Mechanisms of Foxp3$^+$ Regulatory T cell enrichment and High Endothelial Venule formation in tumours

Emily Jayne Colbeck

Cardiff University

Doctor of Philosophy (Ph. D.)

October 2015

Declaration

STATEMENT 1

This work has not previously been accepted in substance for any degree and is not currently submitted in candidature for any degree.

Signed…………………………………(candidate)   Date………………………..

STATEMENT 2

This thesis is being submitted in partial fulfilment of the requirements for the degree of Ph.D.

Signed…………………………………(candidate)   Date………………………..

STATEMENT 3

This thesis is the result of my own independent work / investigation, except where otherwise stated.

Other sources are acknowledged by explicit reference.

Signed…………………………………(candidate)   Date………………………..

STATEMENT 4

I hereby give consent for my thesis, if accepted, to be available for photocopying and for inter-library loan, and for the title and summary to be made available to outside organisations.

Signed…………………………………(candidate)   Date………………………..

STATEMENT 5

I hereby give consent for my thesis, if accepted, to be available for photocopying and for inter-library loan **after expiry of a bar on access previously approved by the Graduate Development committee**.

Signed…………………………………(candidate)   Date………………………..

Acknowledgements

Summary

Foxp3$^+$ Regulatory T cells (Tregs) constitute a major immunosuppressive cell type within tumours. Here, they impinge on anti-tumour immune responses. Modalities aimed at subverting the accumulation and / or suppressive action of Tregs could revolutionise cancer immunotherapies in the future.

By use of the 3-methylcholanthrene (MCA) model of chemical carcinogenesis, I investigated mechanisms of Treg enrichment in tumours. While a large proportion of intra-tumoural Tregs expressed the T_H1 transcription factor, T-bet, there was no role for T-bet-expressing Tregs in tumour control. Additionally, sequestration of Interleukin-2 (IL-2) in the tumour microenvironment (TME) did not represent a mechanism by which Tregs exert dominance at this site. However, the majority of intra-tumoural Tregs expressed CD69, a molecule implicated in retaining T cells at the site of antigen. Furthermore, CD69-expressing Tregs possessed superior suppressive capacity relative to CD69 negative Tregs. Therefore, the consequence of CD69 expression on Tregs may be the retention of tumour-infiltrating super-suppressive Tregs, thereby ensuring Treg dominance within the TME.

By use of the Foxp3^{DTR} mouse model, previous data demonstrated the development of ectopic High Endothelial Venules (HEV) within MCA-induced tumours following depletion of Treg. HEV demonstrated an absolute concordance with increased numbers of T cells inside tumours and reduced tumour growth. I investigated the mechanisms supporting development of HEV in tumours in the absence of Tregs.

I have eliminated a role for B lymphocytes, instead pinpointing CD8$^+$ T cells as key drivers of HEV development in tumours. Ectopic formation of HEV in Treg depleted tumours is Tumour Necrosis Factor (TNF) receptor (TNFR) signalling dependent, and Lymphotoxin (LT) β receptor (LTβR) signalling independent. Furthermore, the proportion of TNFα-producing T cells in the tumour correlated with density of tumour HEV. These data suggest that intra-tumoural development of HEV following Treg depletion is driven by T cell derived TNFα signalling via TNFR(s).

Table of Contents

Abbreviations

ACT, Adoptive Cell Therapy
ADP, Adenosine DiPhosphate
AhR, Aryl hydrocarbon Receptor
AMP, Adenosine MonoPhosphate
APC, Antigen Presenting Cell
ATP, Adenosine TriPhosphate
BEC, Blood Endothelial Cell
BSA, Bovine Serum Albumin
CAR, Chimeric Antigen Receptor
CCL, C-C motif chemokine Ligand
CCR, C-C motif chemokine Receptor
c-FLIP, cellular FLICE (FADD-like IL-1 β-converting enzyme)-Like Inhibitory Protein
CRC, ColoRectal Cancer
CTL, CD8$^+$ Cytotoxic T Lymphocyte
CTLA-4, Cytotoxic T Lymphocyte associated Antigen-4
CTX, Cyclophosphamide
CXCL, C-X-C motif chemokine Ligand
CXCR, C-X-C motif chemokine Receptor
DC, Dendritic Cell
DLN, tumour Draining Lymph Node
DNA, DeoxyriboNucleic Acid
DT, Diphtheria Toxin
DTR, Diphtheria Toxin Receptor
EAE, Experimental Autoimmune Encephalomyelitis
ELS, Ectopic Lymphoid-like Structure
ET$_B$R, EndoThelin B Receptor
FasL, Fas Ligand
FDA, US Food and Drug Administration
FDC, Follicular Dendritic Cell
Foxp3, Forkhead box protein 3
FRC, Follicular Reticular Cell
GATA-3, GATA binding protein 3
GlcNAc6ST, N-acetylglucosamine-6-O-sulfotransferase
GlyCAM-1, Glycosylation-dependent Cell Adhesion Molecule-1
GM-CSF, Granulocyte-Macrophage Colony Stimulating Factor
HEV, High Endothelial Venule
HVEM, Herpes Virus Entry Mediator
IBD, Inflammatory Bowel Disease
ICAM, InterCellular Adhesion Molecule
IDO, Indoleamine 2,3-DiOxygenase
ID2, helix-loop-helix protein Inhibitor of DNA binding 2
IFN, Interferon
IL, Interleukin
ILC, Innate Lymphoid Cell
ILF, Isolated Lymphoid Follicle
i.p, intra-peritoneal
IPEX, Immune dysregulation, Polyendocrinopathy, Enteropathy, X-linked
irAE, immune-related Adverse Events
IRF4, Interferon Regulatory Factor 4
iTreg, *in vitro*-induced Treg
LEC, Lymphatic Endothelial Cell
LFA-1, Lymphocyte Function-associated Antigen 1
LIGHT, LT-related Inducible ligand that competes for Glycoprotein D binding to Herpesvirus entry mediator on T cells
LN, Lymph Node
LPS, LipoPolySaccharide
LT, Lymphotoxin
LTi, Lymphoid Tissue inducer cell

LTo, Lymphoid Tissue organizer cell
mAb, monoclonal Antibody
MAdCAM-1, Mucosal Addressin Cell Adhesion Molecule-1
MAGE-A, Melanoma AntiGEn family A
MALT, Mucosal Associated Lymphoid Tissue
MART-1, Melanoma-associated Antigen Recognised by T cells 1
MCA, 3-Methylcholanthrene
MDSC, Myeloid Derived Suppressor Cell
MeOH, Methanol
MHC, Major Histocompatibility Complex
MZ, Marginal Zone
NBFS, Neutral-Buffered Formalin Solution
NDLN, Non-tumour Draining Lymph Node
NK, Natural Killer cell
NKT, Natural Killer T cell
NOD, Non-Obese Diabetic
NSCLC, Non-Small Cell Lung Cancer
NY-ESO-1, New York ESOphageal squamous cell carcinoma-1
OCT, Optimum Cutting Temperature
PAP, Prostatic Acid Phosphatase
PBS, Phosphate-Buffered Saline
PD-1, Programmed cell Death-1
PD-L1, Programmed cell Death-Ligand 1
PD-L2, Programmed cell Death-Ligand 2
PFA, paraformaldehyde
PGE_2, ProstaGlandin E_2
PLN, Peripheral (subcutaneous) Lymph Node
PNAd, Peripheral Node Addressin
PP, Peyer's Patches
pTreg, peripherally-derived Treg
PU.1, Purine-rich box 1
RAG, Recombination Activating Gene
RIP, Rat Insulin Promoter
RORγt, Retinoid-acid receptor-related Orphan Receptor gamma t
RT, Room Temperature
SCS, SubCapsular Sinus
SLO, Secondary Lymphoid Organ
STAT, Signal Transducer and Activator of Transcription
TAA, Tumour-Associated Antigen
Tconv, conventional $CD4^+$ T cell
TCR, T Cell Receptor
Tfh, T follicular helper
TGFβ, Transforming Growth Factor β
T_H, T helper cell
Ti-BALT, Tumour-induced Bronchus-Associated Lymphoid Tissue
TIL, Tumour Infiltrating Lymphocyte
TLO, Tertiary Lymphoid Organ
TME, Tumour MicroEnvironment
TNF, Tumour Necrosis Factor
TNFα, Tumour Necrosis Factor α
TNFSF, Tumour Necrosis Factor SuperFamily
TRANCE, Tumour Necrosis Factor (TNF)-related activation induced cytokine (TNFSF11; RANKL; OPGL; ODF)
Treg, $Foxp3^+$ Regulatory T cell
tTreg, Thymus-derived Treg
T1D, Type 1 Diabetes mellitus
VCAM, Vascular Cell Adhesion Molecule
VEGF, Vascular Endothelial Growth Factor
WT, Wild-Type
6-sulpho sialyl Lewis X, sialic acid α2-3 Galactose β1-4(Fucose α1-3(sulpho-6))GlcNAcβ1R

Chapter One

1 Introduction

1.1 Cancer Biology and the Process of Tumourigenesis

Cancer is a leading cause of human morbidity and mortality, responsible for approximately 8.2 million deaths worldwide in 2012. Cancer refers to more than 200 different types of disease, afflicting various parts of the body. Lung, liver, stomach, colorectal, breast and oesophageal cancers account for the most cancer-associated deaths. One in every two people in the UK will develop cancer in their lifetime (World Health Organisation; Cancer Research UK).

Cancer development encompasses a multistage process of tumourigenesis, involving discrete genetic events facilitating transformation of healthy cells. Accumulation of spontaneous or inherited genetic mutations results in uncontrolled cellular growth, and eventually the formation of a malignant tumour. This process has been particularly well documented in colorectal cancer (CRC) (Vogelstein et al. 2013). Transformed cells subsequently invade other tissues during metastasis, the major cause of mortality from cancer (World Health Organisation).

Hanahan and Weinberg have defined discrete hallmarks of cancer: traits that cells acquire as they progress to a neoplastic state to enable tumour growth and metastatic dissemination (Figure 1.1) (Hanahan & Weinberg 2000; Hanahan & Weinberg 2011). A fundamental characteristic of cancer cells is the sustenance of chronic proliferation, by deregulating signalling activities of growth factors that maintain normal cell homeostasis. Cancer cells must evade negative regulation of growth, mainly by circumventing growth suppression initiated by tumour suppressor genes. Resistance to programmed cell death is a prerequisite if cancer cells are to progress to malignancy. Furthermore, cancerous cells must acquire replicative immortality: the ability to progress through unlimited cycles of growth and division without being diverted down regulatory pathways involving senescence, a non-replicative but viable state, or crisis, culminating in cell death (Hanahan & Weinberg 2000).
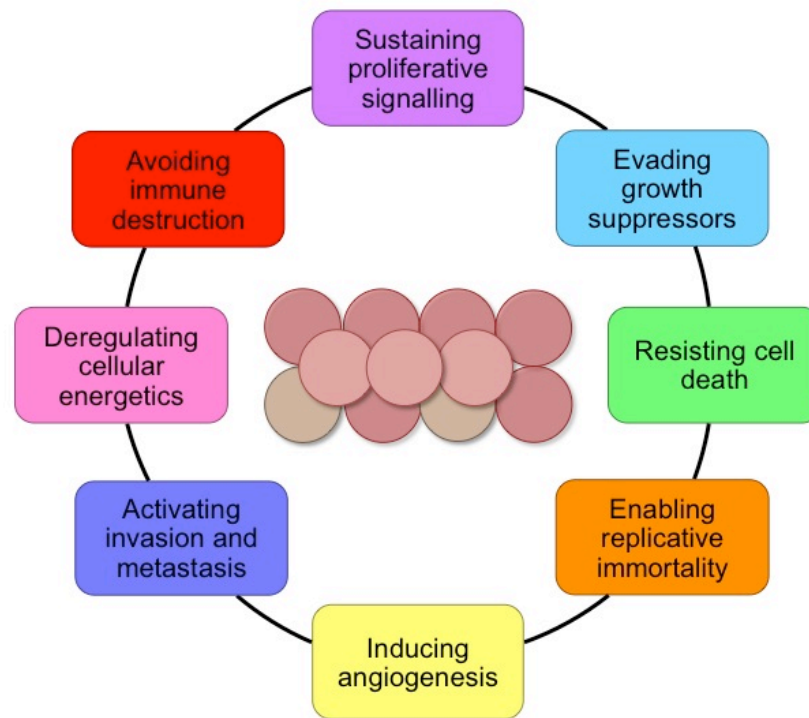
Figure 1.1 | The Eight Hallmarks of Cancer.
The hallmarks of cancer are traits cells acquire as they progress to malignancy. Cancer cells must sustain chronic proliferative signalling, evade negative regulation of growth, resist apoptotic programmed cell death, acquire replicative immortality, initiate angiogenesis, and activate a program of invasion of local tissues and formation of distant metastases. More recently recognised hallmarks are deregulation of cellular energetics, and escape from recognition and attack by a competent immune system. Brown circles represent tumour.
Adapted from (Hanahan & Weinberg 2000; Hanahan & Weinberg 2011).

To guarantee supply of nutrients and oxygen and purge itself of waste products, a tumour must develop its own vascular system by initiating angiogenesis: sprouting of new vessels from existing vasculature (Hanahan & Weinberg 2000). Due to an unbalanced chronic pro-angiogenic signature, tumours are characterized by aberrant heterogeneous vasculature including precocious sprouting, excessive branching and distorted vessels, causing erratic blood flow, leakiness, hypoxia, increased interstitial pressure and micro-haemorrhaging (Hagen et al. 2008). Another key trait is invasion of local tissues and formation of distant metastases (Hanahan & Weinberg 2000).

In 2011, Hanahan and Weinberg updated their review, to include two new emerging hallmarks of neoplastic disease. Firstly, to fuel limitless growth and division, cancerous cells must deregulate cellular energetics. The final emerging hallmark involves evasion of immune system recognition and attack, which is absolutely necessary for progression of a developing tumour (Hanahan & Weinberg 2011).

1.2 Cancer Immunology

1.2.1 A history of Cancer Immunosurveillance

The concept that the immune system can recognize, target and destroy nascent transformed cancer cells was conceived in the early 1900's. Paul Ehrlich proposed that the immune system suppresses formation of what would otherwise be an "overwhelming frequency" of carcinomas. Thereby followed a century of robust debate surrounding immune system involvement in control of tumour formation (Dunn et al. 2002).

Medawar and colleagues clarified a role for cellular components of the immune system in allograft transplant rejection in the mid 1900's (Medawar 1944). However, transplanted tumours from non-inbred mice were destroyed on the basis of allogeneic, rather than tumour-specific, rejection. Successful immunization against carcinogen or virally induced syngeneic tumours in inbred mice established that tumour cells were immunologically distinct from healthy cells, proving the existence of tumour specific antigens (Old & Boyse 1964; Klein et al. 1960). These landmark discoveries supported the formal 'Cancer Immunosurveillance' hypothesis, originally proposed by Burnet and Thomas: that thymus-dependent cells of the immune system act as sentinels in continual surveillance of host tissues for nascent, transformed cells, which they recognize and eliminate (Burnet 1957).

Several studies subsequently tested predictions of the hypothesis; that immunocompromised animals are more susceptible to spontaneous or chemically induced tumours, relative to immunocompetent counterparts (Dunn et al. 2002). 3-methylcholanthrene (MCA) is a polycyclic aromatic hydrocarbon, and a chemical carcinogen found in environmental pollutants. MCA induces tumour formation, usually fibrosarcomas, at the site of injection, and induces cellular transformation via accumulation of multiple random mutations. The MCA carcinogenesis model has been used extensively in tumour immunology studies: this system, in contrast to transplantable tumour models and tumour cell line models, accurately models

reciprocal interactions between the immune system and the tumour during very early stage carcinogenesis (Blankenstein & Qin 2003).

Osias Stutman found no difference in incidence of tumours induced by MCA between athymic nude mice, which carry a genetic immunologic defect, and wild-type (WT) animals (Stutman 1974; Outzen et al. 1975). There was also no difference in incidence of spontaneous non-viral tumour development between WT and nude mice (Rygaard & Povlsen 1974[a]; Rygaard & Povlsen 1974[b]). These studies argued against the Cancer Immunosurveillance hypothesis, which was largely abandoned at the time.

With technological advances and availability of inbred mouse strains genetically deficient for immune system components in the 1990's, came resurgence in the Cancer Immunosurveillance hypothesis. Interferon (IFN)-γ deficient mice or mice lacking perforin (a component of cytolytic granules that mediate CD8^{+} Cytotoxic T Lymphocyte (CTL) or Natural Killer (NK) cell killing) demonstrated increased incidence of transplanted, chemically induced or spontaneous tumours relative to immunocompetent animals (Dunn et al. 2002). In support of lymphocyte involvement in Immunosurveillance, gene-targeted recombination activating gene (RAG)-2 deficient animals, which lack T, B and Natural Killer T (NKT) cells, developed MCA-induced sarcomas quicker and at greater frequency than WT controls (Shankaran et al. 2001).

Indeed, mice lacking various immune constituents, such as NK, NKT, γδ T, and αβ T cells, and IFN-γ and Interleukin (IL)-12, all displayed increased susceptibility to tumour development (Dunn et al. 2002). These studies lent considerable weight to the idea of immune involvement in cancer, and demonstrated involvement of both innate and adaptive arms. Additionally, significant caveats to Stutman's experiments were identified; most notably that nude mice are incompletely immunocompromised. Finally, a landmark study in 2007 provided definitive evidence for the involvement of adaptive immunity in control of tumour development (Koebel et al. 2007). Collectively, this enormous body of work by multiple independent investigators solidified the concept of Cancer Immunosurveillance: that the immune system can recognize and destroy

developing primary tumours, during which lymphocytes and lymphocyte-derived cytokines are key (Dunn et al. 2002; Burnet 1957).

Accumulation of direct evidence for Cancer Immunosurveillance in humans is problematic: anti-tumour immune responses that effectively clear tumour are not recorded by researchers or physicians, as the patient does not present clinically. Conversely, patients that do present clinically are arguably people in which immune-mediated mechanisms of tumour control have failed (Gallimore & Godkin 2008).

Long-term epidemiological data show that immunocompromised patients demonstrate an increased risk for development of non-viral primary tumours relative to the general population (Penn 1999). However, the strongest evidence for Cancer Immunosurveillance in humans is provided by the significant correlation between number of tumour infiltrating lymphocytes (TILs) and prognostic markers, such as patient survival, for many types of cancer, including breast, colon and melanoma (Dunn et al. 2002; Gallimore & Godkin 2008). Specifically, presence of IFN-γ producing CD4^{+} T-helper (T$_H$)1 type cells and CD8^{+} CTLs is associated with better clinical outcome (Naito et al. 1998; Sato et al. 2005; Pagès et al. 2005; Galon et al. 2006). These studies illustrate the existence and physiological relevance of Cancer Immunosurveillance in humans as well as animal models (Gallimore & Godkin 2008).

1.2.2 Cancer Immunoediting

Surveillance of tumour development is now known to represent just one dimension of the complex interaction between the immune system and cancer. It has long been recognized that the immune system can initiate and even promote tumour progression during chronic inflammation (Grivennikov et al. 2010). The Cancer Immunosurveillance hypothesis has undergone extensive resculpturing in recent decades, owing to the recognition that the immune system can also modify the immunogenicity of a developing tumour: tumours originated in immunodeficient hosts are more immunogenic than those developed in immunocompetent environments (Shankaran et al. 2001). Evidence now indicates that the immune system can even

select for and promote emergence of low immunogenicity tumour variants, thereby aiding tumour escape from immune destruction.

The paradoxical ways in which the immune system influences tumour development are recognized in the revolutionized 'Cancer Immunoediting' hypothesis, which encompasses both host-protective and tumour-sculpting functions of the immune system. Cancer Immunoediting consists of three phases that occur independently or sequentially: Elimination, Equilibrium and Escape (Figure 1.2). 'Elimination' refers to classical immunosurveillance, during which transformed cells are eliminated by a collaborative effort between innate and adaptive immune arms. Specific immune components required likely depends on characteristics such as origin, and anatomical location of the tumour (Schreiber et al. 2011; Mittal et al. 2014).

Cancer cell variants that avoid immune destruction may subsequently undergo editing and sculpting by the adaptive immune system during 'Equilibrium'. Tumour outgrowth is controlled during this phase, leading to tumour dormancy (Schreiber et al. 2011). Koebel's study in 2007 unequivocally demonstrated a role for adaptive immunity in maintaining MCA-induced fibrosarcomas in a state of immune-mediated dormancy (Koebel et al. 2007). These data were corroborated by studies in other models (Loeser et al. 2007; Eyles et al. 2010). Immunological restraint of transformed cells is also inferred from reports of tumour development in immunosuppressed patients following transplantation of an organ harbouring occult cancer cells (MacKie et al. 2003).

Immune-mediated dormancy can be a prolonged stage, maintained by the balance between elimination-promoting IL-12 and tumour-promoting IL-23 (Teng et al. 2012). Additionally, the relative balance of immunosuppressive cells, such as Foxp3$^+$ Regulatory T cells (Tregs; described in detail in section 1.5 below) and Myeloid Derived Suppressor Cells (MSDCs), to those underpinning anti-tumour immune responses, such as CD8$^+$ CTLs and NK cells, influences whether tumours are maintained in a state of dormancy (Wu et al. 2013). Transition through Equilibrium also depends on cell intrinsic mechanisms of T cell regulation via co-stimulatory and co-inhibitory receptors and ligands (Mittal et al. 2014). Equilibrium is the target of many cancer

immunotherapies, which largely aim to tip the balance in favour of elimination at the expense of escape (Quezada et al. 2011).

In the final stage of Escape, immunologically edited tumours that have circumvented immune recognition progress to become clinically apparent. Escape mechanisms are highly complex and varied, and involve loss of tumour antigen expression, resistance to cytotoxicity, and establishment of an immunosuppressive microenvironment capable of suppressing further immune attacks (Schreiber et al. 2011). Novel immunotherapies target checkpoint molecules that contribute to immunosuppression (see Section 1.3.3) (Mittal et al. 2014).

The concept of Cancer Immunoediting relies upon the premise that T cells recognize Tumour-Associated Antigens (TAAs), which dictates whether a developing tumour is efficiently eliminated or immunologically sculpted (Mittal et al. 2014). These so-called 'cancer rejection epitopes' presented in Major Histocompatibility Complex (MHC) complexes on tumour cells or Antigen Presenting Cells (APCs) could be non-mutated self non-tolerogenic proteins recognized by T cells, or new proteins, completely absent from the normal human genome, formed by mutational events during tumour formation. The latter are referred to as neo-antigens (Schumacher & Schreiber 2015).

Until recently, the existence of tumour neo-antigens, and those that are recognized by T cells and capable of inducing immune responses, has remained elusive. Matsushita and colleagues used exome sequencing and MHC Class I prediction algorithms to study the mutational landscape of a highly immunogenic, unedited MCA-derived tumour raised in RAG2 deficient mice. A mutation in the gene encoding Spectrin-β2 was discovered as a source of a tumour-associated neo-antigen epitope, which functioned as an immunodominant rejection antigen. Tumour cell clones lacking expression of this antigen displayed decreased immunogenicity and outgrew clones expressing the antigen by a process of T cell-dependent immunoselection (Matsushita et al. 2012). Such data support the notion that Cancer Immunoediting involves T cell mediated elimination and/or immunological sculpting of tumours based

on recognition of tumour-associated neo-antigens. Clinical studies have demonstrated the existence of Cancer Immunoediting reliant upon neo-antigens in humans. Immunoselection and outgrowth of tumours lacking expression of tumour-associated neo-antigens has been found following immunotherapy (Boehmer et al. 2013; Nicholaou et al. 2011). Such studies highlight the requirement to target several TAAs in immunotherapy if outgrowth of low immunogenic tumour variants is to be prevented (Mittal et al. 2014).
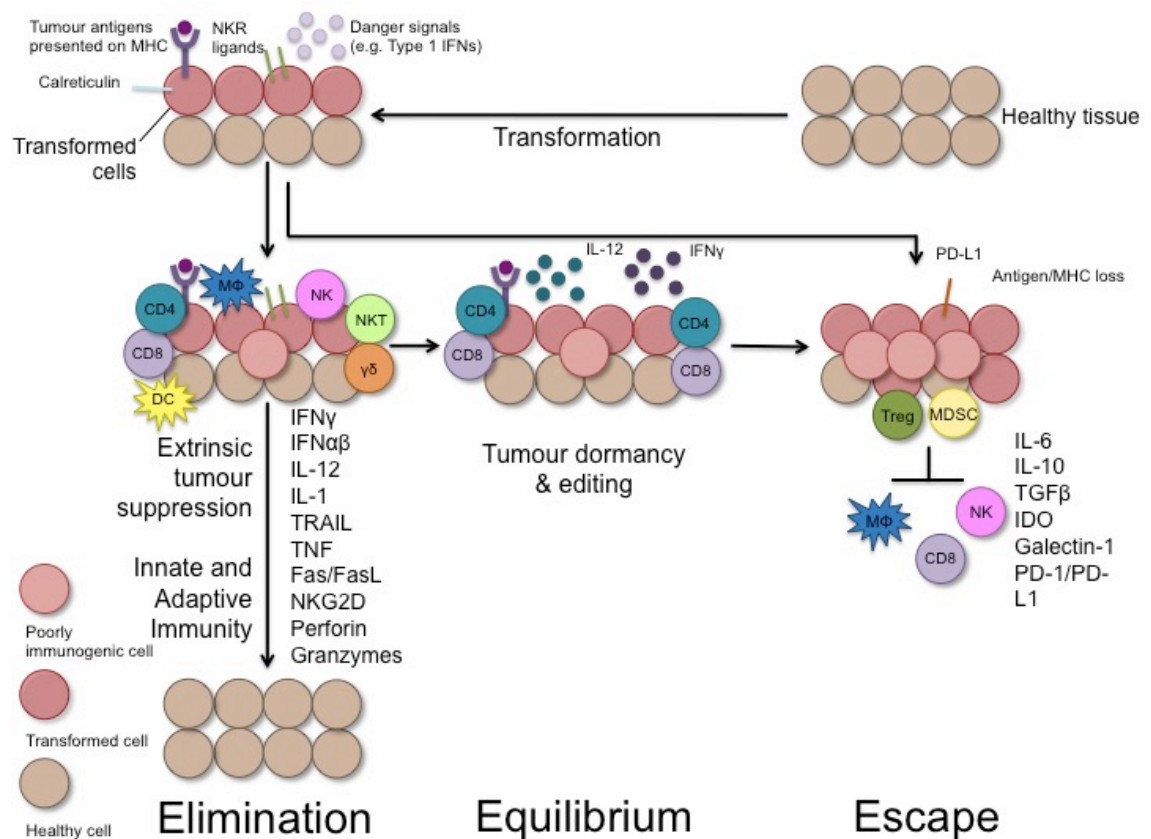
Figure 1.2 | The Concept of Cancer Immunoediting.
Cancer Immunoediting consists of Elimination, Equilibrium and Escape. Immunoediting acts as an extrinsic tumour suppressor, functioning once healthy cells have undergone transformation. The immune system is alerted to the presence of a tumour in ways potentially encompassing release of "danger signals" such a Type 1 IFN; presentation of tumour antigens in MHC complexes; expression of stress ligands, such as ligands for NK receptors (NKR) like NKG2D; and exposure of calreticulin which signals hyperploidy and thereby increases immunogenicity of transformed cells. Elimination involves a collaborative effort between components of innate and adaptive immune systems, as listed/ depicted here. If rare tumour variants escape immune destruction during elimination, they can undergo immunogenicity editing and sculpting during Equilibrium. During this stage, cells of the adaptive immune system, primarily T cells, halt tumour progression to prevent outgrowth by inducing a state of functional dormancy, for which the cytokines IL-12 and IFN-γ are absolutely required. An alternative, however, is the emergence of tumour variants that have lost MHC and/or tumour antigen presentation and are invisible to the immune system. These variants can hence enter the escape phase, where tumour outgrowth to clinical appearance occurs. Other mechanisms leading to tumour escape include increased insensitivity to immune-mediated tumour cell killing, and/or the establishment of an immunosuppressive microenvironment by recruitment of Tregs and MDSCs, which suppress activity of immune cells via the molecules listed, and up-regulation of immunomodulatory molecules on tumour cells, such as PD-L1. Adapted from (Schreiber et al. 2011; Mittal et al. 2014).

1.3 Cancer Immunotherapy

Advances in our understanding of the interplay between developing tumours and the immune system is enabling immunological manipulation to treat human malignancies. Successful immunotherapy proves challenging, due to the plethora of mechanisms underpinning immune-mediated tolerance to self-antigens. A growing appreciation of immune tolerance has accelerated development of new approaches to combat cancer using the immune system, as discussed below (Makkouk & Weiner 2015).

1.3.1 Adoptive Cell Therapy

Adoptive Cell Therapy (ACT) is a highly personalized therapy, involving the infusion of immune cells into a patient. The immune cells administered tend to be naturally occurring autologous lymphocytes isolated from tumour, which exhibit anti-tumour reactivity and are expanded *ex vivo* prior to infusion. Alternatively, host lymphocytes are genetically engineered to express TCRs or Chimeric Antigen Receptors (CARs) specific for tumour antigens (Rosenberg & Restifo 2015).

Clinical trials of ACT therapy for melanoma have consistently yielded impressive objective response rates in approximately 50% of patients, with complete responses observed in up to 22% of patients (Hinrichs & Rosenberg 2014). However, melanomas seem to be one of the only tumour types amenable to ACT therapy (Rosenberg & Restifo 2015). Transfer of lymphocytes engineered to express a TCR specific for the melanoma-melanocyte antigen Melan-A (MART-1) led to tumour regression in patients (Morgan et al. 2006), setting the stage for engineering T cells to express receptors specific for antigens expressed on different tumour types. Transfer of T lymphocytes engineered to express a CAR targeting CD19 led to successful regression of advanced B cell lymphoma (Kochenderfer et al. 2010), and, more recently, sustained remission in up to 67% of leukaemia patients (Maude et al. 2014). However, targeting of antigens over expressed on tumours but expressed at low levels on healthy tissue, such as Melan-A, leads to considerable on-target off-tumour toxicity

in patients (Johnson et al. 2009). Considering the durable and complete tumour regression in metastatic melanoma patients, identification of the antigens recognized by melanoma TILs could enable discovery of suitable tumour-specific targets to translate the clinical benefit of ACT to other cancer types (Rosenberg & Restifo 2015).

1.3.2 Cancer Vaccines

Rationale for cancer vaccines was proven by demonstration of T cell recognition of a melanoma antigen, MAGE-A1 (van der Bruggen et al. 1991). A plethora of TAAs have since been identified (Vigneron et al. 2013). The majority of targets belong to the cancer testis antigen family, a class of proteins with endogenous expression restricted to male germ cells, which are over expressed in tumours. Peptide vaccines targeting one of two cancer testis antigens, MAGE-A3 and NY-ESO-1, have been explored extensively for clinical benefit in trials (Dougan & Dranoff 2009). These approaches have limited efficacy, possibly due to the inability to break immunological tolerance to self. Addition of immune adjuvants, such as IL-2, to boost peptide-specific T cell activation has proven effective in some cases (Makkouk & Weiner 2015).

Whole tumour cell and antigen-pulsed Dendritic Cell (DC) vaccination approaches have also been explored. Tumour cells act as potent multivalent vaccines, generating an immune response against multiple antigens. GVAX is composed of two irradiated prostate cancer cell lines, engineered to express Granulocyte-Macrophage Colony Stimulating Factor (GM-CSF). However, despite evidence of an immune response, clinical trials of GVAX showed no survival benefit (Makkouk & Weiner 2015).

Antigen-pulsed DC vaccines have arguably shown the most promise, evidenced by US Food and Drug Administration (FDA) approval of Sipuleucel-T (Provenge), for metastatic hormone-refractory prostate cancer in 2010, following demonstrable increased overall survival in three independent phase III clinical trails (Higano et al. 2009; Small et al. 2006; Kantoff et al. 2010; Kissick & Sanda 2015). Sipuleucel-T consists of autologous DCs loaded with a fusion protein of Prostatic Acid Phosphatase (PAP) and GM-CSF (Makkouk & Weiner 2015). The failure of cancer

vaccines has been attributed to endogenous T cell exhaustion caused by chronic antigen exposure in the tumour microenvironment, prohibiting the required rapid division of $CD8^+$ T cells in response to antigen presentation. By combining existing cancer vaccines with new modalities aimed at circumventing T cell exhaustion (see Section 1.3.3), efficacy of vaccination could be significantly improved (Kissick & Sanda 2015).

1.3.3 Checkpoint Inhibitors

Checkpoint inhibitor therapy represents a radical shift in cancer immunotherapy. The goal is not to enhance activity of the immune system against tumour cells, but remove inhibition of endogenous T cell activity, circumventing T cell exhaustion. Checkpoint inhibitor therapy works on the premise that activation of naïve T cells by TCR recognition of tumour-antigen-MHC complexes requires co-stimulatory signals in the form of T cell expressed CD28 engagement by B7 ligands CD80 (B7.1) and CD86 (B7.2) expressed on APCs (Sharma & Allison 2015; Salomon & Bluestone 2001).

T cell activation results in proliferation and differentiation but also activation of inhibitory pathways that eventually terminate T cell responses. These inhibitory feedback loops function to mitigate uncontrolled, harmful immune responses (Sharma & Allison 2015; Quezada & Peggs 2013). One major inhibitory pathway is mediated by Cytotoxic T Lymphocyte associated Antigen 4 (CTLA-4). CTLA-4 binds CD80 and CD86 with higher affinities than CD28 and therefore opposes CD28-mediated T cell stimulation, promoting down-regulation of T cell responses (Sharma & Allison 2015).

Early studies in mouse models demonstrated that CTLA-4-mediated inhibitory signals limit anti-tumour immune responses, and blockade of CTLA-4 enabled sufficient persistence of anti-tumour T cell responses to facilitate tumour rejection, without prior knowledge of TAAs (Leach et al. 1996; Krummel & Allison 1996). Two seminal phase III clinical trials demonstrated considerable improved overall survival in metastatic melanoma patients treated with Ipilimumab, a fully human anti-CTLA-4 monoclonal antibody (Hodi et al. 2010; Robert et al. 2011), resulting in FDA approval in

2011 (Sharma & Allison 2015). Crucially, a durable response of survival up to 4 years was observed in approximately 20% of treated patients, with a subset of patients surviving to 10 years or more (Schadendorf et al. 2015). However, anti-tumour affects of Ipilimumab are accompanied by considerable immune-related Adverse Events (irAE) in approximately 60% of patients (Hodi et al. 2010).

It was initially suggested that Ipilimumab functions via direct blockade of CTLA-4 on effector T cells (Walunas et al. 1994; Krummel & Allison 1995; Krummel & Allison 1996; Sutmuller et al. 2001). However, as CTLA-4 is constitutively expressed at high levels on both murine and human Tregs (see Section 1.5.4.2) (Read et al. 2000; Takahashi et al. 2000; Wing et al. 2008; Dieckmann et al. 2001), anti-CTLA-4 could directly deplete Tregs or inhibit their suppressive capacity (Read et al. 2006). Quezada and colleagues demonstrated a requirement for anti-CTLA-4 to bind both effector T cells and Tregs for full anti-tumour activity (Peggs et al. 2009). Many groups have shown that anti-CTLA-4 in fact expands the Treg compartment in both mice and humans (Quezada et al. 2006; Schmidt et al. 2009; Kavanagh et al. 2008). However, successful rejection of tumour following anti-CTLA-4 treatment is commonly associated with an increased effector T cell : Treg ratio, specifically in the tumour (Shrikant et al. 1999; Quezada et al. 2006; Kavanagh et al. 2008; Liakou et al. 2008; Chen et al. 2009; Curran & Allison 2009; Waitz et al. 2012). Quezada and colleagues have elegantly demonstrated through T cell tracking experiments that anti-CTLA-4 therapy results in an increase in absolute numbers of effector T cells and Tregs in lymph nodes, but a reciprocal decrease in absolute numbers of Tregs with an increase in absolute numbers of effector T cells in the tumour. Depletion of Tregs in the tumour was shown to be dependent on the presence of Fcγ-receptor expressing macrophages, explaining the paradoxical effects of this antibody therapy on T cell ratios in lymphoid organs and tumour (Simpson et al. 2013).

In 2000, another immune checkpoint molecule, Programmed cell Death (PD) 1 (PD-1), was found to circumvent the responses of activated T cells (Freeman et al. 2000). In contrast to CTLA-4, PD-1 interferes with TCR signalling, when activated by

one of two ligands, PD-Ligand (PD-L)1 or PD-L2 (Sharma & Allison 2015). PD-1 is also up-regulated on T cells following activation, but unlike CTLA-4 is more broadly expressed on B cells, monocytes and NKT cells in addition to T cells (Greenwald et al. 2005). PD-L1 is broadly expressed on T and B cells, DCs, and macrophages, and is significantly up-regulated on several human tumours, possibly in response to T cell-derived IFNγ, where it is thought to attenuate anti-tumour immune responses. PD-L2 is expressed mostly on macrophages and DCs following activation (Madorsky Rowdo et al. 2015; Quezada & Peggs 2013).

PD-1 is highly expressed on Tregs, and promotes their function when bound to a cognate ligand, leading to the hypothesis that PD-1 blockade could attenuate the number or function of intra-tumoural Tregs (Madorsky Rowdo et al. 2015). Blockade of the PD-1 pathway in mouse models increased anti-tumour T cell activity (Dong et al. 2002; Iwai et al. 2002; Fife et al. 2009). The humanized anti-PD-1 monoclonal antibody, pembroluzimab, received FDA approval in 2014, following good clinical response rates in advanced melanoma patients (Hamid et al. 2013; Robert et al. 2014; Topalian et al. 2012; Topalian et al. 2014). However, as for anti-CTLA-4, Pembroluzimab results in toxic effects in 79% of patients (Hamid et al. 2013), and can induce autoimmune diabetes (Martin-Liberal et al. 2015). A second anti-PD-1 monoclonal antibody, Nivolumab, has been approved for metastatic melanoma and metastatic or advanced NSCLC (Robert et al. 2015; Sharma & Allison 2015).

The distinct mechanisms of action of anti-CTLA-4 and anti-PD-1 antibodies suggest that combinatorial therapy may result in more efficacious T cell responses (Parry et al. 2005; Sharma & Allison 2015). Pre-clinical studies have shown better outcome following combined therapy relative to either therapy alone (Curran et al. 2010). A phase I clinical trial recently demonstrated tumour regression (most with regression of ≥80%) in approximately half of advanced melanoma patients treated with combination therapy (Wolchok et al. 2013).

Checkpoint blockade therapies have achieved unprecedented overall response rates in the clinic. However, complete response rates remain at the few per cent for

both therapies, indicating room for improvement. Furthermore, the observed irAE, consistent with a mechanism of action based on general activation of the immune system, could represent a significant limitation. Improving lymphocytic infiltration into the tumour mass could improve efficacy and selectivity of these treatments in the future (Madorsky Rowdo et al. 2015).

1.3.4 Neo-antigens in Cancer Immunotherapy

The clinical studies mentioned above demonstrate the inherent tumouricidal potential of endogenous T lymphocytes and the ability of therapies to potentiate robust anti-tumour immune responses without prior knowledge of tumour antigens. However, therapies designed by exploitation of information regarding tumour specific neo-antigens are now becoming feasible. The neo-antigens expressed by a tumour from one patient are unlikely to be shared at any considerable frequency with those from another patient's tumour, and hence are largely patient specific. Attempts to interrogate T cell reactivity towards any particular neo-antigen therefore need to be centred entirely on the genome of an individual patient's tumour. With the advent of deep sequencing, it is now feasible to sequence an individual patient's tumour exome (the protein-encoding part of the genome) to find mutated proteins, from which putative neo-antigens for T cell recognition can be predicted using computational algorithms. The feasibility of this approach has been demonstrated by several recent seminal studies in mouse and human (Castle et al. 2012; Matsushita et al. 2012; Robbins et al. 2013; van Rooij et al. 2013; Schumacher & Schreiber 2015).

1.4 The Tumour Microenvironment as a Hostile Site of Immune Privilege

A prerequisite of successful cancer immunotherapy is physical contact between anti-tumour T cells and target cancer cells. Stromal and immune cells resident of the Tumour Microenvironment (TME) can restrict access of tumour-specific T cells (Joyce & Fearon 2015). A study in 1960 demonstrated the inability of an immune response initiated by a primary MCA-induced tumour to control tumour growth, despite the ability of this response to inhibit establishment of a secondary tumour derived from primary

tumour cells. Hence tumours establish an immune-privileged microenvironment, shielding themselves from immune recognition and attack (Klein et al. 1960).

Immune suppression by the TME was demonstrated in humans by the co-existence of progressing melanoma in patients with T cells capable of recognizing MAGE-A1 (van der Bruggen et al. 1991). Such studies illustrate that induction of tumour antigen-specific T cells via vaccination or ACT may be insufficient for robust control of tumour growth. Indeed, infiltration of highly activated anti-tumour effector T cells via tumour vasculature is a frequently overlooked prerequisite for successful immunotherapy (Chen et al. 2003). This hurdle could explain that, despite the induction of vast quantities of circulating T cells by vaccination and no evidence for cancer cell antigen shedding, melanoma patients frequently demonstrate disease recurrence (Rosenberg et al. 2005). The difference in composition and penetrability of the microenvironment of leukaemias relative to solid tumours could explain the limited efficacy of ACT in the latter (Joyce & Fearon 2015).

Clinical success of checkpoint blockade therapies could be attributed to their ability to overcome some of the immunosuppressive functions of the TME (Joyce & Fearon 2015). As previously mentioned, anti-CTLA-4 therapy in mice results in a reduction in the number of immunosuppressive Foxp3^{+} Tregs in tumours (Simpson et al. 2013). PD-1 pathway blockade is thought to function by preventing the negative regulatory signals derived from tumour cell-expressed PD-L1. The inability to achieve objective clinical responses in a large fraction of patients following checkpoint inhibitor therapy, however, could reflect the plethora of immunosuppressive mechanisms employed by tumours (Joyce & Fearon 2015).

1.4.1 The Tumour Vasculature: a Prominent Component of the Immunosuppressive Tumour Microenvironment

Due to the aberrant exposure to pro-angiogenic factors such as Vascular Endothelial Growth Factor (VEGF)-A, tumours develop a highly disorganized, distorted vasculature (Hagen et al. 2008). Tumour vasculature represents a major component of

the immunosuppressive TME, employing multiple mechanisms to selectively recruit or exclude cells (Figure 1.3) (Joyce & Fearon 2015; Motz & Coukos 2011). VEGF additionally acts as an immunosuppressive factor, and elevated VEGF levels on endothelium of human ovarian tumours is associated with decreased infiltration of effector anti-tumour T cells and a worse prognosis (Zhang et al. 2003). The anti-VEGF-A monoclonal antibody, Bevacizumab, became the first anti-angiogenesis agent approved for treatment of metastatic CRC by the FDA in 2004 (Ellis & Hicklin 2008). Low doses of anti-VEGF-A therapy results in so-called "normalization" of tumour vasculature, involving reversal of the highly chaotic structure to a mature, healthy vascular bed (Jain 2005; Tong et al. 2004; Willett et al. 2004). Vascular normalization by antiangiogenic therapy significantly improves infiltration of effector T cells, boosting ACT or vaccine efficacy in mouse models (Shrimali et al. 2010; Huang et al. 2012).

Molecules expressed by tumour endothelial cells enforce a barrier to anti-tumour T cells (Joyce & Fearon 2015). One study revealed establishment of a "tumour endothelial death barrier" via endothelial expression of the apoptosis inducer Fas ligand (FasL) within human ovarian, breast, bladder, prostate, colon and renal cancers. High endothelial FasL expression was associated with a paucity of $CD8^+$ CTLs and an abundance of Tregs in tumours; the latter are thought to protect themselves against FasL-mediated killing by high expression of c-FLIP, an apoptosis inhibitor. In mouse models, FasL inhibition significantly increased infiltration of anti-tumour T cells, which mediated tumour control, and substantially improved efficacy of ACT. FasL expression was induced by immunosuppressive factors in the TME, including VEGF, prostaglandin E_2 (PGE_2), and IL-10 (Motz et al. 2014). The vasculature of human ovarian tumours also expresses endothelin B receptor (ET_BR), which correlates with lower frequencies of infiltrating T cells and poor outcome. ET_BR inhibition increased effector T cell infiltration into tumours and significantly improved efficacy of vaccination (Buckanovich et al. 2008). Expression of B7-H3, another ligand for CTLA-4, on tumour endothelium has also been associated with reduced T cell infiltration and worse clinical outcome in ovarian carcinoma patients (Figure 1.3) (Zang et al. 2010).
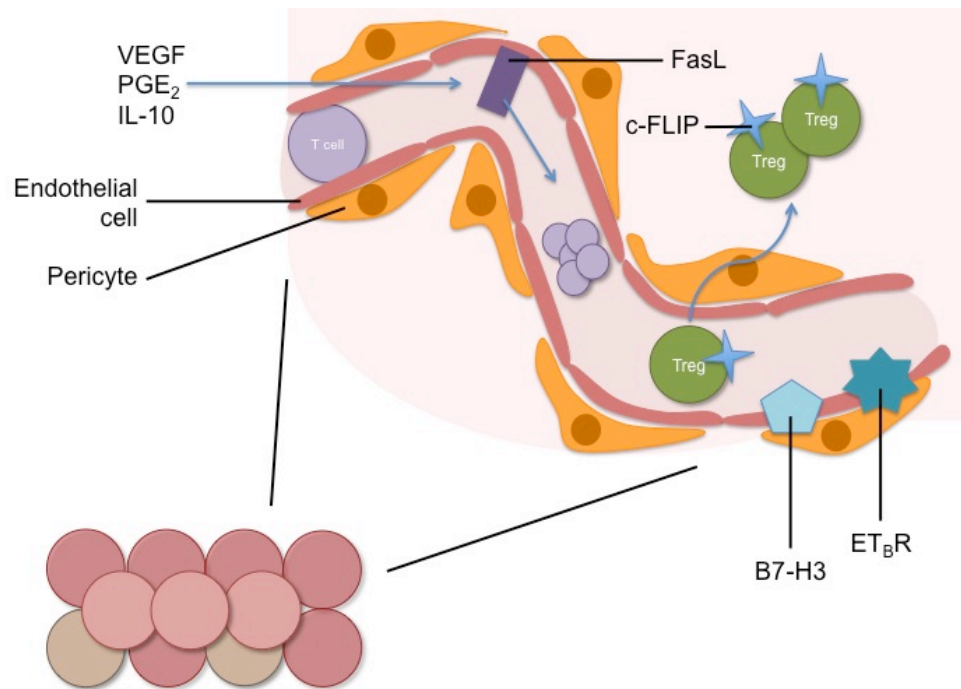
Figure 1.3 | The Immunosuppressive Tumour Vasculature.
Tumours display highly aberrant vasculature, including incomplete pericyte coverage. Tumour endothelium expresses FasL, which is induced by VEGF, PGE_2 and IL-10. FasL induces apoptosis of anti-tumour effector T cells, while Tregs are refractory to FasL-induced killing due to their high surface expression of c-FLIP. Other immunosuppressive molecules expressed on tumour endothelium include B7-H3, a ligand for CTLA-4, and ET_BR. FasL, Fas Ligand; VEGF, Vascular Endothelial Growth Factor; PGE_2, Prostaglandin E_2; IL-10, Interleukin-10; c-FLIP, cellular FLICE (FADD-like IL-1 β-converting enzyme)-Like Inhibitory Protein; ET_BR, Endothelin B Receptor. Adapted from (Joyce & Fearon 2015).

Tumour vessels are characterized by sub-threshold expression of lymphocyte trafficking molecules (Fisher et al. 2011). Tumour vasculature is also incredibly refractory to endothelial activation induced by pro-inflammatory cytokines. Tumour Necrosis Factor (TNF)α potently induces expression of vascular adhesion molecules on peritumoural vessels during inflammation, aiding lymphocytic recruitment. Local administration of TNFα in mouse models results in only marginal improvements in leukocyte adhesion to tumour vessels, whilst nearby normal vasculature is fully responsive (Chen et al. 2003). Induction of biophysical stress responses by fever-range thermal therapy can increase tumour vascular perfusion and selective adhesion of CD8$^+$ CTLs at the expense of Tregs (Repasky et al. 2013). Collectively, the aforementioned studies illustrate an important requirement to modulate the tumour vasculature to drive anti-tumour T cell infiltration into the TME for efficient tumour clearance (Joyce & Fearon 2015).

1.5 Foxp3^{+} Regulatory T cells

1.5.1 Introducing Foxp3^{+} Regulatory T cells

CD4^{+} CD25^{+} Forkhead box protein 3 (Foxp3)[+] Regulatory T cells (Treg) represent a major immunosuppressive cell type within tumours, where they impinge on many of the anti-tumour immune responses discussed in detail above (Nishikawa & Sakaguchi 2010; Gallimore & Godkin 2008). Anti-tumour T cells are reactive to self-antigens aberrantly expressed by tumour cells, such as cancer testis antigens as described earlier (see Section 1.3.2). It was therefore reasoned that mechanisms responsible for maintaining immunological tolerance to self could also inhibit anti-tumour immune responses (Scanlan et al. 2004; Nishikawa & Sakaguchi 2010).

Two major processes underpin tolerance to self, which is essential for continued preservation of immune homeostasis. Central tolerance encompasses a process whereby T cells harbouring a high affinity self-antigen specific TCR undergo negative selection (clonal deletion) in the thymus, and are directed to programmed cell death by apoptosis. Peripheral tolerance is established by differentiation of Tregs (clonal deviation) in the thymus, which exert immunosuppression to maintain tolerance to self at peripheral sites throughout the lifetime of an animal (Klein et al. 2014).

According to the model of thymocyte selection, the developmental fate of T cells in the thymus is specified by the nature (i.e. strength) of the interaction between their TCR and cognate self-peptide-MHC complexes expressed by thymic APCs (Klein et al. 2014). Treg differentiation appears to occur within an intermediate window of TCR affinity for self-antigen that lies between the upper limit imposed by TCR interactions that drive negative selection and the lower limit demarked by TCR interactions driving positive selection (Jordan et al. 2001). Positive selection is the process by which CD4^{+} CD8^{+} double positive thymocytes that express low affinity TCRs specific for self-peptide-MHC complex differentiate into either mature CD4^{+} or CD8^{+} single positive thymocytes (Hsieh et al. 2012).

Tregs are indispensible for maintenance of immune homeostasis and promotion of peripheral immunological tolerance to self-antigens. Tregs prevent autoimmunity by

keeping in check the activation and expansion of over-reactive immune cells, therefore limiting excessive and harmful immune responses. Tregs largely control the responses of self-reactive T cells, which have escaped thymic deletion and entered the peripheral T cell pool. Developmental or functional defects in Tregs result in profound autoimmune and inflammatory disease pathology in both humans and animals, illustrating their physiological significance as a dominant, cell-extrinsic mechanism of self-tolerance (see Section 1.5.2) (Sakaguchi et al. 2008; Attridge & Walker 2014).

The vast majority of endogenous Tregs develop in the thymus as a functionally distinct, mature population of T cells, termed Thymus-derived Tregs or 'tTregs' (Sakaguchi 2005; Huehn & Beyer 2015). Tregs can also be generated *de novo* in the periphery by conversion of conventional naïve Foxp3$^-$ CD4$^+$ T cells into Foxp3$^+$ Tregs following antigen exposure, termed peripherally derived Tregs or 'pTregs'. pTregs are thought to make an essential contribution to the peripheral Treg TCR repertoire by supplying TCR specificities directed towards non-pathogenic foreign antigens, including those derived from food, commensal gut microbiota, and foetal proteins. Lastly, induced Tregs or 'iTregs' encompasses Tregs induced *in vitro* from naïve conventional CD4$^+$ T cells by TCR stimulation and IL-2 and Transforming Growth Factor (TGF)-β cytokine exposure (Huehn & Beyer 2015; Abbas et al. 2013).

Two early studies in which autoimmune disease developed following either neonatal thymectomy or adult thymectomy with sublethal X-irradiation made a significant contribution to the early appreciation of a Treg-mediated mechanism of self-tolerance (Nishizuka & Sakakura 1969; Penhale et al. 1973). In both cases, the autoimmunities were suspected to be a result of a loss of a suppressor T cell subset (Sakaguchi et al. 1982; Penhale et al. 1976). Evidence for the existence of an immunosuppressive CD4$^+$ T cell population also came from studies of spontaneous rodent models of autoimmunity: transfer of WT CD4$^+$ T cells to non-obese diabetic (NOD) mice or Bio-Breeding (BB) rats, which normally develop spontaneous Type 1 Diabetes mellitus (T1D), prevented disease onset. Transfer of diabetogenic T cells to

T-cell deficient hosts can also induce disease, but co-transfer of pathogenic T cells with normal CD4$^+$ T cells prevents disease (Greiner et al. 1987; Boitard et al. 1989).

Attempts were then made to define this immunosuppressive subset of cells by expression of a cell surface molecule. Co-transfer of CD5^{high} T cells inhibited autoimmunity induced by the transfer of CD5-depleted CD4$^+$ T cells alone (Sakaguchisaka 1985; Sugihara et al. 1988). Subsequent studies used CD45RB to differentiate between immunosuppressive CD4$^+$ T cells (CD45RB^{low}) and inflammatory CD4$^+$ T cells (CD45RB^{high}) (Powrie et al. 1993; Morrissey et al. 1993). The cell surface CD25 (IL-2 receptor α chain (IL-2Rα)) molecule was then identified as the first putative marker of suppressive T cells and the term 'regulatory T cell' was coined: CD25$^+$ T cells were contained in the CD5^{high} CD45RB^{low} CD4$^+$ population and constituted 5-10% of the peripheral CD4$^+$ T cell pool and <1% of peripheral CD8$^+$ T cells in both mice and humans. Critically, co-transfer of a small number of CD25$^+$CD4$^+$ T cells alongside CD4$^+$ T cells was sufficient to inhibit the development of autoimmunity that occurs in syngeneic athymic nude mice transferred with CD25-depleted CD4$^+$ T cell suspensions. Furthermore, depletion of CD25$^+$CD4$^+$ Tregs not only provoked autoimmunity but also augmented responses to non-self-antigens, including microbial and tumour antigens (Sakaguchi et al. 1995).

1.5.2 The discovery of Foxp3

Immune deregulation, polyendocrinopathy, enteropathy, X-linked (IPEX) syndrome was first described in 1982 as a fatal X-linked immunodeficiency syndrome in humans. X-linked Scurfy mutant mice, initially identified in the 1950s, but more extensively characterized in the 1990s, exhibit hyperactivation of CD4$^+$ T cells, extensive multi-organ immune infiltration and elevated proinflammatory cytokine secretion (Sakaguchi 2004). The defective gene in Scurfy mice was later identified and coined *Foxp3*, a member of the forkhead/winged-helix family of transcriptional regulators (Brunkow et al. 2001). Several independent studies confirmed that mutations in the human ortholog of the murine *Foxp3* gene were responsible for IPEX

syndrome (Chatila et al. 2000; Wildin et al. 2001; Bennett et al. 2001). *Foxp3* expression was predominantly restricted to CD4$^+$ CD25$^+$ Treg in the thymus and periphery, and was essential and sufficient for development of functional, suppressive Tregs (Hori et al. 2003; Fontenot et al. 2003; Khattri et al. 2003). Collectively these studies implicated *Foxp3* as a master regulatory gene in Treg cell-lineage commitment, differentiation and function (Sakaguchi 2004). Subsequent studies confirmed that *Foxp3* was also the Treg-lineage specific transcriptional master regulator in humans (Yagi et al. 2004; Roncador et al. 2005). In addition to its crucial role in Treg differentiation, sustained Foxp3 expression is also critical for maintenance of the Treg differentiation and functional program in mature T cells in adults (Lahl et al. 2007; Kim et al. 2007; Williams & Rudensky 2007; Zheng & Rudensky 2007).

Foxp3 is a multi domain transcription factor encoded by an X-chromosome encoded gene (Huehn & Beyer 2015). In Foxp3-deficient humans and mice, hemizygous males carrying the mutant *Foxp3* allele on their X chromosome are afflicted whereas heterozygous females harbouring the mutant *Foxp3* allele on one of their X chromosomes are healthy. The *Foxp3* mutation does not affect random X chromosome inactivation in T cells, and hence this process results in genetic mosaicism of defective and normal Treg cells. Therefore, Treg cells expressing WT *Foxp3* allele are competent in terms of keeping in check hyperactive T cells and mediating peripheral tolerance in a dominant manner (Zheng & Rudensky 2007).

1.5.3 Foxp3$^+$ Treg Characteristics

The central defining feature of Tregs is their immunosuppressive activity, mediated through a variety of mechanisms (see Section 1.5.4) (Shevach 2009; Josefowicz et al. 2012). The induction of immunosuppressive function by Tregs is antigen specific, and relies on TCR stimulation. However, the suppressive capacity of Tregs seems to be antigen non-specific *in vitro* (Thornton & Shevach 2000), while it is still unclear whether antigen-specific suppression is important *in vivo* (Corthay 2009). Of note, Foxp3 expression can be temporarily induced in activated T cells in mouse or

human where it is not associated with suppressor activity, demonstrating potential plasticity of Foxp3 expression in T cells (Miyao et al. 2012; Gavin et al. 2006; Miyara et al. 2009). Additional important characteristics of Tregs include absolute dependence on the cytokine interleukin 2 (IL-2; see Section 1.5.5), immunosuppressive cytokine production, and unique intracellular metabolic regulation (Xudong Li & Zheng 2015).

One of the cardinal features of Foxp3$^+$ Tregs is exhibition of anergy (a reversible antiproliferative state) *in vitro*: in contrast to other CD4$^+$ T cells, Tregs are unresponsive to agonistic TCR ligation in culture (Takahashi et al. 1998; Thornton & Shevach 1998; Read et al. 1998; Itoh et al. 1999; Kuniyasu et al. 2000). The development of transgenic Tregs with a known TCR specificity has greatly benefitted our understanding of physiological homeostasis and function of Tregs *in vivo* (Attridge & Walker 2014). Despite some contradictory results reporting an anergic state of Tregs following peptide-MHC complex presentation and costimulation *in vivo* (Gavin et al. 2002), tracking of TCR-transgenic Tregs in multiple independent studies demonstrated the rapid hyperproliferation displayed by Tregs during a response to cognate antigen *in vivo* (Walker et al. 2003; Klein et al. 2003). Human Tregs also demonstrated *in vitro* proliferative anergy, but Tregs from blood displayed significantly higher proliferation than conventional CD4$^+$ T cells, and the proliferative response of Tregs in secondary lymphoid organs was even higher than those in blood (Ng et al. 2001; Taams et al. 2001; Vukmanovic-Stejic et al. 2008; Peters et al. 2013). These studies highlighted that local antigenic environments shape population dynamics of Tregs *in vivo*. As for other T cells, Tregs are capable of homeostasis-driven proliferation, as demonstrated by rapid proliferation in response to lymphopenia when transferred to RAG-1$^{-/-}$ hosts (Gavin et al. 2002; Annacker et al. 2001). *In vitro* anergy in CD25$^+$ Tregs is closely linked to the inherent suppressive capacity of this cellular population: Treg suppression is simultaneously abrogated upon breaking of their anergic state by addition of high doses of IL-2 or an anti-CD28 monoclonal antibody (Takahashi et al. 1998).

1.5.4 Mechanisms of Treg-Mediated Suppression

A key challenge is understanding modes of Treg-mediated suppression, and their relevance for distinct disease states (Sakaguchi et al. 2008). Antigen stimulated murine and human Tregs suppress proliferation, cytokine production, and differentiation of naïve T cells *in vitro* in the presence of APC (Thornton & Shevach 1998; Takahashi et al. 1998; Read et al. 1998). Additionally, Tregs directly inhibit T cell proliferation in the absence of APCs (Ermann et al. 2001; Dieckmann et al. 2001). Tregs are also capable of functional suppression of differentiated CD4$^+$ and CD8$^+$ T, NK, NKT, and B cells, and DCs, macrophages and osteoclasts (Sakaguchi et al. 2008).

Four mechanisms of Treg-mediated suppression of Foxp3$^-$ CD4$^+$ conventional T cells have been described based on results of *in vitro* Treg suppression assays (Figure 1.4). These mechanisms act either directly on responder T cells, indirectly on responder T cells via direct action on APCs, or both (Schmidt et al. 2012; Vignali 2012). Other molecules expressed on the surface of Tregs, such as Galectin-1 and Neuropilin-1 (Nrp-1), might also contribute to immunosuppression (Shevach 2009).
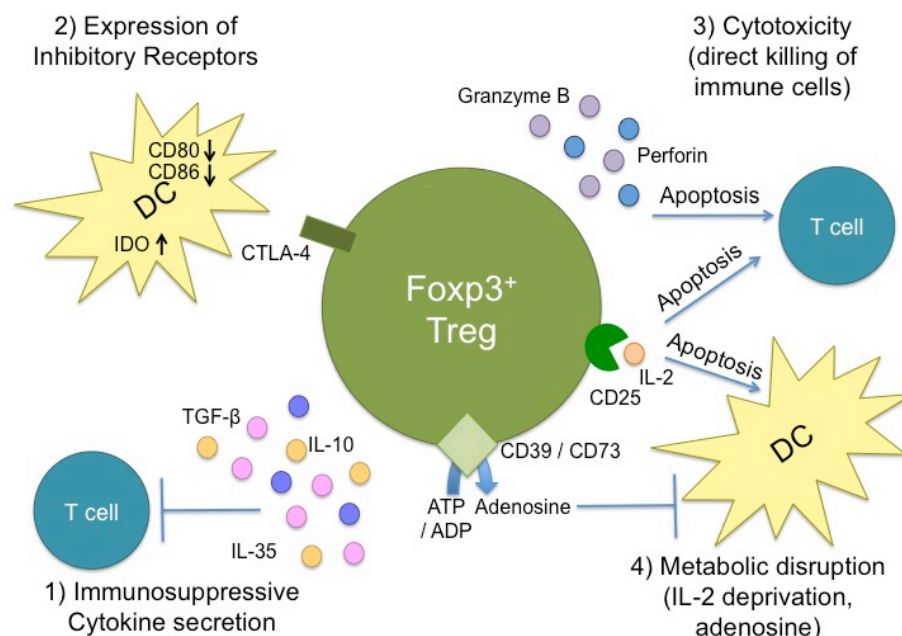
Figure 1.4 | Mechanisms of Treg-Mediated Suppression.
Mechanisms include 1) secretion of immunosuppressive cytokines IL-35, TGF β and IL-10, 2) expression of inhibitory receptors such as CTLA-4, which down-regulates CD80 and CD86, and up-regulates IDO on DCs, 3) direct killing via Granzyme B and perforin, and 4) metabolic disruption, including CD39/ CD73 mediated conversion of ATP or ADP to Adenosine, or 'scavenging' of IL-2.
Adapted from (Sakaguchi et al. 2009; Schmidt et al. 2012; Vignali 2012; Shevach 2009).

1.5.4.1 Synthesis of Inhibitory Cytokines

One recently discovered cytokine implicated in Treg-mediated suppression is IL-35. IL-35 is formed of the proteins encoded by the Epstein-Barr Virus-induced gene 3 (*Ebi3*) and *Il12a*, both of which are significantly up-regulated in actively suppressing murine Tregs. Tregs from *Ebi3*^{-/-} or *Il12a*^{-/-} mice are severely functionally compromised *in vitro*, and *Ebi3*^{-/-} and *Il12a*^{-/-} animals are unable to regulate excessive immune responses in an *in vivo* Inflammatory Bowel Disease (IBD) model (Collison et al. 2007).

TGF-β is required for conversion of non-Tregs into pTregs, generation of iTregs and Treg homeostasis (Chen et al. 2003; Liu et al. 2008; Marie et al. 2005). However, whether TGF-β mediates Treg suppression remains controversial: use of anti-TGF-β antibodies *in vitro* has produced contrasting results (Nakamura et al. 2001; Piccirillo et al. 2002; Shevach 2009). Some studies have shown that while TGF-β deficient Tregs are capable of conventional T cell suppression *in vitro*, Treg-expressed TGF-β is necessary for control of colitis *in vivo* (Read et al. 2000; Izcue et al. 2009). In contrast, other studies have shown that TGF-β deficient Tregs are competent at controlling diseases such as IBD *in vivo* (Mamura et al. 2004; Fahlén et al. 2005).

The anti-inflammatory cytokine IL-10 seems to play a crucial role in Treg-mediated suppression (Belkaid 2007; McGeachy et al. 2005). Despite the failure of *in vitro* suppression assays to identify a suppressive function of Treg-generated IL-10, IL-10 secretion by Tregs *in vivo* seems to be important for control of gut inflammation, infection and Experimental Autoimmune Encephalomyelitis (EAE) but dispensable for regulation of other autoimmunities and control of allergic responses (Schmidt et al. 2012). A recent study has revealed that Treg-derived IL-10, but not IL-35 or TGF-β, is required to regulate effector T cell derived IFN-γ in the skin (Sojka & Fowell 2011; Schmidt et al. 2012).

1.5.4.2 Expression of Inhibitory Receptors

One mechanism of direct APC inhibition involves expression of the coinhibitory molecule CTLA-4, which is constitutively expressed by both murine and human Tregs

(Read et al. 2000; Takahashi et al. 2000; Dieckmann et al. 2001). Addition of Tregs can ameliorate the spontaneous autoimmunity induced by genetic deficiency of CTLA-4 or CTLA-4 blockade (Bachmann et al. 1999; Takahashi et al. 2000). Furthermore, anti-CTLA-4 abrogates the immunosuppressive effects of Tregs *in vivo*, thereby exacerbating murine colitis (Read et al. 2000). Selective CTLA-4 deficiency in Tregs is sufficient to induce fatal systemic autoimmunity, underpinning the significance of Treg-specific CTLA-4 expression in maintenance of immune tolerance (Wing et al. 2008). However, some studies have shown that murine CTLA-4-deficient Tregs are still capable of suppression *in vivo* and *in vitro*, reportedly via mechanisms involving TGF-β and / or IL-10 (Tang et al. 2004; Read et al. 2006). Similar contradictory results have been obtained for human Tregs (Schmidt et al. 2012).

Treg-expressed CTLA-4 down-regulates co-stimulatory molecules CD80 and CD86 on the surface of DCs or other APCs (Wing et al. 2008; Cederbom et al. 2000; Misra et al. 2004; Serra et al. 2003). Furthermore, CTLA-4 ligation with CD80 or CD86 can result in up-regulation of indoleamine 2,3-dioxygenase (IDO), a potent regulatory enzyme that generates proapoptotic metabolites, ultimately leading to starvation and induction of cell cycle arrest in effector T cells (Fallarino et al. 2003; Onodera et al. 2009; Grohmann et al. 2002). Lastly, CTLA-4 is capable of removing CD80 and CD86 ligands from the surface of APCs by trans-endocytosis, thereby impairing future costimulation to the APC (Qureshi et al. 2011). Binding of another Treg-expressed inhibitory receptor LAG3 (CD223) to DC-expressed MHC-Class II molecules suppresses maturation and co-stimulatory ability of DCs (Liang et al. 2008). Together, these downstream affects of inhibitory receptor expression by Tregs result in a heightened threshold for T cell activation by DCs, ultimately prohibiting autoreactive T cell activation (Schmidt et al. 2012).

1.5.4.3 Direct Killing of Immune Cells (Cytotoxicity)

Tregs are capable of direct cytolysis of target responder cells (Shevach 2009). Perforin is a pore-forming toxin and Granzymes are proapoptotic serine proteases;

together, these two molecules form the perforin/granzyme cell death pathway, which is the principal cytotoxic mechanism executed by NK lymphocytes and CTLs against intracellular pathogens and transformed cells (Hoves et al. 2010). Human Foxp3^{+} Tregs express Granzyme B upon activation and directly kill activated CD4^{+} and CD8^{+} T cells, as well as other immune cells including APCs, in a manner dependent on Perforin but independent of Fas-FasL interactions (Grossman et al. 2004). Murine Foxp3^{+} Tregs also up-regulate Granzyme B once activated (Shevach 2009), and have been shown to exhibit granzyme B-dependent killing of responder cells in a perforin-independent manner (Gondek et al. 2005). Another report described an inability of Granzyme B-expressing Tregs to kill responder cells, despite killing of antigen-presenting B cells (Zhao et al. 2006).

Up to 30% of Tregs in tumour microenvironments produce Granzyme B and can induce lysis of NK and CTLs in a manner dependent on both Granzyme B and perforin (Cao et al. 2007). Furthermore, using two-photon live microscopy, Boissonnas and colleagues have observed direct perforin-dependent killing of DCs by Tregs in tumour-draining lymph nodes *in vivo* (Boissonnas et al. 2010). Additionally, Granzyme B-mediated Treg suppression seems to be required for maintenance of tolerance following transplant (Gondek et al. 2008).

1.5.4.4 Metabolic Disruption of Immune Cells

Extracellular Adenosine Triphosphate (ATP) is an indicator of cell damage and trauma in the immune system, and is sensed by DCs (Shevach 2009). CD39 is an ectoenzyme constitutively expressed on the surface of murine Tregs and approximately 50% of human Tregs that converts ATP or Adenosine diphosphate (ADP) to Adenosine monophosphate (AMP) (Borsellino et al. 2007; Shevach 2009). A proportion of Tregs co-express another ectoenzyme CD73 which further degrades AMP to Adenosine, a nucleoside with direct immunosuppressive effects on T cells and DCs (Schmidt et al. 2012). Deaglio and colleagues demonstrated that pericellular adenosine could inhibit the function of effector T cells (Deaglio et al. 2007). Therefore,

inactivation of ATP danger signals and generation of adenosine could represent important immunosuppressive mechanisms of Tregs. Deprivation of the cytokine IL-2 represents another potential Treg-mediated mechanism of suppression, as discussed in detail in the following section (Schmidt et al. 2012; Shevach 2009).

1.5.5 The Role of IL-2 in Treg Homeostasis and Suppression

Interleukin-2 (IL-2) is required for expansion of T_H1 and CD8^{+} CTLs. However, IL-2 is also necessary for survival and expansion of Tregs, and therefore plays a crucial role in both promotion of immunity and maintenance of immune tolerance (Boyman & Sprent 2012; Sakaguchi et al. 2008). The critical reliance upon IL-2 for Treg differentiation, survival and suppressor function is illustrated by animals deficient in IL-2 or components of the IL-2 receptor, which are devoid of peripheral Tregs and demonstrate severe autoimmunity. Furthermore, transfer of CD25^{+} CD4^{+} Tregs to mice harbouring these genetic deficiencies prevents the onset of disease (Sakaguchi 2004; Malek 2008; Gasteiger & Kastenmuller 2012). Neutralization of IL-2 by administration of monoclonal antibodies also reduces Treg numbers and concurrently induces autoimmune disease reminiscent of that elicited by Treg depletion (Setoguchi et al. 2005; Murakami et al. 2002). Furthermore, IL-2 is necessary for maintained Foxp3 and CD25 expression and suppression activity by Tregs *in vitro* (Fontenot et al. 2005; Shevach et al. 2006; Thornton et al. 2004).

IL-2 stimulates signalling via either the high affinity trimeric IL-2 receptor (IL-2R) or the weak affinity dimeric IL-2R. The dimeric IL-2R consists of CD122 (IL-2Rβ) and the common cytokine receptor γ chain ($γ_c$; CD132), and must be expressed at high levels for IL-2 responsiveness. The trimeric IL-2R has in addition CD25 (IL-2Rα), which increases the affinity for IL-2 by 10-100 fold (Boyman & Sprent 2012).

Dimeric receptor expression is low on naïve CD8^{+} and memory CD4^{+} T cells, and high on memory CD8^{+} T and NK cells. Following TCR stimulation, CD4^{+} and CD8^{+} T cells transiently up-regulate the trimeric IL-2R. Tregs constitutively express CD25 at high levels, presumably endowing them with a superior ability to exploit the IL-2

resource provided by other T cells. In addition to TCR stimulation, exposure to IL-2 also results in up-regulation of CD25 expression on T cells (Boyman & Sprent 2012; Malek 2008).

Under steady state conditions, IL-2 is secreted primarily by Foxp3$^-$ CD4$^+$ T$_H$ cells within secondary lymphoid organs and other activated Foxp3$^-$ CD4$^+$ T cells. IL-2 can also be synthesized by CD8$^+$ T cells, NK cells, NKT cells and, under certain conditions, activated DCs and mast cells (Malek 2008; Boyman & Sprent 2012). Tregs cannot synthesize significant amounts of IL-2, due to Foxp3-dependent repression of *il2* transcription (Boyman & Sprent 2012; Wu et al. 2006; Ono et al. 2007).

Under homeostatic conditions equilibrium is reached between Tregs and Tconvs where Foxp3$^+$ Tregs make up 10-15% of the peripheral CD4$^+$ T cell pool in normal animals (Sakaguchi et al. 2008). The frequency of peripheral Tregs is regulated by the number of IL-2 producing T cells (Almeida et al. 2006). Conversely, limitation of IL-2 production by other cells and/or sequestration of IL-2 are potential Treg-mediated immunosuppressive mechanisms (Figure 1.4) (Shevach 2009; Schmidt et al. 2012).

In vitro, Tregs are capable of inducing transcriptional repression of *il2* in Foxp3$^-$ CD4$^+$ T cells (Takahashi et al. 1998; Thornton & Shevach 1998; Oberle et al. 2007; Barthlott et al. 2005). Instead, Pandiyan and colleagues proposed a model whereby Tregs compete with conventional CD4$^+$ T cells for IL-2 protein in the microenvironment and scavenge it, causing IL-2 deprivation-mediated apoptosis of responder T cells (Pandiyan et al. 2007). However, human Tregs can actively suppress proliferation of mouse responder T cells when IL-2 is prohibited from binding to Treg-expressed CD25 (Tran et al. 2009). Furthermore, extensive *in vitro* and *in vivo* studies conducted by Szymczak-Workman and colleagues demonstrated the ability of Tregs to suppress transgenic conventional T cells that were resistant to cytokine-withdrawal mediated apoptosis, in complete contrast to the results of Pandiyan and colleagues (Szymczak-Workman et al. 2011). Such contradictory results have meant that the importance of competitive consumption of IL-2 by Tregs as a mechanism of suppression has remained controversial (Schmidt et al. 2012; Shevach 2009).

1.5.6 Specialization of Regulatory T cells

Naïve CD4$^+$ T lymphocytes differentiate into functionally distinct effector T_H cell, T follicular helper (Tfh) cell, or Treg subsets depending on the nature of the antigen signal they receive and cytokines secreted by APCs (Figure 1.5). A unique cytokine profile and effector, or immunosuppressive function, defines each lineage. Lineage specification depends on intrinsic and extrinsic factors, which determine the genetic program. Lineage-specific transcription factors are crucial (Tripathi & Lahesmaa 2014).

Typically, intracellular pathogens induce T_H1 immune responses. T_H1 cells produce signature cytokines IFNγ, IL-2, TNFα and Lymphotoxin (LT). The cytokine IL-12 initiates T_H1 differentiation and T-bet is the master transcription factor that regulates the T_H1 distinct program of gene expression (Szabo et al. 2000; Szabo et al. 2003).

T_H2 cells are typically involved in responses against parasitic helminths and nematodes, and produce cytokines IL-4, IL-5, IL-6 and IL-13 (Zhu & Paul 2010). GATA-3 is the transcriptional regulator necessary and sufficient for T_H2 differentiation (Zheng & Flavell 1997). IL-4 is the initiator for T_H2 differentiation (Ansel et al. 2006).

Yeasts, fungi and extracellular bacteria induce T_H17 responses, involving production of IL-17, IL-22 and IL-23 (Zhu & Paul 2010). RORγt is the master transcription factor in T_H17 differentiation, but others are also involved (Ivanov et al. 2006). IL-6, IL-23 and TGFβ can initiate T_H17 differentiation (Chen et al. 2007).

More recently identified sub-types of CD4$^+$ T cell include T_H9 and T_H22 cells and Tfh cells. T_H9 differentiation *in vitro* is initiated by TCR activation with IL-4 and TGFβ, which stimulate expression of IRF4 and Purine-rich box 1 (PU.1) transcription factors, respectively (Tripathi & Lahesmaa 2014). A recent study clarified a role for the IRF1 transcription factor, induced in T_H9 cells by IL-1β, in enhancement of T_H9 function (Végran et al. 2014). Transcriptional control of the T_H22 lineage requires IL-6 and TNF, and the Aryl hydrocarbon receptor (AhR). Tfh differentiation is stimulated by IL-6 and IL-21, which induce expression of the transcription factor Bcl6 which is necessary and sufficient for Tfh lineage commitment (Tripathi & Lahesmaa 2014). Tfh cells are

essential for generation of T-cell dependent B cell responses in germinal centres (Crotty 2014).
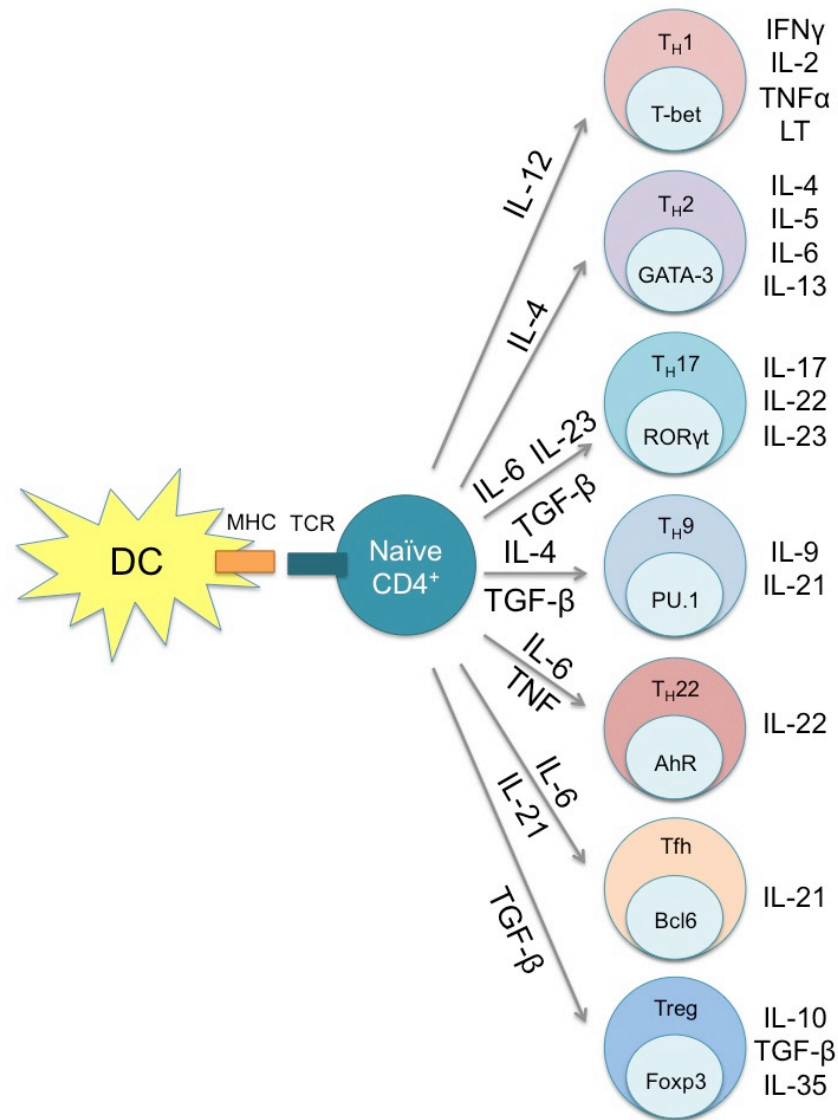
Figure 1.5 | Differentiation of Naïve CD4$^+$ T cells.
Upon TCR-peptide-MHC-complex ligation with a DC, naïve CD4$^+$ T cells differentiate into one of a number of different T helper cell (T$_H$) subtypes. Alternatively, naïve CD4$^+$ cells can differentiate into T follicular helper (Tfh) cells, or Foxp3$^+$ regulatory T cells (Tregs). Different cytokines are influential in this process of lineage commitment, and each T$_H$ cell subset is defined by the expression of a lineage specific transcription factor (shown in the cell nucleus). Each distinct cell lineage is defined by the production of a set repertoire of effector or immunosuppressive cytokines, shown on the far right. Adapted from (Tripathi & Lahesmaa 2014).

Recently, studies have highlighted expression of canonical T$_H$-cell lineage transcription factors by Tregs, and thus 'mirroring' of the T$_H$ polarized immune response by the Treg population (Campbell & Koch 2011; Linterman et al. 2011). T-bet is expressed by a subset of Treg cells in response to IFNγ, and T-bet$^+$ Tregs accumulate at sites of T$_H$1-type immune responses. Furthermore, T-bet expression

was found to be required for Treg-mediated control of T_H1-orientated inflammatory responses (Koch et al. 2009). In a different study, a proportion of Tregs were shown to express IRF4, a transcription factor important for T_H2 differentiation. IRF4^{+} Tregs were required for suppression of T_H2-directed inflammatory responses, as ablation of IRF4 specifically in Foxp3^{+} T cells resulted in deregulated T_H2 responses (Zheng et al. 2009). Treg-expression of the T_H17 associated transcription factor STAT3 has also been reported, and control of T_H17-driven intestinal inflammation was dependent on STAT3 expression by Tregs (Chaudhry et al. 2009). Lastly, Linterman and colleagues demonstrated differentiation of Tfh cell repressor Tregs, via expression of the Tfh-specific Bcl6 transcription factor. These follicular Tregs were required for control of Tfh cell number and germinal centre responses *in vivo* (Linterman et al. 2011). Hence, Tregs may co-opt components of the canonical T_H-associated transcriptional machinery to effectively hamper a corresponding type of immune response (Campbell & Koch 2011).

1.6 Regulatory T cells in Cancer

1.6.1 The Role of Regulatory T cells in Anti-Tumour Immunity

Seminal studies in the 1970s and 1980s began establishing a critical role for 'suppressor' T cells in the anti-tumour immune response, although the identity of the cellular subset was yet to be determined (Zou 2006). In a series of pioneering studies, Robert North and colleagues demonstrated that despite induction of an effective anti-tumour T cell response to Meth A tumours (a tumour cell line model in which the cells are derived from MCA-induced fibrosarcomas), the immune response was unable to completely prohibit tumour growth due to suppressor T cell activity induced by the tumour. Indeed, concomitant immunity, defined as rejection of a second inoculum of an identical tumour cell line in a host already bearing tumour, decreased over time, simultaneous with the establishment of suppressor T cell function (North & Bursuker 1984; Gallimore & Godkin 2008). The suppressor T cell subset in question was later revealed as CD4^{+} CD8^{-} T cells, and specific depletion of CD4^{+} T cells using monoclonal antibodies resulted in efficient tumour rejection (Awwad & North 1988).

These early studies illustrated the ability of naturally occurring Tregs to dampen effective anti-tumour immune responses (Gallimore & Godkin 2008). With the identification of CD25 as a specific Treg marker in 1995 (see Section 1.5.1) (Sakaguchi et al. 1995), use of depleting anti-CD25 monoclonal antibodies was shown to induce effective anti-tumour CD8^{+} T cell responses, and confer control of tumour growth in a number of different tumour cell line models (Onizuka et al. 1999; Shimizu et al. 1999). Other groups corroborated these findings and demonstrated that tumour rejection and long-term CD4^{+} and/or CD8^{+} T cell mediated immunity against tumour cells could be established in mice depleted of CD25^{+} Tregs (Sutmuller et al. 2001; Jones et al. 2002). Similar studies reported that depletion of CD25^{+} Tregs also resulted in effective concomitant immunity (Turk et al. 2004). Furthermore, adoptive transfer of CD25^{+} Tregs into tumour bearing hosts provided a direct functional link between Treg presence and abrogation of anti-tumour immunity (Turk et al. 2004; Antony et al. 2005).

However, most early studies only demonstrated efficacy of CD25^{+} T cell depletion if conducted in a prophylactic setting prior to tumour cell inoculation: efficacy was lost when antibodies were administered simultaneously with tumour cell inoculation or after inoculation, likely as a result of depletion of CD25^{hi} anti-tumour effector T cells as well as Tregs (Onizuka et al. 1999; Shimizu et al. 1999; Sutmuller et al. 2001; Jones et al. 2002; Li et al. 2003; Teng et al. 2010; Ko et al. 2005; Quezada et al. 2008; Tanaka et al. 2002). However, efficient rejection of established tumours could sometimes be initiated, for instance by intra-tumoural injection of anti-CD25 antibodies (Yu et al. 2005).

These early studies were almost entirely conducted using tumour cell line models. These models preclude study of the effect of CD25^{+} Tregs on rejection of tumours that have developed *in vivo* in the context of mechanisms of Cancer Immunoediting (Gallimore & Godkin 2008). Analyses of tumours induced by injection of MCA revealed a reduction in the rate and frequency of tumour development in animals devoid of CD25^{+} T cells relative to WT counterparts, even if CD25^{+} T cell depletion is only transient in nature (Tawara et al. 2002; Betts et al. 2007).

Following the identification of Foxp3 as a Treg-specific marker, several independent studies demonstrated the prevention of tumour development or regression of established tumour, following efficient and selective depletion of Foxp3^{+} Tregs (Klages et al. 2010; Li et al. 2010; Teng et al. 2010; Hindley et al. 2012). These studies made use of transgenic mouse lines in which Foxp3-expressing cells express the primate diphtheria toxin receptor (DTR): selective depletion of Foxp3^{+} Tregs is achieved in these models by diphtheria toxin (DT) administration (Lahl et al. 2007; Kim et al. 2007). Such studies underpin the idea that Tregs play a central role in the generation of immunity against developing tumours *in vivo.*

The tightly controlled homeostatic ratio of Tconv to Treg under normal conditions is significantly perturbed in patients with cancer and mouse models (Quezada et al. 2011). Many murine tumour models exhibit a preferential accumulation of Tregs within the tumour mass (Betts et al. 2007; Hindley et al. 2011). Furthermore, a plethora of studies have demonstrated selective enrichment of Tregs in peripheral blood or TME of patients with a range of malignancies, including liver, lung, pancreatic, breast, gastrointestinal tumours and melanomas, relative to peripheral blood or healthy tissue in healthy controls (Nishikawa & Sakaguchi 2010; Whiteside 2012; Wilke et al. 2010; Quezada et al. 2011; Scurr et al. 2012). Importantly, some of these studies illustrated the correlation between high numbers of tumour-infiltrating Tregs and a poor clinical outcome (Curiel et al. 2004; Sato et al. 2005; Bates et al. 2006; Perrone et al. 2008). Strikingly, several of these studies demonstrated that an elevated CD8^{+} CTL to Foxp3^{+} Treg ratio was significantly associated with an improved clinical prognosis (Gao et al. 2007; Sinicrope et al. 2009; Sato et al. 2005). This correlation between effector T cell to Treg ratio and outcome is also observed in mouse models: CTLA-4 blockade together with GVAX vaccine therapy in the B16 melanoma model resulted in a significantly altered ratio of effector T cells to Tregs, in favour of effectors, which correlated with tumour rejection (Quezada et al. 2006). Collectively, such studies establish the importance of the balance between effector anti-tumour T cells and immunosuppressive Tregs in dictating disease outcome. Hence, therapies aimed at

altering this balance, to steer the response in the direction of an effector response at the expense of regulation, could be beneficial in the future (Quezada et al. 2011).

Crucially, it is becoming evident that the type of cancer dictates whether a high infiltration of Foxp3^{+} Tregs determines a good or bad clinical outcome (Whiteside 2012). For certain types of cancer, inflammation is considered a major driving force in progression to malignancy (Ruffell et al. 2010). This raises the possibility that Tregs could exert some anti-tumourigenic effect via their demonstrable ability to suppress cancer-promoting inflammation (Erdman et al. 2005; Grivennikov et al. 2010).

Paradoxically, presence of Tregs in Hodgkin's lymphoma correlates with improved prognosis (Alvaro et al. 2005). Many studies reported that density of tumour infiltrating Tregs correlates with improved prognosis and survival for CRC patients (Scurr et al. 2012). However, tumour antigen-specific Tregs are capable of suppressing beneficial anti-tumour T cell responses in CRC (Bonertz et al. 2009). Furthermore, suppression of tumour antigen specific T cells by Tregs prior to tumour resection positively correlates with recurrence 1 year later (Betts et al. 2012). Confirmation of the prognostic value of Tregs in different types of cancer is crucial for development of strategies targeting them (Scurr et al. 2012; Whiteside 2012).

1.6.2 Mechanisms of Treg Enrichment in Tumours

Several mechanisms of intra-tumoural Treg enrichment have been suggested (Figure 1.6) (Ondondo et al. 2013). Both tTregs and pTregs can suppress anti-tumour immune responses in mice (Zhou & Levitsky 2007). However, the relative contribution of pTregs and tTregs to anti-tumour immunity remains a contentious issue (Tanchot et al. 2013). Adoptively transferred CD4^{+} CD25^{-} T cells convert into Foxp3^{+} CD25^{+} CD4^{+} Tregs *in vivo* (Valzasina et al. 2006; Schreiber et al. 2012; Weiss et al. 2012). Some studies have shown that the high levels of TGF-β made by tumour cells and/or DCs within tumours enable conversion of conventional CD4^{+} T cells into Tregs *in situ* (Ghiringhelli et al. 2005; Liu et al. 2007). However, many of these studies utilized adoptive transfer systems, which do not robustly reflect mechanisms underpinning Treg enrichment in tumours *in vivo*.
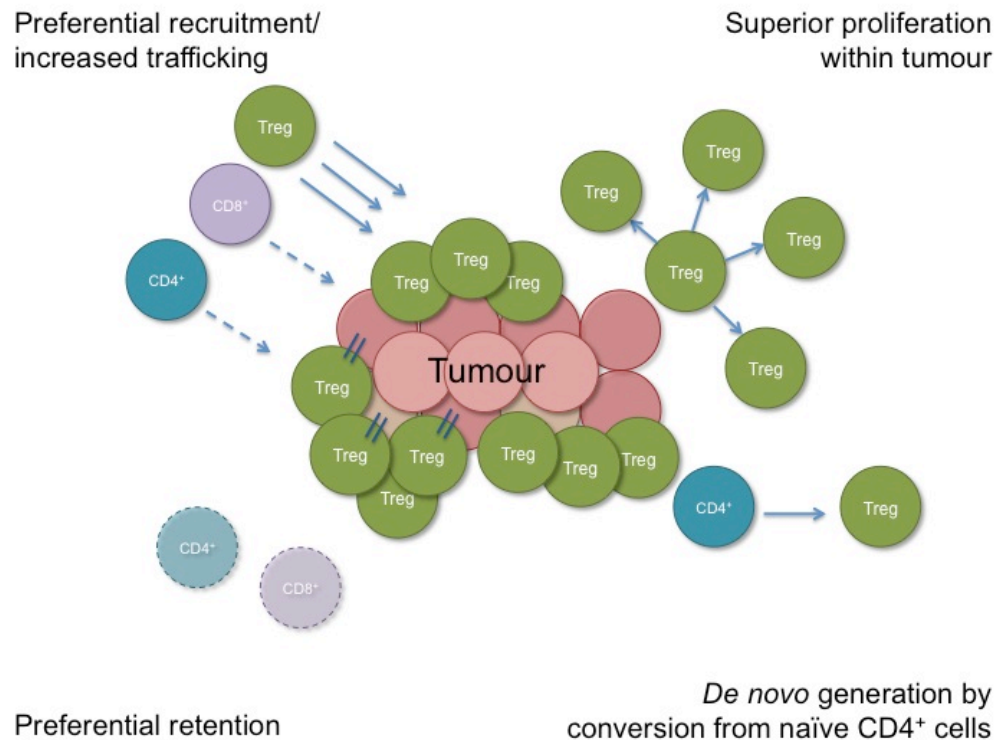
Figure 1.6 | Mechanisms of Foxp3$^+$ Treg Enrichment in Tumours.
Mechanisms include preferential recruitment or trafficking over other populations of T cells, and/ or superior proliferation once within the tumour microenvironment, possibly by exploitation of a limited resource. *De novo* generation of Tregs, by conversion from naïve CD4$^+$ conventional T cells has also been suggested. Lastly, preferential retention of Tregs by unknown mechanisms could contribute to dominance of Tregs in the tumour.
Adapted from (Ondondo et al. 2013).

The debate has been fuelled by the lack of a specific marker for pTregs or tTregs (Ondondo et al. 2013). Helios, an Ikaros transcription factor, has been identified as a specific marker of tTregs in both mouse and human (Thornton et al. 2010). Nrp-1, a type 1 transmembrane protein, is also a purported tTreg specific marker (Bruder et al. 2004). A large number of studies support the hypothesis that the majority of Tregs enriched in mouse or human tumours are Helios and / or Nrp-1 expressing tTregs (Curiel et al. 2004; Ghiringhelli et al. 2005; Wainwright et al. 2011; Bui et al. 2006; Hansen et al. 2012; Teng et al. 2010; Weiss et al. 2012; Elkord et al. 2011). Work from our own lab has demonstrated that Tregs enriched in MCA-induced fibrosarcomas are tTregs: intra-tumoural Tregs demonstrated an entirely distinct TCR repertoire relative to tumour-derived naïve conventional T cells (Hindley et al. 2011). Our more recently published work corroborated these data in demonstrating expression of Helios by the vast majority of intra-tumoural Tregs in MCA tumours (Colbeck et al. 2015).

Collectively, definitive evidence supporting a role for conversion of non-Treg cells into suppressive Tregs in tumours is lacking.

Preferential recruitment by a selective chemokine axis is another possible mechanism of Treg enrichment in tumours. Chemokine axes responsible for recruitment of Tregs include inflammatory chemokine ligand receptor pairs C-C motif chemokine receptor (CCR)5- C-C motif chemokine ligand (CCL)5, CCR4-CCL17/CCL22, and C-X-C motif chemokine receptor (CXCR)3- C-X-C motif chemokine ligand (CXCL)9/10/11. However, data support a critical role for CCR5 and CXCR3 axes in recruitment of effector anti-tumour T cells, as well as Tregs, to tumours. Furthermore, expression of IFN-γ-induced chemokine ligands for CCR5 and CXCR3 by tumour cells is associated with a favourable prognosis in multiple human cancers (Ondondo et al. 2013). In support of these data, our recently published study demonstrated that Foxp3$^+$ Tregs and Foxp3$^-$ T cells utilize multiple and overlapping chemokine axes to access MCA-induced tumours, and selective recruitment of Tregs cannot be accounted for by a distinct chemokine axis (Ondondo et al. 2014[a]).

CCR4 signalling seems to be influential in mediating Treg accumulation in multiple human cancers (Ondondo et al. 2013). Anti-CCR4 monoclonal antibody treatment selectively depletes Tregs, unleashing an anti-tumour immune response in melanoma patient derived peripheral blood mononuclear cells (PBMC) *ex vivo* (Sugiyama et al. 2013). The hypoxic conditions within tumours can also induce up-regulation of hypoxic chemokines CCL28 and CXCL12, which bind CCR10 and CXCR4, respectively. These chemokines have been shown to contribute to accumulation of Tregs expressing cognate receptors in human and mouse tumours (Ondondo et al. 2013). In particular, the CXCR4-CXCL12 axis seems to direct preferential migration of Tregs (Wald et al. 2006; Jaafar et al. 2009).

The CCR7-CCL21 axis, classically associated with lymphocyte migration in secondary lymphoid organs, is implicated in Treg enrichment in B16 tumours (Shields et al. 2010; Förster et al. 2008). However, a body of evidence supports a crucial role for this chemokine axis in facilitating entry of effector anti-tumour immune cells and

subsequent tumour control in mouse and human tumours. Hence, while targeting CCR5 / CXCR3 / CCR7 axes will unlikely result in the desired outcome, targeting CCR4 / CXCR4 axes could selectively deplete Tregs from tumours without hindering infiltration of beneficial anti-tumour T cells (Ondondo et al. 2013).

Studies have highlighted a superior proliferative ability of Foxp3$^+$ Tregs relative to other T cells (Attridge & Walker 2014). Bui and colleagues noted preferential proliferation of Tregs within carcinogen-induced tumours, relative to Tregs in tumour draining lymph nodes and CD25$^-$ CD4$^+$ T cells within the tumour (Bui et al. 2006). Moreover, Helios$^+$ Foxp3$^+$ tTregs within tumours of a mouse model of glioblastoma were significantly more proliferative than Helios$^-$ and / or Foxp3$^-$ counterparts (Wainwright et al. 2011). Tumour derived TGF-β and / or VEGF-A could be responsible for driving superior Treg proliferation (Ghiringhelli et al. 2005; Terme et al. 2013). These studies highlight superior proliferation as a major mechanism contributing to expansion of Tregs within tumours (Ondondo et al. 2013; Attridge & Walker 2014).

1.6.3 Methods for Manipulating Tregs in Cancer Immunotherapy

The significant enrichment of Tregs in tumours represents a major obstacle tempering successful immunotherapy. All *in vitro* and *in vivo* data to date support a model whereby Tregs exert their suppressive effects in a dose-dependent manner (Quezada et al. 2011). Hence, depletion of Tregs has been investigated as a potential method to encourage tumour regression either alone or in combination with vaccination programs. Preclinical studies have underpinned the efficacy of such an approach to augment powerful anti-tumour immune responses (see Section 1.6.1).

Cyclophosphamide (CTX; *N,N*-bis (2-chloroethyl)-1,3,2-oxazaphosphinan-2 amine 2-oxide) is a nitrogen mustard alkylating agent. High doses of CTX are used as a chemotherapy for human tumours as this compound displays direct selective cytotoxicity for tumour cells (Sistigu et al. 2011). However, the activity of CTX is dose dependent: low doses induce effective anti-tumour immune responses in mouse and human. This affect is at least partly due to modulation of the Treg compartment by low-

dose CTX, including a reduction in suppressive capacity of Tregs, and apoptosis induction (Le & Jaffee 2012). In a phase II clinical trial, low dose CTX reduced Treg numbers and boosted anti-tumour immune responses induced by vaccination, increasing overall survival in renal cell carcinoma patients (Walter et al. 2012).

As the balance between effector T cells and Tregs is crucial in dictating an effective anti-tumour immune response, attempts are now being made to tip the balance away from suppressive Tregs, in favour of effector T cells (Quezada et al. 2006; Quezada et al. 2011). To this end, costimulatory therapies, including anti-CTLA-4 and anti-PD-1 therapies, are proving successful in simultaneously increasing intra-tumoural numbers of CD8^{+} CTL and reducing intra-tumoural accumulation of Tregs, in both mice (Quezada et al. 2006; Curran et al. 2010; Curran & Allison 2009) and human cancer patients (Chen et al. 2009; Liakou et al. 2008). A better understanding of mechanisms leading to Treg enrichment in tumours and how immunotherapies lead to increased effector T cell to Treg ratios will aid modification of future immunotherapy regimes to maximize beneficial clinical outcome (Quezada et al. 2011).

1.6.4 The link between Regulatory T cells and Tumour Angiogenesis

Despite the induction of powerful anti-tumour immune responses following depletion of Tregs, infiltration of activated T cells into tumours represents a significant bottleneck to effective tumour control (Hindley et al. 2012; Quezada et al. 2008). There is an emerging link between tumour angiogenesis and establishment of peripheral immune tolerance in the TME (Joyce & Fearon 2015; Motz & Coukos 2011). Tumour vasculature impairs infiltration of effector T cells, while enabling entry of immunosuppressive Tregs and MDSCs (Huang et al. 2013; Ganss et al. 2002; Ryschich et al. 2002; Buckanovich et al. 2008; Facciabene et al. 2011; Gabrilovich et al. 2012; Carretero et al. 2015). Furthermore, anti-VEGF-A prevents infiltration of Tregs, enhancing immune responses initiated by vaccination (Li et al. 2006).

Interestingly, in what appears to be a reciprocal relationship, immunosuppressive cells in tumours promote angiogenesis (Motz & Coukos 2011).

Tregs, recruited to the tumour by hypoxic chemokine CCL28 expression, contribute to the VEGF-A rich microenvironment, and depletion of Tregs decreases available VEGF-A and inhibits tumour angiogenesis (Facciabene et al. 2011). Hence, Tregs promote disease progression via pro-angiogenic reprogramming of the TME, in addition to canonical anti-tumour immunity subversion (Facciabene et al. 2012). In line with these data, depletion of Tregs results in normalization of tumour vasculature, which promotes effector T cell infiltration (Li et al. 2010; Hamzah et al. 2008). Hence, tumour immune tolerance and angiogenesis work in concert to promote tumour outgrowth.

Tumour angiogenesis is generally associated with disease progression (Martinet & Girard 2013; Joyce & Fearon 2015). However, development of specialised tumour-associated blood vessels, termed High Endothelial Venules (HEV), has recently been associated with a good prognosis for multiple cancers in several reports (Ager & May 2015; Goc et al. 2013). Furthermore, our lab have discovered tumour-associated HEV in MCA-induced tumours in the absence of Tregs, underpinning the link between tumour angiogenesis and immunosuppression (Hindley et al. 2012).

1.7 High Endothelial Venules

1.7.1 Introducing Secondary Lymphoid Organs

Secondary Lymphoid Organs (SLOs) in mice and humans function primarily in initiation of adaptive immune responses to pathogens. SLOs provide a location for interactions between rare, antigen-specific naïve lymphocytes and APCs. SLOs are also sites where rapid recall responses to a returning antigen are mounted via central memory T cells (van de Pavert & Mebius 2010; Andrian & Mempel 2003).

SLOs comprise Lymph Nodes (LN), splenic white pulp, appendix (in humans) and Mucosal Associated Lymphoid Tissues (MALTs), the latter including intestinal Peyer's patches (PP) and isolated lymphoid follicles (ILF). SLOs are strategically placed at predetermined sites throughout the body, forming a sophisticated network that continually surveys interstitial areas, mucosal surfaces and the blood. SLOs have

highly organised architecture, specifically adapted to promote cellular interactions necessary for immune response initiation (Randall et al. 2008; Drayton et al. 2006).

Development of SLOs is a genetically pre-programmed process initiated during embryogenesis. Whilst some SLOs (LNs, PP) develop prenatally, the organogenesis of some SLOs occurs in early postnatal development. Prenatal and postnatal development follows a similar underlying program, despite some differences reflecting distinct anatomical sites in which SLOs develop (van de Pavert & Mebius 2010).

1.7.2 High Endothelial Venules in the Lymph Node

The basic architecture of all SLOs is similar. The structure of the LN, as the prototypical SLO, is described in Figure 1.7. In brief, LNs comprise a capsule and subcapsular sinus (SCS), within which cells are topologically segregated into the cortex, paracortex and medulla. The cortex consists of B cells and Follicular Dendritic Cells (FDCs), tightly packed into primary follicles. The paracortex harbours loosely arranged T cells, DCs and Fibroblastic Reticular Cells (FRCs). Lymphatic tissues constitute the medulla (Ruddle & Akirav 2009; Girard et al. 2012; Drayton et al. 2006).

LNs contain two distinct vasculature systems: lymphatic vasculature, and High Endothelial Venules (HEVs; Figure 1.7). Afferent lymphatic vessels deliver lymph carrying soluble antigen and immune cells, primarily DCs. Lymph percolates through cortical and medullary sinuses, and leaves the LN via the efferent lymphatic vessel, which delivers lymph to the venous blood (Girard et al. 2012; Drayton et al. 2006).

HEV are specialised post-capillary venules found in the blood vascular bed within the paracortical region of the LN and other SLOs, except the Spleen (Ager & May 2015). The primary function of HEV is homeostatic delivery of naïve B and T lymphocytes from the adjacent bloodstream. Central memory T cells, Tregs, plasmacytoid DCs (pDCs) and NK cells also extravasate via HEV under homeostatic conditions (Girard et al. 2012). Endothelial cells lining HEV have a distinct plump, cuboidal morphology, engendering the name 'High' endothelial venules (Rosen 2004). The HEV network is spatially organised to control the anatomical site of cellular entry
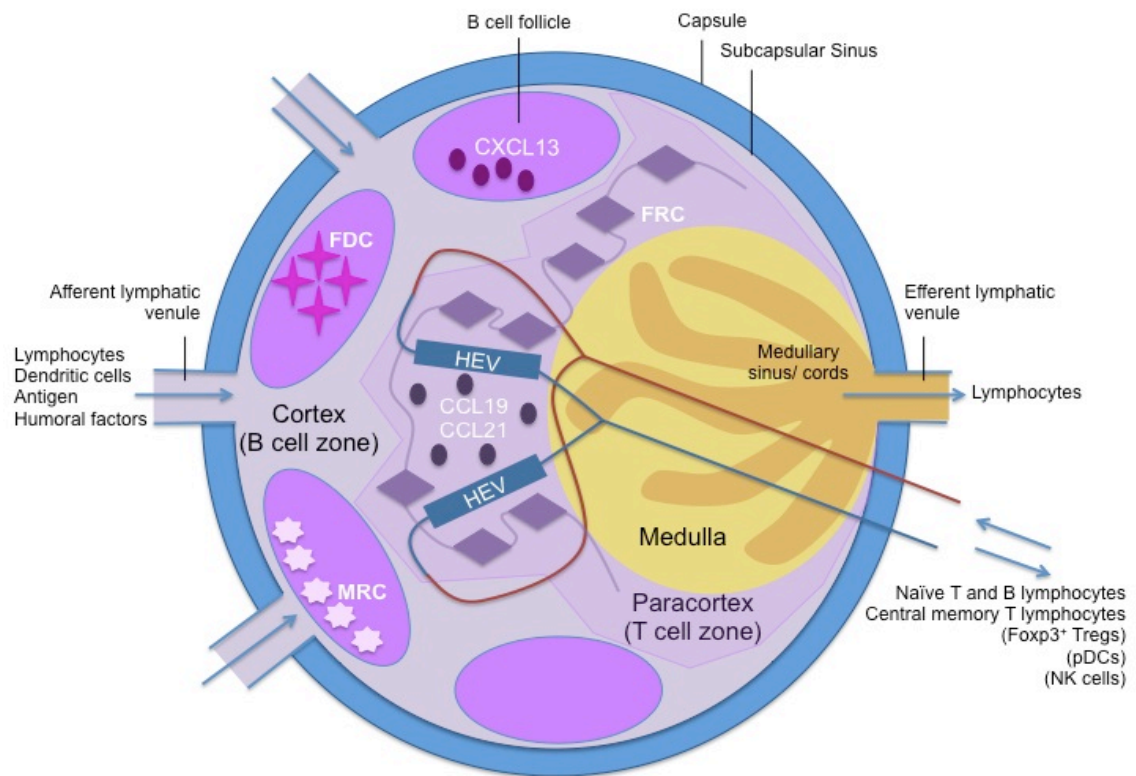
Figure 1.7 | The Structure of the Lymph Node.
Lymph nodes comprise a collagen-rich fibrous capsule and an underlying SCS. Cells are segregated into 1) the cortex, consisting of B cells and FDCs arranged in primary follicles, in which B cells survey antigens presented on the FDC stromal network, and 2) the paracortex, which accommodates T cells and DCs, and FRCs that form stromal cell networks and reticular fibres, along which T cells and DCs migrate. The inner medulla is composed of lymphatic tissues (medullary cords) separated by medullary sinuses consisting of lymph. FRCs express CCL19 and CCL21, whereas CXCL13 is expressed by FDCs. MRCs form a third stromal cell network, situated just under the SCS. Lymph nodes contain lymphatic vasculature and HEV. Afferent lymphatic vessels deliver lymph containing antigen and immune cells, and HEV are specialised post-capillary venules that primarily deliver naïve and central memory lymphocytes. SCS, subcapsular sinus; FDC, Follicular Dendritic Cell; DC, Dendritic Cell; FRC, Fibroblastic Reticular Cell; MRC, Marginal Reticular Cell; HEV, High Endothelial Venule. Adapted from (Girard et al. 2012; Drayton et al. 2006).

and contribute to overall structural organisation of the tissue (Ager & May 2015). T and B lymphocytes continually circulate through LNs, entering the tissue via HEV and exiting through efferent lymphatic vessels (Drayton et al. 2006).

Sir James Gowans was the first to definitely demonstrate extensive but selective infiltration of HEV by lymphocytes, suggesting a special affinity of lymphocytes for HEV endothelial cells (Gowans & Knight 1964). Lymphocytes extravasate through HEV according to a multistep adhesion cascade, involving tethering, rolling and arrest, dictated by the expression of adhesion molecules and chemokines on the HEV endothelial cell surface (Figure 1.8) (Girard et al. 2012). Mechanisms of lymphocyte homing to SLOs differ, with the process of naïve

lymphocyte homing to peripheral (subcutaneous) lymph nodes (PLN) in the mouse remaining the best understood (Figure 1.8) (Rosen 2004).

Homing is initiated by tethering of the lymphocyte to the surface of an endothelial cell via the lymphocyte-expressed homing receptor, L-selectin (CD62L). L-selectin recognises the carbohydrate epitope 6-sulpho sialyl Lewis X, present on *N*-glycans and extended core 1 and 2 *O*-glycans that decorate heavily sulphated, fucosylated and sialylated sialomucins. 6-sulpho sialyl Lewis X decorated sialomucins are collectively referred to as peripheral node addressins (PNAd), and are highly specific to HEV. HEV sialomucins include the CD34 family, nepmucin, endomucin, murine Glycosylation-dependent Cell Adhesion Molecule-1 (GlyCAM-1) and Mucosal Addressin Cell Adhesion Molecule-1 (MAdCAM-1) (Girard et al. 2012).
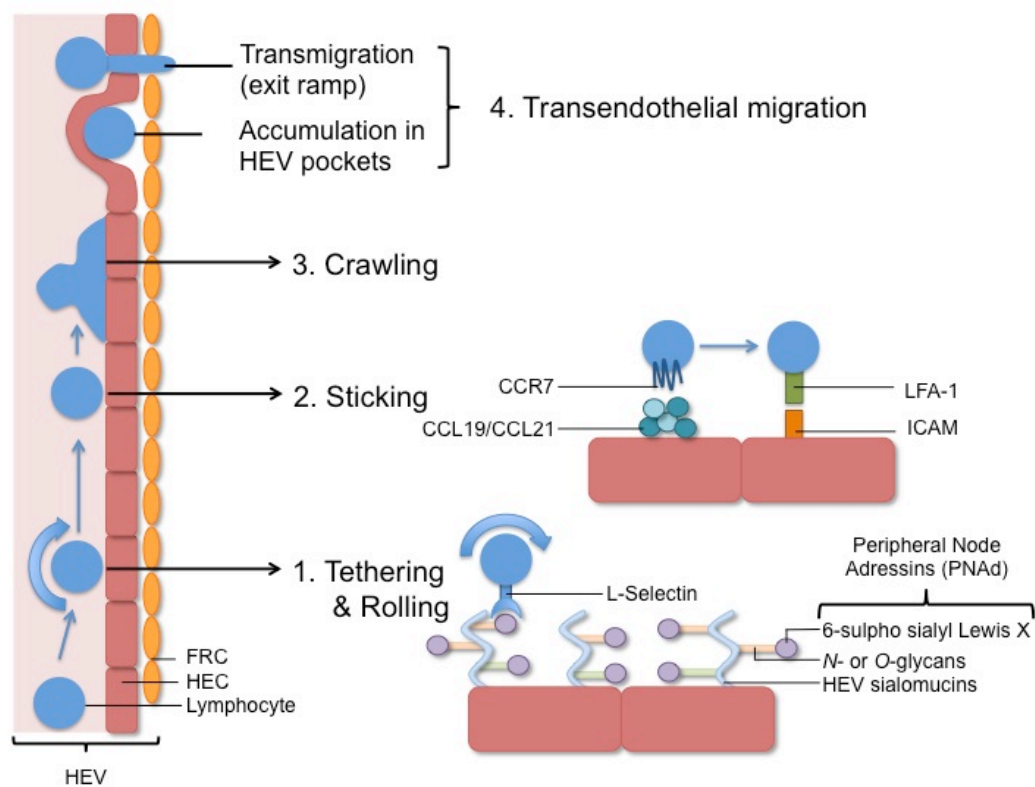
Figure 1.8 | The Multistep Adhesion Cascade of Naïve Lymphocyte Homing to Peripheral Lymph Nodes.
Tethering involves interactions between lymphocyte expressed L-Selectin and 6-sulpho sialyl Lewis X carbohydrate epiptopes expressed on *N*- or *O*-Glycans decorating sialomucins expressed on endothelial cells (PNAd). This facilitates reversible adhesion, manifested as rolling (1). CCL19 / CCL21 signalling via CCR7 allows LFA-1 to interact with ICAM-1 and/ or 2, resulting in integrin-mediated arrest (2). Lymphocytes then 'crawl' on the endothelium (3) before rapidly transmigrating via 'exit ramps' (4). Some lymphocytes transiently accumulate in 'HEV pockets'. HEV, High Endothelial Venule; PNAd, peripheral node addressin; LFA-1, Lymphocyte function-associated antigen 1; ICAM-1, InterCellular Adhesion Molecule-1; FRC, Follicular Reticular Cell.
Adapted from (Girard et al. 2012).

Initial tethering via the L-selectin-PNAd interaction leads to reversible adhesion, which manifests as lymphocyte 'rolling' along the endothelium under the force of blood flow. Rolling lymphocytes encounter CCL19 and CCL21 immobilized on the surface of endothelial cells. Signalling of CCL19 / CCL21 via the cognate lymphocyte-expressed CCR7 receptor activates lymphocyte-expressed integrin Lymphocyte function-associated antigen 1 (LFA-1; $\alpha_L\beta_2$). LFA-1 engages adhesion molecules InterCellular Adhesion Molecule (ICAM)-1 and/or ICAM-2 expressed on endothelial cells, resulting in integrin-mediated arrest. The lymphocyte will then 'crawl' along the surface of the endothelium for several minutes before rapidly transmigrating the endothelial layer via 'exit ramps' formed by FRCs. Alternatively, lymphocytes temporarily reside in HEV endothelial cell 'pockets' before transmigrating (Girard et al. 2012).

HEV are detected in mouse and human using the anti-PNAd antibody (clone MECA-79), which recognizes the 6-sulpho sialyl Lewis X epitope expressed on core 1 *O*-glycans, highly specific to HEV. Other HEV-specific markers include enzymes involved in synthesis of the HEV sialomucins, GlcNAc6ST-2 and fucosyltransferase 7 (FucTVII). MAdCAM-1 is expressed on the surface of HEV in mucosal lymphoid organs such as mesenteric LNs, where it facilitates lymphocyte arrest via lymphocyte-expressed $\alpha_4\beta_7$ integrin (Girard et al. 2012). However, MAdCAM-1 is not HEV-specific, due to broad expression on blood vessels of the lamina propia, marginal sinus-lining cells of the spleen and stromal cells within embryonic LNs (Ager & May 2015).

Following recruitment of lymphocytes and DCs, positioning of these cells within the LN is dictated by compartmentalised expression of lymphoid chemokines by stromal cell populations (Drayton et al. 2006). Constitutive expression of CCL19 and CCL21 by stromal FRCs and FRC networks allows directed migration of CCR7^{+} T cells and DCs along FRC networks to T cell zones. CXCL13 is constitutively expressed by FDCs in the centre of B cell follicles, and is responsible for directing B cells that express the CXCL13 receptor, CXCR5, to these areas (Girard et al. 2012). On their way to B cell follicles, B cells crawl along FRC networks in the T cell zones (Bajénoff et al. 2006).

1.7.3 Lymph Node Development during Embryogenesis

Many of the molecular mechanisms involved in LN development have been defined (Figure 1.9). A body of work has demonstrated that successful development of LNs critically depends upon coordinated interactions between stromal lymphoid tissue organizer cells (LTo) and haematopoietic lymphoid tissue inducer cells (LTi). These interactions occur via signalling between the $LT\alpha_1\beta_2$ ligand, expressed on the surface of LTi cells, and the LTβ Receptor (LTβR), expressed on LTo cells (van de Pavert & Mebius 2014; van de Pavert & Mebius 2010; Mebius 2003).

The first haematopoietic precursor LTi (pre-LTi) cells are attracted to sites of future LNs (LN anlagen) between embryonic day post-coitus (E)12.5 and E13.5, by the chemokine CXCL13, expressed by local stromal cells (van de Pavert & Mebius 2014; van de Pavert & Mebius 2010). To migrate to such locations, pre-LTi cells must express CXCR5 (van de Pavert & Mebius 2014). Mice genetically deficient in CXCL13 or CXCR5 lack several PLNs, have a reduced number of PP, and a full complement of mesenteric LNs (van de Pavert et al. 2009; Luther et al. 2003; Ansel et al. 2000; Förster et al. 1996; Ohl et al. 2003). Animals deficient in both CXCR5 and CCR7 develop no PLNs, implying cooperation between these two receptors (Ohl et al. 2003; Luther et al. 2003). However, all LNs form in mice deficient in CCR7/CCL21 but competent in CXCR5/CXCL13 signalling (Förster et al. 1999). Hence CXCL13 expression is a crucial event in early LN development, by initiating LTi clustering. Retinoic acid (RA), potentially derived from proximal nerve fibres, induces CXCL13 expression by stromal cells (van de Pavert et al. 2009).

Following recruitment, $LT\alpha_1\beta_2$ expression is induced on pre-LTi cells (see Section 1.7.3.1). $LT\alpha_1\beta_2$ expressing pre-LTi cells differentiate into mature LTi cells, which form stable interactions with LTβR-expressing stromal cells, causing them to differentiate into stromal LTo cells (van de Pavert & Mebius 2010). Signalling via LTβR results in expression of CCL19, CCL21 and CXCL13, and adhesion molecules Vascular Cell Adhesion Molecule-1 (VCAM-1), ICAM-1 and MAdCAM-1, by stromal LTo cells, which are absolutely required for attraction and retention of further

haematopoietic cells leading to LN growth (van de Pavert & Mebius 2010; Cupedo et al. 2004; Roozendaal & Mebius 2011).
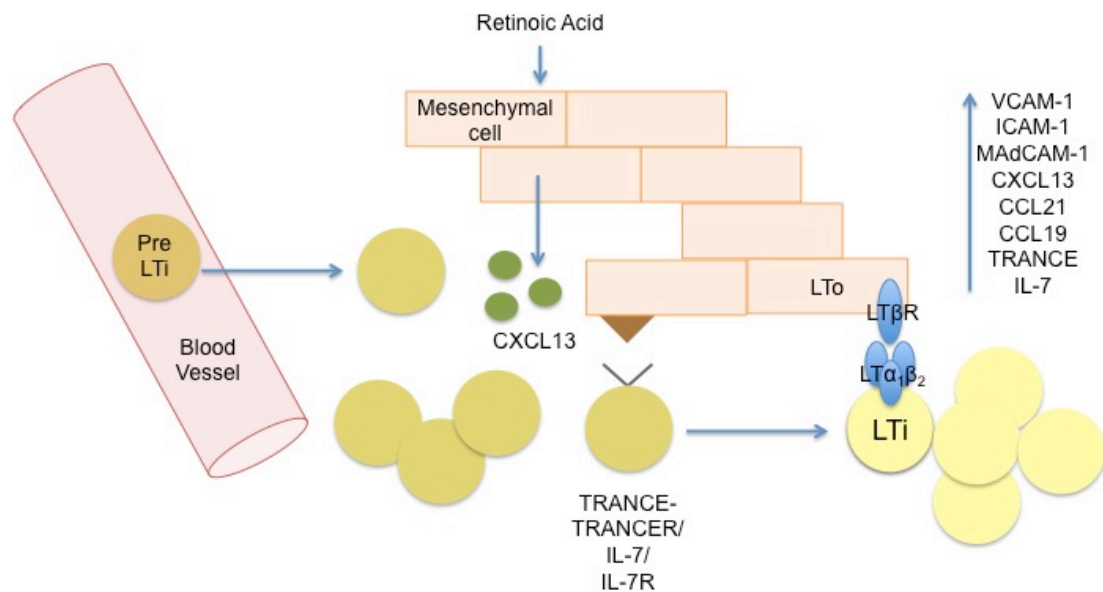
Figure 1.9 | Molecular Mechanisms of Lymph Node Development.
Retinoic Acid (RA) induces expression of CXCL13 by local mesenchymal stromal cells at the site of the future Lymph Node. This attracts CXCR5-expressing precursor LTi cells (pre-LTi cells) from the blood, and these form the first haematopoietic cell clusters. Clustering of these cells facilitates signalling via either TRANCE-TRANCER or IL-7-IL-7R between stromal cells and pre-LTi cells, which induces $LT\alpha_1\beta_2$ expression on the pre-LTi cell. These pre-LTi cells then differentiate into mature LTi cells. Signalling of LTi-expressed $LT\alpha_1\beta_2$ via $LT\beta R$ expressed on stromal cells causes the latter to differentiate into LTo cells. This crucial interaction between LTi and LTo causes the up-regulation of adhesion molecules VCAM-1, ICAM-1 and MAdCAM-1 and chemokines CXCL13, CCL21 and CCL19 by stromal LTo cells, leading to further recruitment of haematopoietic cells, fostering lymph node growth. $LT\alpha_1\beta_2$-$LT\beta R$ signalling also causes expression of TRANCE and IL-7, constituting a positive feedback loop to facilitating $LT\alpha_1\beta_2$-$LT\beta R$ signalling between stromal cells and newly arriving pre-LTi cells. TRANCE, tumour necrosis factor (TNF)-related activation induced cytokine; LTi, lymphoid tissue inducer cell; LTo, lymphoid tissue organizer cell; VCAM-1, Vascular Cell Adhesion Molecule-1; ICAM-1, InterCellular Adhesion Molecule-1; MAdCAM-1, Mucosal Addressin Cell Adhesion Molecule-1. Adapted from (van de Pavert & Mebius 2010).

LTβR signalling also results in up-regulation of IL-7 and tumour necrosis factor (TNF)-related activation induced cytokine (TRANCE) expression by LTo cells, which induces $LT\alpha_1\beta_2$ expression on newly arriving pre-LTi cells, thereby constituting a positive feedback loop (Mebius 2003; Yoshida et al. 2002; Vondenhoff et al. 2009; Honda et al. 2001). Furthermore, LTβR signalling induces expression of the lymphangiogenic factor, VEGF-C, by stromal LTo cells, which aids connection of the developing LN to surrounding lymphatic vasculature (Vondenhoff et al. 2009). The developing LN is colonized by infiltrating lymphocytes around day E15.5, eventually giving rise to a highly organized LN (van de Pavert & Mebius 2010).

1.7.3.1 Lymphoid Tissue Inducer cells in Lymph Node Development

LTi cells were originally described in the mouse by the Mebius and Nishikawa groups (Mebius et al. 1996; Mebius et al. 1997; Adachi et al. 1997; Yoshida et al. 1999). LTis are haematopoietic cells that derive from a lymphoid progenitor found in mouse foetal livers (Mebius et al. 2001; Yoshida et al. 2001), and express a defined repertoire of markers (Table 1.1) (Lane et al. 2012[a]; Lane et al. 2012[b]). An absolute requirement for LTi cells in LN development is evident by the complete lack of LNs in animals genetically deficient in either one of two genes required for LTi development and maturation: the *Rorc* gene, which encodes the transcription factor RORγt, and the *Id2* gene (Sun et al. 2000; Eberl et al. 2004; Yokota et al. 1999).

Table 1.1 | Marker Expression of Murine Lymphoid Tissue inducer (LTi) cells

Marker		**Expression**
Th17-associated gene	IL-22	+
	IL-17A	+
	IL-23 receptor	+
Transcription factor	retinoic acid receptor-related orphan receptor-γt (RORγt)	+
	helix-loop-helix protein inhibitor of DNA binding 2 (ID2)	+
Surface marker	CD3	-
	CD4	+/-
	CD117	+
	IL-7Rα (CD127)	+
	IL-2Rα (CD25)	+
TNFSF members	TRANCE	+
	TNF, LTα, LTβ	++
Chemokine receptors	CXCR5	+
	CCR7	+
	CCR6	+

Adapted from (Lane et al. 2012[a]; Lane et al. 2012[b]).

Both IL-7 and TRANCE induce $LT\alpha_1\beta_2$ expression by LTi cells, and are differentially required in different SLOs (Yoshida et al. 2002). The function of LTi cells is absolutely dependent on expression of $LT\alpha_1\beta_2$ (Yoshida et al. 2001; Yoshida et al. 2002). However, initial LTi clustering proceeds uninterrupted when $LT\alpha_1\beta_2$ expression by LTi cells, or LTβR expression by LTo cells is prevented (van de Pavert & Mebius 2010). Moreover, over expression of TNFα can compensate for the loss of classical

RORγt$^+$ LTis to a certain degree, enabling organogenesis of some functional LNs, in a LTβR signalling dependent manner (Furtado et al. 2014).

1.7.3.2 Cellular Signalling in Lymph Node Development

1.7.3.2.1 Introducing the Tumour Necrosis Factor Superfamily

The extended Tumour Necrosis Factor (TNF) superfamily consists of 19 ligands and 29 receptors. TNF superfamily signalling results in diverse immunological outcomes, from pro-inflammatory functions to cell survival signals to promotion of cellular apoptosis (Aggarwal et al. 2012). TNF superfamily cytokines exert such effects by initiating rapid transcription of genes, primarily via activation of the Nuclear Factor κB (NFκB) family of inducible transcription factors (Hayden & Ghosh 2014).

The immediate TNF/LT family comprises four cytokines, TNFα, LTα, LTβ, and LT-related inducible ligand that competes for glycoprotein D binding to herpesvirus entry mediator on T cells (LIGHT), and five communal receptors. This signalling circuitry is complex, consisting of both unique and overlapping ligand-receptor interactions (Figure 1.10). LTα can exist as part of an exclusively secreted LTα$_3$ homotrimer, which signals via one of the two structurally similar but functionally distinct TNF receptors, TNFR1 (p55) and TNFR2 (p75). LTα can alternatively form part of one of two membrane-anchored heterotrimers together with LTβ. The predominant LTα$_1$β$_2$ binds to the high affinity LTβ receptor (LTβR), whereas LTα$_2$β$_1$ is expressed by fewer than 2% of T cells, has no defined role, and is capable of engaging TNFR1, TNFR2 and LTβR but only with low avidity (Ware 2005; Aggarwal et al. 2012).

TNFα is expressed as a homotrimeric transmembrane protein (mTNFα), or a cleaved extracellular soluble ligand (sTNFα). It has been reported that while sTNFα results in robust activation of TNFR1 but limited or no activation of TNFR2, mTNFα primarily signals via TNFR2 (Grell et al. 1995; Grell et al. 1998; Aggarwal 2003). LIGHT signals via either herpes virus entry mediator (HVEM) receptor or LTβR. Decoy receptor 3 (DcR3) is a secreted receptor for LIGHT, which limits engagement of LIGHT in active signalling (Ware 2005; Aggarwal et al. 2012).

Stromal cells including fibroblasts, and epithelial and myeloid cells constitutively express LTβR. LTα$_1$β$_2$ is expressed by activated T, B and NK cells. TNFα is expressed in diverse cell types in response to inflammatory stimuli, but is produced in substantial quantities by myeloid cells. TNFR1 is ubiquitously expressed, whereas TNFR2 expression is mostly restricted to immune cells: TNFR2 is constitutively expressed on monocytes and inducible on T and B cells. TNFR1 facilitates most of the proinflammatory, apoptotic and cytotoxic functions traditionally associated with TNFα. LIGHT demonstrates constitutive expression on myeloid cells and inducible expression on T cells. HVEM is widely distributed in lymphoid and non-lymphoid compartments (Chen & Oppenheim 2011; Ware 2005).
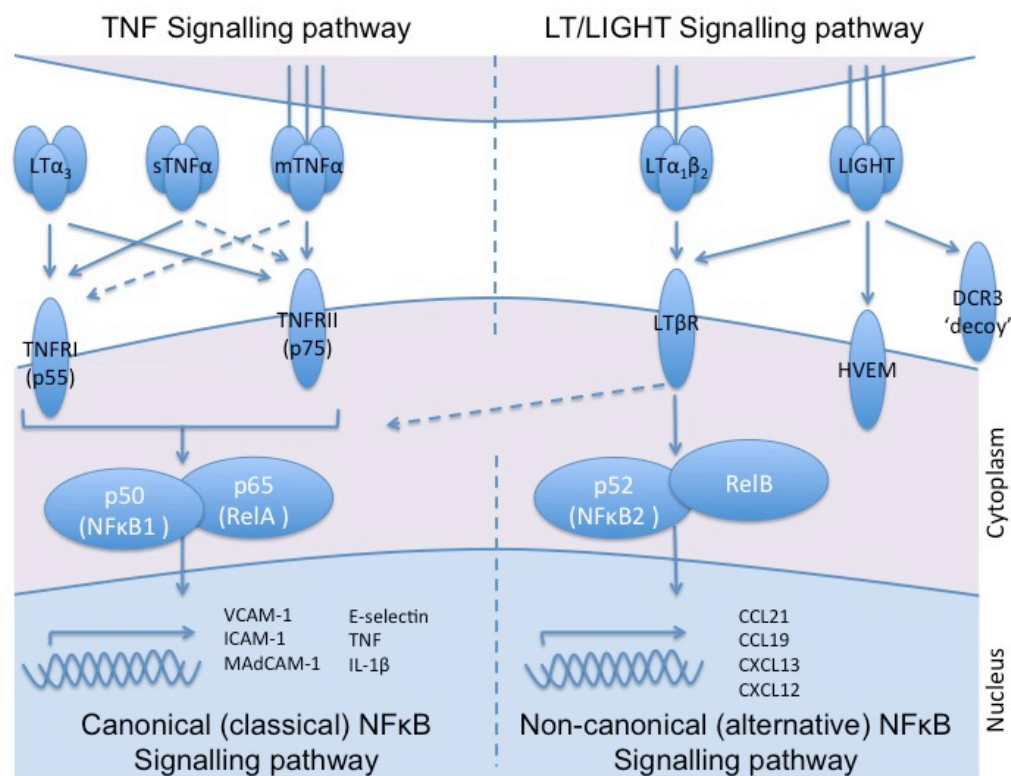
Figure 1.10 | The Immediate TNF/ LT Family and their Signalling Circuitry.
Two distinct signalling pathways can be defined: the TNF signalling pathway is activated by TNFα or LTα$_3$, which bind TNFR1 (p55) or TNFR2 (p75). TNFα exists as a membrane bound ligand (mTNFα) or soluble ligand (sTNFα). Both ligands are capable of binding either receptor, but mTNFα initiates most of its signalling via TNFR2 and sTNFα signals primarily via TNFR1. Signalling via either TNFR activates the p50/p65 cytoplasmic complex for target gene transcription. The p50/p65 complex belongs to the canonical (classical) NFκB pathway, leading to transcription of genes encoding adhesion molecules and cytokines as shown. The LT/ LIGHT signalling pathway consists primarily of two dominant ligands, LTα$_1$β$_2$ and LIGHT, both of which signal via LTβR. LIGHT also interacts with HVEM and DcR3. Signalling via the LTβR initiates the non-canonical (alternative) NFκB pathway. This activates the p52/ RelB complex for transcription of genes including those encoding the chemokines shown. Signalling via the LTβR can also initiate the canonical NFκB pathway. TNF, Tumour Necrosis Factor; LT, Lymphotoxin; TNFR, TNF receptor; LIGHT, LT-related inducible ligand that competes for glycoprotein D binding to herpesvirus entry mediator on T cells; HVEM, Herpes Virus Entry Mediator; DcR3, Decoy receptor 3.

TNFα was discovered over a century ago: following reports of regression of established tumours in human patients after bacterial infection by a German physician, William Cooley, an American oncologist, successfully treated some human cancers with bacterial extracts, later named 'Coley's toxins' (Coley 1891; Coley 1910; Aggarwal 2003). Lipopolysaccharide (LPS) within the bacterial extracts was the agent responsible for regression of tumours, as it induced haemorrhagic tumour necrosis. The anti-tumour effects of LPS were indirect and were facilitated by the production of a factor within the serum in response to LPS, at the time referred to as tumour-necrotizing factor (Aggarwal 2003). Lloyd Old's group coined the name tumour necrosis factor (TNF) in 1975, and demonstrated that TNF was produced in serum in response to endotoxin and caused necrosis when injected directly into tumours (Carswell et al. 1975). LT was initially described in the 1960s, as a factor produced by lymphocytes, capable of killing tumour cells (Williams & Granger 1968).

The NFκB family consists of five transcription factors: p50 (NFκB1), p52 (NFκB2), p65 (RelA), RelB and cRel (Rel). These proteins exist as homodimers or heterodimers, and bind directly to DNA to either induce or repress target gene transcription. Cytosolic NFκB dimers are prevented from binding to DNA targets during the resting state by an association with inhibitor of κB (IκB) proteins. Two IκB proteins, IκBα and p100, represent the primary regulators of the 'canonical' or 'classical' and 'non-canonical' or 'alternative' NFκB signalling pathways, respectively (Hayden & Ghosh 2014). Signalling via TNFRs triggers transduction via the canonical NFκB pathway, whereas signalling via the LTβR can initiate signal transduction via both canonical and non-canonical pathways (Figure 1.10) (Mebius 2003).

1.7.3.2.2 Lymphotoxin/ Tumour Necrosis Factor Signalling in Lymph Node Development

The absolute requirement for LTβR signalling for LN development is illustrated by failure of lymphoid organogenesis in mouse models genetically deficient in components of the LTβR signalling pathway (Mebius 2003). De Togni and colleagues

were the first to report complete absence of all PLNs and PP in LTα-deficient mice (De Togni et al. 1994). Banks and colleagues largely confirmed these findings, but noted rudimentary LN-like structures in the mesentery of some LTα$^{-/-}$ mice; an early indication of the differential requirement for LT signalling in the organogenesis of SLOs in distinct anatomical sites (Banks et al. 1995). Expression of the LTα transgene under the control of the rat insulin promoter (RIP) in the pancreas, kidney and skin of LTα$^{-/-}$ mice (RIPLT.LTα$^{-/-}$ mice) restored LNs, supporting a critical role for LTα (Sacca et al. 1997).

Despite significant similarities between LTα and TNFα, mice genetically deficient in TNFα, TNFR1 or TNFR2, displayed relatively normal LN organogenesis. However, mice harbouring disruptions at the TNFα or TNFR genetic loci display defective PP development, which were either completely absent or reduced in number and structurally disrupted. These data implicated TNFα-TNFR signalling in PP organogenesis (Körner et al. 1997; Pasparakis et al. 1996; Pasparakis et al. 1997; Erickson et al. 1994; Kuprash et al. 2005; Neumann et al. 1996; Pfeffer et al. 1993; Rothe et al. 1993).

The discrepancy between LTα and TNFα/TNFR genetically deficient mouse models indicated that LTα may be controlling lymphoid organogenesis independent of TNFRs (De Togni et al. 1994). These data were resolved by the observation that LTα forms heterotrimers with LTβ (Androlewicz et al. 1992; Browning et al. 1993), and the resulting membrane bound ligand signals through the then newly discovered LTβR (Rennert et al. 1996; Crowe et al. 1994). A role for LTαβ-LTβR signalling in orchestration of SLO development was soon confirmed by a series of studies of LTβ- or LTβR-deficient animals, showing either a complete lack of all LNs and PP (Fütterer et al. 1998) or formation of only cervical, mesenteric and sacral LNs (Koni et al. 1997; Alimzhanov et al. 1997; Kuprash et al. 1999; Soderberg et al. 2004).

Injection of soluble LTβR-immunoglobulin antagonist fusion protein during embryogenesis inhibited formation of some LNs and PP (Yamamoto et al. 2000; Rennert et al. 1996; Rennert et al. 1997; Rennert et al. 1998). Importantly, the first of these studies also elegantly demonstrated sequential development of LNs during

embryogenesis: injection of the protein on various gestational days affected development of distinct LNs (Rennert et al. 1996). Abolished development of LNs in LTα$^{-/-}$ mice is rescued by in utero injection of agonist anti-LTβR monoclonal antibodies (Rennert et al. 1998). These studies unequivocally demonstrate the absolute requirement for LTα$_1$β$_2$-LTβR signalling for LN and PP development.

The fact that LTα$^{-/-}$ mice lack all LNs (De Togni et al. 1994; Banks et al. 1995) while LTβ$^{-/-}$ mice retain cervical, sacral and mesenteric LNs (Koni et al. 1997; Alimzhanov et al. 1997; Kuprash et al. 1999) suggests a degree of cooperation between surface and membrane bound ligands. Additionally, as the aforementioned LNs can develop in LTβ$^{-/-}$ but not LTβR$^{-/-}$ mice (Fütterer et al. 1998), the alternative LTβR ligand, LIGHT, is implicated specifically in development of cervical, sacral and mesenteric lymphoid organs. Indeed, LIGHT$^{-/-}$ LTβ$^{-/-}$ mice harbour a lower frequency of mesenteric LNs compared to that of LTβ$^{-/-}$ mice. However, intact development of all LNs, including those in the mesentery, in LIGHT$^{-/-}$ animals suggests LTα$_1$β$_2$-LTβR signalling holds a dominant role (Scheu et al. 2002).

A number of LNs, including mesenteric, cervical, lumbar and sacral, were still able to form when LTβR-immunoglobulin fusion protein was administered during utero (Rennert et al. 1996; Rennert et al. 1997). In contrast, development of all LNs was completely blocked by in utero treatment with LTβR.Ig and either a TNFR1 immunoglobulin fusion protein (TNFRp55.Ig) or an anti-TNF antibody. This study illustrates that TNF-TNFRp55 signalling also contributes to SLO development, perhaps in a redundant fashion to LTβR signalling (Rennert et al. 1998).

Simultaneous triggering of canonical and non-canonical NFκB pathways is required for expression of the adhesion molecules and chemokines necessary for successful SLO development (Randall et al. 2008). Mice harbouring a spontaneous mutation in the *aly* gene, which encodes for NFκB-inducing kinase (NIK), an essential component of the non-canonical NFκB pathway (Miyawaki et al. 1994; Shinkura et al. 1999), or NIK$^{-/-}$ mice (Yin et al. 2001), lack all PP and LNs. Conversely, *Rela x tnfr1$^{-/-}$*

mice, which cannot initiate canonical NFκB signalling, also lack all PP and LNs (Alcamo et al. 2002).

1.7.4 High Endothelial Venule Development and Maintenance in Lymph Nodes

The final steps of LN development require recruitment and positioning of lymphocytes. This is delayed until approximately 3 days after birth, due to sequential expression of addressins on HEV, the portals for lymphocytic infiltration. Before day 3, LN HEV exclusively express MAdCAM-1 (Mebius et al. 1996). Hence only cells expressing the cognate selectin $\alpha_4\beta_7$, such as LTi cells and γδ T cells, can access the LN via HEV (Yoshida et al. 2001; Mebius et al. 1997; Mebius et al. 1998). Around day 3, MAdCAM-1 expression is down-regulated concurrently with the up-regulation of PNAd, enabling L-selectin-expressing naïve T and B cells to gain entry (Mebius et al. 1996; Randall et al. 2008).

Generation of PNAd on the surface of HEV endothelial cells is critically reliant upon two enzymes, GlcNAc6ST-1 and GlcNAc6ST-2, which sulfate core glycoproteins (Rosen 2004). GlcNAc6ST-2 demonstrates a highly restricted pattern of expression in LN HEV, where it is responsible for the expression of PNAd on the inner, apical surface of HEV endothelial cells: luminal PNAd (Hemmerich et al. 2001). In contrast, GlcNAc6ST-1 is broadly expressed and is thought to facilitate generation of both luminal and abluminal PNAd (Uchimura et al. 2005; Uchimura et al. 2004; Kawashima et al. 2005). Loss of both GlcNAc6ST-1 and -2 enzymes completely abolishes PNAd expression on HEV, rolling of lymphocytes on HEV endothelial cells and lymphocyte homing to all PLN (Uchimura et al. 2005; Kawashima et al. 2005).

Abluminal PNAd expression on ectopic HEV is initiated by overexpression of the LTα transgene in pancreas and kidney (Kratz et al. 1996; Drayton et al. 2003). Residual abluminal PNAd expression also remains on LN HEV in LTβ$^{-/-}$ animals, or mice in which LTβR signalling has been blocked by antagonist LTβR.Ig (Browning et al. 2005; Drayton et al. 2003; Liao & Ruddle 2006). In line with these data, LTα$_3$-TNFR1 signalling has been implicated in regulation of abluminal PNAd expression on HEV, but

a direct role has not yet been demonstrated (Drayton et al. 2003). In contrast, GlcNAc6ST-2 and GlyCAM-1 expression, required for luminal PNAd expression, requires co-expression of LTβ with LTα, and thus $LT\alpha_1\beta_2$-LTβR signalling directly controls luminal PNAd expression on HEV (Drayton et al. 2003; Drayton et al. 2004; Hemmerich et al. 2001).

The stromal compartment of LNs actively maintains the differentiated status of HEV: PNAd expression and cuboidal morphology of HEV endothelial cells, as well as lymphocyte transmigration across endothelial cells, are rapidly down-regulated following isolation from adult mice (Ager & May 2015). Early studies during which afferent lymphatic flow to LNs was ligated illustrated an essential requirement for components of lymph in active maintenance of LN architecture and function (Mebius et al. 1991; Mebius et al. 1993; Swarte et al. 1998; Liao & Ruddle 2006). Within 1 week of afferent lymphatic occlusion, lymphocytic influx into the LN is significantly decreased, accompanied by a loss in the characteristic 'high' morphology of HEV endothelial cells and changes in adhesion molecule expression. Specifically, HEV revert from a mature ($MECA-79^{hi}$ $GlyCAM1^{hi}$ $FucTVII^{hi}$ $GlcNAc6ST-2^{hi}$ $MAdCAM-1^{lo}$) to an immature ($MECA-79^{lo}$ $GylCAM1^{lo}$ $FucTVII^{lo}$ $GlcNAc6ST-2^{lo}$ $MAdCAM-1^{hi}$) phenotype (Mebius et al. 1991; Mebius et al. 1993; Swarte et al. 1998). Hence, lymphatic flow and presumably factors within lymph are required for homeostatic maintenance of HEV, although the identity of such factors remains elusive (van de Pavert & Mebius 2014). Additionally, LTβR signalling is required for normal homeostatic maintenance of HEV structure and function (Lu & Browning 2014). Administration of a LTβR.Ig decoy receptor to adult mice phenocopies afferent lymphatic occlusion in that adhesion molecule expression by HEV endothelial cells is altered and HEV function is impaired (Browning et al. 2005; Liao & Ruddle 2006).

DCs, well known for their role in antigen presentation, are implicated in the modulation and maintenance of the HEV phenotype in the adult, via expression of the LTβ ligand. Following depletion of $CD11c^+$ DCs in adult mice, cellularity and size of PLNs was significantly reduced, expression of HEV markers was down-regulated and

homing of lymphocytes to LNs impaired. The authors noted a similar reversion of HEV to an immature phenotype as induced by afferent lymphatic occlusion. This effect was the result of a direct interaction between DCs and endothelial cells, presumably via LT ligands expressed by DCs and endothelial cell-expressed LTβR (Moussion & Girard 2011).

Due to arrested development of lymphoid organs in LT deficient mice, the role of LT signalling in development of LN HEV has been more difficult to elucidate. However, HEV addressin expression is reduced in mesenteric LNs of LTβ^{-/-} mice and rudimentary LNs of mice treated with LTβ blocking reagents during gestation (Rennert et al. 1997; Alimzhanov et al. 1997). Indeed, HEV express LTβR and are capable of responding to LTαβ ligands (Liao & Ruddle 2006; Browning et al. 2005; Drayton et al. 2003). A recent study illustrated that LTβR signalling is directly required for development of functional HEV in PLNs. When LTβR was ablated in vascular endothelial cells beginning at day E8 (before initial stages of LN development), mice failed to develop up to 45% of PLNs. Importantly, in LNs that did develop, the HEV network was severely impaired, as noted by a significant reduction in addressin molecule and chemokine expression, and a loss of cuboidal morphology. These structural and phenotypic defects translated to a significant reduction in lymphocyte homing via HEV. However, the phenotype of animals in which vascular LTβR expression was ablated was not absolute: HEV were not completely absent in PLNs that did develop (Onder et al. 2013). These data suggest the existence of complex levels of redundancy in signalling circuitries underpinning HEV development in LNs, and illustrate the on-going gap in our knowledge surrounding normal HEV genesis.

1.8 High Endothelial Venule Neogenesis in Chronic Inflammation and Cancer

1.8.1 Tertiary Lymphoid Organs

Soon after birth, developmental programs driving lymphoid organogenesis are turned off (Drayton et al. 2006). However, tissues can support development of lymphoid organs into adulthood. This recapitulation of SLO organogenesis is

manifested in the formation of Tertiary Lymphoid Organs (TLOs). TLOs, also termed Ectopic Lymphoid-like Structures (ELSs), form at sites of microbial infection or chronic inflammation and have been reported in autoimmune disease, and more recently cancer (Pitzalis et al. 2014). *De novo* development of TLOs is referred to as ectopic lymphoid neogenesis (Pitzalis et al. 2014; Kratz et al. 1996). TLO development has been documented in practically all organ settings during chronic inflammation. 'TLO' refers to structures of varying organization, from simple clusters of lymphocytes, to sophisticated, histologically organized organs highly reminiscent of SLOs (Neyt et al. 2012; Lu & Browning 2014; Pitzalis et al. 2014; Stranford & Ruddle 2012; Aloisi & Pujol-Borrell 2006; Carragher et al. 2008).

1.8.1.1 Tertiary Lymphoid Organs in Cancer

TLOs of varying degrees of organization have been reported in multiple types of primary and metastatic cancer (Table 1.2) (Goc et al. 2013). PNAd[+] HEV can be found within tumours in the presence or absence of TLOs (Ager & May 2015). Tumour TLOs and / or isolated PNAd[+] HEV are largely associated with a favourable clinical prognosis (Goc et al. 2013). In a retrospective study of 74 NSCLC patients, Dieu-Nosjean and colleagues reported the presence of tumour-induced bronchus-associated lymphoid tissue (Ti-BALT), consisting of organized DC and T cell clusters, and B cell follicles. The density of mature DC-LAMP[+] DCs, a marker of Ti-BALT, correlated with increased overall, disease-specific and disease-free survival (Dieu-Nosjean et al. 2008). Martinet and colleagues found a significant correlation between presence of intra-tumoural PNAd[+] HEV, located within lymphocyte-rich clusters, and increased disease-free, metastasis-free and overall survival in 146 breast cancer patients (Martinet et al. 2011). Furthermore, regression of primary cutaneous melanoma correlated with presence of PNAd[+] HEV within the tumour mass (Avram et al. 2013). An interpretation of these data is that TLO and / or isolated HEV serve to facilitate trafficking of naïve T cells, which become primed and sensitized to tumour antigens locally at the tumour site (Ruddle 2014).

However, some studies have demonstrated a protumoural role for TLOs and / or HEV. Development of HEV-containing TLO in B16 melanomas engineered to express CCL21 led to rapid recruitment of immunosuppressive Tregs and MDSCs, which promoted tumour growth (Shields et al. 2010). Furthermore, high numbers of Tregs within lymphoid aggregates of primary breast tumours was indicative of an increased risk of disease relapse or death (Gobert et al. 2009; Bates et al. 2006; Bohling & Allison 2008). A detailed study in our own lab using resected tumour samples from 62 CRC patients found that despite identification of PNAd$^+$ HEV in the extra-tumoural area of most patients, intra-tumoural HEV were rare. Extra-tumoural HEV were associated with lymphoid aggregates which correlated with advanced disease (Bento et al. 2015). It will therefore be important to establish characteristics of tumour-associated TLO / HEV that correlate with good prognostic features in the future.

Table 1.2 | Tertiary Lymphoid Organs in Human Cancer

Cancer type	TLO features	References
Lung	T cells, mature DCs, HEVs	(de Chaisemartin et al. 2011)
Lung (non-small-cell)	T cells, Mature DCs	(Goc et al. 2014)
	T cells, B cells, mature DCs, FDCs	(Dieu-Nosjean et al. 2008)
Colorectal carcinoma	T cells, B cells, mature DCs	(Suzuki et al. 2002)
	T cells, B cells, HEVs	(Bento et al. 2015)
	T cells, mature DCs	(McMullen et al. 2010)
	T cells, B cells, FDCs	(Coppola et al. 2011)
	T cells, B cells, FDCs	(Bergomas et al. 2011)
	T cells, B cell, HEVs	(Martinet et al. 2011)
	T cells, B cells, mature DCs	(Remark et al. 2013)
Colorectal carcinoma (with lung metastases)	T cells, B cells, mature DCs	(Remark et al. 2013)
Colorectal carcinoma (with liver metastases)	Mature DCs	(Miyagawa et al. 2004)
Breast carcinoma	T cells, mature DCs	(Bell et al. 1999)
	T cells, B cells, FDCs	(Coronella et al. 2002)
	T cells, B cells, FDCs	(Gu-Trantien et al. 2013)
	T cells, B cells, PCs, FDCs	(Nzula et al. 2003)
	T cells, B cell, HEVs	(Martinet et al. 2011)
	T cells, B cells, mature DCs, HEVs	(Martinet et al. 2013)
	Lymphocytes	(Gobert et al. 2009)
Melanoma	T cells, B cells, HEVs	(Martinet et al. 2012)
	Memory T cells, mature DCs	(Ladányi et al. 2007)
	T cells, B cells, mature DCs	(Messina et al. 2012)
	T cells, B cells, mature DCs, FDCs, HEVs	(Cipponi et al. 2012)
	Lymphocytes, HEVs	(Avram et al. 2013)
Ovarian	T cells, B cells, HEVs	(Martinet et al. 2011)
	T cells, B cells	(Nielsen et al. 2012)
Seminoma	T cells, HEVs	(Sakai et al. 2014)
Renal cell carcinoma	T cells, B cells, mature DCs	(Remark et al. 2013)
Renal cell carcinoma (with lung metastases)	T cells, B cells, mature DCs	(Remark et al. 2013)
Mucosal-associated lymphoid tissue lymphoma	T cells, B cells, FDCs	(Bombardieri et al. 2007)
	T cells, B cells, FDCs	(Barone et al. 2008)
	T cells, HEVs	(Kobayashi et al. 2011)

Adapted from (Pitzalis et al. 2014; Neyt et al. 2012; Ager & May 2015; Goc et al. 2013).

1.8.2 Development of Tertiary Lymphoid Organs

Ontogenic development of SLOs provides a paradigm for understanding TLO formation. Despite structural differences, data from studies utilizing knockout and transgenic mouse models have indicated cooperation between TNF superfamily members and lymphoid chemokines in TLO neogenesis, much as in SLO development. However, a detailed understanding of exact mechanisms by which TLOs form in various pathogenic settings is still lacking (Drayton et al. 2006; van de Pavert & Mebius 2014; van de Pavert & Mebius 2010; Pitzalis et al. 2014).

1.8.2.1 Lymphotoxin/ Tumour Necrosis Factor Signalling in Tertiary Lymphoid Organ Neogenesis

Overexpression of *Ltα* in kidney and pancreas results in chronic inflammation and induction of functional, highly organized TLO, displaying T and B cell compartmentalization, and HEV expressing HEV-specific adhesion molecules (Kratz et al. 1996). Although TLO can form in *Ltα* deficient mice, the observed structures are much less organized than those in WT animals, and lack many TLO features including FDC networks and HEV (Moyron-Quiroz et al. 2004; Moyron-Quiroz et al. 2006). Interestingly, TNFR1 expression, but not LTβ expression, is required for LTα-induced chemokine expression and TLO neogenesis in the *Ltα* over-expression model (Hjelmström et al. 2000; Sacca et al. 1998). Meanwhile, TLOs in RIPLTαβ transgenic animals displayed more distinct T and B cell zone separation, higher expression of CXCL13, CCL19 and CCL21, luminal expression of PNAd on HEV, and increased infiltration of naïve lymphocytes, relative to RIPLTα mice (Drayton et al. 2003). Hence, LTα plays a crucial role in TLO development in at least some settings, and when present in combination with LTβ, TLO formation can be enhanced (Pitzalis et al. 2014).

In models of TLO induction in pancreatic islets, loss of $LT\alpha_1\beta_2$-LTβR signalling resulted in reversion of many aspects of TLO formation, including HEV dedifferentiation (Luther et al. 2000). Additionally, administration of the LTβR.Ig fusion protein to NOD mice resulted in reversion of key features of TLO, including PNAd[+] HEV, that form in

association with Sjögren syndrome (SS)-like salivary gland disease (Gatumu et al. 2009; Fava et al. 2011). Development of TLOs in the aortas of atherosclerosis mouse models is also a LTβR signalling dependent process, as demonstrated by significant interruption of TLO neogenesis following LTβR.Ig administration (Gräbner et al. 2009). Lastly, overexpression of LTαβ specifically in the acinar cells of the pancreas resulted in robust TLO induction in a mouse model of autoimmune pancreatitis (Seleznik et al. 2012). Such studies implicate $LT\alpha_1\beta_2$-LTβR signalling in TLO neogenesis at sites of chronic inflammation, and in particular in the development and maintenance of particular TLO associated lymphoid structures, namely FDC networks and HEV (Lu & Browning 2014).

Signalling via the LTβR has also been implicated in neogenesis of TLOs and / or HEV in cancer. Targeting of an antibody-LTα fusion protein directly to mouse melanomas resulted in neogenesis of TLO-like lymphoid aggregates including PNAd[+] HEV (Schrama et al. 2001). These LTα-induced TLO aggregates could foster an active anti-tumour immune response in the absence of canonical SLOs in LTα^{-/-} animals (Schrama et al. 2008). Expression of LIGHT in a fibrosarcoma cell line resulted in up-regulation of CCL21 and MAdCAM-1, facilitating recruitment of vast numbers of naïve CD8^{+} T lymphocytes, which were then sufficiently activated *in situ* to facilitate rejection of established tumours (Yu et al. 2004). Martinet and colleagues demonstrated that DC-LAMP[+] DCs were the major producers of LTβ ligand in human breast tumours, a cytokine overexpressed in tumour displaying a high density of HEV. Furthermore, the authors showed that DC-LAMP[+] DCs positively correlated with HEV density and were significantly associated with a favourable clinical prognosis (Martinet et al. 2013). Presence of DC-LAMP[+] DCs was also shown to correlate with HEV density in primary melanoma (Martinet et al. 2012). However, despite clustering of DCs around HEVs in breast cancer, the vast majority of DCs are located outside basal laminal layers encapsulating HEV, as in LNs, and are therefore unlikely to be capable of direct contact with endothelial cells; a likely prerequisite for functional LTβR signalling to drive HEV neogenesis (Martinet et al. 2013; Ager & May 2015). Therefore, the precise role

of LT and / or TNF signalling in TLO and / or HEV development within tumours remains to be established.

1.8.2.2 Chemokine Involvement in Tertiary Lymphoid Organ Neogenesis

Chronically inflamed tissues containing TLOs display heightened expression of homeostatic chemokines involved in SLO development, including CXCL12, CXCL13, CCL19 and CCL21 (Pitzalis et al. 2014). In the pancreas, all four lymphoid chemokines are individually capable of inducing TLO formation when overexpressed (Luther et al. 2000; Luther et al. 2002; Chen et al. 2002; Fan et al. 2000; Marinkovic et al. 2006). Conversely, loss of CXCL13, CXCR5, or CCR7 prohibits formation of TLO in disease settings (Rangel-Moreno et al. 2007; Wengner et al. 2007; Winter et al. 2010). These chemokines seem to function upstream of $LT\alpha_1\beta_2$ signalling, as $LT\alpha_1\beta_2$ expression on T or B cells is induced by CCL19, CCL21 or CXCL13 (Luther et al. 2000; Luther et al. 2002).

Human studies have implicated chemokines CCL19, CCL21 and CXCL13 in the formation of intra-tumoural TLOs (Goc et al. 2013). Up-regulated expression of these lymphoid chemokines was found in tumour TLOs of both lung carcinoma and breast carcinoma patients (Gu-Trantien et al. 2013; de Chaisemartin et al. 2011). In lung carcinoma associated TLOs, CCL19 expressing cells belonged predominantly to the mature DC-LAMP[+] DC population, CXCL13 expression was detected on FDCs within GC-like areas, and CCL21 expression was restricted to lymphatic vessels (de Chaisemartin et al. 2011). Alternatively, CXCL13-expressing CD4^{+} Tfh were found in breast carcinoma TLOs, and a strong Tfh signature robustly predicted an increased patient survival rate (Gu-Trantien et al. 2013).

1.8.2.3 Requirement for LTi cells in Tertiary Lymphoid Organ Neogenesis

The recent discovery of adult RORγt^{+} LTi cells, members of the innate lymphoid cell (ILC) family, prompted speculation that such a population could direct TLO neogenesis (Schmutz et al. 2009; Sawa et al. 2010; Pitzalis et al. 2014). Meier and colleagues demonstrated that induction of ectopic lymphoid tissue by over expression

of IL-7 was entirely dependent on adult LTi cells, as TLOs failed to develop in the absence of *RORγt* (Meier et al. 2007). Another study demonstrated the ability of adult WT LTi cells, adoptively transferred into neonatal CXCR5$^{-/-}$ mice, to induce TLOs in the intestine (Schmutz et al. 2009).

However, TLOs can develop in the absence of canonical RORγt^{+} LTi cells. In a mouse model of TLO formation induced by CCL21 overexpression, absence of LTi cells results in a complete lack of LNs and PP, but normal development of TLOs. Instead, mature CD3^{+} CD4^{+} T cells are absolutely required for TLO development (Marinkovic et al. 2006). TLOs also develop in the colon of *Rorc(*γt)$^{-/-}$ animals following inflammatory insult (Lochner et al. 2011). Furthermore, inducible-BALT (iBALT) form in the lungs of *Rorc(*γt)$^{-/-}$ animals subjected to pulmonary inflammation (Rangel-Moreno et al. 2011). Interestingly, *TNF/Rorc(*γt)$^{-/-}$ mice demonstrate development not only of some SLOs but also TLOs in the absence of LTi cells, provided TNFα signalling is increased. However, although TNFα compensates for LTi cell loss to a certain degree, *Id2* expression and LTβR signalling are required for complete SLO organogenesis and *de novo* TLO neogenesis (Furtado et al. 2014).

In the study by Rangel-Moreno and colleagues, the investigators concluded that CD4^{+} T cell-derived IL-17 was responsible for iBALT development by inducing LTα-independent CXCL13 expression (Rangel-Moreno et al. 2011). Other studies have linked IL-17 and/ or T$_{H}$17 cells to TLO neogenesis (Deteix et al. 2010; Peters et al. 2011). A recently published study demonstrated the involvement of T$_{H}$17 and Tfh cells in synovial ectopic lymphoid structure development in both experimental and clinical rheumatoid arthritis (RA). This process was under the control of IL-27, a cytokine that is often elevated in RA patient synovial and serum samples (Jones et al. 2015). Interestingly, the IL-17 producing capability of LTi cells indicates an ancestral relationship between LTis and T$_{H}$17 cells (Pitzalis et al. 2014). However, the identity of a distinct TLO-inducing cell type remains elusive, with B cells and TNF-producing myeloid cells also representing candidates (Lochner et al. 2011; Furtado et al. 2014; Pitzalis et al. 2014).

1.9 High Endothelial Venules in Treg Depleted Carcinogen-Induced Tumours

The Gallimore group has extensively investigated the feasibility of Treg depletion as a mechanism of facilitating a robust effective anti-tumour immune response in the Foxp3^{DTR} mouse model of carcinogenesis. In this model, we induce the formation of fibrosarcomas by injection of MCA into the hind leg. As previously mentioned, near complete ablation of Foxp3$^+$ Treg can be achieved by administration of DT to Foxp3^{DTR} mice (Kim et al. 2007). This strategy has proven effective at unleashing a powerful CD8$^+$ T cell centred anti-tumour immune response that is capable of stunting tumour growth in both B16 melanoma models and MCA models of carcinogenesis (Klages et al. 2010; Teng et al. 2010). However, this strategy is limited, as only a proportion of established tumours in Treg depleted animals demonstrate significant regression. As previously mentioned, it has been suggested that inefficient infiltration of effector T cells into the tumour mass represents a significant impediment to realizing the potential of Treg depletion (Quezada et al. 2008).

To definitively assess the factors underlying an effective anti-tumour immune response following Treg depletion, Hindley and colleagues set out to determine the features distinguishing regressing from progressing tumours (Hindley et al. 2012). Despite profound activation of Foxp3$^-$ CD4$^+$ and CD8$^+$ T cells, and an overall highly significant reduction in tumour growth rate following Treg ablation in this model, a large proportion of Treg depleted animals displayed no significant alteration in tumour control (Kim et al. 2007; Hindley et al. 2012). Tumour growth rate was inversely correlated with the extent of CD4$^+$ and CD8$^+$ T cell infiltration into the tumour mass, rather than T cell activation status, suggesting T cell infiltration following Treg depletion dictates successful tumour control. Critically, successful tumour control was determined by the development of ectopic, isolated HEV within the tumour mass of a proportion of animals. HEV were only ever observed in tumours following Treg depletion, and there was an absolute concordance between HEV presence, high numbers of TIL and tumour growth control (Hindley et al. 2012).

1.10 Hypothesis and Aims

My hypothesis states that Foxp3$^+$ Tregs, having been recruited to the tumour by incompletely understood mechanisms, exert local suppression of immune cell/s. Following Treg depletion and the lifting of immunosuppression, extensive and robust activation of immune cells enables the production of 'HEV-inducing' cytokine(s) or signalling molecule(s) that directs HEV neogenesis in MCA tumours. Considering the profound activation of T and B lymphocytes following Treg depletion, I hypothesise that T and / or B cells are the immune cells responsible for initiating a program of HEV neogenesis in tumours.

Furthermore, in light of data described above, I hypothesise that the 'HEV-inducing' cytokine(s) are LT and / or TNF. My hypothesis then follows that development of PNAd$^+$ HEV in tumours facilitates infiltration of vast numbers of CD4$^+$ and CD8$^+$ T lymphocytes, and possibly other immune cells. These infiltrating immune cells underpin an effective anti-tumour immune response to promote tumour regression (Figure 1.11).

The aims of this PhD thesis were:

1) To investigate mechanisms underlying enrichment of Foxp3$^+$ Tregs in MCA fibrosarcomas (see Chapter Three)

2) To investigate the involvement of;

2a) T and B lymphocytes (see Chapter Four), and

2b) LT and TNF (see Chapter Five)

in HEV neogenesis in MCA fibrosarcomas following Foxp3$^+$ Treg depletion in Foxp3^{DTR} animals

Figure 1.11 | Hypothesis of HEV Neogenesis in Carcinogen-Induced Tumours after Treg Depletion.
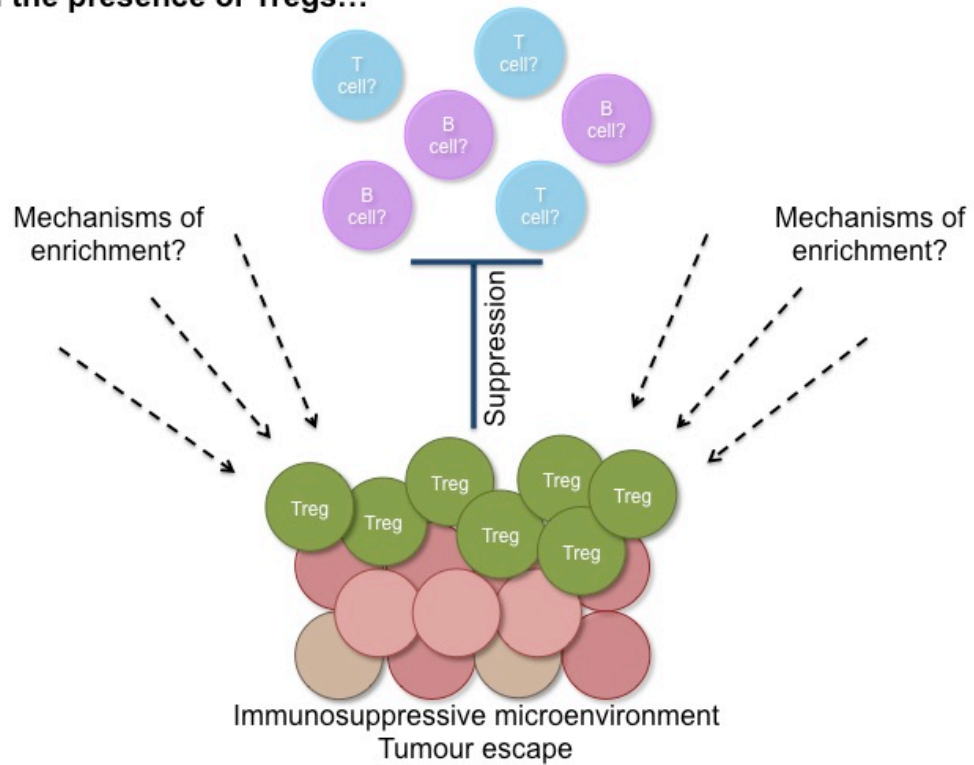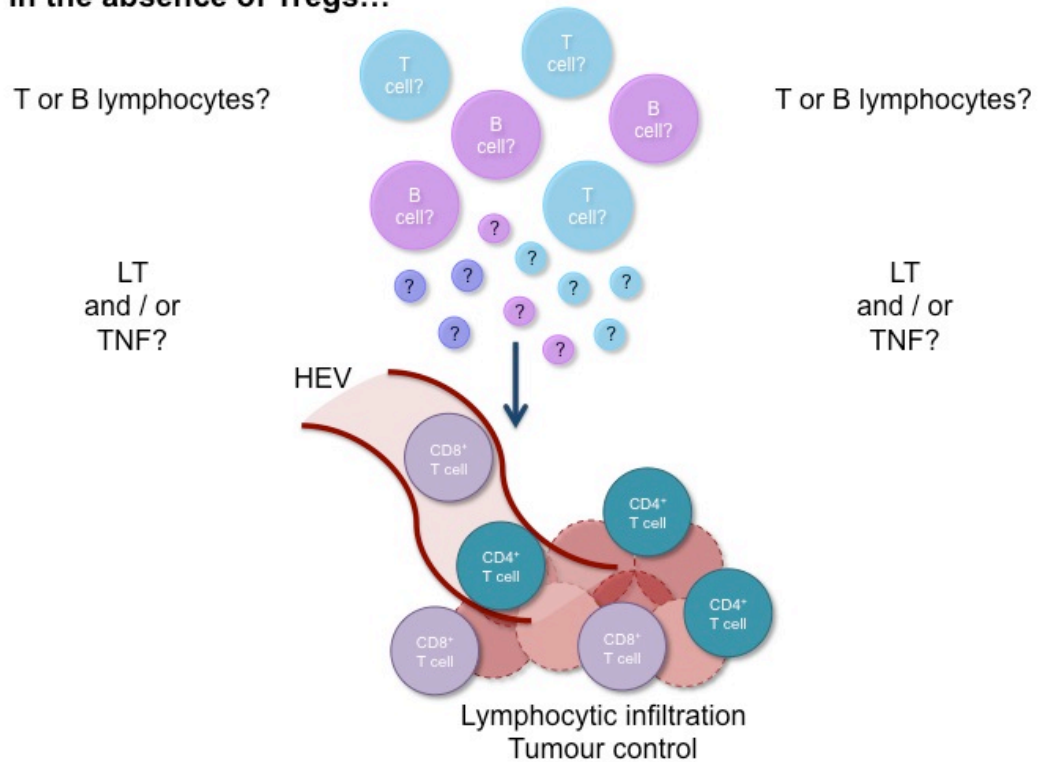
Chapter Two

2 Materials and Methods

2.1 *In vivo* mouse work

2.1.1 Mice

Genetically engineered Foxp3^{DTR} mice, gratefully received from Professor Alexander Rudensky, have been described previously (Kim et al. 2007). Foxp3^{DTR} mice were backcrossed with C57BL/6 mice (bred in house) for ≥5 generations by the host lab. T-bet$^{fl/fl}$Foxp3-Cre conditional KO mice, gratefully received from Professor Stephen Anderton, have been described previously (McPherson et al. 2015). Mice were housed in accordance with UK Home Office regulations, and isolator-bred before being housed in filter-top cages for the duration of experiments.

2.1.2 Tumour Induction, Diphtheria Toxin Administration and Tumour Monitoring

For tumour induction, Foxp3^{DTR} mice, T-bet$^{fl/fl}$Foxp3-Cre conditional KO mice, or Wild-Type C57BL/6 mice, aged 8 to 15 weeks, were anesthetized and injected subcutaneously with 400µg of 3-methylcholanthrene carcinogen (MCA; Sigma-Aldrich) suspended in 100µl olive oil into the left hind leg, as previously described (Hindley et al. 2011). Following MCA injection, mice were monitored for tumour development weekly for up to 18 months. Tumour-bearing mice were sacrificed before their tumours reached 1.5cm in diameter, or if tumours caused apparent discomfort.

For *in vivo* depletion of Foxp3^{+} Tregs, 0.1µg of diphtheria toxin (DT; Sigma-Aldrich) diluted in 100µl sterile phosphate buffered saline (PBS) was administered by intra-peritoneal (i.p.) injection every other day, after development of a palpable tumour.

Tumour size, in mm, was measured using calipers, every other day. The following measurements were taken: tumour leg width, non-tumour leg width, tumour width and tumour height. Tumour growth rate (k, days^{-1}) was calculated using the difference between the tumour and non-tumour leg diameters, using the statistical software package Prism 5 (GraphPad) by the following equation for exponential growth: Y= Y0 x exp (k x X).

2.1.3 Depletion of Immune Cells or Blocking of Signalling Molecule Activity

Hybridomas secreting CD4- and CD8- specific monoclonal antibodies (mAb) have been described previously (Qin et al. 1987; Cobbold et al. 1984). Depleting CD4- and CD8- specific antibodies were produced and purified in house as previously described (Jones 2002). To achieve depletion of CD4$^+$ or CD8$^+$ T cells, or simultaneous depletion of CD4$^+$ and CD8$^+$ T cells, 100µg of anti-CD4$^+$ (clones YTS-191 & YTA-3) and/or anti-CD8$^+$ (clones YTS-156 & YTS-169) mAb were administered by i.p. injection in sterile PBS, alongside DT treatment, at amounts and times stated in Figure 2.1.

Anti-mouse CD20 mAb (clone 18B12 m2a) was gratefully received from Professor Martin Glennie and has been described previously (Williams et al. 2013). To achieve depletion of B cells, a single i.p. injection of 250µg of anti-CD20 was administered on Day 0, after which DT treatments were given every other day starting on Day 1, according to the protocol in Figure 2.1.

For *in vivo* blockade of Lymphotoxin (LT)β receptor (LTβR) signalling, a mouse LT-βR decoy fusion protein (LTβR.Ig) was gratefully received from Dr Jane Grogan or Professor Carl Ware, and has been described previously (Chiang et al. 2009; Benedict et al. 2001; Rooney et al. 2000). LTβR.Ig was administered by i.p. injection every other day, at a dose of 10mg per kg of body weight, according to the protocol in Figure 2.1. For *in vivo* blockade of Tumour Necrosis Factor (TNF) Receptor (TNFR) signalling, clinical grade Etanercept (trade name Enbrel®, Amgen/Wyeth, Cambridge, UK), consisting of a dimeric fusion protein of human TNFR2 (TNFRII) fused to human IgG1 (TNFRII.Ig), gratefully received from Dr Anwen Williams, was dissolved in the supplied vehicle according to the manufacturers' instructions and diluted using sterile PBS. The agent was administered by i.p. injection either every day, at a dose of 2.5mg per kg of body weight, or every other day, at a dose of 5mg per kg of body weight, according to the protocol in Figure 2.1. For an alternative method of *in vivo* blockade of TNFR signalling, an antagonistic rat anti-mouse TNF-α mAb (clone MP6-XT22) was administered by i.p. injection in sterile PBS at amounts and times in Figure 2.1.

Figure 2.1 | Immune Cell Depletion and Cytokine Blockade Treatment Regimes.

2.1.4 Administration of Anti-IL-2 or Anti-IL-2 / IL-2 Complexes

To neutralise IL-2 *in vivo*, 200µg of anti-IL-2 mAb (JES6-1A12; Bio-Xcell) was administered by i.p. injection on 3 consecutive days prior to sacrifice. Control mice were treated with an equal volume of sterile PBS. For treatment with Anti-IL-2/IL-2 complexes, complexes were prepared by incubating 5µg recombinant murine IL-2 (PeproTech) with 50µg of an anti-IL-2 mAb (JES6-1A12 or S4B6-1; Bio-Xcell) for 10 minutes at room temperature (RT), prior to i.p. injection in 200µl of solution on 3 consecutive days prior to sacrifice.

2.1.5 Dissection of Tissues

Spleen, inguinal Lymph Nodes (LN) and occasionally mesenteric LN, were carefully removed from naïve or tumour-bearing mice upon dissection. When required, blood was taken directly from the heart upon dissection and pipetted into Microvette® lithium heparin containing tubes, which were then centrifuged at 13,000 rpm in a microfuge for 5 minutes at RT for plasma isolation. Plasma was stored at -80°C until required. The inguinal LN on the tumour (left) side of tumour-bearing mice was analysed as a 'tumour draining lymph node' (DLN). The inguinal LN on the non-tumour (right) side of tumour-bearing mice was analysed as a 'non-tumour draining lymph node' (NDLN). For naïve (control) mice, the left and right inguinal LN were pooled for analysis. Tumours were carefully resected from tumour bearing mice avoiding local muscle, other normal tissues, and in particular, the local popliteal LN.

2.2 Flow Cytometry

2.2.1 Preparation of Single Cell Suspensions from Tissues

Spleen and LN were homogenized in a multiwell plate using the back of a syringe plunger. Tumours were diced into small pieces in a petri dish, almost to a pulp, using a scalpel blade, before being forced through a 70µm cell strainer (BD Biosciences) using the back of a syringe plunger. Homogenized tissues were resuspended in complete RPMI (RPMI [Invitrogen] supplemented with 2mM L-glutamine, 1mM sodium pyruvate, 50µg/ml penicillin streptomycin and 10% foetal calf

serum) before being passed through a 70μm cell strainer. The single cell suspension was washed by pelleting the cells via centrifugation at 1,500rpm (approx. 450 X G) for 5 minutes, aspirating the supernatant, and resuspending the pellet in complete RPMI. Prior to antibody staining, red blood cells in tumour and spleen cell pellets were lysed by resuspending pellets in 5ml of RBC lysis buffer (Biolegend) for 90 seconds at RT. 20ml of complete RPMI was then added to stop the reaction, and cells were pelleted once more at 1,500rpm for 5 minutes, after which the supernatant was discarded.

2.2.2 Cell Surface Staining

Single cell suspensions were plated out in a 96 round-bottomed well plate at a density of 0.5-1 million cells per well. Cells were washed twice in PBS prior to staining for dead cells using a fixable dead cell staining kit (LIVE/DEAD Aqua; Invitrogen), by adding 3μl (or 6μl for tumour cells) of diluted (1:10 in PBS) LIVE/DEAD Aqua to the cell pellet and mixing. Cells were stained for 15 minutes in the dark prior to washing twice with FACS buffer. Fc Receptors were blocked by adding diluted anti-CD16/32 (93; eBioscience) antibody directly to the cells and incubating for 10 minutes at 4°C in the dark. After another two washes in FACS buffer, cells were stained with a surface stain panel by adding 25-50μl of diluted (in FACS buffer) antibody master mix to the cells, and incubating at 4°C in the dark for 10-15 minutes. Surface antibodies are listed in Table 2.1 below.

2.2.3 Intracellular Antigen and Cytokine Staining

For intracellular cytokine analysis, single cell suspensions (0.5-1 million cells per well) were stimulated in 24 well plates with complete RPMI containing 20 nM phorbol myristate acetate (PMA; Sigma-Aldrich) and 1μg/ml ionomycin (Sigma-Aldrich), at 37°C for 4 hours, prior to surface staining. After 1 hour of incubation, 1μl/ml of GolgiStop (containing monensin; BD Bioisciences) was added to each well. Surface stained cells were subsequently stained for intracellular antigen following 40 minutes to 16 hours of Fixation/Permeabilisation (Foxp3-staining kit, eBiosciences). Intracellular antibodies are listed in Table 2.1 below. For flow cytometric analysis, samples were

acquired on a FACS Canto II flow cytometer (BD Biosciences). Unless stated otherwise, numbers presented in example flow cytometric histograms and dot plots included in Figures represent 'proportion of parent population' statistics. In some cases, absolute number of cells in the daughter population gate per x number of total live cells is presented: this statistic was calculated using the number of acquired events in total and daughter population gates on the flow cytometer.

2.2.4 Flow Cytometric Analysis

Flow cytometric data were analysed using FlowJo software. As a large proportion of data were gathered surrounding expression of markers by conventional CD4$^+$ Foxp3$^-$ T cells (Tconv) and CD4$^+$ Foxp3$^+$ Regulatory T cells (Tregs), an example gating strategy is shown in Figure 2.2. Additionally, the gating strategy for analysis of CD19$^+$ B220$^+$ CD21^{hi} CD23^{lo} CD1d^{hi} Marginal Zone (MZ) B cells in the spleen is shown in Figure 2.3.

Table 2.1 | Flow Cytometry Antibodies

Antigen	Conjugate	Clone	Isotype	Company	Final Concentration (µg/ml)
Surface Antibodies					
CD1d (CD1.1, Ly-38)	Pacific Blue	1B1	Rat IgG2b, κ	Biolegend	10
CD3	PE-Cy5	17A2	Rat IgG2b, κ	BD Biosciences	2
CD4	APC-eFluor 780	RM4-5	Rat IgG2a, κ	eBioscience	2
CD8a	Pacific Blue	53-6.7	Rat IgG2a, κ	BD Biosciences	4
CD8a	APC	53-6.7	Rat IgG2a, κ	eBioscience	2
CD19	PerCP-Cy5.5	1D3	Rat IgG2a, κ	BD Biosciences	2
CD21/CD35	APC	7G6	Rat IgG2b, κ	BD Biosciences	2
CD23	PE	B3B4	Rat IgG2a, κ	Biolegend	2
CD25	PE	PC61	Rat IgG1, λ	BD Biosciences	4
CD45R/ B220	FITC	RA3-6B2	Rat IgG2a, κ	Biolegend	5
CD69	APC	H1.2F3	Armenian Hamster IgG	Biolegend	10
CD69	FITC	H1.2F3	Armenian Hamster IgG1, λ3	BD Biosciences	2.5
CD127 (IL-7Rα)	Brilliant Violet 605	A7R34	Rat IgG2a, κ	Biolegend	1.2
CD183 (CXCR3)	APC	CXCR3-173	Armenian Hamster IgG	eBioscience	4
CD183 (CXCR3)	Brilliant Violet 421	CXCR3-173	Armenian Hamster IgG	Biolegend	4
Intracellular Antibodies					
Foxp3	PE-Cy7	FJK-16s	Rat IgG2a, κ	eBioscience	4
Ki67	Brilliant Violet 421	16A8	Rat IgG2a, κ	Biolegend	2.5
Ki67	FITC	B56	Mouse IgG1	BD Biosciences	2
T-bet	PerCP-Cy5.5	eBio4B10	Mouse IgG1	eBioscience	2
TNFα	FITC	MP6-XT22	Rat IgG1, κ	eBioscience	5
Isotype control antibodies					
Mouse IgG1, κ	PerCP-Cy5.5	MOPC-21	-	Biolegend	(matched to primary)
Armenian Hamster IgG1, κ	FITC	-	-	BD Biosciences	(matched to primary)

Figure 2.2 | Gating Strategy for CD4$^+$ Foxp3$^-$ Tconv and CD4$^+$ Foxp3$^+$ Treg
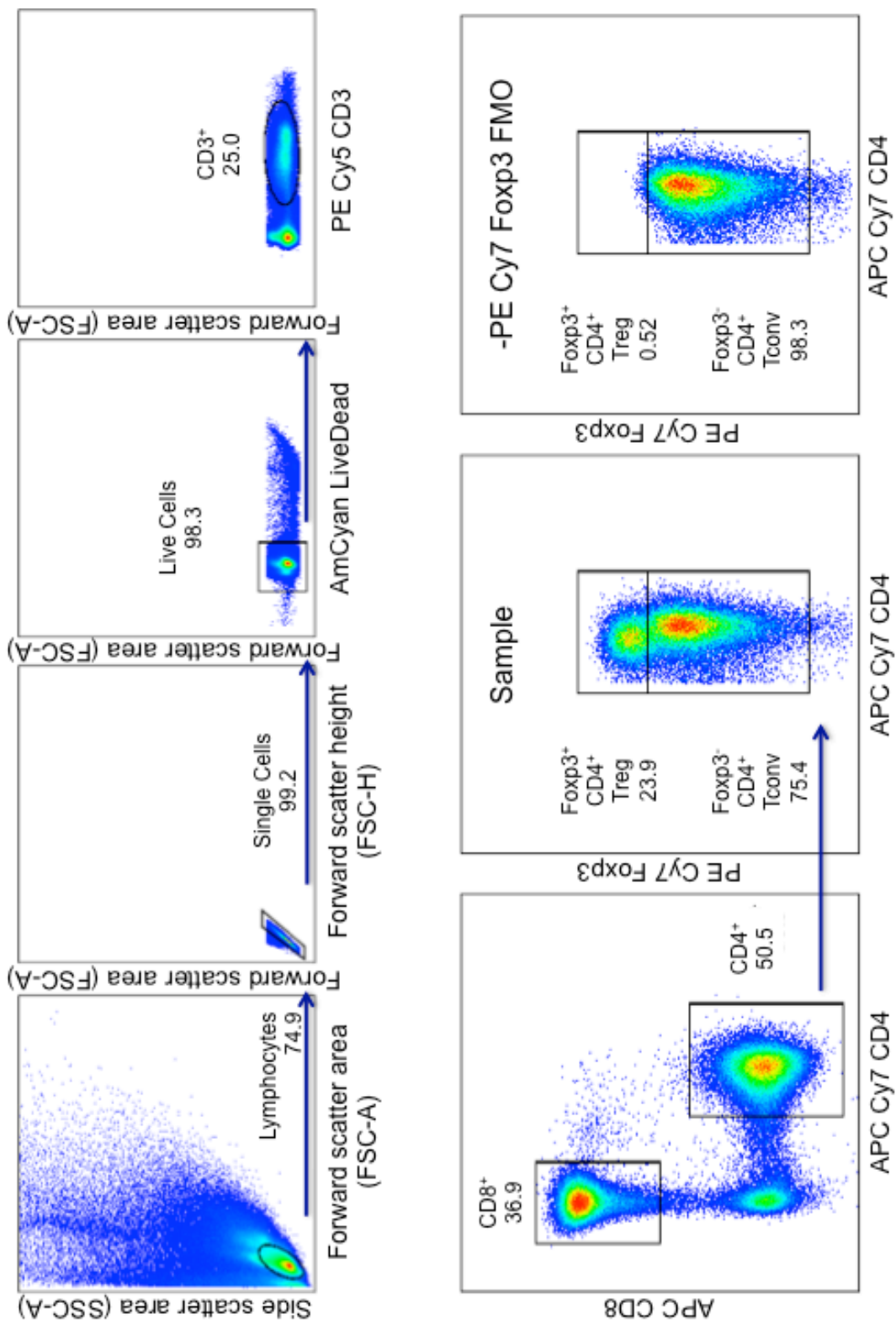
Figure 2.3 | Gating Strategy for Marginal Zone B cells of the Spleen
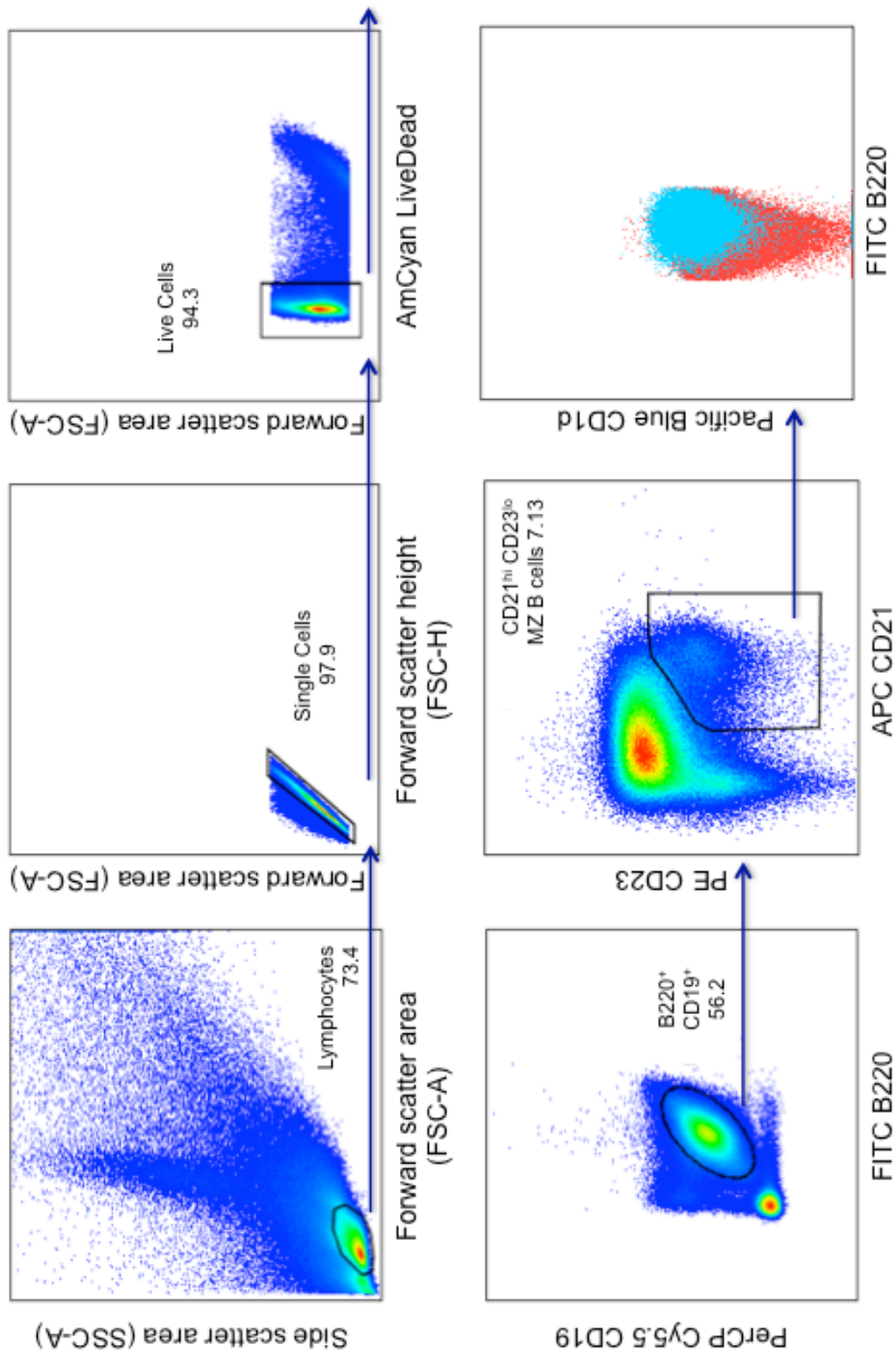
2.3 Immunohistochemistry

2.3.1 Paraffin Sections

Portions of tumours and spleens collected from Foxp3^{DTR} mice were fixed in neutral-buffered formalin solution (NBFS) and embedded in paraffin. 5μm thick sections were cut on a microtome and mounted on glass slides, and then dewaxed in xylene (3 x 5 minutes) and rehydrated via an alcohol gradient (2 x 3 minutes at 100% Methanol (MeOH); 1 x 3 minutes at 90% MeOH; 1 x 3 minutes at 70% MeOH; 1 x 5 minutes in running tap water). Slides were then washed in distilled H$_2$O. For antigen retrieval, slides were microwaved for 8 minutes in pre-warmed 10mmol/L Tris, 1mmol/L EDTA buffer (pH9), cooled for 30 minutes and equilibrated in 1x PBS. Endogenous peroxidase activity was quenched by incubation in Peroxidase Suppressor (Thermo Scientific) for 10-15 minutes at RT. After 3x 3 minute washes in 1x PBS, non-specific antibody binding was blocked by incubating slides in 2.5% Normal Horse Serum Blocking Solution (VectorLabs) for 30 minutes at RT. Slides were incubated in the primary antibody diluted to the appropriate concentration in 1% Bovine Serum Albumin (BSA) in PBS overnight at 4^{0}C. Primary antibodies are listed in Table 2.2 below. The following day, after 3x 3 minute washes in 1x PBS, primary antibodies were detected via a 30 minute incubation using the relevant ImmPRESS^{TM} Horseradish Peroxidase (HRP) Polymer Detection Kit, and subsequently visualized by brief incubation in either Impact DAB (3, 3'-diaminobenzidine; brown) or Vector very intense purple (VIP; purple) HRP substrate (all VectorLabs). Following detection, slides were rinsed briefly in dH$_2$O before counterstain in haematoxylin for 1 minute. Following a 2 minute wash in running tap water, sections were dehydrated via the following alcohol series: 1x 3 minutes at 70% MeOH; 1x 3 minutes at 90% MeOH; 2x 3 minutes at 100% MeOH; 3x 5 minutes in Xylene. Sections were then mounted in mounting medium (distyrene, a plasticizer, and xylene; DPX) and glass coverslips and allowed to dry in a 60^{0}C oven overnight. Sections were analysed using a Nikon microscope, and then scanned for quantification as detailed below.

2.3.2 Frozen Sections

Portions of tumours, spleens and LNs were embedded in optimum cutting temperature (OCT) compound (RA Lamb) and frozen on dry ice. 5µm thick sections were cut using a cryostat machine and fixed in ice-cold acetone for 10 minutes before being aired dried at RT. Slides were washed in 1x PBS (3x 3 minutes). If biotinylated antibodies were to be used, endogenous biotin, biotin receptors and avidin binding sites were blocked by incubation in Avidin D solution for 15 minutes at RT, followed by a brief rinse in 1x PBS, and incubation in Biotin solution for a further 15 minutes at RT. Non-specific antibody binding was blocked by incubating in 2.5% Normal Horse Serum Blocking Solution (VectorLabs) for 30 minutes at RT. Slides were incubated in the primary antibody diluted to the appropriate concentration in 1% BSA in PBS overnight at 4^0C. The following day, after 3x 3 minute washes in 1x PBS, primary antibodies were detected by incubation in a fluorophore-conjugated secondary antibody diluted to the appropriate concentration in 1% BSA in PBS, for 60 minutes at RT. Primary and secondary antibodies are listed in Table 2.2 below. When sections were double or triple stained with more than one unconjugated primary antibody of the same isotype, the first primary antibody was detected with a secondary antibody, prior to fixation in 1% paraformaldehyde (PFA) for 10 minutes at RT. Slides were incubated in the second primary antibody for 60 minutes at RT before detection of this antibody using an appropriate secondary antibody. After 3x 3 minute washes in 1x PBS, slides were fixed in 1% PFA for 10 minutes. Slides were washed a further 2 times in 1xPBS, before excess unreacted PFA on the sections was quenched by a 3 minute wash in 0.3Molar Glycine in PBS. After a final wash in 1x PBS, sections were mounted using Vectashield mounting medium with DAPI (4, 6-diamidino-2-phenylindole; VectorLabs) and glass coverslips, and sealed with nail varnish. Sections were imaged using a Zeiss LSM5 Pascal confocal microscope and serial images assembled using Adobe Photoshop software.

Table 2.2 | Immunohistochemistry Antibodies

Antigen	Conjugate	Clone	Isotype	Company	Final Concentration (µg/ml)
Primary antibodies					
CD4	Purified	RM4-5	Rat IgG2a, κ	Biolegend	1
CD8a (Ly-2)	Purified	53-6.7	Rat IgG2a, κ	eBioscience	1
CD21/CD35	APC	7G6	Rat IgG2b, κ	BD Biosciences	2
CD31 (PECAM-1)	FITC	390	Rat IgG2a, κ	eBioscience	2
CD35	Purified	8C12	Rat IgG2a, κ	BD Biosciences	1
CD45R/ B220	Biotin	RA3-6B2	Rat IgG2a, κ	eBioscience	1
CD45R/B220	Purified	RA3-6B2	Rat IgG2a, κ	eBioscience	2
PNAd	Purified	MECA-79	Rat IgM, κ	Biolegend	2.5
PNAd	Biotinylated	MECA-79	Rat IgM, κ	Biolegend	1
MAdCAM-1	Purified	MECA-367	Rat IgG2a, κ	eBioscience	1
Secondary antibodies					
Rat IgG	Alexa Fluor® 488	-	Donkey IgG	Life Technologies	2
Rat IgG	Alexa Fluor® 568	-	Goat IgG	Life Technologies	2
Streptavidin	Alexa Fluor® 555	-	-	Life Technologies	1
Streptavidin	FITC	-	-	Biolegend	1
Isotype control antibodies					
Rat IgG2a	Biotinylated	MRG2a-83	Mouse IgG	Biolegend	(matched to primary)
Rat IgM κ	Biotinylated	RTK2118	-	Biolegend	(matched to primary)
Rat IgG2a, κ	Purified	RTK2758	-	Biolegend	(matched to primary)
Rat IgM, κ	Purified	RTK2118	-	Biolegend	(matched to primary)
Rat IgG2a κ	FITC	RTK2758	-	Biolegend	(matched to primary)
Rat IgG2b κ	APC	-	-	eBioscience	(matched to primary)

2.4 Quantification of T cells in Tumour Tissue

Immunofluorescently stained frozen tumour sections were used to quantify numbers of CD4$^+$ and / or CD8$^+$ T cells within tumour tissue. Using a fluorescent microscope, numbers of T cells were counted per high power field of view by eye. The average of 10 high power fields of view was calculated for each section.

2.5 Quantification of High Endothelial Venules in Tumour Tissue

Paraffin-embedded tumour sections stained using the anti-mouse PNAd (clone MECA-79) antibody were scanned using a high-resolution digital Zeiss Axio Scan.Z1 slide scanner. Absolute numbers of PNAd$^+$ vessels present within total tumour area, calculated in μm^2, were quantified per slide using Zeiss Zen software, and the density of HEV (HEV density/μm^2) was calculated for each sample. Each individual tumour HEV vessel was drawn around using measurement tools in Zen software, to obtain the vessel area, so that average tumour HEV area could be calculated per sample (see Figure 2.4). Tumours with zero vessels were excluded from the calculation of average vessel area. Calculation of the area occupied by each individual vessel in each tumour enabled the 'total HEV area' to also be calculated, as a proportion of the total tumour area. A summary of the parameters measured is shown in Table 2.3 below.

2.6 Quantification of Lymph Node Cellularity by Haemocytometer Count

20µl of a single cell suspension generated from mashed lymph nodes, as described above, was mixed with 20µl of 0.4% Trypan Blue solution (Thermo Scientific) by pipetting. 20µl of mixed solution was pipetted into one chamber of a disposable haemocytometer. Viable cells, which had not taken up the blue dye, were counted in a block of 16 (4x4) squares by eye under a light microscope, and the number of cells per ml of solution was calculated by: count x 2 x 10^4/ml.

Figure 2.4 | Example of High Endothelial Venule Quantification
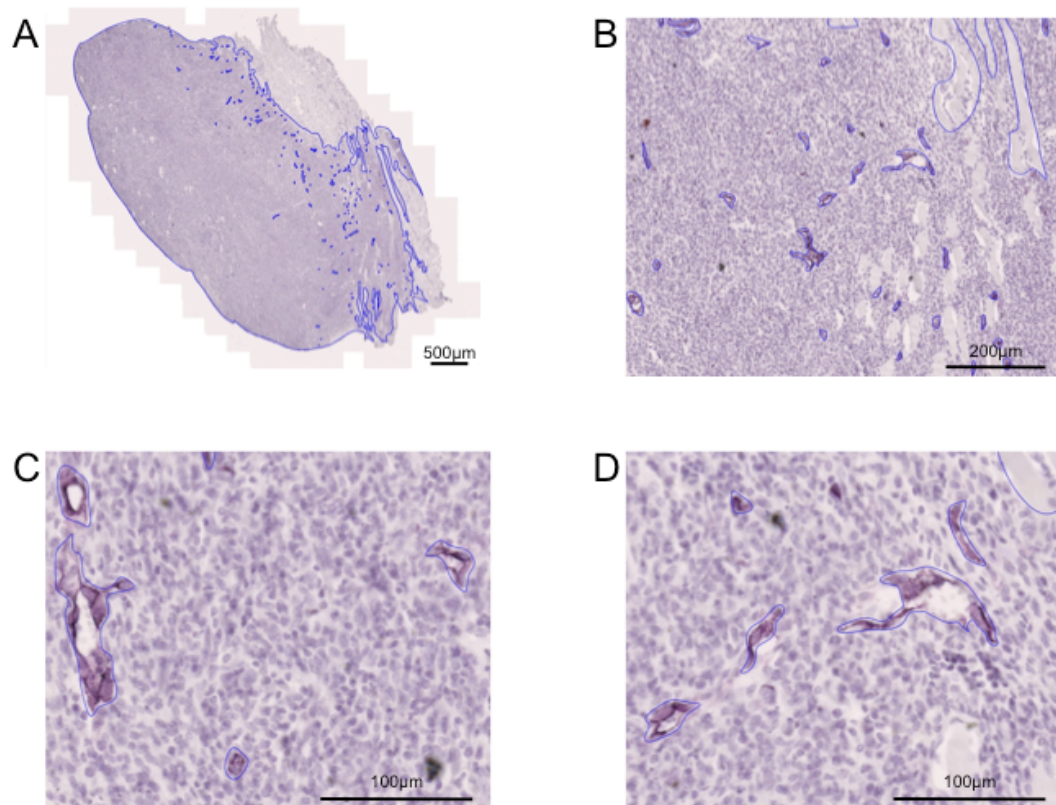
Figure 2.4 | High Endothelial Venules (HEV) were quantified in stained paraffin embedded tumour sections by drawing around individual vessels using a graphics tool in Zen software (blue lines). In addition, the total tumour area (μm^2) was calculated by drawing around the entire tumour mass using the same graphics tool (also blue line, around perimeter). A) Low power image of a quantified tumour section. B) Higher power image of part of a quantified tumour section. Some blue lines are encapsulating HEV vessels while other blue lines are highlighting areas of the tissue that are not tumour tissue and will be exluded from final analysis. C & D) High power images of parts of a quantified tumour section, showing some HEV vessels, and some parts of the tissue to be excluded from analysis (D).

Table 2.3 | High Endothelial Venule Parameters Measured

Parameter	Calculation
HEV Density (per 10^6 μm^2)	(Absolute HEV number / Total tumour area (μm^2)) x 10^6
Total HEV area (%)	(Total HEV area (μm^2) / Total tumour area (μm^2)) x 100
Average HEV area (μm^2)	Total HEV area (μm^2) / Absolute HEV number

2.7 TNFα Enzyme Linked ImmunoSorbent Assay

Enzyme Linked Immunosorbent assay (ELISA) for quantification of TNFα in plasma was performed using the eBioscience Mouse TNF alpha ELISA Ready-Set-Go!® kit, according to the manufacturers specifications. Briefly, the plate was coated

with 100µl / well of capture antibody and incubated overnight at 4°C. Wells were washed 3x before blocking with 200µl / well of 1x Assay Diluent for 1 hour at RT. Standards were diluted in Assay Diluent by two-fold serial dilution; samples were diluted three-fold and added at 50-100µl / well. The plate was incubated for 2 hours at RT, and then washed 5x. 100µl / well of Detection Antibody diluted in Assay Diluent was added per well and the plate incubated for 1 hour at RT. The plate was washed 5x prior to adding 100µl / well of Avidin-HRP diluted in Assay Diluent and incubating for 30 minutes. The plate was washed 7x before adding 50µl / well of Substrate solution and incubating for 15 minutes. 50µl / well of Stop Solution (1Molar H_3PO_4) was added prior to reading the plate at 450nm on a FLUOstar OPTIMA Microplate Reader.

2.8 Gene Expression Analysis

Data previously generated by gene expression profiling were analysed for statistically significant differences in expression of TNF superfamily genes between groups (Hindley et al. 2012). Briefly, gene expression profiling was carried out using MouseRef-8v2.0 whole genome expression bead chip (Illumina) as recommended by the manufacturer. Probe intensity values were corrected by background subtraction in GenomeStudio software and subsequently log_2 and baseline (median) transformed using Genespring software (Agilent) before analysis of genes. Data are therefore presented as relative gene expression, calculated as log_2-fold change relative to the global median of genes.

2.9 *In vitro* Treg Suppression Assay

Spleen and NDLN were a source of effector T cells, and NDLN and DLN, Spleen and Tumour were a source of CD69$^-$ and CD69$^+$ Tregs. Single cell suspensions were prepared as above. Cell suspensions were stained in a 96 well round bottomed plate using LIVE/DEAD Aqua, anti-CD3, anti-CD4, anti-CD25 and anti-CD127 mAb. CD3$^+$ CD4$^+$ CD25^{lo} Tconvs, CD3$^+$ CD4$^+$ CD25^{hi} CD127^{lo} CD69$^+$ Tregs and CD3$^+$ CD4$^+$ CD25^{hi} CD127^{lo} CD69$^-$ Tregs were sorted using a customized 20-parameter FACSAria

II flow cytometer (BD Biosciences). Post-sort purity checks on practice cell sorts using the same panel of antibodies 2 days earlier revealed greater than 98% purity.

Following sorting, Tconvs were washed in Hank's Balanced Salt Solution (HBSS) and pelleted cells resuspended in warm complete RPMI, at a concentration of 1×10^6 cells per ml. 0.4µl of 2.5mM CellTrace stock solution prepared in Dimethyl sulfoxide (DMSO; Invitrogen) was added per ml of cell suspension, and cells incubated for 20 minutes at RT, away from light. 5x the original staining volume of complete RPMI was added and the cells were incubated for 5 minutes at RT. Cells were pelleted by centrifugation (5 minutes, 1500rpm), and resuspended in warm complete RPMI at a concentration of 2.8×10^5 cells per ml, to deliver 14,000 effector cells in 50µl.

Sorted Treg populations were washed once in HBSS, pelleted and resuspended in warm complete RPMI culture medium (complete RPMI supplemented with β-Mercaptoethanol, Minimal Essential Media Non Essential Amino Acids (MEM NEAA 100X; gibco) and 5mM N-2-hydroxyethylpiperazine-N-2-ethane sulfonic acid (HEPES buffer solution; gibco)). 14,000 Tconvs per well were incubated with anti-mouse CD3/CD28 dynabeads (Invitrogen) at a ratio of 1:2 (beads:Tconvs), with titrating numbers of Tregs, in complete RPMI culture medium for 120 hours. After 72 hours, 100µl of fresh, warm complete RPMI culture medium was added to each well. At the end of culture, cells were stained with LIVE/DEAD Aqua, and Fc Receptors were blocked prior to cell surface staining with anti-CD3, anti-CD4 and anti-CD25. Dilution of the CellTrace Violet dye was measured by flow cytometry on a FACS Canto II flow cytometer (BD Biosciences). Addition of the CD25 antibody enabled exclusion of the CellTrace Violet negative, CD25^{hi} Tregs present in some samples.

2.10 Statistical Analyses

All statistical analyses were performed using GraphPad Prism software, except for Linear Models, which were performed in R-statistics software with the help of an in-house biostatistician. Details of statistical tests used are shown in Figure legends and / or in text (footnotes).

Chapter Three

3 Results: Mechanisms of Foxp3$^+$ Treg Enrichment in Tumours

3.1 Introduction

The observation that Foxp3$^+$ Tregs are enriched in tumours has been made in numerous mouse models and human cancer patients (Ondondo et al. 2013). In fact, Tregs can represent up to 40-50% of the CD4$^+$ T cell pool in the MCA-induced fibrosarcomas studied herein (Betts et al. 2007). Our lack of knowledge concerning mechanisms of Treg enrichment significantly impedes the design of therapies to prevent the accumulation of these immunosuppressive cells in tumours.

Several mechanisms could explain the accumulation of Tregs in tumours (see Section 1.6.2 in Chapter One). One idea involves preferential migration of Tregs in response to chemokines expressed by tumour cells and/or the surrounding tumour stroma (Ondondo et al. 2013). Our recently published study investigated the chemokine profile of MCA-induced tumours and compared chemokine receptor expression profiles between tumour infiltrating Foxp3$^-$ Tconv and Foxp3$^+$ Treg. Whilst both Foxp3$^-$ and Foxp3$^+$ T cells employ multiple, overlapping chemokine receptors to migrate to the tumour, a site characterised by expression of type-1 inflammatory chemokines, specific recruitment of Foxp3$^+$ Tregs does not occur via a distinct chemokine axis (Ondondo et al. 2014[a]).

Mouse and human CD4$^+$ Tregs in peripheral lymphoid organs including LNs and spleen demonstrate more active proliferation than CD4$^+$ Tconv under normal physiological conditions (Hori et al. 2002; Fisson et al. 2003; Attridge & Walker 2014; Pierson et al. 2013). However, our recently published data indicate that the difference between the proportions of proliferating Tconv and Treg cells is significantly greater within the tumour compared to LNs and spleen. This difference is due to a significant increase in the percentage of proliferating Tregs within the tumour (approximately 45%), compared to normal lymphoid tissue (approximately 20%) (Colbeck et al. 2015). The vast majority of proliferating Foxp3$^+$ T cells in MCA tumours also express Helios,

[1] One-Way ANOVA with Tukey's multiple comparison test [2] Mantel-Cox log rank test
[3] Mann Whitney test

which is expressed predominantly in tTregs (Thornton et al. 2010). These data confirm that Tregs in MCA tumours are highly proliferative, and thymus-derived. These findings are in support of previous data published by our group demonstrating the largely distinct TCR clonotypes of Foxp3^{-} and Foxp3^{+} CD4^{+} tumour-infiltrating T cell sub-populations, suggesting a minimal contribution by conversion of Tconv into Tregs in Treg enrichment (Hindley et al. 2011).

Under normal physiological conditions, the considerable cellular proliferation demonstrated by Tregs *in vivo* is coupled to enhanced cell death: Tregs exhibit an enhanced propensity to undergo apoptosis relative to Foxp3^{-} CD4^{+} T cells (Pandiyan & Lenardo 2008; Vukmanovic-Stejic et al. 2006; Taams et al. 2001). Cytokine-withdrawal induced apoptosis in fact plays a key role in setting the size of the peripheral Treg pool during homeostasis (Pierson et al. 2013). In line with these data, we have previously observed that a lower proportion of Tregs than Tconv express the anti-apoptotic factor Bcl-2 in LNs and spleen of tumour-bearing animals. However, the proportion of tumour infiltrating Treg and Tconv expressing Bcl-2 is almost equal. Furthermore, whilst Tregs incorporate higher levels of the dead cell exclusion dye 7AAD than Tconvs in lymphoid tissues, a significantly lower proportion of intra-tumoural Tregs take up 7AAD than intra-tumoural Tconv (unpublished data). These data corroborate the notion that Tregs within the tumour are less prone to death by apoptosis than their counterparts in lymphoid tissues. Taken together, these data indicate that enhanced proliferation and survival of tumour infiltrating Tregs cooperatively promote enrichment of Tregs in tumours. We have found that Tregs also demonstrate enhanced activation relative to Tconvs in MCA tumours, by virtue of their heightened expression of a number of cell surface activation markers (Colbeck et al. 2015).

I aimed to investigate further the mechanisms underlying accumulation of Foxp3^{+} Tregs in tumours, using the well-established mouse model of MCA-induced carcinogenesis. I hypothesised that in addition to heightened proliferation and activation, and enhanced survival, Tregs ensure dominance over Tconv in the tumour microenvironment by expression of particular cell surface and/ or intracellular markers,

[1] One-Way ANOVA with Tukey's multiple comparison test [2] Mantel-Cox log rank test
[3] Mann Whitney test

perhaps facilitating their retention, and by exploitation of limited resources within the tumour microenvironment (Figure 3.1). Specifically, I investigated:

- expression of early activation and retention markers on intra-tumoural Foxp3^{+} Tregs;

- a role for competition for limited IL-2 with conventional T cells in enrichment of intra-tumoural Foxp3^{+} Tregs within the tumour;

- expression of the T_H1-associated transcription factor T-bet on intra-tumoural Foxp3^{+} Tregs.

Figure 3.1 | Hypothesis of Treg Enrichment in MCA-Induced Tumours.
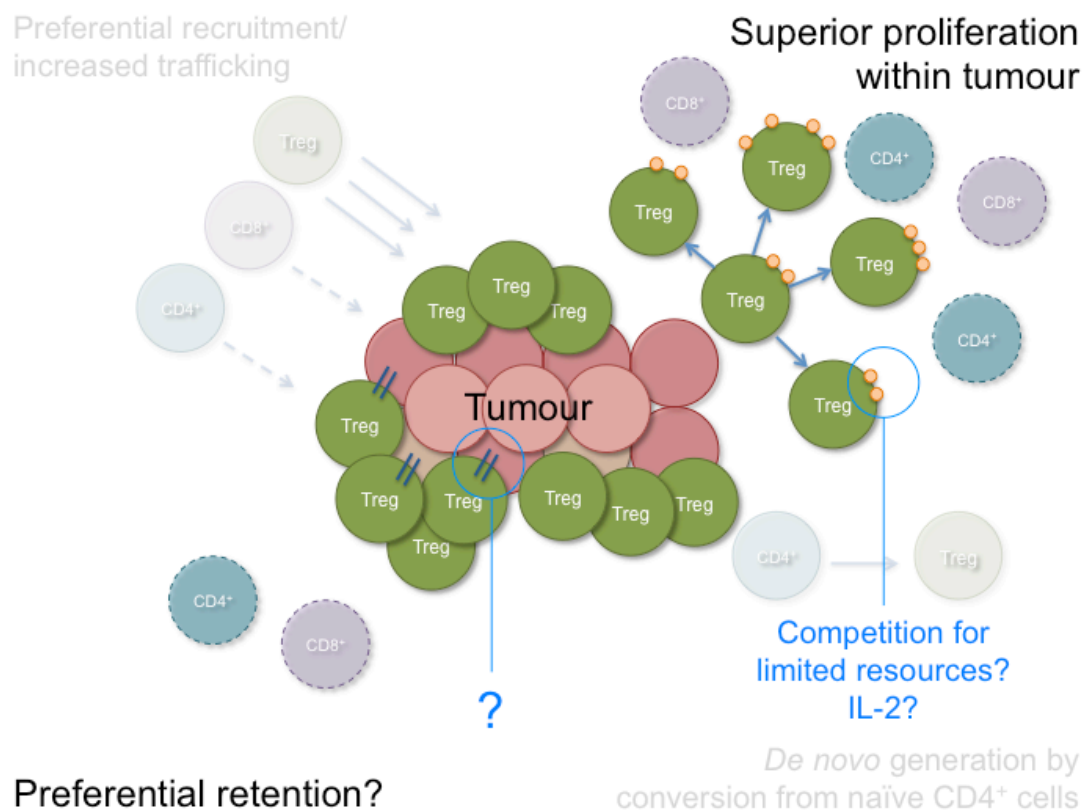
3.2 Results: Tumour-infiltrating CD4^{+} T cells are Enriched for Inflammation-Seeking T_H1-like Tregs

Previous studies have reported that Tregs can express the T_H1 associated chemokine receptor CXCR3 in response to T_H1 polarising cues, and that these CXCR3^{+} Tregs accumulate at peripheral sites of inflammation to specifically suppress T_H1 and CTL responses (Campbell & Koch 2011; Redjimi et al. 2012; Koch et al. 2009; O'Connor et al. 2012). Considering the multitude of studies highlighting a crucial role for T_H1 and CTL cells in the anti-tumour response to MCA induced fibrosarcomas, I explored the possibility that the enriched pool of intra-tumoural Tregs reflect this T_H1 orientated immune response (Koebel et al. 2007; Ondondo et al. 2013). When I analysed tumour-infiltrating T cells for CXCR3 expression, a high proportion of tumour-infiltrating Tregs were CXCR3^{+} (Figure 3.2). In fact, the majority of intra-tumoural Tregs expressed CXCR3 (56.34% mean ± 6.267 SD; Figure 3.3 A). Furthermore, the majority of Ki67^{+} proliferating Tregs in the tumour expressed CXCR3 (59.54% mean ± 5.231 SD), as was true for intra-tumoural Tconvs (Figure 3.3 B). The proportion of either total or Ki67^{+} proliferating Tregs expressing CXCR3 was significantly greater in the tumour relative to the spleen and LNs, and in the tumour draining LN (DLN) relative to the non-draining LN (NDLN)[1] (Figure 3.3 A-B).

Several studies have reported that CXCR3^{+} Tregs are "T_H1-like" by virtue of transient expression of T-bet, the master regulator of T_H1 cells (Szabo et al. 2000; Koch et al. 2009; Campbell & Koch 2011; Redjimi et al. 2012; O'Connor et al. 2012). In line with these data, I consistently found T-bet expression in a proportion of both intra-tumoural Foxp3^{-} and Foxp3^{+} CD4^{+} T cells (Figure 3.4). Significantly higher proportions of intra-tumoural Foxp3^{-} and Foxp3^{+} CD4^{+} T cells expressed T-bet than those cells in other compartments[1] (Figure 3.5 A). Collectively these data are compatible with the hypothesis that in MCA-induced tumours, the accumulating Tregs are so-called T_H1-like Tregs mirroring the T_H1-orientated immune response targeted for suppression.

---

[1] One-Way ANOVA with Tukey's multiple comparison test [2] Mantel-Cox log rank test [3] Mann Whitney test
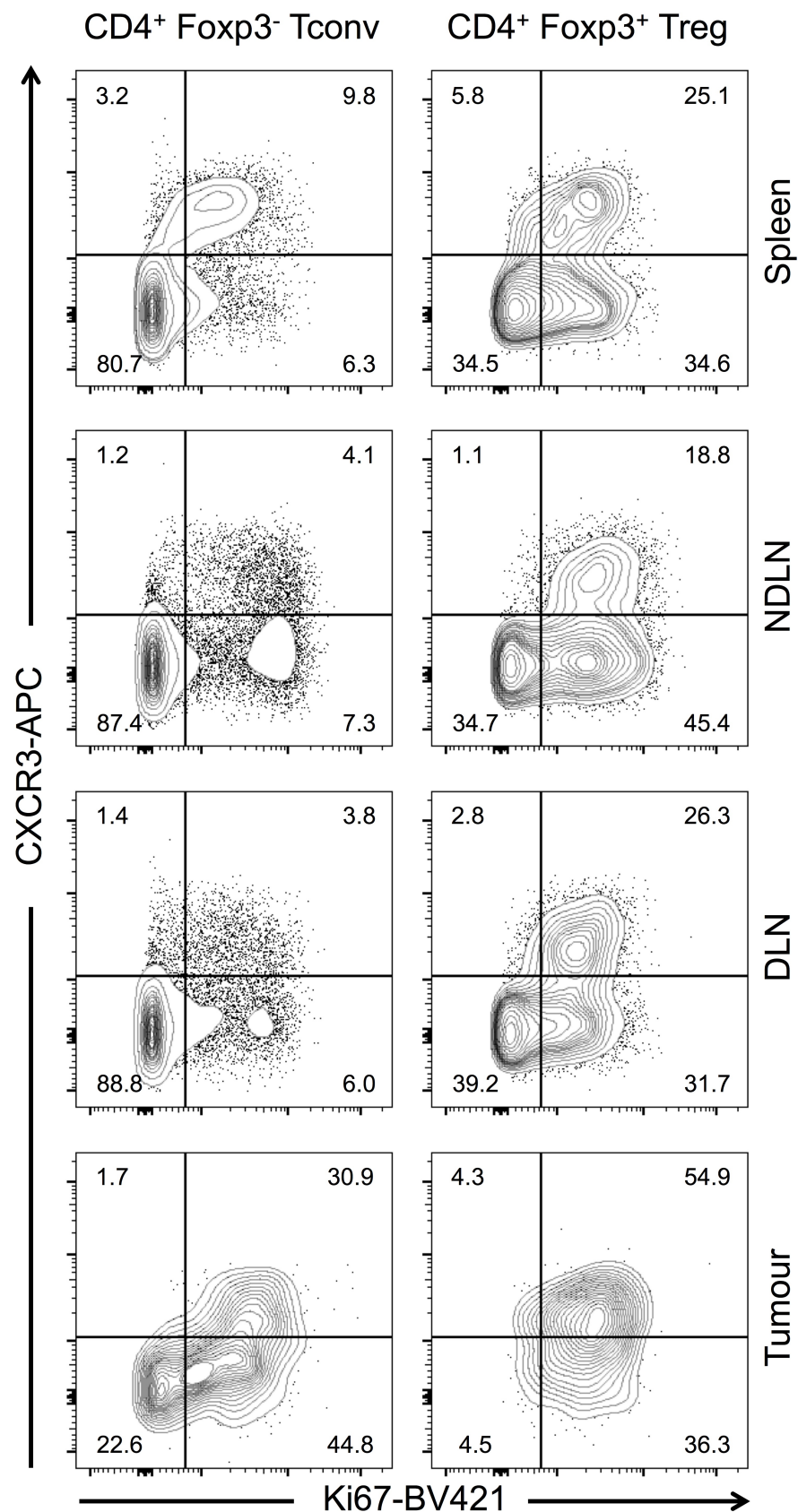
Figure 3.2 | The majority of tumour infiltrating Foxp3^{+} Treg express CXCR3.
Representative flow cytometry plots showing proportion of T cells expressing CXCR3 (y axis) and Ki67 (x axis) in Spleen, tumour non-draining lymph nodes (NDLN), tumour draining lymph node (DLN) and tumour of one animal. Cells are gated on live CD4^{+} Foxp3^{-} conventional T cells (Tconv; left column), or live CD4^{+} Foxp3^{+} regulatory T cells (Treg; right column). Numbers represent proportion of cells in each quadrant.
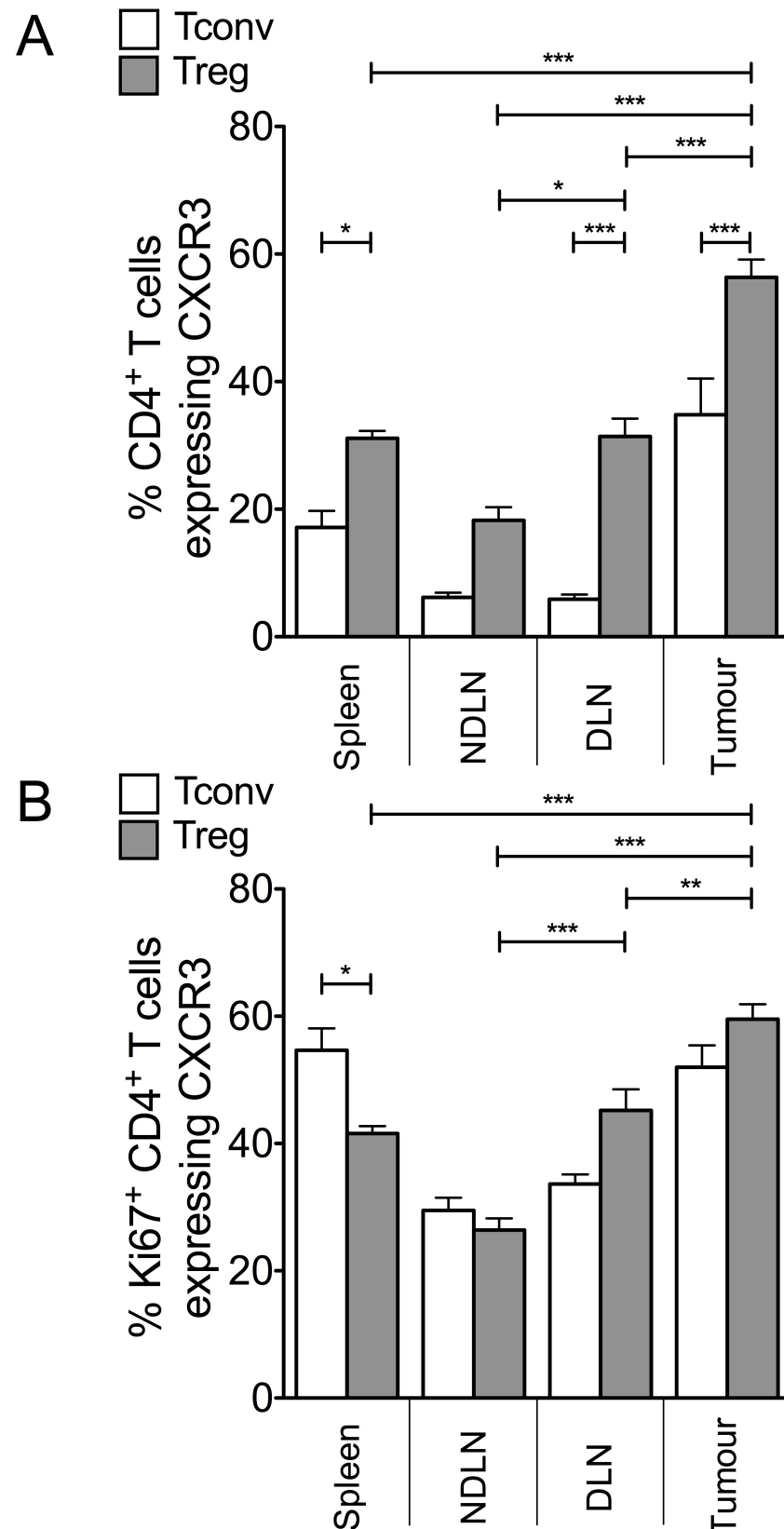
Figure 3.3 | A large proportion of total and Ki67^{+} proliferating Tconv and Treg express CXCR3 in tumour.

Bar charts showing the proportion of total CD4^{+} Foxp3^{-} conventional T cells (Tconv; white bars), and total CD4^{+} Foxp3^{+} regulatory T cells (Tregs; grey bars) (A), and those expressing Ki67 (B), that also express CXCR3, in spleen, tumour non-draining lymph node (NDLN), tumour draining lymph node (DLN), and tumour. N = 5. Data are presented as mean ± standard deviation (SD). Statistical significance was determined by One-way ANOVA with Tukey's multiple comparison tests to compare pairs of means (* = $P{\le}0.05$, ** = $P{\le}0.01$, *** = $P{\le}0.001$).

[1] One-Way ANOVA with Tukey's multiple comparison test [2] Mantel-Cox log rank test
[3] Mann Whitney test
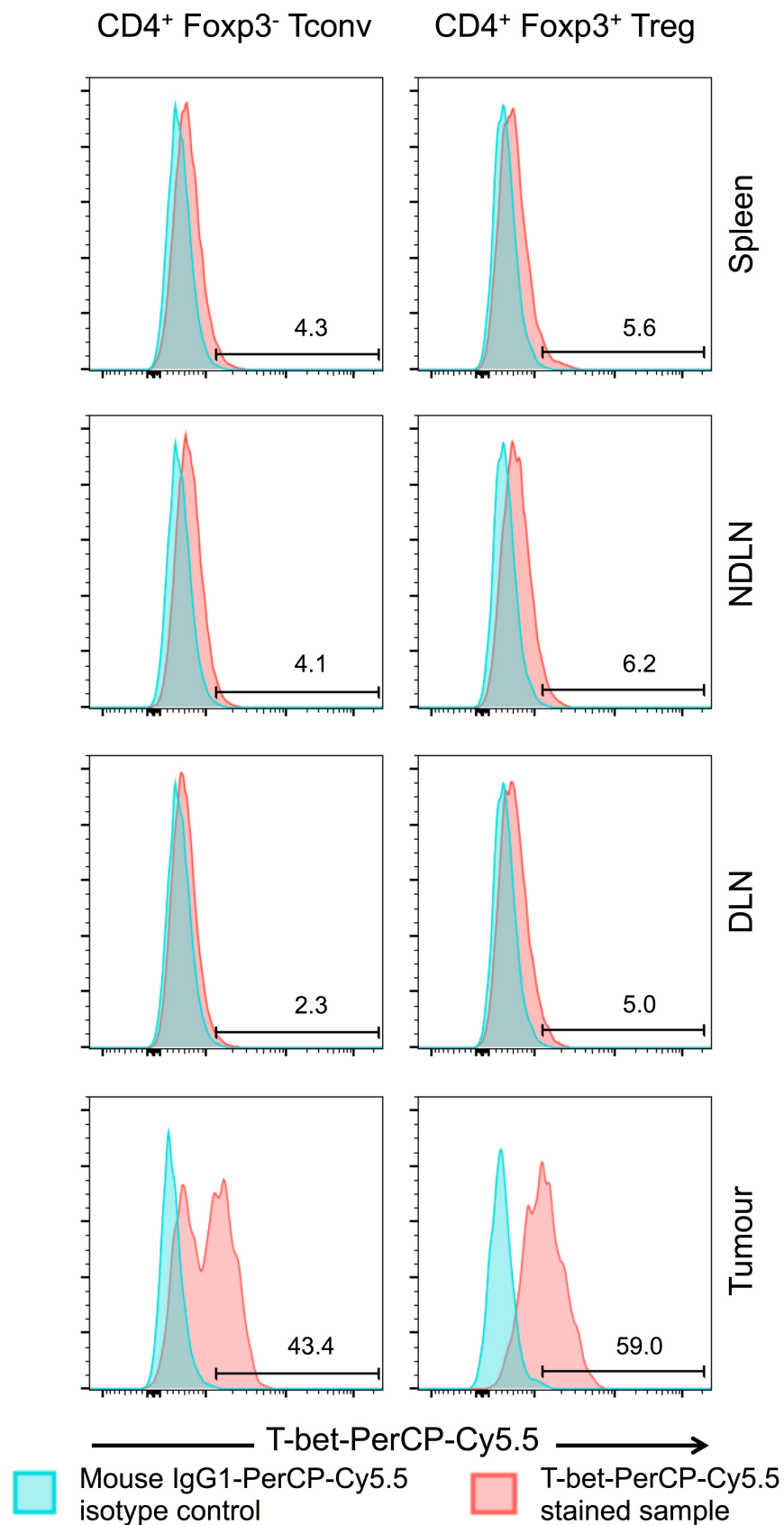
Figure 3.4 | A large proportion of Tconv and Treg express T-bet in tumour.
Representative flow cytometry plots showing proportion of T cells expressing T-bet (x axis) in spleen, tumour non-draining lymph node (NDLN), tumour draining lymph node (DLN), and tumour of one animal. Cells are gated on live CD4$^+$ Foxp3$^-$ conventional T cells (Tconv; left column), or live CD4$^+$ Foxp3$^+$ regulatory T cells (Treg; right column). Numbers represent proportion of cells positive for T-bet expression. Stained samples are shown in red; samples stained using the isotype control are shown in blue.

[1] One-Way ANOVA with Tukey's multiple comparison test [2] Mantel-Cox log rank test
[3] Mann Whitney test
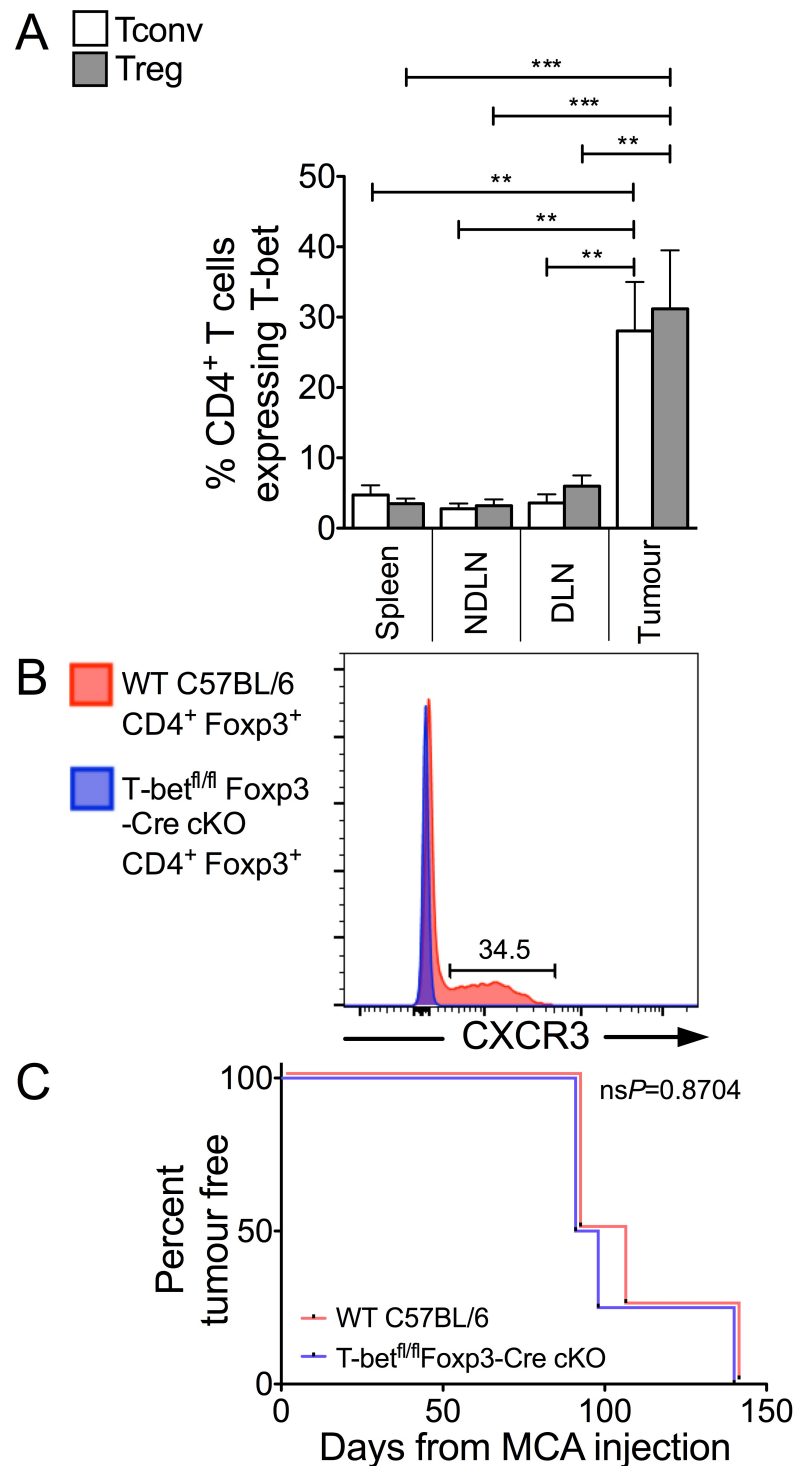
Figure 3.5 | T-bet expression by Treg is dispensable for Treg-mediated suppression of anti-tumour immune responses.

(A) Bar chart showing the proportion of total CD4^{+} Foxp3^{-} conventional T cells (Tconv; white bars) and total CD4^{+} Foxp3^{+} regulatory T cells (Treg; grey bars) that express T-bet in spleen, tumour non-draining lymph node (NDLN), tumour draining lymph node (DLN) and tumour. N = 5. Data are presented as mean ± standard deviation (SD). Statistical significance was determined by One-way ANOVA with Tukey's multiple comparison tests to compare pairs of means (* = $P \leq 0.05$, ** = $P \leq 0.01$, *** = $P \leq 0.001$). (B) A representative flow cytometry plot showing the proportion of CD4^{+} Foxp3^{+} Tregs (gated on live CD4^{+} Foxp3^{+} lymphocytes) that express CXCR3 in blood of Wild Type C57BL/6 (red) and T-bet^{fl/fl}Foxp3-Cre conditional knock out (cKO) animals (purple). The number represents the proportion of Tregs expressing CXCR3 in Wild Type. (C) Incidence of MCA-induced tumours (per cent of animals tumour free X days after MCA injection) for Wild Type C57BL/6 mice (red) and T-bet^{fl/fl}Foxp3-Cre cKO mice (purple). N = 4. Statistical significance was determined by a log rank (Mantel-Cox) test.

[1] One-Way ANOVA with Tukey's multiple comparison test [2] Mantel-Cox log rank test
[3] Mann Whitney test

I hypothesised that if T-bet expression is necessary for the ability of Tregs to suppress T_H1 responses, as is suggested in the literature (Campbell & Koch 2011; Koch et al. 2009), and promote tumour growth, then tumour development should be better controlled in the absence of T-bet expressing Tregs. I used mice genetically engineered to lack T-bet expression specifically in Foxp3^{+} cells (T-bet^{fl/fl}Foxp3-Cre conditional KO mice) (McPherson et al. 2015). As CXCR3 expression is under the control of T-bet in Treg cells, Treg in T-bet^{fl/fl}Foxp3-Cre conditional KO mice also display abolished CXCR3 expression (Koch et al. 2009; McPherson et al. 2015). The lack of CXCR3 expression in Foxp3^{+} Tregs in T-bet^{fl/fl}Foxp3-Cre conditional KO mice was confirmed by flow cytometric analysis of blood from the conditional KO animals relative to that from control Wild Type C57BL/6 animals (Figure 3.5 B). To test the hypothesis, I compared the incidence of MCA-induced tumours in T-bet^{fl/fl}Foxp3-Cre conditional KO and WT C57BL/6 mice and found that tumour incidence was comparable between the groups as there was no statistically significant difference[2] (Figure 3.5 C). Thus, whilst these data show that in MCA-induced tumours, approximately 50% of tTregs are "T_H1-like", I have no evidence that T-bet is required for Treg-mediated suppression in the tumour environment.

[1] One-Way ANOVA with Tukey's multiple comparison test [2] Mantel-Cox log rank test
[3] Mann Whitney test

3.3 Results: Competition for IL-2 does not account for the Enrichment of Intra-Tumoural Foxp3^{+} Tregs

The ratio of Tregs to Tconvs under homeostatic conditions is tightly controlled by bioavailability of IL-2. Tregs are unable to synthesize IL-2 but constitutively express CD25, part of the high affinity IL-2 receptor, suggesting they may have the ability to exploit the IL-2 resource provided by other T cells (Boyman & Sprent 2012). Tregs have been shown to indirectly induce apoptosis of conventional CD4^{+} T cells via deprivation of pro-survival cytokines that signal through the common cytokine γ-chain receptor, such as IL-2 (Pandiyan et al. 2007). Furthermore, Tregs have been shown *in vitro* and *in vivo* to out-compete Tconvs for IL-2, particularly under conditions where its production is limited (Almeida et al. 2006).

I postulated that competition for a limited resource of IL-2 in the tumour represents a key component of intra-tumoural Treg proliferation and subsequent enrichment. Studies in our lab have shown that a lower proportion of Tconvs within MCA tumours express intracellular IL-2 compared to those in spleen and LNs (Colbeck et al. 2015). Analysis of intracellular IL-2 expression by intra-tumoural Tconvs represents a surrogate measure of the available IL-2 present in the tumour microenvironment.

I therefore hypothesised that IL-2 is limited in the tumour and that Tregs out-compete Tconvs for this limited resource by virtue of CD25 expression. To test this hypothesis I injected tumour-bearing mice with anti-IL-2 monoclonal antibodies (JES6-1A12) for three consecutive days and analysed T cell proportions and marker expression by flow cytometry. Whilst IL-2 neutralisation resulted in a significant decrease in the proportion of Ki67^{+} proliferating CD4^{+} Tconv, CD4^{+} Treg and CD8^{+} T cells in lymphoid organs, the observed trend towards a decrease in proliferation of these cell subsets in the tumour failed to reach significance[3] (Figure 3.6). Furthermore, neutralisation of IL-2 did not affect the ratio of Treg to Tconv in any of the compartments studied including the tumour[3]: this was observed when data were analysed as either percentage of CD4^{+} T cells (Figure 3.7) or absolute number of

[1] One-Way ANOVA with Tukey's multiple comparison test [2] Mantel-Cox log rank test
[3] Mann Whitney test

Tconv and Treg (data not shown). These data suggest that limited IL-2 is not responsible for dictating the perturbed ratio of Treg to effector T cells in tumour microenvironments. IL-2 neutralisation did significantly decrease the proportion of CD4^{+} Tregs expressing CD25 in all compartments studied, including the tumour, in corroboration of previous data showing that IL-2 directly regulates CD25 gene expression[3] (Figure 3.8) (Kim et al. 2001). The proportion of CD8^{+} T cells expressing CD25 was also significantly decreased in LNs[3] (Figure 3.8). These CD25 data confirm that the antibody successfully accessed the tumour microenvironment.

To further explore the potential role of IL-2 in maintenance of an altered Treg: Tconv ratio in tumours, I injected anti-IL-2/IL-2 complexes into tumour-bearing hosts and again analysed T cell proportions and marker expression by flow cytometry. I used two different anti-IL-2 monoclonal antibody-IL-2 complexes, which exhibit functional dichotomy in terms of the cellular subsets they expand or restrict *in vivo*. The JES6-1A12 antibody binds IL-2 in such a way that precludes the interaction of this cytokine with low affinity IL-2 receptors, so that the JES6-1A12-IL-2 complex favours stimulation of cells expressing the high affinity IL-2 receptor, namely Foxp3^{+} Tregs. Conversely, binding of a second anti-IL-2 monoclonal antibody, S4B6, apparently occludes interactions between IL-2 and the high affinity IL-2 receptor but allows interactions with the lower affinity receptor. Complexes formed between this antibody and IL-2 therefore favour preferential stimulation of CD8^{+} T cells and other low affinity IL-2 receptor bearing cells such as Foxp3^{-} Tconvs, over Foxp3^{+} Tregs (Boyman et al. 2006; Boyman & Sprent 2012; Rojas et al. 2014).

[1] One-Way ANOVA with Tukey's multiple comparison test [2] Mantel-Cox log rank test
[3] Mann Whitney test
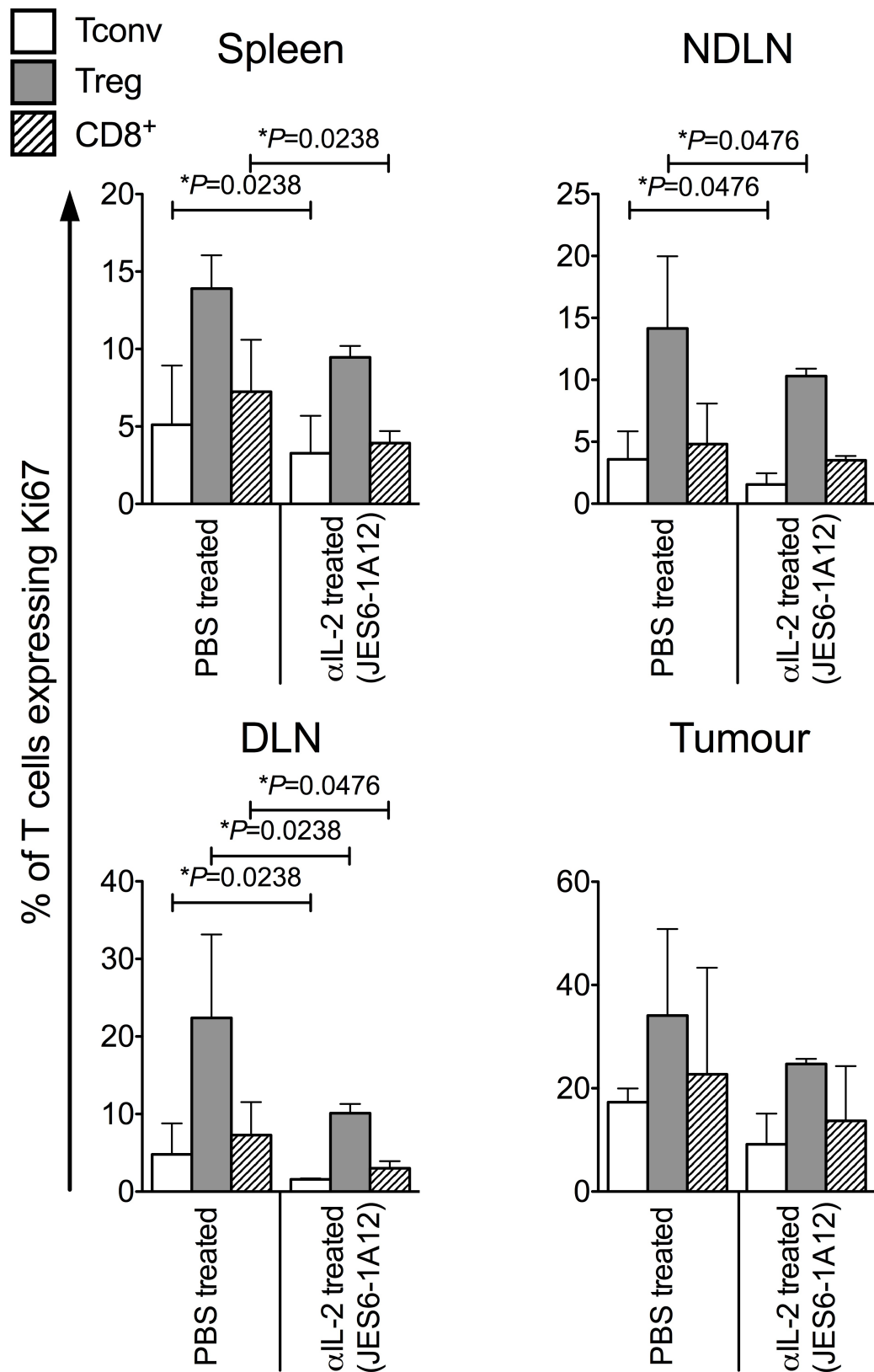
Figure 3.6 | Neutralisation of IL-2 results in significant reductions in the proportions of proliferating T cells in lymphoid organs, but only modest reductions in tumour.

Bar charts showing the proportion of CD4+ Foxp3- conventional T cells (Tconv; white bars), CD4+ Foxp3+ regulatory T cells (Treg; grey bars) and CD8+ T cells (dashed bars) expressing Ki67 in spleen, tumour non-draining lymph node (NDLN), tumour draining lymph node (DLN) and tumour of PBS-treated control animals or experimental animals treated with the JES6-1A12 anti-IL-2 monoclonal antibody. N = 3 experimental; 6 control. Data are presented as median ± interquartile range (IQR). Statistical significance was determined by individual Mann Whitney *t* tests between each cell type in control and treated groups.

[1] One-Way ANOVA with Tukey's multiple comparison test [2] Mantel-Cox log rank test
[3] Mann Whitney test
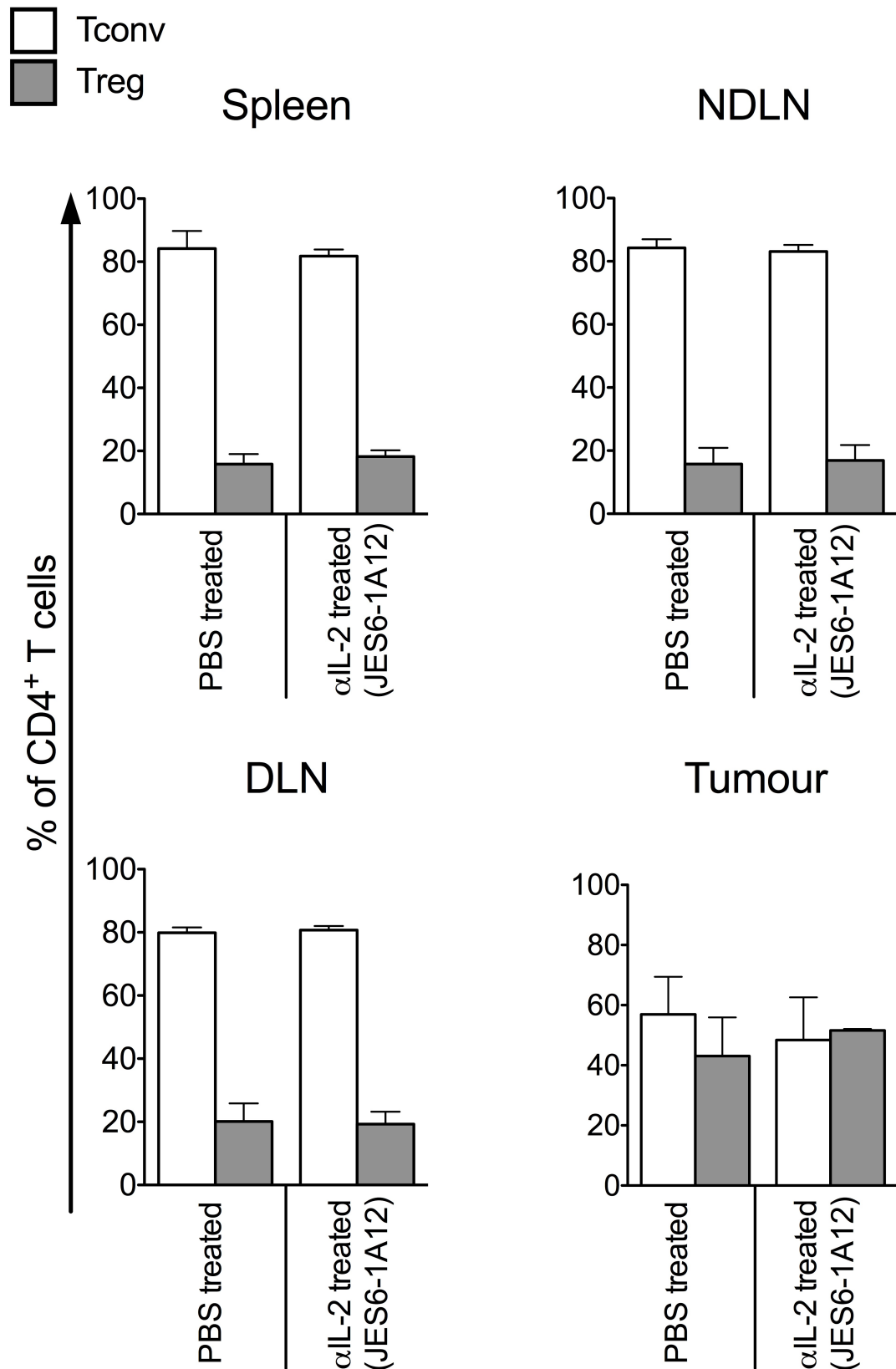
Figure 3.7 | Neutralisation of IL-2 does not alter the Tconv : Treg ratio in lymphoid organs or in tumour.
Bar charts showing the proportion of CD4^{+} T cells that are Foxp3^{-} (Tconv; white bars) or Foxp3^{+} (Treg; grey bars) in spleen, tumour non-draining lymph node (NDLN), tumour draining lymph node (DLN) and tumour of PBS-treated control animals or experimental animals treated with the JES6-1A12 anti-IL-2 monoclonal antibody. N = 3 experimental; 6 control. Data are presented as median ± interquartile range (IQR). Statistical significance was determined by Mann Whitney *t* tests between each cell type in control and treated groups.

[1] One-Way ANOVA with Tukey's multiple comparison test [2] Mantel-Cox log rank test
[3] Mann Whitney test

Figure 3.8 | Neutralisation of IL-2 alters CD25 expression by T cells in lymphoid organs and in tumour.
Bar charts showing the proportion of CD4^{+} Foxp3^{-} conventional T cells (Tconv; white bars), CD4^{+} Foxp3^{+} regulatory T cells (Treg; grey bars) and CD8^{+} T cells (dashed bars) expressing CD25 in spleen, tumour non-draining lymph node (NDLN), tumour draining lymph node (DLN) and tumour of PBS-treated control animals or experimental animals treated with the JES6-1A12 anti-IL-2 monoclonal antibody. N = 3 experimental; 6 control. Data are presented as median ± interquartile range (IQR). Statistical significance was determined by Mann Whitney t tests between each cell type in control and treated groups.
[1] One-Way ANOVA with Tukey's multiple comparison test [2] Mantel-Cox log rank test
[3] Mann Whitney test

Injection of pre-formed JES6-1A12/IL-2 complexes into tumour-bearing hosts resulted in a significant increase in proliferation of Tregs in all lymphoid organs studied, and also Tconvs and CD8^{+} T cells in the spleen[3]. However, no significant increase in proliferation in any of these cellular subsets was observed in the tumour[3] (Figure 3.9). The observed change in cellular proliferation resulted in a net effect of increasing the ratio of Treg to Tconv in lymphoid organs, whilst no change in the Treg to Tconv ratio was observed in the tumour, again, when data were analysed as either percentage of CD4^{+} T cells (Figure 3.10) or absolute number of Tconv and Treg (data not shown)[3]. This complex also resulted in significantly increased proportions of Tregs expressing CD25 in lymphoid organs, and Tconv and CD8^{+} T cells expressing CD25 in the spleen, but no alteration in CD25 expression was observed in cells isolated from tumour[3] (Figure 3.11).

[1] One-Way ANOVA with Tukey's multiple comparison test [2] Mantel-Cox log rank test
[3] Mann Whitney test
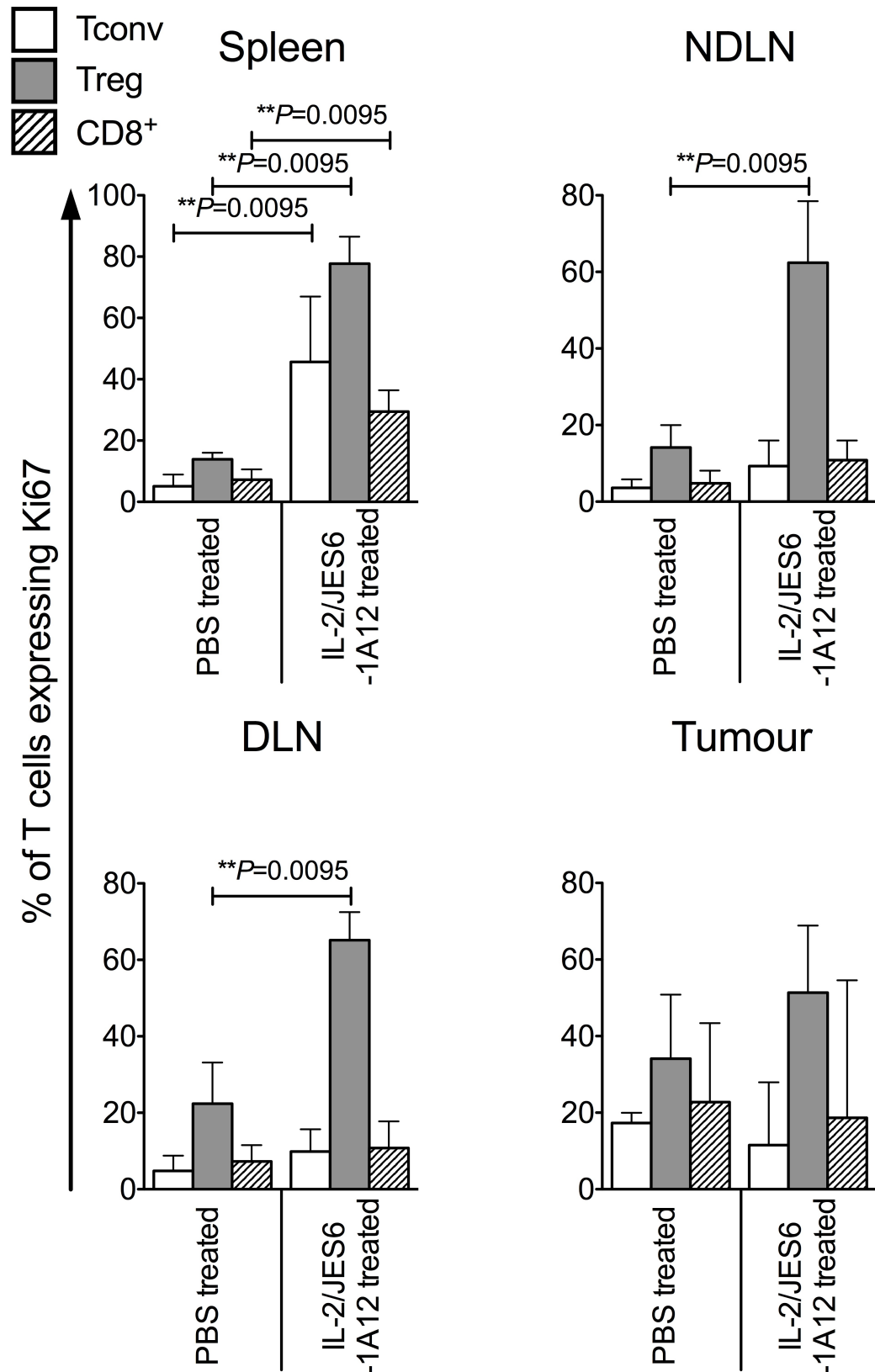
Figure 3.9 | Administration of IL-2/anti-IL-2 (JES6-1A12) complexes results in increased T cell proliferation in lymphoid organs but not in tumour.

Bar charts showing the proportion of CD4$^+$ Foxp3$^-$ conventional T cells (Tconv; white bars), CD4$^+$ Foxp3$^+$ regulatory T cells (Treg; grey bars) and CD8$^+$ T cells (dashed bars) expressing Ki67 in spleen, tumour non-draining lymph node (NDLN), tumour draining lymph node (DLN) and tumour of PBS-treated control animals or experimental animals treated with the IL-2/JES6-1A12 anti-IL-2 complex. N = 4 experimental; 6 control. Data are presented as median ± interquartile range (IQR). Statistical significance was determined by Mann Whitney t tests between each cell type in control and treated groups.

[1] One-Way ANOVA with Tukey's multiple comparison test [2] Mantel-Cox log rank test
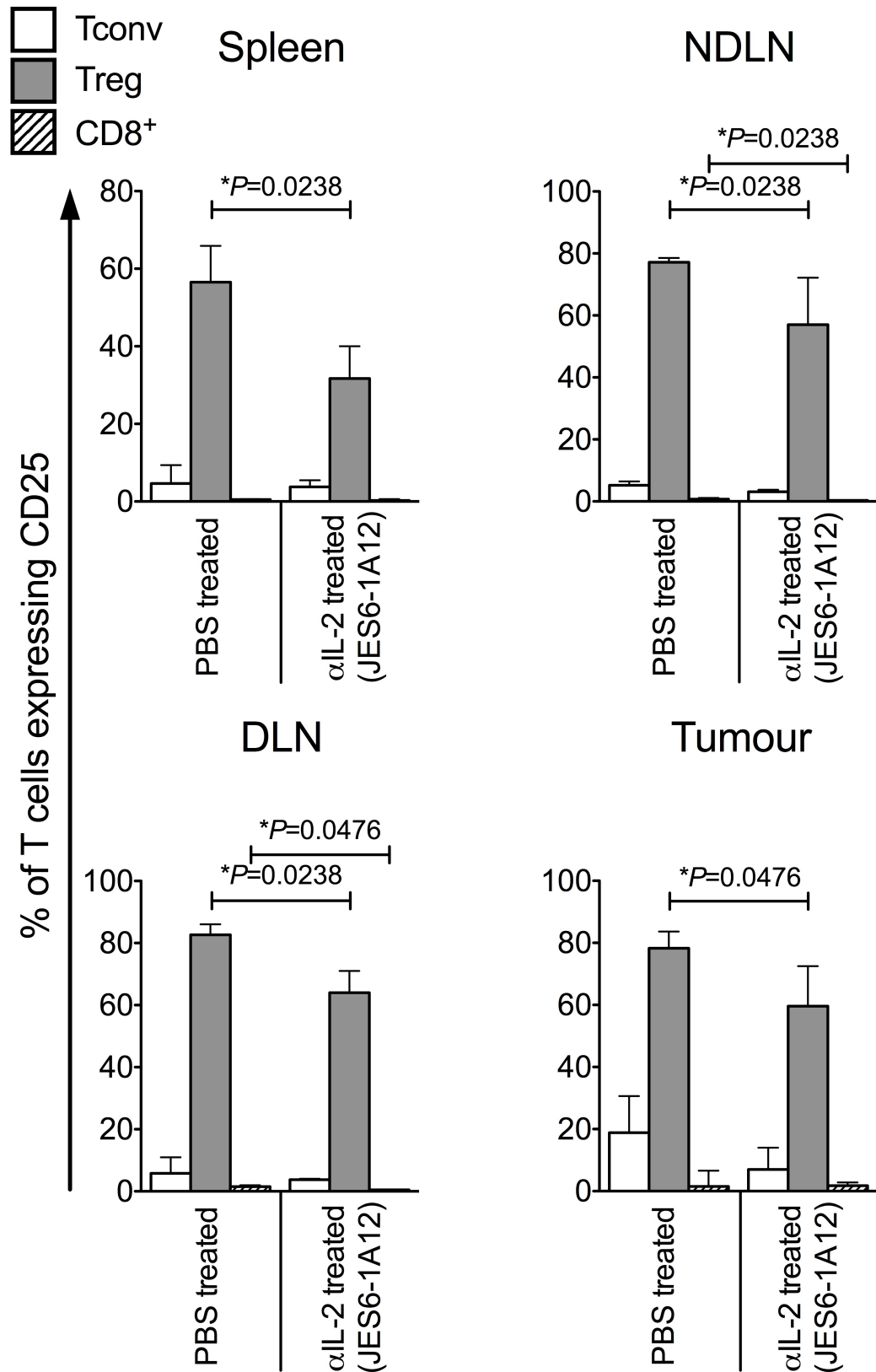[3] Mann Whitney test

Figure 3.10 | Administration of IL-2/anti-IL-2 (JES6-1A12) complexes alters the Tconv : Treg ratio in lymphoid organs but not in tumour.

Bar charts showing the proportion of CD4$^+$ T cells that are Foxp3$^-$ (Tconv; white bars) or Foxp3$^+$ (Treg; grey bars) in spleen, tumour non-draining lymph node (NDLN), tumour draining lymph node (DLN) and tumour of PBS-treated control animals or experimental animals treated with the IL-2/JES6-1A12 anti-IL-2 complex. N = 4 experimental; 6 control. Data are presented as median ± interquartile range (IQR). Statistical significance was determined by Mann Whitney t tests between each cell type in control and treated groups.

[1] One-Way ANOVA with Tukey's multiple comparison test [2] Mantel-Cox log rank test
[3] Mann Whitney test

Figure 3.11 | Administration of IL-2/anti-IL-2 (JES6-1A12) complexes alters CD25 expression by T cells in lymphoid organs but not in tumour.

Bar charts showing the proportion of $CD4^+$ $Foxp3^-$ conventional T cells (Tconv; white bars), $CD4^+$ $Foxp3^+$ regulatory T cells (Treg; grey bars) and $CD8^+$ T cells (dashed bars) expressing CD25 in spleen, tumour non-draining lymph node (NDLN), tumour draining lymph node (DLN) and tumour of PBS-treated control animals or experimental animals treated with the IL-2/JES6-1A12 anti-IL-2 complex. N = 4 experimental; 6 control. Data are presented as median ± interquartile range (IQR). Statistical significance was determined by Mann Whitney t tests between each cell type in control and treated groups.

[1] One-Way ANOVA with Tukey's multiple comparison test [2] Mantel-Cox log rank test [3] Mann Whitney test

Administration of preformed S4B6-IL2 complexes also resulted in a highly significant increase in proliferation of CD4^{+} Tconv, CD4^{+} Treg and CD8^{+} T cells to a comparable degree in secondary lymphoid tissues[3]. Again, a significant increase in proliferation of CD4^{+} Tconv and CD4^{+} Treg was not observed in the tumour[3] (Figure 3.12). However, in line with previous reports, the S4B6-IL2 complex resulted in preferential and considerable expansion of CD8^{+} T cells in the tumour, confirming successful tumour access by the complex[3] (Boyman et al. 2006; Boyman & Sprent 2012). The S4B6-IL-2 complex increased the proportion of Tregs and CD8^{+} T cells, and sometimes CD4^{+} Tconv, expressing CD25 in lymphoid organs[3] (Figure 3.13). Furthermore, the proportion of Tregs expressing CD25 was also significantly increased in the tumour following S4B6-IL-2 complex administration[3] (Figure 3.12). However, whilst S4B6/IL-2 administration resulted in an increased ratio of Treg to Tconv in lymphoid tissues, the ratio of Treg to effector T cells, including both Tconv and CD8^{+} T cells, remained unchanged in the tumour, when data were analysed as either percentage of CD4^{+} T cells (Figure 3.14) or absolute number (data not shown).

These data collectively indicate that increasing the availability of IL-2 has no impact on the ratio of Tregs to Tconvs at the tumour site.

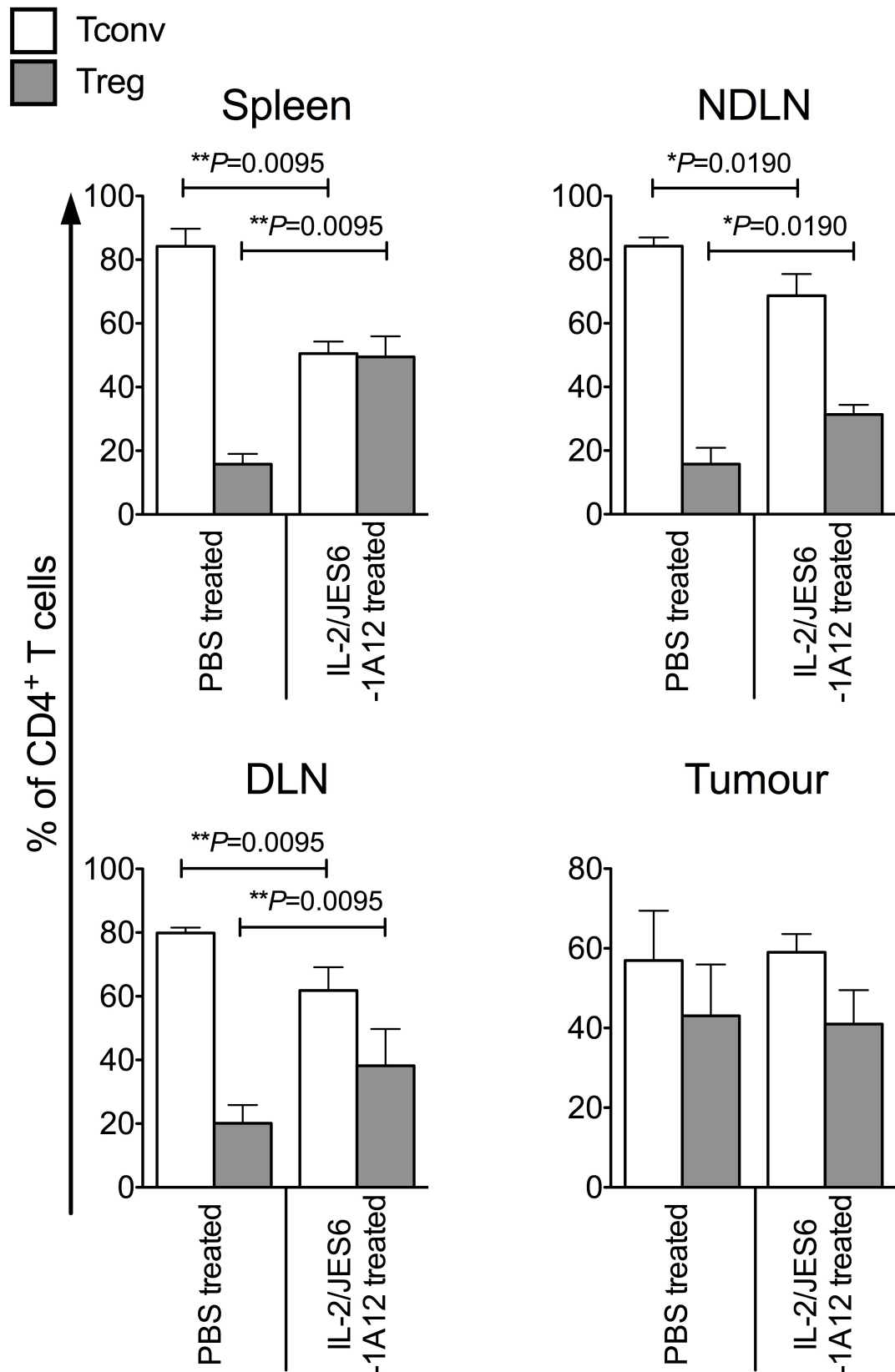[1] One-Way ANOVA with Tukey's multiple comparison test [2] Mantel-Cox log rank test
[3] Mann Whitney test
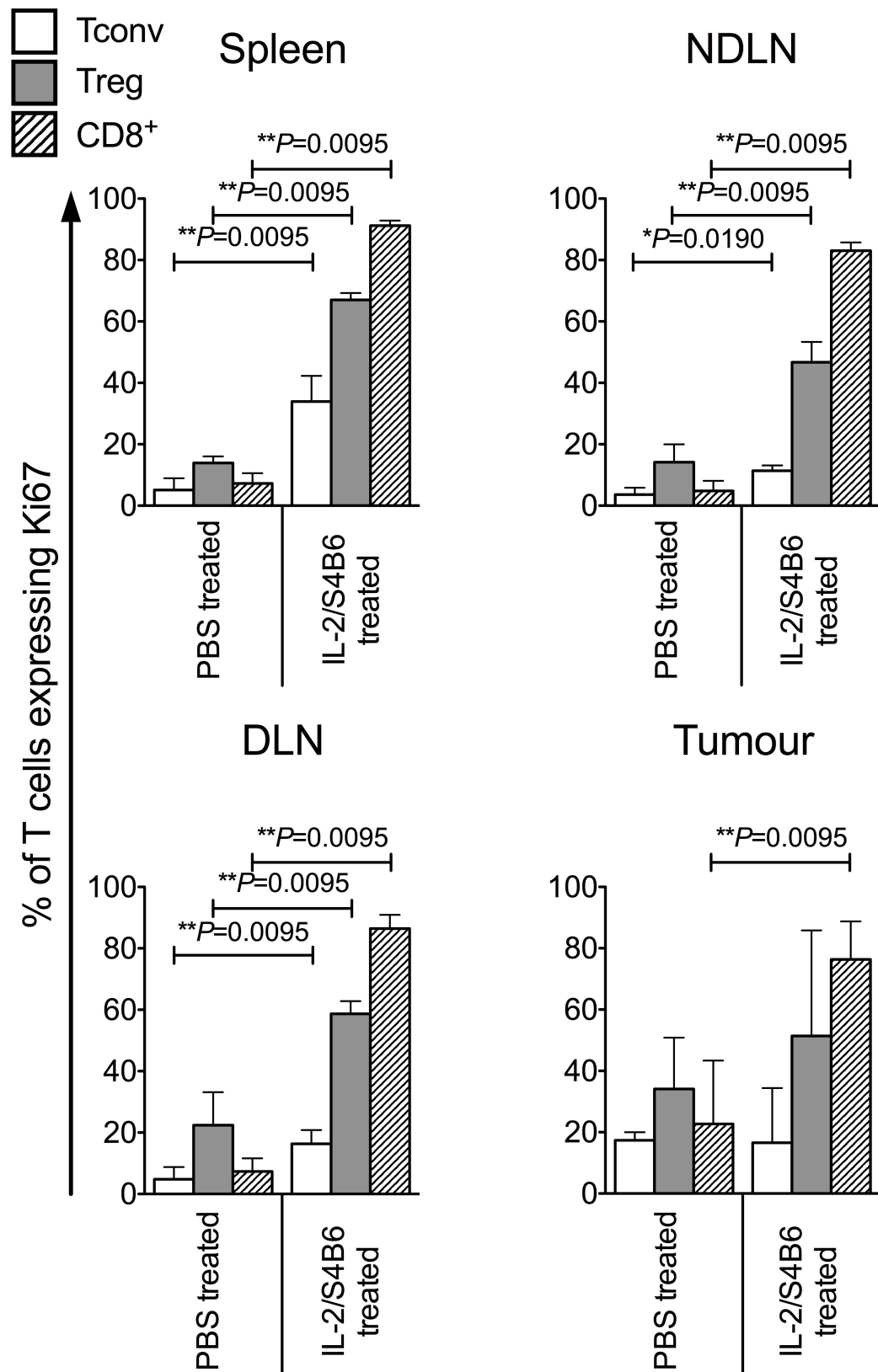
Figure 3.12 | Administration of IL-2/anti-IL-2 (S4B6) complexes results in increased T cell proliferation in lymphoid organs and in tumour.

Bar charts showing the proportion of CD4$^+$ Foxp3$^-$ conventional T cells (Tconv; white bars), CD4$^+$ Foxp3$^+$ regulatory T cells (Treg; grey bars) and CD8$^+$ T cells (dashed bars) expressing Ki67 in spleen, tumour non-draining lymph node (NDLN), tumour draining lymph node (DLN) and tumour of PBS-treated control animals or experimental animals treated with the IL-2/S4B6 anti-IL-2 complex. N = 4 experimental; 6 control. Data are presented as median ± interquartile range (IQR). Statistical significance was determined by Mann Whitney *t* tests between each cell type in control and treated groups.

[1] One-Way ANOVA with Tukey's multiple comparison test [2] Mantel-Cox log rank test
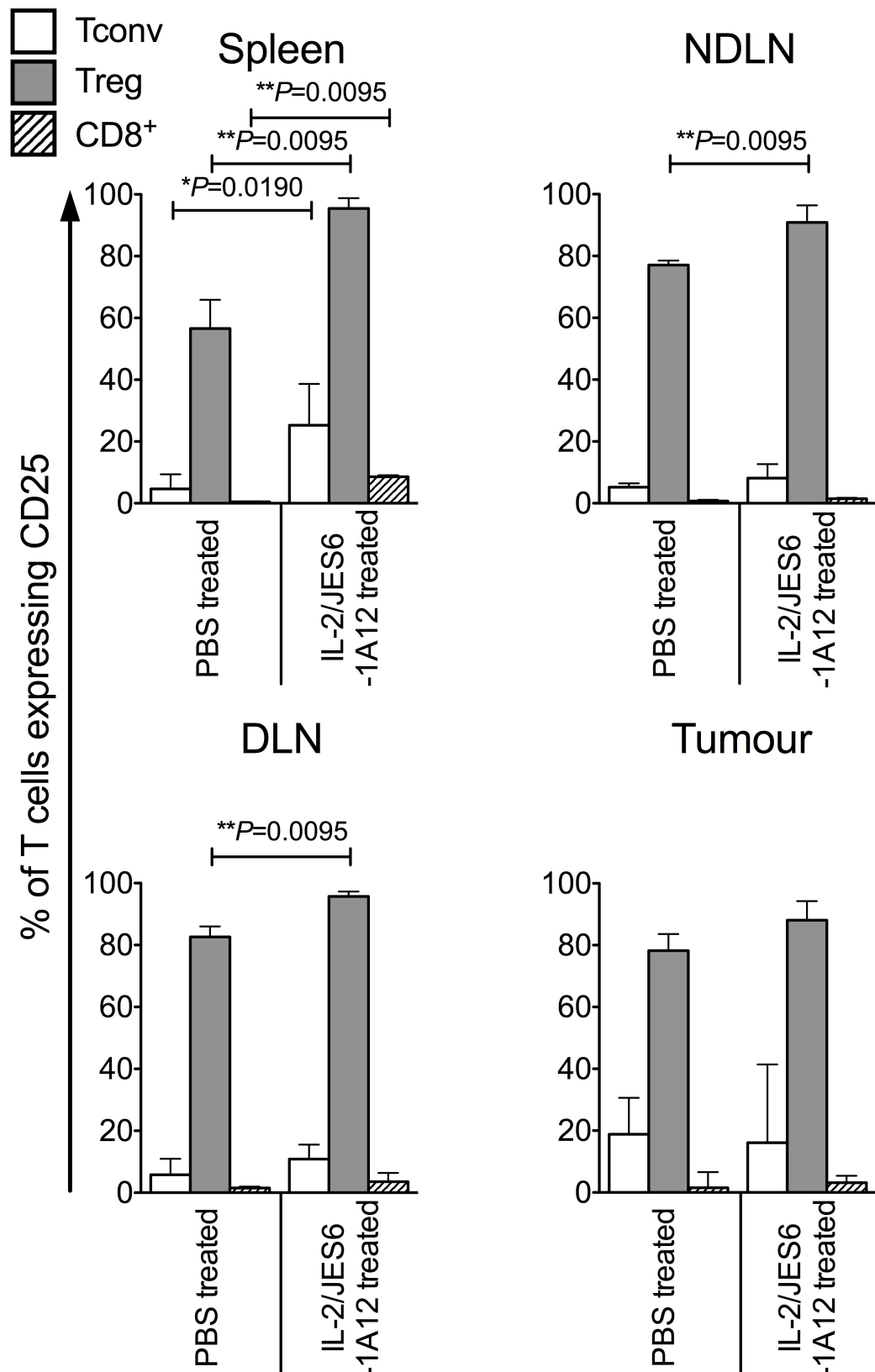[3] Mann Whitney test

Figure 3.13 | Administration of IL-2/anti-IL-2 (S4B6) complexes alters CD25 expression by T cells in lymphoid organs and in tumour.

Bar charts showing the proportion of CD4^{+} Foxp3^{-} conventional T cells (Tconv; white bars), CD4^{+} Foxp3^{+} regulatory T cells (Treg; grey bars) and CD8^{+} T cells (dashed bars) expressing CD25 in spleen, tumour non-draining lymph node (NDLN), tumour draining lymph node (DLN) and tumour of PBS-treated control animals or experimental animals treated with the IL-2/S4B6 anti-IL-2 complex. N = 4 experimental; 6 control. Data are presented as median ± interquartile range (IQR). Statistical significance was determined by Mann Whitney *t* tests between each cell type in control and treated groups.

[1] One-Way ANOVA with Tukey's multiple comparison test [2] Mantel-Cox log rank test
[3] Mann Whitney test

Figure 3.14 | Administration of IL-2/anti-IL-2 (S4B6) complexes alters the Tconv : Treg ratio in lymphoid organs but not in tumour.

Bar charts showing the proportion of CD4^{+} T cells that are Foxp3^{-} (Tconv; white bars) or Foxp3^{+} (Treg; grey bars) in spleen, tumour non-draining lymph node (NDLN), tumour draining lymph node (DLN) and tumour of PBS-treated control animals or experimental animals treated with the IL-2/S4B6 anti-IL-2 complex. N = 4 experimental; 6 control. Data are presented as median ± interquartile range (IQR). Statistical significance was determined by Mann Whitney t tests between each cell type in control and treated groups.

[1] One-Way ANOVA with Tukey's multiple comparison test [2] Mantel-Cox log rank test
[3] Mann Whitney test

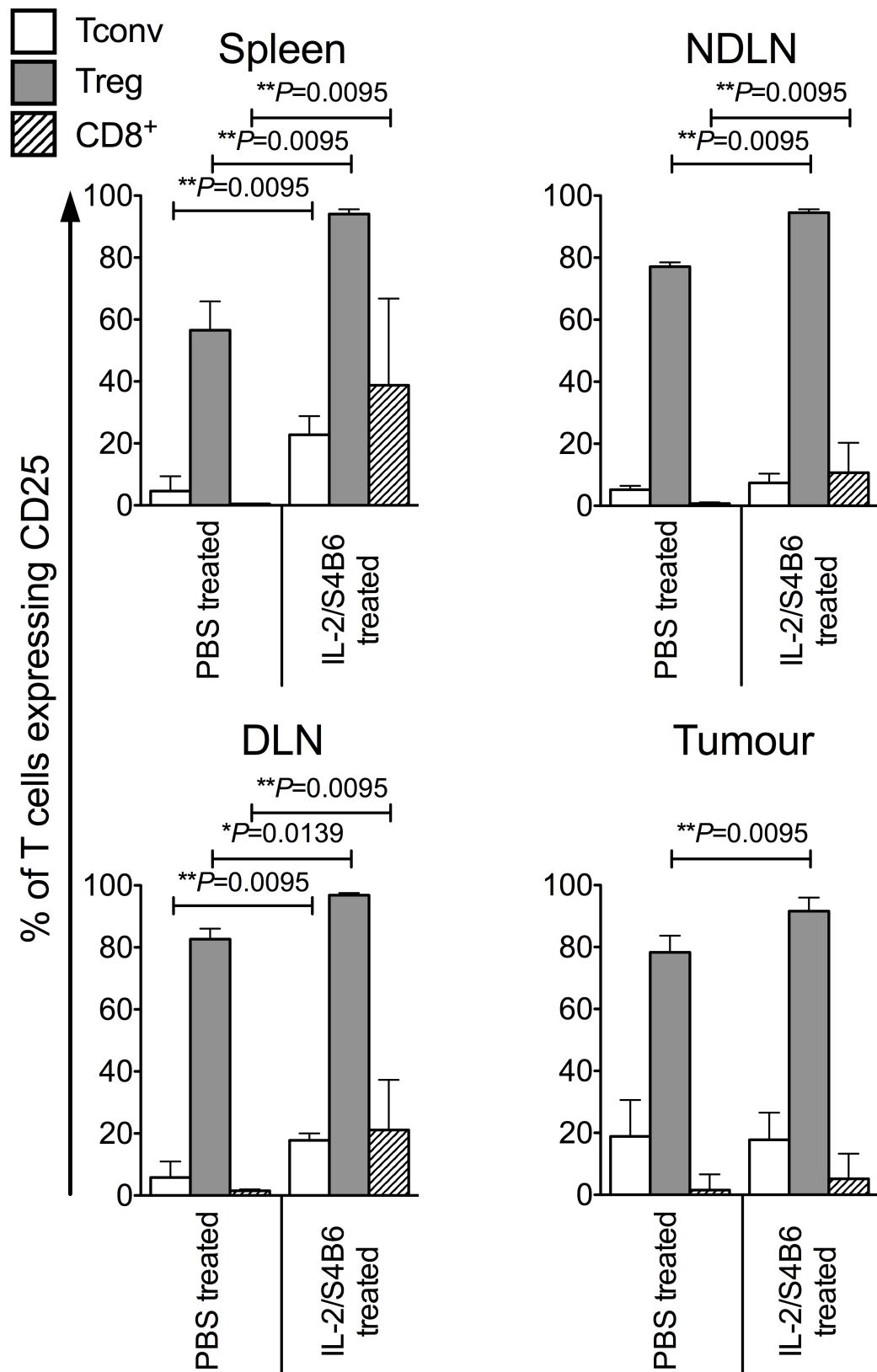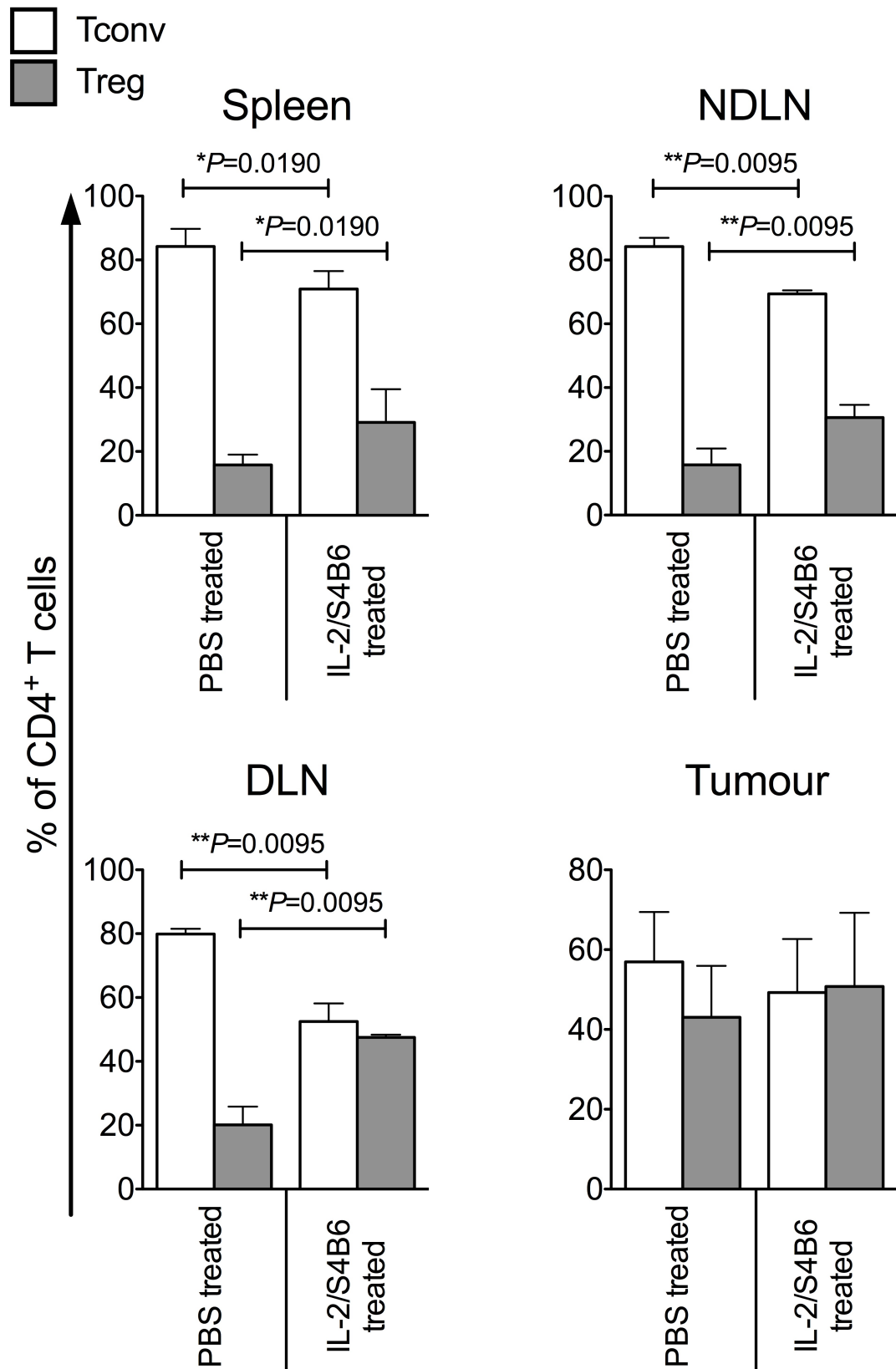3.4 Results: CD69 is highly Expressed on Intra-Tumoural Foxp3^{+} Tregs

CD69 is classically described as a marker of early T cell activation (González-Amaro et al. 2013). In recent years however, it has become apparent that through reciprocal regulation of sphingosine 1-phosphate receptor 1 ($S1P_1$), CD69 also plays a role in retaining T cells at the site of antigen (Shiow et al. 2006; Matloubian et al. 2004; Chu et al. 2003; Bankovich et al. 2010; Mackay et al. 2015). I compared CD69 expression on MCA tumour-derived Foxp3^{-} and Foxp3^{+} CD4^{+} T cells and found a striking difference (Figure 3.15). A significantly greater proportion of intra-tumoural Foxp3^{+} T cells expressed CD69, than tumour derived conventional Foxp3^{-} T cells[1] (Figure 3.16 A). The proportion of Foxp3^{+} Tregs expressing CD69 was also statistically greater than the proportion of CD69-expressing Foxp3^{-} T cells in LNs and spleen[1]. Furthermore, the proportion of CD69-expressing Foxp3^{+} Tregs in the tumour was statistically greater than in any lymphoid tissue[1] (Figure 3.16 A).

To investigate the relevance of this finding in the context of another tumour model, I also compared CD69 expression in Foxp3^{-} and Foxp3^{+} CD4^{+} T cells isolated from tumours induced by injection of the 4T1 mammary carcinoma cell line (Figure 3.17) (Miller et al. 1983; Miller 1983). These data strongly corroborated my findings in the MCA-induced fibrosarcomas, as I observed that a significantly greater proportion of tumour derived Foxp3^{+} CD4^{+} T cells expressed CD69 relative to tumour derived Foxp3^{-} CD4^{+} T cells, and Foxp3^{+} Tregs in all other lymphoid compartments[1] (Figure 3.16 B). Again, a greater proportion of Foxp3^{+} Tregs than Foxp3^{-} CD4^{+} T cells expressed CD69 in lymphoid compartments, as observed in the MCA-induced model, although this did not reach statistical significance here[1] (Figure 3.16 B). Collectively, these data from two different tumour models strongly support the notion that Tregs are far more likely than Foxp3^{-} T cells to remain tumour-resident by virtue of their heightened expression of CD69, thereby contributing to their accumulation within the tumour-infiltrating T cell pool (Figure 3.18).

[1] One-Way ANOVA with Tukey's multiple comparison test [2] Mantel-Cox log rank test [3] Mann Whitney test
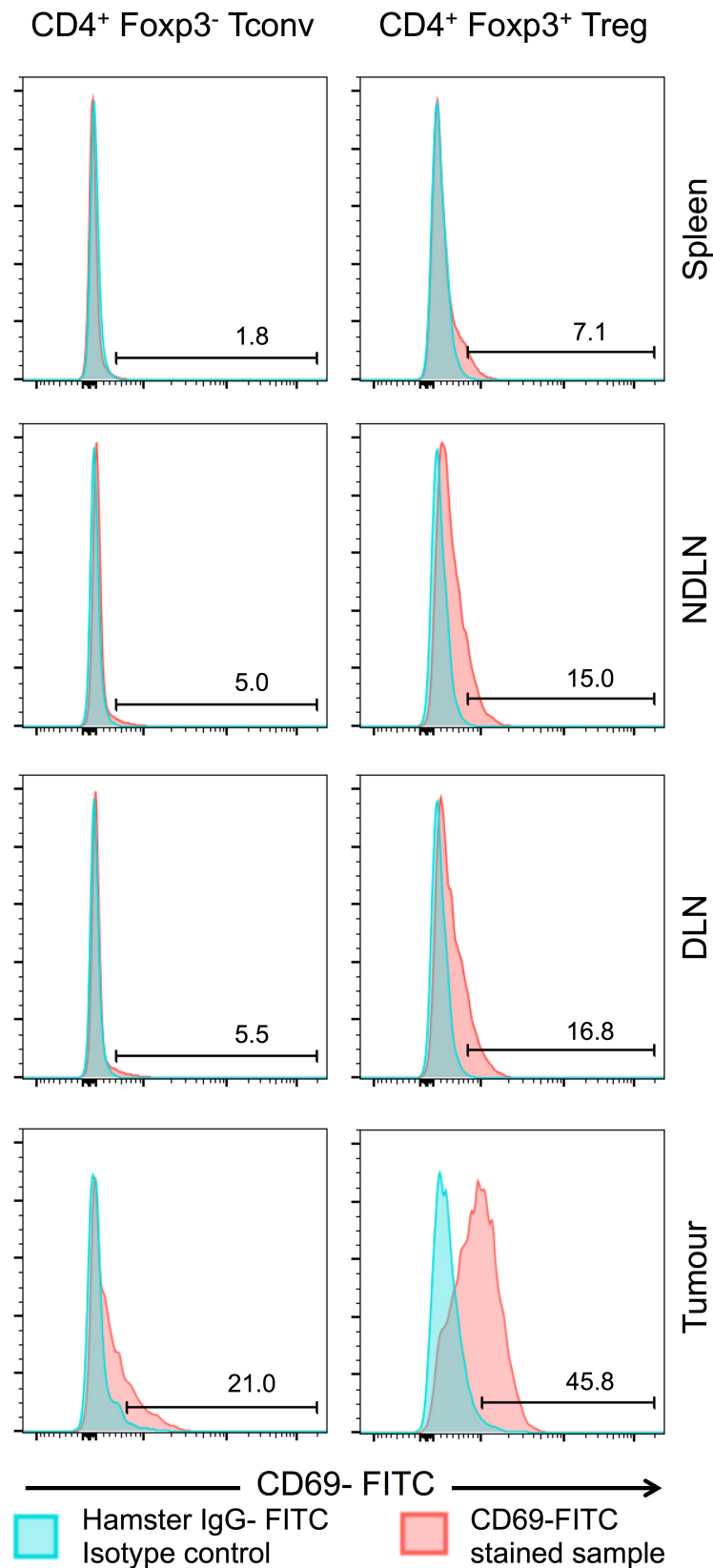
Figure 3.15 | Intra-tumoural Tregs of MCA fibrosarcomas express high levels of CD69. Representative flow cytometry plots showing proportion of T cells expressing CD69 (x axis) in spleen, tumour non-draining lymph node (NDLN), tumour draining lymph node (DLN), and tumour of one animal model of MCA-induced fibrosarcoma. Cells are gated on live $CD4^+$ $Foxp3^-$ conventional T cells (Tconv; left column), or live $CD4^+$ $Foxp3^+$ regulatory T cells (Treg; right column). Numbers represent proportion of cells positive for CD69. Stained samples are shown in red; samples stained using the isotype control are shown in blue.

[1] One-Way ANOVA with Tukey's multiple comparison test [2] Mantel-Cox log rank test
[3] Mann Whitney test
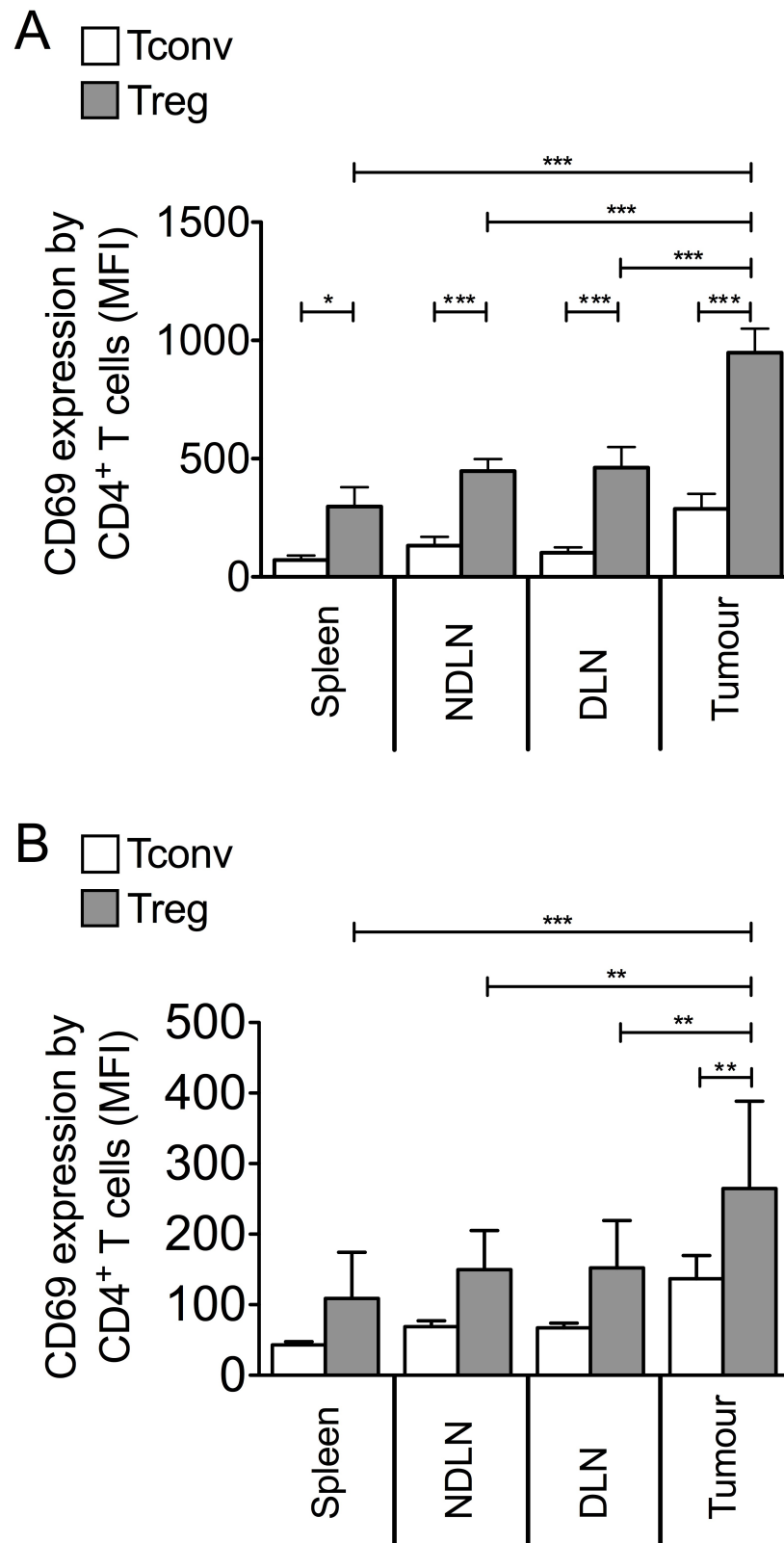
Figure 3.16 | Tregs express higher levels of CD69 than Tconv in lymphoid organs and tumours of two separate tumour models.

Bar charts showing the proportion of CD4$^+$ Foxp3$^-$ conventional T cells (Tconv; white bars) and CD4$^+$ Foxp3$^+$ regulatory T cells (Treg; grey bars) that express CD69 in spleen, tumour non-draining lymph node (NDLN), tumour draining lymph node (DLN) and tumour, expressed as Mean Fluorescence Intensity (MFI) in animal models of MCA-induced fibrosarcoma (A), or 4T1 breast carcinoma (B). N = 3 (A), N = 8 (B). Data are presented as mean ± standard deviation (SD). Statistical significance was determined by One-way ANOVA with Tukey's multiple comparison tests to compare pairs of means (* = $P \leq 0.05$, ** = $P \leq 0.01$, *** = $P \leq 0.001$).
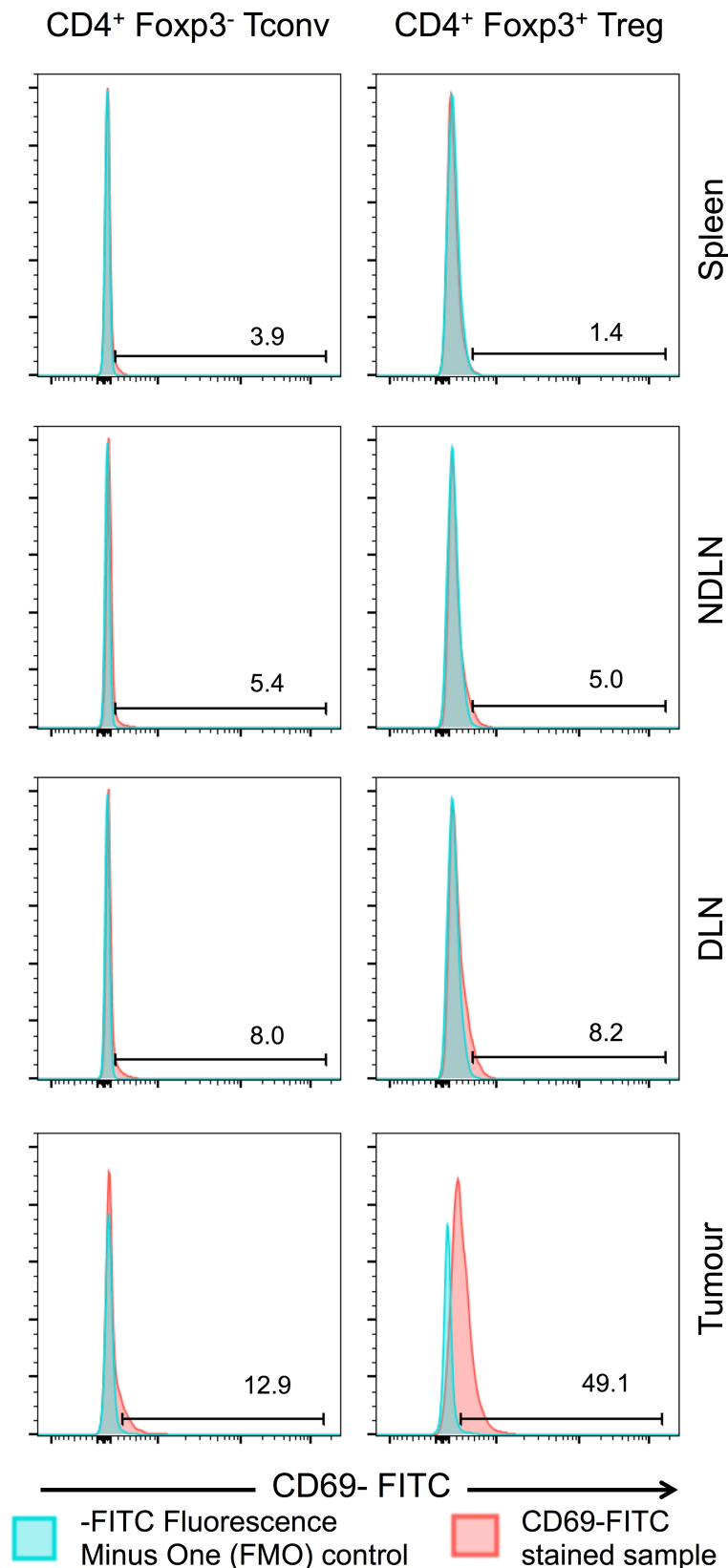
Figure 3.17 | Intra-tumoural Tregs of 4T1 mammary carcinomas express high levels of CD69. Representative flow cytometry plots showing proportion of T cells expressing CD69 (x axis) in spleen, tumour non-draining lymph node (NDLN), tumour draining lymph node (DLN), and tumour of one animal model of 4T1 breast carcinoma. Cells are gated on live CD4^{+} Foxp3^{-} conventional T cells (Tconv; left column), or live CD4^{+} Foxp3^{+} regulatory T cells (Treg; right column). Numbers represent proportion of cells positive for CD69. Stained samples are shown in red; samples stained using the –FITC fluorescence minus one control are shown in blue.

[1] One-Way ANOVA with Tukey's multiple comparison test [2] Mantel-Cox log rank test [3] Mann Whitney test
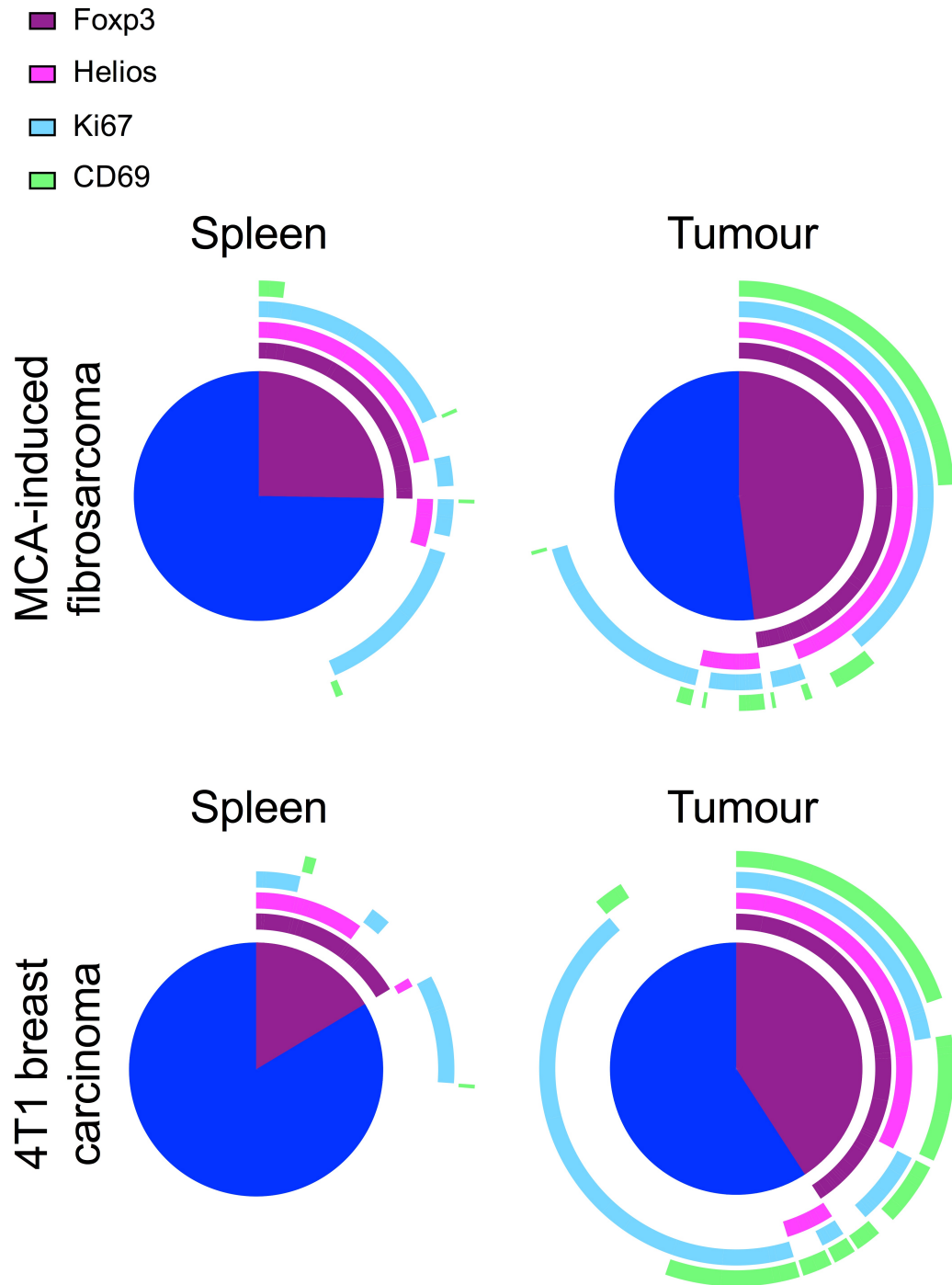
Figure 3.18 | MCA induced fibrosarcomas and 4T1 mammary carcinomas demonstrate a significant enrichment of Helios[+] thymus-derived Foxp3^{+} Tregs, which express heightened levels of Ki67 and CD69 relative to those in Spleen. Spice diagrams showing proportions of CD4^{+} T cells expressing certain markers in one representative spleen and tumour of the MCA-induced fibrosarcoma model (top) and the 4T1 mammary carcinoma model (bottom). Each arc denotes a marker as detailed in the key.

[1] One-Way ANOVA with Tukey's multiple comparison test [2] Mantel-Cox log rank test
[3] Mann Whitney test

3.5 Results: CD69 Expression Confers Superior Suppressive Capacity on Foxp3^{+} T cells

CD69 is a well-established marker of early leukocyte activation (González-Amaro et al. 2013) yet CD69^{-/-} animals paradoxically display enhanced anti-tumour immunity and enhanced susceptibility to autoimmune diseases (Esplugues et al. 2003; Sancho et al. 2003). These data indicate that CD69 could also therefore act as a negative regulator of T cell activation somehow. A recent study indicated that Foxp3+ Tregs could indirectly mediate this negative regulatory effect, as CD69^{+} Foxp3^{+} Tregs were found to be more efficient at limiting inflammation than CD69^{-} counterparts (Cortés et al. 2014).

Having found a significant population of CD69^{+} Foxp3^{+} Tregs in MCA-induced tumours, I next sought to assess the suppressive capacity of this population of Foxp3^{+} Treg. CD4^{+} CD25^{lo} Tconvs were sorted from lymphoid tissue and co-cultured in the presence of anti-CD3 and anti-CD28 beads with either CD69^{+} or CD69^{-} Tregs sorted from DLN or NDLN, at varying Tconv : Treg ratios. Treg were sorted as CD4^{+} CD25^{hi} CD127^{lo} (CD69^{+} or CD69^{-}) cells: low cell surface expression of the IL-7 receptor α-chain (CD127) is used to discriminate and isolate live Tregs by cell sorting as intra-cellular Foxp3 staining cannot be used (Liu et al. 2006). After 120 hours of culture, proliferation of labelled Tconvs was measured by flow cytometry.

Strikingly, CD69^{+} Tregs, recovered from DLN and NDLN, were more suppressive of Tconv proliferation than their CD69^{-} counterparts (Figure 3.19). I observed that CD69^{+} Tregs are 2 x and 1.3 x more suppressive than CD69^{-} Tregs at a Tconv : Treg ratio of 8 : 1 in the DLN and NDLN, respectively. Similarly, CD69^{+} Tregs are 1.2 x and 1.3 x more suppressive than CD69^{-} Tregs at a Tconv : Treg ratio of 4 : 1 in the DLN and NDLN, respectively (Figure 3.19). These data are indicative of a superior ability of CD69^{+} Foxp3^{+} Tregs to not only be retained at the site of antigen, but to suppress proliferation of anti-tumour Tconv cells, in relation to CD69^{-} Foxp3^{+} Tregs. Collectively, these data might point to a role for CD69 in retaining highly proliferative, super-suppressive Tregs at the tumour site.

[1] One-Way ANOVA with Tukey's multiple comparison test [2] Mantel-Cox log rank test [3] Mann Whitney test
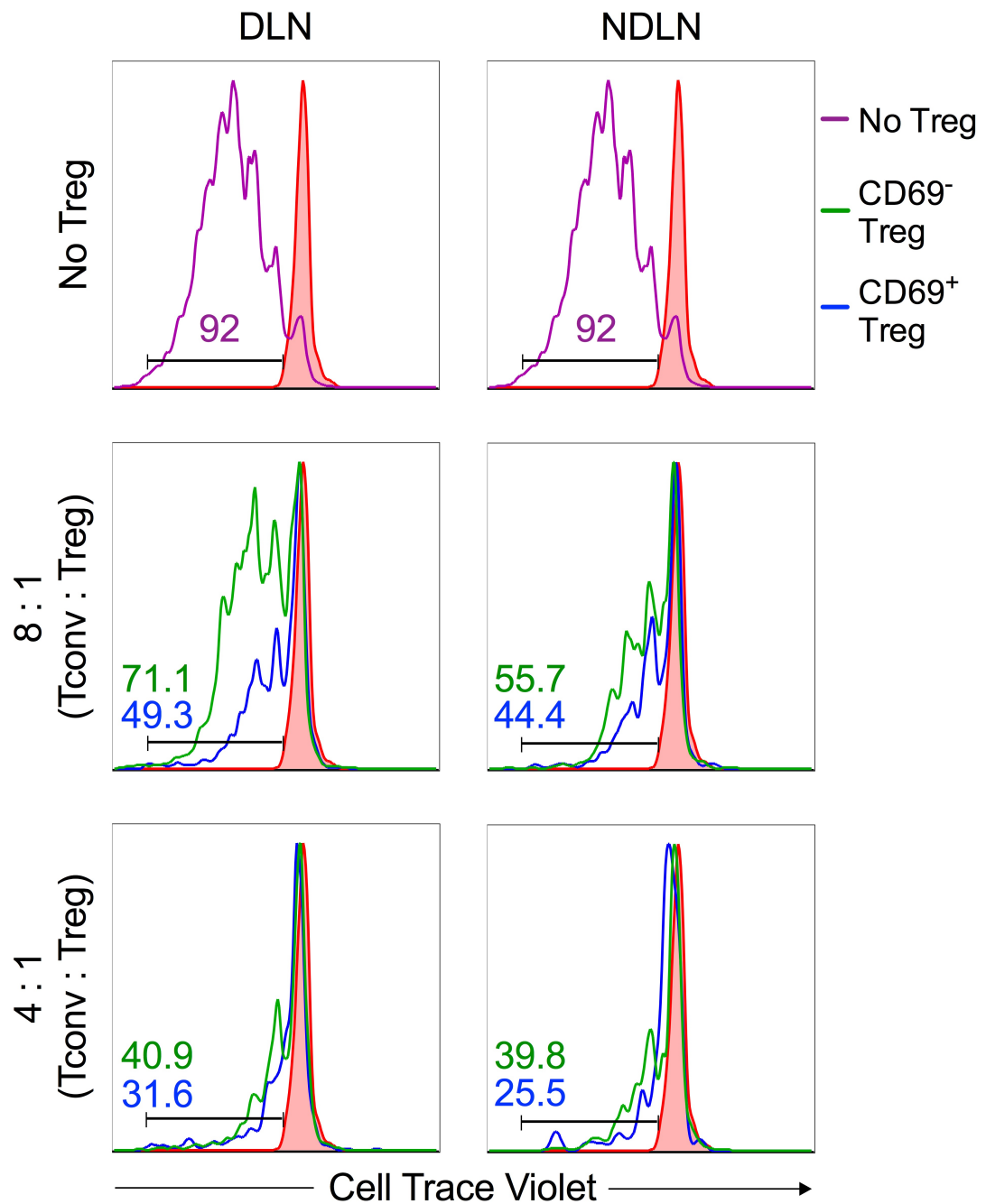
Figure 3.19 | CD69$^+$ Tregs from Lymph Nodes demonstrate heightened suppression of Tconv proliferation relative to CD69$^-$ Tregs *in vitro*.
Representative flow cytometry plots showing proportion of divided Tconv cells according to dilution of CellTrace Violet dye (x axis) with no CD3/CD28 stimulation (filled in red peak), with stimulation (purple peak), with stimulation and CD69$^-$ Tregs (green peak), and with stimulation and CD69$^+$ Tregs (blue peak). Data are shown for CD4$^+$ CD25^{hi} CD127^{lo} CD69$^+$ or CD69$^-$ Tregs from tumour draining lymph nodes (DLN) and tumour non-draining lymph nodes (NDLN).

[1] One-Way ANOVA with Tukey's multiple comparison test [2] Mantel-Cox log rank test
[3] Mann Whitney test

3.6 Discussion

It is clear that T_H1 cells and CTL are the key cells involved in immune control of MCA-induced tumours (Koebel et al. 2007). I have found that the proliferating Tregs in MCA tumours express both the chemokine receptor CXCR3 and the transcription factor T-bet, in-keeping with a "T_H1-like" lineage. Redjimi and colleagues reported that CXCR3^{+} T-bet[+] Tregs are prevalent in human ovarian tumours. These data imply that 'mirroring' of the anti-tumour T_H1-orientated immune response may be required for effective immunosuppression by Tregs in tumours (Redjimi et al. 2012). Indeed, Koch and colleagues previously observed that T-bet deficient Tregs were inferior to wild-type Tregs during control of T_H1-mediated multi-organ autoimmunity (Koch et al. 2009). However, several studies have reported either no alteration in suppressive capacity of Tregs when T-bet is absent, or even superior suppressive function of T-bet deficient Tregs (Neurath et al. 2002; Bettelli et al. 2004; Finotto et al. 2005). A recent study of experimental autoimmune encephalomyelitis (EAE) reported that lack of T-bet expression in Foxp3^{+} Tregs did not hinder their infiltration of the inflamed central nervous system, which is important for EAE resolution. T-bet deficient Tregs were also capable of preventing the development of T cell-driven colitis (McPherson et al. 2015). My studies provide no evidence that T-bet expression defines Tregs with a superior capacity to suppress anti-tumour T_H1-orientated immune responses. These data also corroborate recent data from our laboratory that excluded a role for CXCR3 in preferential homing of Tregs to the tumour (Ondondo et al. 2014[a]).

I postulated that as IL-2 might be a limiting resource in the tumour environment, preferential proliferation and accumulation of Tregs in the tumours could be due to competition for IL-2. IL-2 serves to promote both tolerance and immunity. Whilst it is needed to potentiate differentiation and expansion of both T_H1 cells and CD8^{+} CTL, Tregs also depend on IL-2 for their expansion and survival (Malek 2008). Although high doses of IL-2 have proven an effective component of immunotherapy against renal cell cancer in some patients (< 20%), its administration is associated with high levels of toxicity and may result in a significant increase in Treg numbers (Fyfe et al. 1995;

[1] One-Way ANOVA with Tukey's multiple comparison test [2] Mantel-Cox log rank test
[3] Mann Whitney test

Ahmadzadeh & Rosenberg 2006; Cesana et al. 2006; van der Vliet et al. 2007). My data indicate that while IL-2 is a limiting factor for proliferation of Tregs, Tconvs and CD8$^+$ T cells in lymphoid compartments and tumour, as evidenced by changes in Ki67 expression following anti-IL-2 or IL-2/anti-IL-2 administration, altering the availability of IL-2 has no significant impact on the ratio of Tregs to Tconvs or Tregs to CD8$^+$ effector T cells at the tumour site.

I found that a significantly higher proportion of intra-tumoural Tregs express CD69 than intra-tumoural Tconvs and Tconvs in other, lymphoid tissues. Furthermore, intra-tumoural Tregs consistently expressed the highest levels of CD69 relative to Tregs in lymphoid organs. Lastly, my data indicate that CD69-expressing Tregs in lymphoid organs are more suppressive of CD4$^+$ Tconv proliferation than their CD69$^-$ counterparts. However, these are preliminary data from one experiment, and would need to be repeated before firm conclusions regarding the suppressive capacity of CD69$^+$ and CD69$^-$ Tregs could be drawn.

CD69 is a type-II C-lectin transmembrane receptor, up-regulated on T cells upon antigen stimulation via the TCR (González-Amaro et al. 2013). It has also become apparent that CD69 plays a role in retaining T cells at the site of antigen, through preventing expression of S1P$_1$, thereby stopping lymphocyte egress from the site of antigen recognition (Shiow et al. 2006). Furthermore, it is now known that lack of expression of S1P$_1$ in resident memory T cells is responsible for their retention in non-lymphoid tissues (Skon et al. 2013).

Although CD69 is considered a classical marker of T cell activation, CD69$^{-/-}$ paradoxically mice exhibit enhanced tumour immunity and heightened susceptibility to autoimmune disease and allergic inflammation, raising the possibility that the molecule could act as a negative regulator of T cell activation (Esplugues et al. 2003; Sancho et al. 2003; Martin et al. 2010). It is possible that this effect of CD69 expression is mediated by Foxp3$^+$ Tregs. Several recent studies in mouse and human have provided data linking CD69 expression to the generation and suppressive function of Foxp3$^+$ Tregs (González-Amaro et al. 2013). Double positive thymocytes expressing high

[1] One-Way ANOVA with Tukey's multiple comparison test [2] Mantel-Cox log rank test
[3] Mann Whitney test

levels of CD69 represent the precursors to Foxp3^{+} tTregs in human (Martín-Gayo et al. 2010). Consistent with these data, peripheral CD69-expressing Tregs in mice differ from CD69 negative Tregs in terms of expression levels of Treg associated markers such as glucocorticoid-induced TNFR family related gene (GITR), CTLA-4 and inducible co-stimulator (ICOS), supporting the idea that CD69^{+} Treg represent a distinct subset of Treg (Cortés et al. 2014). Compromised Foxp3^{+} Treg suppressive function in systemic sclerosis patients is associated with diminished CD69 expression on Tregs (Radstake et al. 2009). A more recent study has demonstrated that mouse CD69^{+} Foxp3^{+} Tregs limit inflammation more efficiently than CD69^{-} Tregs (Cortés et al. 2014). $S1P_1$ signalling has also been shown to up-regulate the Akt-mTOR signalling pathway, which results in diminished suppressor activity in Tregs (Liu et al. 2009). Hence, CD69 expression on Tregs following TCR activation may not only serve to retain Tregs at the site of antigen but may also, through repression of $S1P_1$ signalling, favour strong suppressor activity by the retained CD69^{+} Tregs. Thus, in the case of the tumours described herein, the consequence of CD69 expression on Tregs may be the retention of tumour-infiltrating super-suppressive Tregs at the site of antigen, thereby ensuring Treg dominance within the local tumour microenvironment.

CD69 expression on intra-tumoural Tregs could of course be a simple reflection of heightened activation status. To tease apart activation and suppressive capacity of Tregs in future experiments would be challenging, as these are intricately linked in Foxp3^{+} Tregs. However, the fact that most T cells inside the tumour are highly activated (unpublished data) argues for a fundamental difference in the functional activity of CD69^{+} Tregs.

In conclusion, I have eliminated competition for a limited IL-2 resource as a means by which Tregs become significantly enriched in tumours. Despite the discovery of an accumulation of T_H1-like Tregs in tumours, this feature did not contribute to the functional ability of Tregs to control anti-tumour immune responses. Instead, my observations highlight that as well as increased proliferation with superior survival, retention of highly suppressive Tregs within the tumour microenvironment by virtue of

[1] One-Way ANOVA with Tukey's multiple comparison test [2] Mantel-Cox log rank test
[3] Mann Whitney test

CD69 expression is a key mechanism by which Tregs exert dominance over intra-tumoural Tconvs (Figure 3.20). Further analyses investigating the relevance of these observations in different tumour models will enable more successful manipulation of these immunosuppressive cells in cancer immunotherapy regimes.

Figure 3.20 | Modified Hypothesis of Treg Enrichment in MCA Tumours.
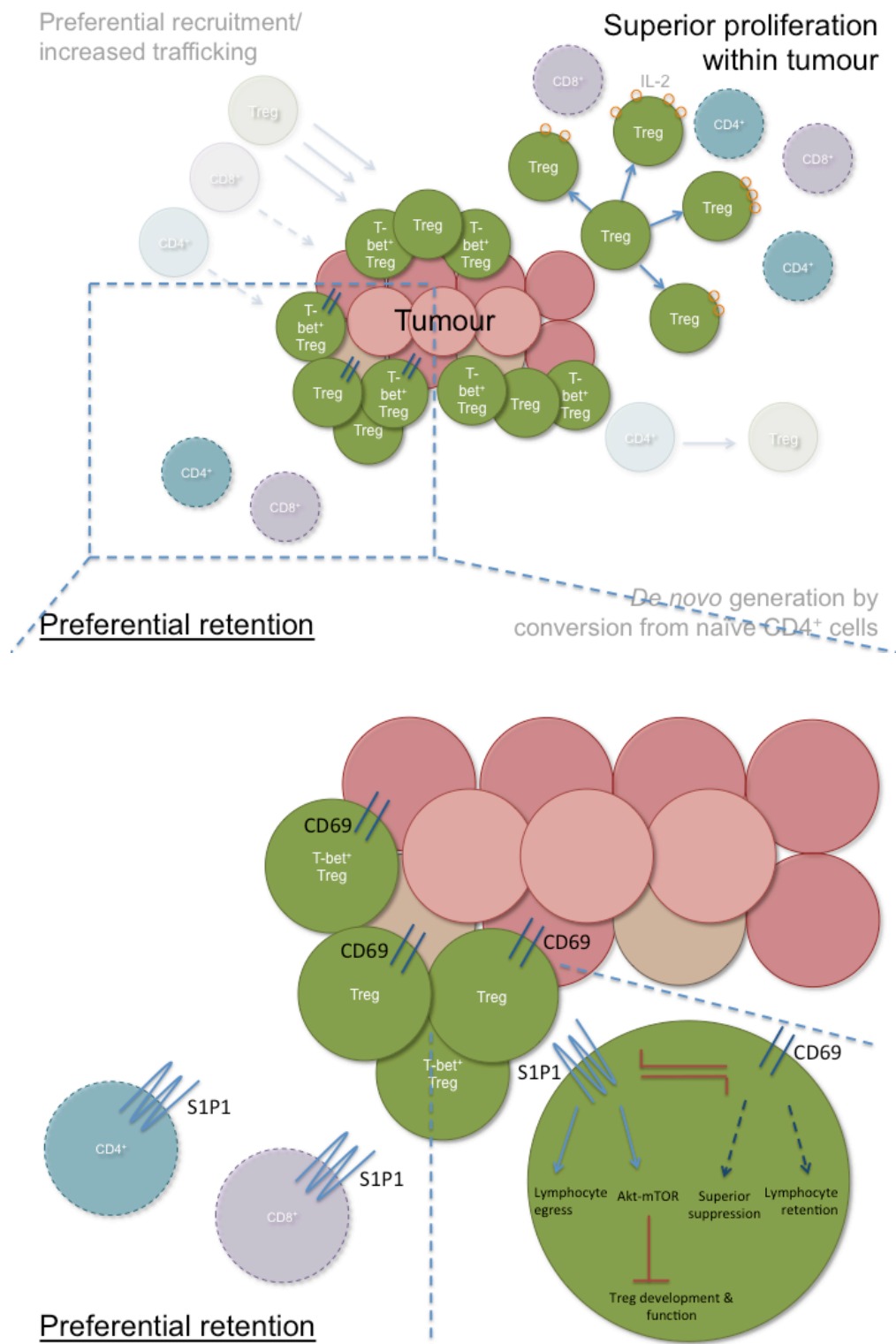
Chapter Four

4 Results: Cellular Subsets Responsible for Directing High Endothelial

Venule Neogenesis in Tumours

4.1 Introduction

HEV develop during ontogeny as part of the pre-programmed process of SLO development, which is kick-started by interactions between stromal LTo and haematopoietic LTi cells (Mebius 2003). Previous immunohistochemical analyses conducted in our lab revealed an absence of canonical $CD3^-$ $CD4^+$ $IL-7R\alpha^+$ $ROR\gamma t^+$ LTi cells in HEV positive and negative tumours of Treg depleted $Foxp3^{DTR}$ animals (Hindley et al. 2012). These data indicate that HEV neogenesis in MCA tumours proceeds along a distinct molecular pathway to that observed during normal lymphoid organ development.

The precise mechanisms and cellular subsets directing HEV development within LNs remain incompletely defined. Recent evidence has pointed to a crucial role for $CD11c^+$ DCs in modulation and maintenance of the specialised HEV phenotype in LNs (Moussion & Girard 2011). There is also evidence that DCs regulate the overall size of the HEV vascular tree, possibly via LTβR-induced VEGF expressed by FRCs, suggesting an additional role for DCs in control of HEV growth (Wendland et al. 2011; Webster et al. 2006; Chyou et al. 2008; Ager & May 2015).

Whether LTi-like cells or DCs dictate HEV neogenesis in solid human tumours remains unknown (Ager & May 2015). Recent studies have implicated LTβ-producing mature $DC-LAMP^+$ DCs in the process of HEV neogenesis in human breast tumours. Martinet and colleagues observed that clusters of mature DCs surround HEV in tumour tissue and that DCs were the major producers of LTβ in tumours. Furthermore, DC abundance correlated positively with density of tumour-associated HEV (Martinet et al. 2013; Martinet & Girard 2013). However, direct evidence for involvement of DCs in HEV neogenesis in tumours is still lacking. Considering Treg depletion in $Foxp3^{DTR}$ mice results in a profound increase in both numbers and activation status of DCs (Kim

[1] Spearman's correlation [2] Mann Whitney non-parametric *t* test [3] Kruskal-Wallis One-Way ANOVA with Dunn's multiple comparisons test [4] Linear Regression

et al. 2007), it is possible that DCs could be instrumental in driving HEV neogenesis in MCA tumours of Treg depleted Foxp3^{DTR} mice. Current ongoing work in our lab is aimed at determining whether these immune cells regulate HEV neogenesis in this scenario.

Due to the complete absence of HEV in Treg replete tumours of our MCA-Foxp3^{DTR} model, it is entirely possible that other immune cells, which become highly activated as a result of Treg depletion (Kim et al. 2007; Hindley et al. 2012), coordinate HEV formation in these tumours. T and B lymphocytes, as well as DCs, are capable of producing TNF superfamily cytokines involved in HEV development during ontogeny (Ware 2005), and therefore represent strong candidates for 'HEV-initiator'-type cells in tumours. Under this premise, I aimed to determine whether there is a role for:

- B cells,

- CD4$^+$ T cells, and / or

- CD8$^+$ T cells,

    in HEV neogenesis in Treg depleted tumours.

4.2 Results: HEV in Tumours of Treg Depleted Animals Share Similarities with but also Differ from Lymph Node HEV

HEV in tumours of Treg depleted Foxp3^{DTR} animals were detected by immunohistochemical staining of paraffin embedded sections or immunofluorescence staining of frozen sections using the MECA-79 monoclonal antibody that detects PNAd expressed on endothelial cells (Figure 4.1). MECA-79 staining co-localised with the pan-endothelial marker CD31, confirming the detection of vascular endothelial cells. However, the vast majority of CD31$^+$ blood vessels in the tumour did not express PNAd (data not shown).

PNAd$^+$ HEV within tumours of Treg depleted Foxp3^{DTR} animals differed from HEV within LNs of Treg replete Foxp3^{DTR} mice according to several criteria (Figure 4.2). While LN HEV are composed of endothelial cells with a characteristic and distinctive cuboidal, or 'high' morphology (Figure 4.2) (Gowans & Knight 1964; Rosen 2004), endothelial cells lining PNAd$^+$ HEV in tumours seemed much less plump: vessels were often lined by flat endothelial cells (Figure 4.1). LN HEV are situated within the post-capillary network, and increase in size from the cortical-paracortical junction, where they are smallest, to the paracortex, where they are largest. HEV therefore conform to an orderly and uniform architectural organisation within LNs (Ager & May 2015). In contrast, HEV within the tumours described herein displayed varying degrees of uniformity in relation to morphology and size, with no apparent pattern of distribution within the tumour mass (Figures 4.1 and 4.2).

Mature LN HEV are characterised by luminal expression of PNAd. When analysing the pattern of PNAd distribution in tumour HEV, there looked to be PNAd staining throughout the vessel wall (Figure 4.1). However, it was not possible to definitively determine the contribution of luminal versus abluminal PNAd expression, as this was not directly measured here. Interestingly, in contrast to HEV reported in some human cancers (see Table 1.2 in Chapter One), development of HEV within the fibrosarcomas described herein was not accompanied by the formation of isolated lymphoid aggregates (Figure 4.1). While PNAd$^+$ HEV were often observed in close

[1] Spearman's correlation [2] Mann Whitney non-parametric *t* test [3] Kruskal-Wallis One-Way ANOVA with Dunn's multiple comparisons test [4] Linear Regression

proximity to clusters of lymphocytes within the tumour mass, the vessels were certainly not embedded within discrete lymphoid follicles.

Tumour HEV also differed from classical LN HEV by co-expression of MAdCAM-1, an addressin normally restricted to mucosal lymphoid organs such as mesenteric LNs in adult animals (Figure 4.1) (Girard et al. 2012). MAdCAM-1 is expressed by endothelial cells of HEV in all LNs early in development, after which it is rapidly downregulated concurrent with the upregulation of PNAd expression on HEV (Mebius et al. 1996). Dedifferentiation of HEV in LNs involves reversion from a mature (MECA-79^{hi} MAdCAM-1^{lo}) phenotype to an immature (MECA-79^{lo} MAdCAM-1^{hi}) phenotype (Mebius et al. 1993; Mebius et al. 1991; Swarte et al. 1998). MAdCAM-1 expression is therefore associated with an immature HEV phenotype (Drayton et al. 2006), and could reflect an early developmental status of HEV in tumours of Treg depleted animals. However, upon antigen challenge, HEV in reactive LNs undergo extensive remodelling during which they re-express MAdCAM-1 and downregulate PNAd (Liao & Ruddle 2006; Herzog et al. 2013). MAdCAM-1 expression on HEV is hence indicative of two entirely divergent biological scenarios: dedifferentiation concurrent with reversion to an immature phenotype, or robust activation of the endothelium. Some intra-tumoural vessels expressed MAdCAM-1 but not PNAd, suggesting the existence of a range of vessels at various states of differentiation and / or activation in the tumour (Figure 4.1). Interestingly, the anti-MAdCAM-1 antibody also reacted with PNAd^{+} HEV in LNs of Treg replete Foxp3^{DTR} animals, in contrast to reports of HEV in inguinal LN being MAdCAM-1 negative (Figure 4.2) (Girard et al. 2012). Further study, including functional analyses, will be required to determine the relevance of MAdCAM-1 expression on both tumour HEV and HEV of inguinal LNs in Foxp3^{DTR} animals.
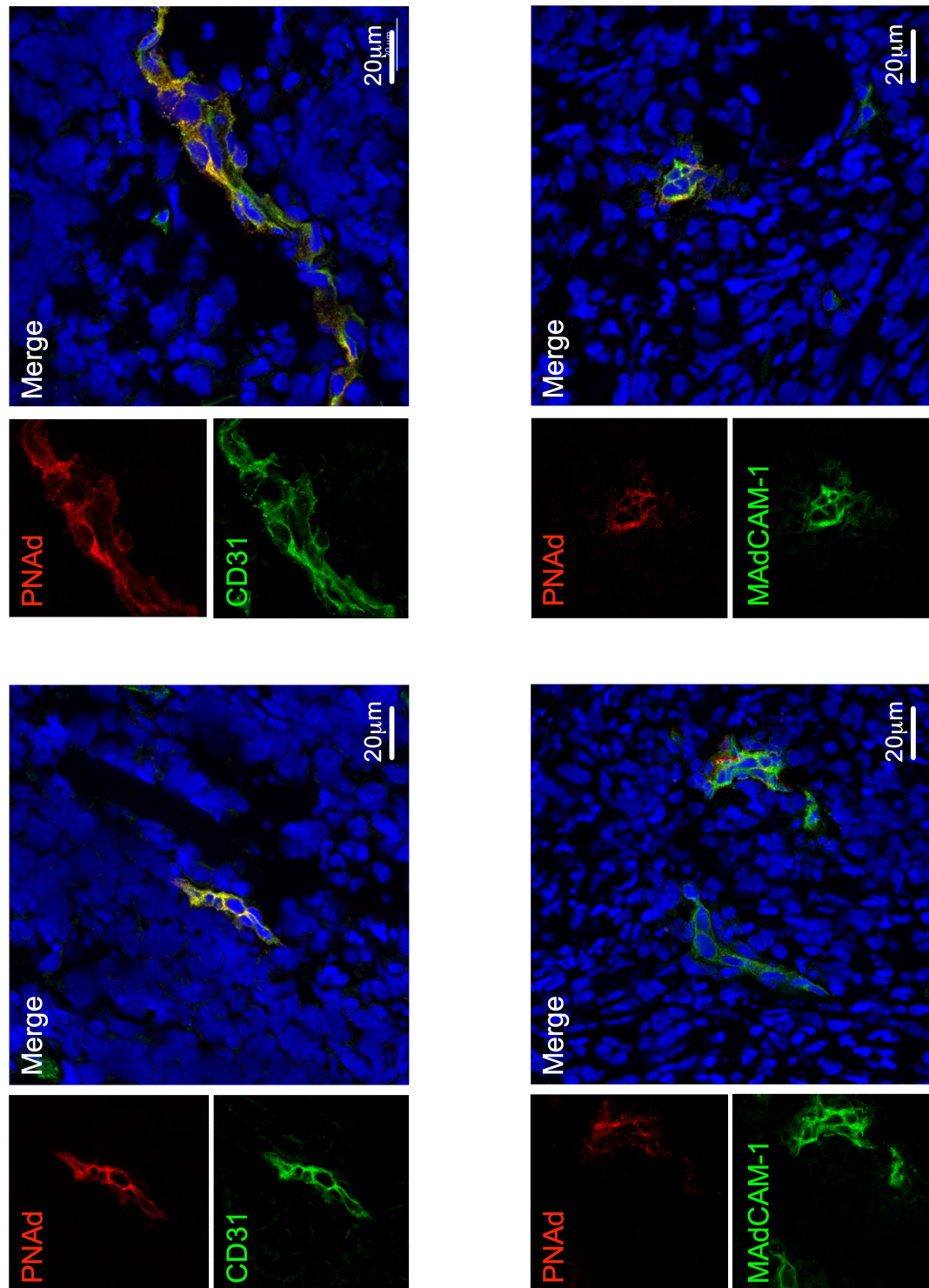
Figure 4.1 | High Endothelial Venules present in a range of morphologies in MCA-induced tumours in the absence of Tregs.
High power confocal images of High Endothelial Venules (HEV) within tumours of Treg depleted Foxp3[DTR] animals. Endothelial cells of HEV were detected by immunofluorescence staining using a biotinylated rat anti-PNAd primary antibody (clone MECA-79) and streptavidin Alexa Fluor® 555 secondary antibody (red). Tumour sections were dual-stained for PNAd and either CD31 (rat anti-CD31-FITC; green; top panels) or MAdCAM-1 (rat anti-MAdCAM-1 antibody followed by donkey anti-rat Alexa Fluor® 488 secondary antibody; green; bottom panels). Merged images include the nuclear stain DAPI (blue). Scale bars are shown.

[1] Spearman's correlation [2] Mann Whitney non-parametric t test [3] Kruskal-Wallis One-Way ANOVA with Dunn's multiple comparisons test [4] Linear Regression

Figure 4.2 | High Endothelial Venules in peripheral Lymph Nodes conform to a uniform morphology and size.
High power confocal images of High Endothelial Venules (HEV) within Lymph Nodes of Treg replete Foxp3^{DTR} animals. Endothelial cells of HEV were detected by immunofluorescence staining using a biotinylated rat anti-PNAd primary antibody (clone MECA-79) and streptavidin Alexa Fluor® 555 secondary antibody (red). Lymph Node sections were dual-stained for PNAd and either CD31 (rat anti-CD31-FITC; green; top panels) or MAdCAM-1 (rat anti-MAdCAM-1 antibody followed by donkey anti-rat Alexa Fluor® 488 secondary antibody; green; bottom panels). Merged images include the nuclear stain DAPI (blue). Scale bars are shown.

[1] Spearman's correlation [2] Mann Whitney non-parametric *t* test [3] Kruskal-Wallis One-Way ANOVA with Dunn's multiple comparisons test [4] Linear Regression

In addition to the profound splenomegaly and lymphadenopathy induced by Treg depletion in Foxp3^{DTR} animals (Kim et al. 2007), I noted significant disruption to the general organisation and morphology of LN microarchitecture, including HEV, after depletion of Tregs (Figures 4.3 and 4.4). Demarcation between T and B cell zones was almost completely lost; instead T cells could be found throughout the swollen LN. HEV had lost their distinctive orderly and uniform organisation within the LN: vessels of varying sizes were located randomly throughout the node (Figure 4.3). Furthermore, HEV were generally larger in size, with particularly open lumen, relative to LN HEV of Treg replete Foxp3^{DTR} animals. However, HEV maintained PNAd and MAdCAM-1 expression, which could on occasion be seen to be upregulated, relative to HEV of Treg replete animals (Figure 4.4). The observed alterations to the LN HEV network following Treg depletion are reminiscent of previous reports of expansion of HEV in peripheral LN following depletion of Treg in the Foxp3^{DTR} model (Kumar et al. 2012). By optical projection tomography analysis, Kumar and colleagues reported increases in HEV segment length, number of branching points and overall HEV length following Treg depletion, although it remains unknown whether the observed vascular expansion was a result of the autoinflammatory lymphadenopathy induced by Treg depletion, or direct Treg activity on the LN vasculature.

[1] Spearman's correlation [2] Mann Whitney non-parametric *t* test [3] Kruskal-Wallis One-Way ANOVA with Dunn's multiple comparisons test [4] Linear Regression
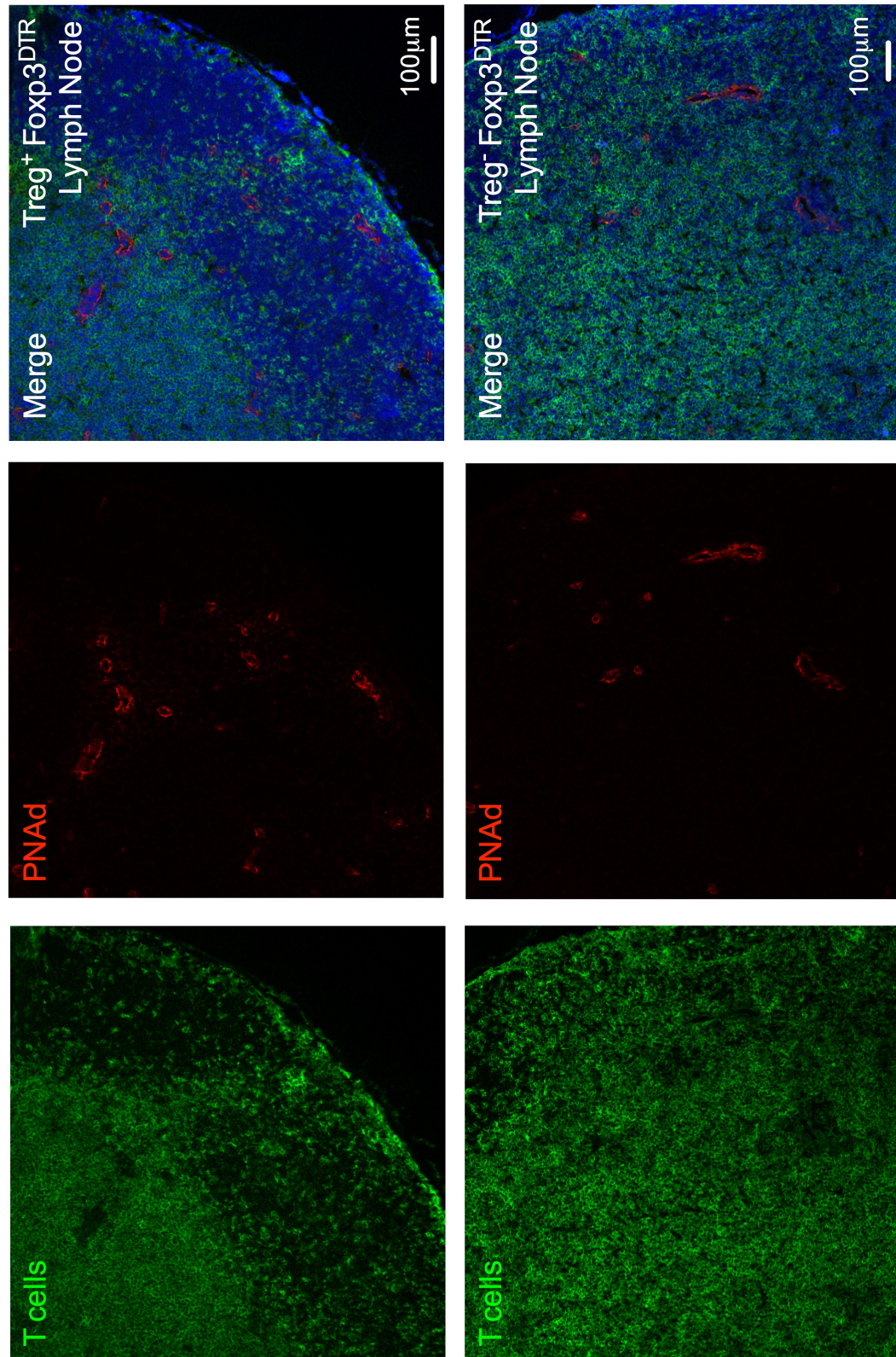
Figure 4.3 | Treg depletion induces profound microarchitectural changes in peripheral Lymph Nodes.
Low power confocal images of High Endothelial Venules (HEV) and T cells within Lymph Nodes of Treg replete (upper panels) and Treg depleted (lower panels) Foxp3[DTR] animals. Lymph node sections were immunofluorescently co-stained using a biotinylated rat anti-PNAd primary antibody (clone MECA-79), which was detected using a streptavidin Alexa Fluor® 555 secondary antibody (red), and rat anti-CD4 and rat anti-CD8a primary antibodies, which were detected using a donkey anti-rat Alexa Fluor® 488 secondary antibody (green). Merged images include the nuclear stain DAPI (blue). Scale bars are shown.
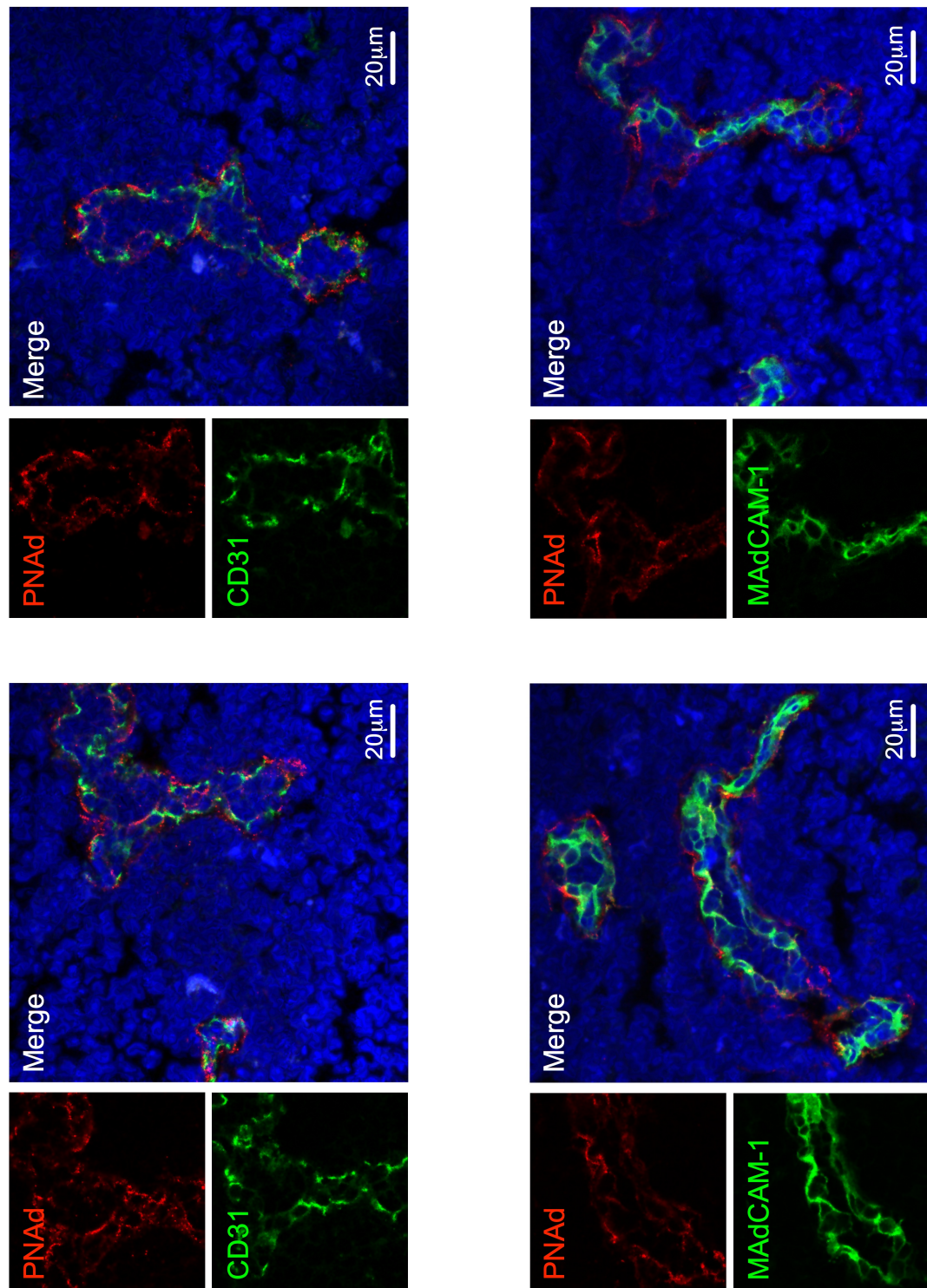
[1] Spearman's correlation [2] Mann Whitney non-parametric *t* test [3] Kruskal-Wallis One-Way ANOVA with Dunn's multiple comparisons test [4] Linear Regression
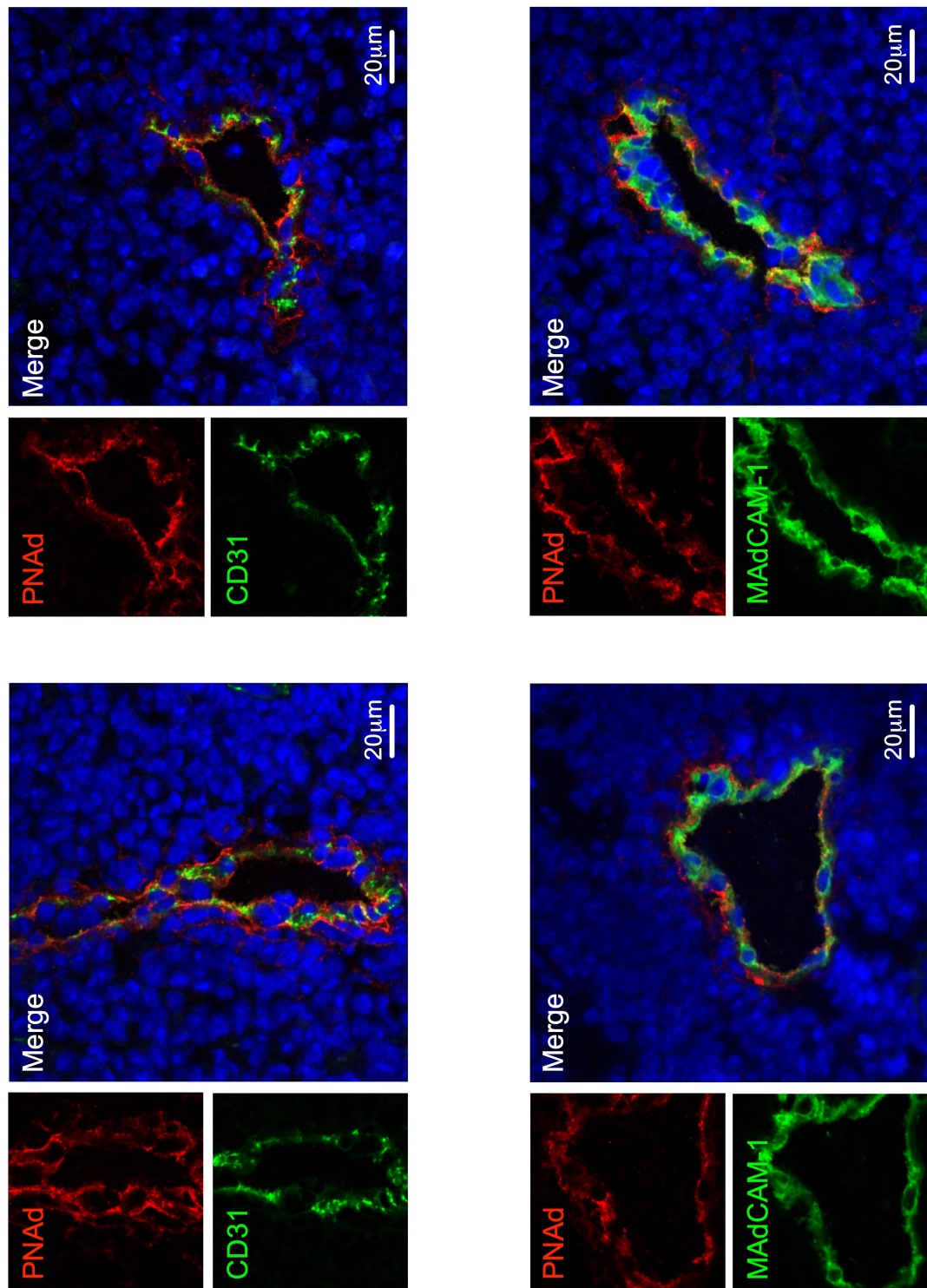
Figure 4.4 | Treg depletion induces significant alterations in High Endothelial Venule morphology in peripheral Lymph Nodes.

High power confocal images of High Endothelial Venules (HEV) within Lymph Nodes of Treg depleted Foxp3[DTR] animals. Endothelial cells of HEV were detected by immunofluorescence staining using a biotinylated rat anti-PNAd primary antibody (clone MECA-79) and streptavidin Alexa Fluor[®] 555 secondary antibody (red). Lymph Npde sections were dual-stained for PNAd and either CD31 (rat anti-CD31-FITC; green; top panels) or MAdCAM-1 (rat anti-MAdCAM-1 antibody followed by donkey anti-rat Alexa Fluor[®] 488 secondary antibody; green; bottom panels). Merged images include the nuclear stain DAPI (blue). Scale bars are shown.

4.3 Results: HEV Density Correlates with Increased T cell Infiltration and Reduced Tumour Growth Rate in Treg Depleted Tumours

Tumours of Treg depleted Foxp3[DTR] animals that contain HEV contain significantly increased numbers of CD8^{+} T cells and display significantly reduced tumour growth rates, relative to HEV negative tumours of Treg depleted animals, and tumours of Treg replete mice (Hindley et al. 2012). However, delineating tumours into "HEV positive" or "HEV negative" categories over-simplified the biological scenario: "HEV positive" tumours varied greatly in terms of numbers of vessels per unit area. In order to more accurately represent the observed variation, I developed a method of quantitating HEV in tumours. Using Zen software and scanned images of immunohistochemically stained tumour sections (Figure 4.5 A), I obtained quantitative measures of number of PNAd[+] HEV per unit area of tumour (HEV density), average area of HEV vessels per tumour (Average HEV area) and proportion of tumour area occupied by HEV vessels (Total HEV area; see Table 4.1 below). By quantifying HEV, I obtained measures by which to assess the impact of various treatments on HEV neogenesis in tumours, as described in the following Results sections.

Table 4.1 | Quantitative Parameters of Tumour HEV

Parameter	Calculation
HEV Density (per 10^6 μm^2)	(Absolute HEV number / Total tumour area (μm^2)) x 10^6
Total HEV area (%)	(Total HEV area (μm^2) / Total tumour area (μm^2)) x 100
Average HEV area (μm^2)	Total HEV area (μm^2) / Absolute HEV number

Both HEV density and total HEV area data fit a bifurcated pattern of distribution, whereby, within the dataset, one group of data points is very low or null, and the other group of data points is above this threshold and demonstrate positivity for the measure (Figure 4.5 B and D). These data corroborate the observation that approximately 50% of Treg depleted tumours contain HEV (Hindley et al. 2012). The average area of HEV of Treg depleted tumours varied significantly, ranging from less than 50 μm^2 to over 450 μm^2 (Figure 4.5 C).

[1] Spearman's correlation [2] Mann Whitney non-parametric *t* test [3] Kruskal-Wallis One-Way ANOVA with Dunn's multiple comparisons test [4] Linear Regression

I found a striking statistically significant positive correlation between HEV density and number of T cells in tumours of Treg depleted animals (r = 0.4781, *P=0.0284 for CD4^{+} T cells[1]; r = 0.6221, **P=0.0026 for CD8^{+} T cells[1]; Figure 4.6 A-B). There was also a positive correlation between total HEV area and number of T cells in tumours (r = 0.3806, nsP=0.0887 for CD4^{+} T cells[1]; r = 0.6286, **P=0.0023 for CD8^{+} T cells[1]; data not shown). These data support my hypothesis stating that T cells access the tumour via HEV following Treg depletion. Of note, those tumours with high numbers of CD4^{+} T cells generally also contained high numbers of CD8^{+} T cells.

Number of CD4^{+} T cells and CD8^{+} T cells negatively correlated with tumour growth rate, which did not reach statistical significance for CD4^{+} T cells (r = -0.3384, nsP=0.1335 for CD4^{+} T cells[1]; r = 5481, *P=0.0101 for CD8^{+} T cells[1]; Figure 4.6 C-D). These data indicate that following Treg depletion, infiltration of T cells, particularly CD8^{+} T cells, contributes towards tumour growth control. Interestingly, HEV density and total HEV area both displayed highly statistically significant negative correlations with tumour growth rate (r = -0.6519, **P=0.0014 for HEV density[1]; r = -0.7390, ***P=0.0001 for total HEV area[1]; Figure 4.6 E-F). The greater association between total HEV area and tumour growth rate than between HEV density and tumour growth rate suggests that not only number but relative area of HEV in tumours is important for dictating HEV-mediated tumour control. Furthermore, the more striking correlation between measures of HEV and tumour growth rate than between number of tumour infiltrating T cells and tumour growth rate suggests that HEV-mediated tumour control is a function not only of T cell infiltration via HEV, but also perhaps infiltration of other anti-tumour immune cells. For instance, HEV density also displays a weak positive correlation with number of CD45R^{+} B cells in tumours of Treg depleted animals (r = 0.4659, nsP=0.1275[1]; Figure 4.7). Collectively, these data support my hypothesis stated in Chapter One: intra-tumoural HEV facilitate control of tumour growth and tumour rejection by enabling infiltration of high numbers of anti-tumour T cells.

[1] Spearman's correlation [2] Mann Whitney non-parametric t test [3] Kruskal-Wallis One-Way ANOVA with Dunn's multiple comparisons test [4] Linear Regression
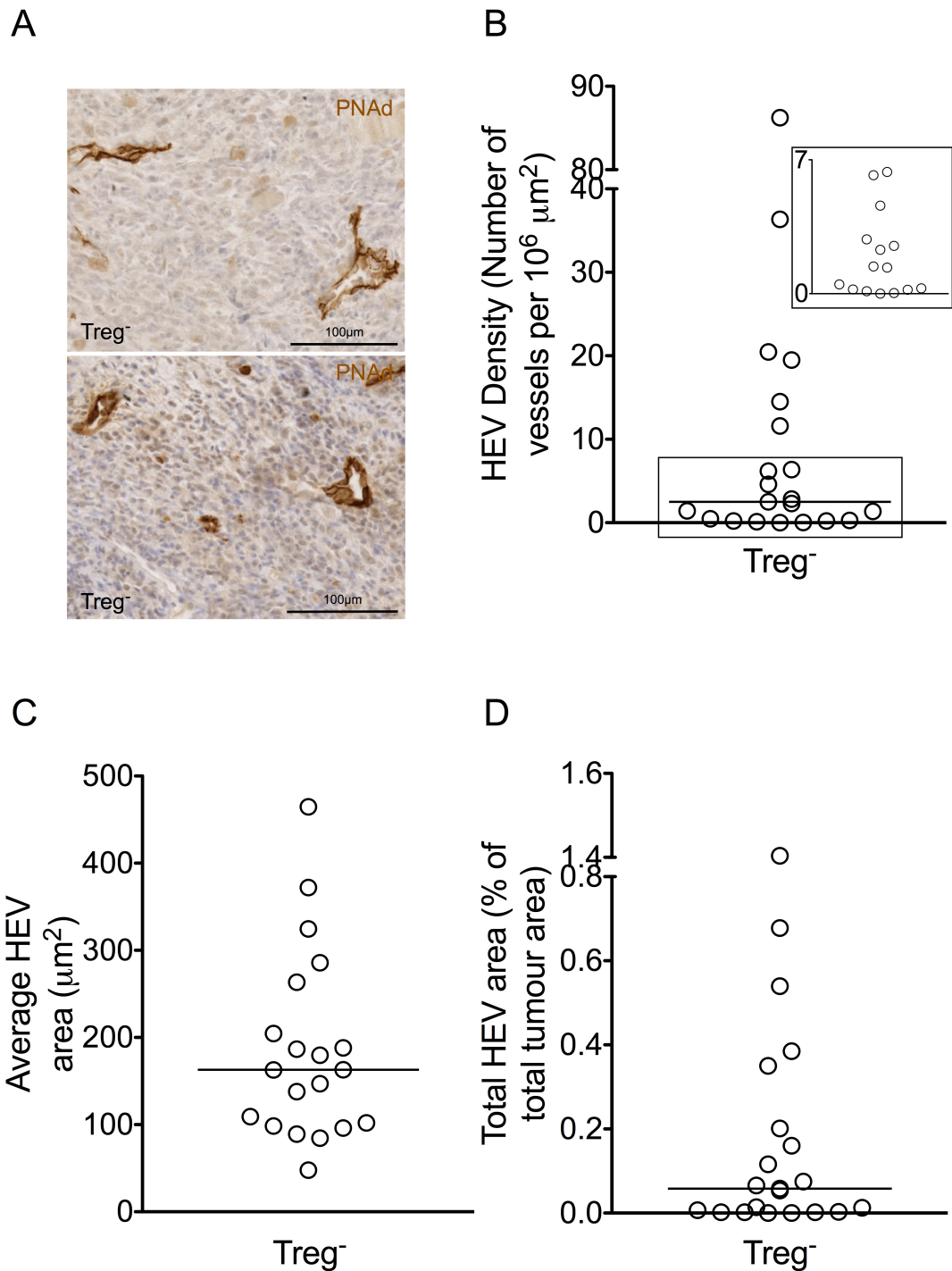
Figure 4.5 | MCA-induced tumours develop ectopic High Endothelial Venules following Treg depletion.
Quantitative measures of High Endothelial Venules (HEV) in tumours of Treg depleted Foxp3[DTR] animals. (A) Representative microscope images of HEV in paraffin embedded tumours. The anti-PNAd antibody (clone MECA-79) was detected using DAB chromogen (brown staining). Sections were counterstained using haematoxylin. Scale bars are shown. (B) HEV density was calculated per unit area of tumour (μm^2). The insert shows an enlarged version of the boxed area. (C) Average area of HEV vessels calculated in μm^2. (D) Total HEV area as a proportion of total tumour area, calculated as a percentage. Data are presented as individual datapoints plus median. Statistical significance was determined by Mann Whitney t tests. N = 21 (20 in C).

[1] Spearman's correlation [2] Mann Whitney non-parametric t test [3] Kruskal-Wallis One-Way ANOVA with Dunn's multiple comparisons test [4] Linear Regression
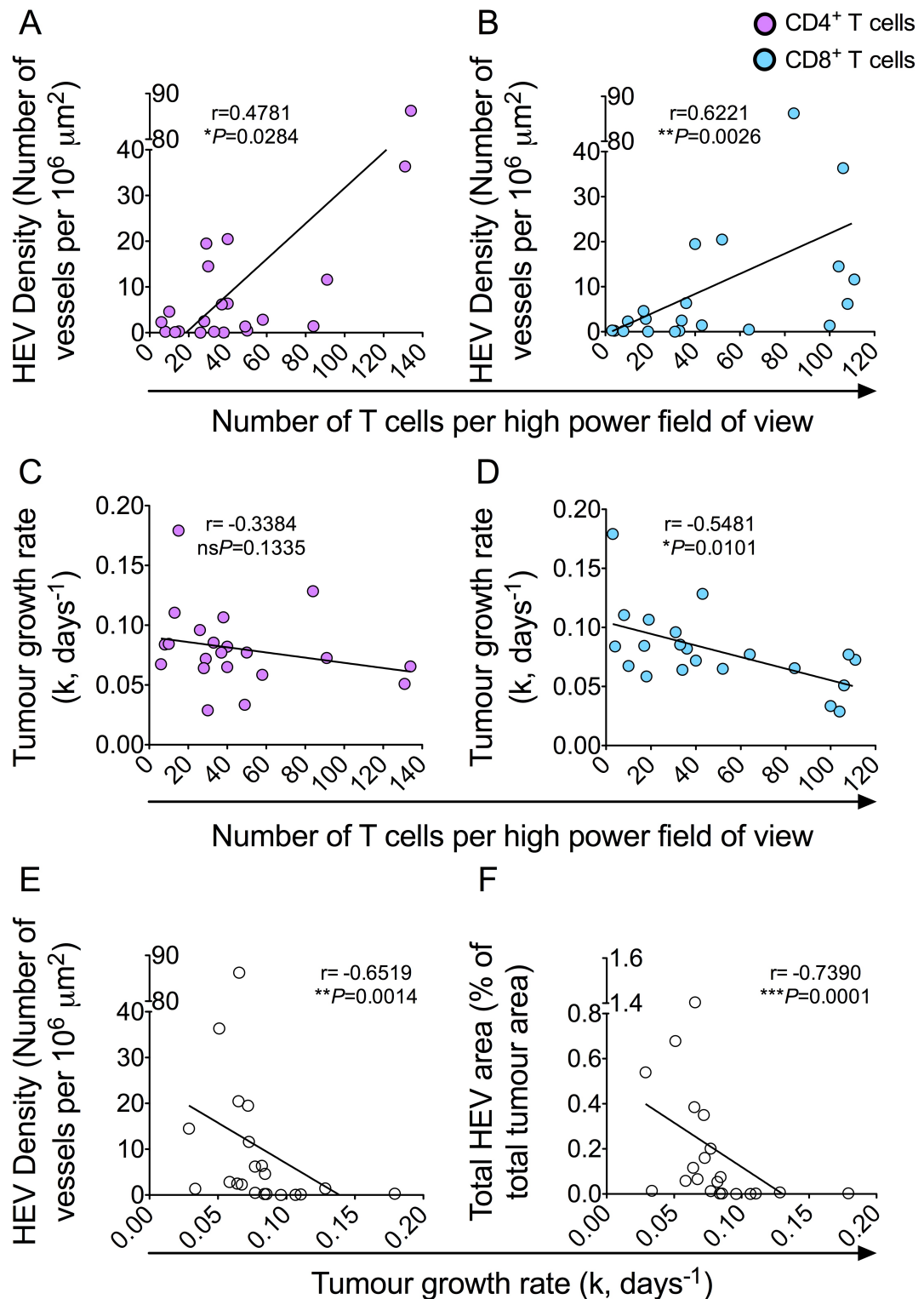
Figure 4.6 | Intra-tumoural High Endothelial Venules correlate with higher numbers of infiltrating T cells and reduced tumour growth rate.
Correlations between numbers of intra-tumoural CD4^{+} and CD8^{+} T cells, High Endothelial Venule (HEV) density and total HEV area, and tumour growth rates for Treg depleted Foxp3[DTR] animals. (A-B) Numbers of intra-tumoural CD4^{+} and CD8^{+} T cells plotted against tumour HEV density; CD4^{+} T cells (A; purple); CD8^{+} T cells (B; blue). (C-D) Numbers of intra-tumoural CD4^{+} and CD8^{+} T cells plotted against tumour growth rates (k, days[-1]); CD4^{+} T cells (C; purple); CD8^{+} T cells (D; blue). (E-F) HEV density (E) and total HEV area (as proportion of total tumour area; F) plotted against tumour growth rate (k, days[-1]). Statistical significance was determined by the non-parametric Spearman's correlation coefficient test, and the r statistic and P values are shown. N = 21.

[1] Spearman's correlation [2] Mann Whitney non-parametric t test [3] Kruskal-Wallis One-Way ANOVA with Dunn's multiple comparisons test [4] Linear Regression
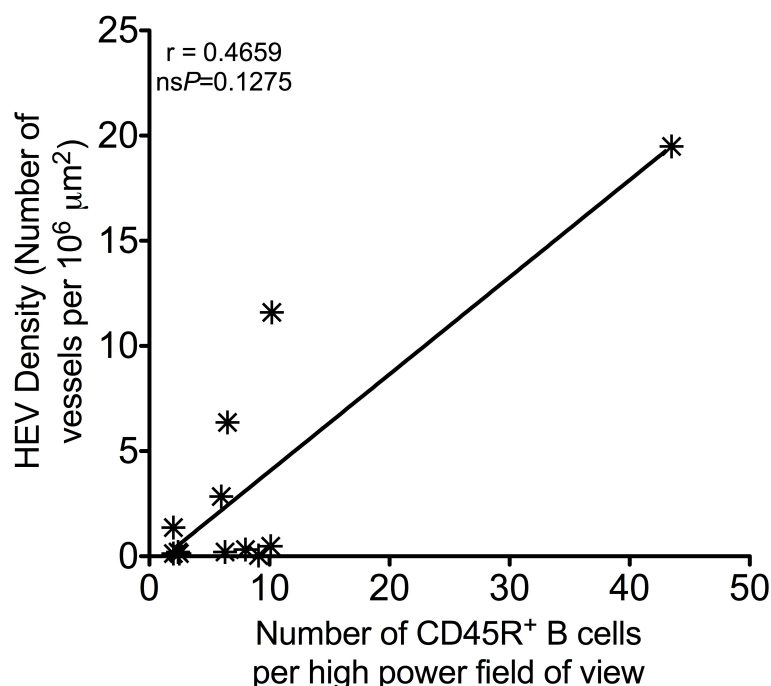
Figure 4.7 | High Endothelial Venule density correlates with numbers of CD45R^{+} B cells inside tumours.
Correlation between number of intra-tumoural CD45R^{+} B cells and High Endothelial Venule (HEV) density, in Treg depleted Foxp3[DTR] animals. Statistical significance was determined by the non-parametric Spearman's correlation coefficient test, and the r statistic and *P* values are shown. N = 12.

4.4 Depletion of B cells does not Abrogate HEV Neogenesis in Tumours

Foxp3[+] Tregs are capable of direct suppression of B cell proliferation and Immunoglobulin (Ig) production, and B cell killing (Lim et al. 2005; Zhao et al. 2006; Wang & Zheng 2013). In line with this, Treg depletion results in a significant increase in numbers of CD45R^{+} B cells in LN and spleen and dysregulated antibody production (Morgan et al. 2003; Kim et al. 2007). CD45R^{+} B cells are detectable in tumours of Foxp3[DTR] mice (unpublished data), and numbers of B cells in Treg depleted tumours correlates with HEV density (Figure 4.7). Furthermore, B cells are prolific producers of TNF superfamily cytokines involved in development of HEV-containing LN when activated (Ware 2005), raising the possibility that these cells could contribute to HEV formation in tumours following Treg depletion. For this reason, I set out to determine whether B cells are important for HEV neogenesis in tumours. I injected tumour-bearing animals with an anti-CD20 antibody to deplete B cells according to the protocol in Chapter Two and analysed tumour sections for HEV presence by immunohistochemistry.

[1] Spearman's correlation [2] Mann Whitney non-parametric *t* test [3] Kruskal-Wallis One-Way ANOVA with Dunn's multiple comparisons test [4] Linear Regression

To confirm efficacy of the anti-CD20 antibody, proportions of CD45R$^+$ B cells were analysed in tumour draining LN (DLN) and non-draining LNs (NDLN), and spleen by flow cytometry, and in tumour by counting of immunofluorescently stained frozen sections. A single administration of the anti-CD20 antibody at the beginning of the Treg depletion regime resulted in a significant decrease in both the proportion and absolute number of CD45R$^+$ B cells in spleen and lymph nodes, and absolute number of B cells in tumour (Figure 4.8).

PNAd$^+$ HEV were easily detectable in frozen tumour sections of Treg depleted animals in the absence of B cells (Figure 4.9). PNAd staining co-localised with CD31, confirming detection of vascular endothelial cells of vessels (data not shown). PNAd$^+$ HEV were also readily detectable in paraffin embedded tumour sections of the same B cell depleted, Treg depleted tumours (Figure 4.10 A). Quantification of PNAd$^+$ HEV demonstrated that there was no significant difference in HEV density in anti-CD20 treated Treg depleted tumours relative to Treg depleted tumours, despite a slight decrease in anti-CD20 tumours (ns*P*=0.1604[2], Figure 4.10 B). There was also no significant difference in the total HEV area between anti-CD20 treated Treg depleted tumours and Treg depleted tumours (ns*P*=0.4209[2], Figure 4.10 D). However, there was a highly significant increase in the average HEV area in anti-CD20 treated Treg depleted tumours relative to Treg depleted control tumours (***P*=0.0007[2], Figure 4.10 C).
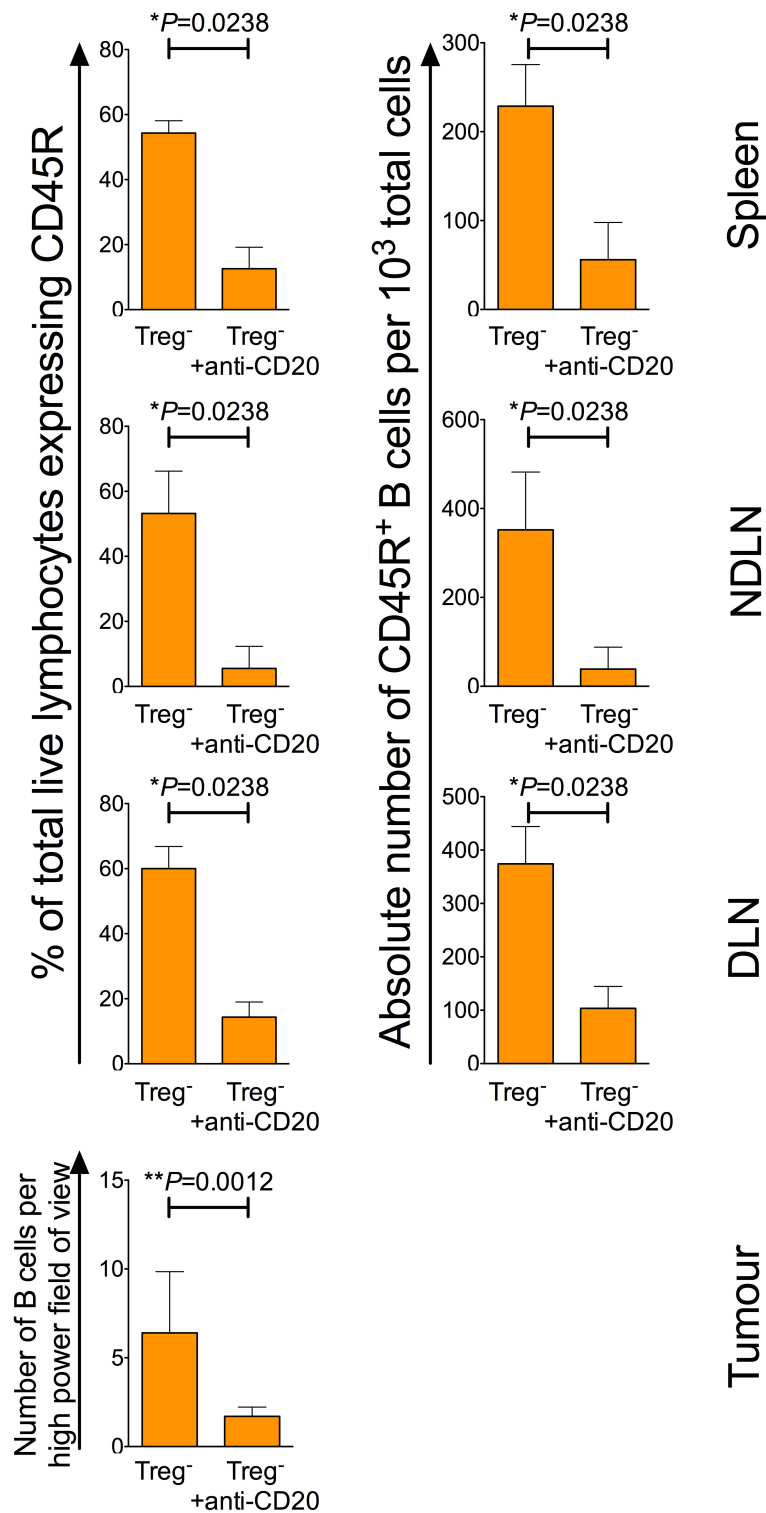
Figure 4.8 | Treatment with an anti-CD20 monoclonal antibody depletes CD45R^{+} B cells from lymphoid organs and tumour.

Proportion and absolute number of CD45R^{+} B cells in spleen, non tumour-draining lymph node (NDLN), tumour-draining lymph node (DLN) and tumour, determined by flow cytometry or counting of immunofluorescently stained tumour sections, in Treg depleted and anti-CD20 treated, Treg depleted Foxp3[DTR] animals, at the end of treatment. Data shown are: proportion of total live lymphocytes expressing CD45R (left), absolute number of CD45R^{+} B cells (middle) or counts of CD45R^{+} B cells per high power field of view for tumour (bottom left). Data are presented as median ± Interquartile range. Statistical significance was determined by Mann Whitney *t* tests. N = 6 (anti-CD20 treated Treg depleted); N = 3 (Treg depleted; lymphoid organs); N = 12 (anti-CD20 treated, Treg depleted and Treg depleted Foxp3[DTR] animals; tumours).

[1] Spearman's correlation [2] Mann Whitney non-parametric *t* test [3] Kruskal-Wallis One-Way ANOVA with Dunn's multiple comparisons test [4] Linear Regression
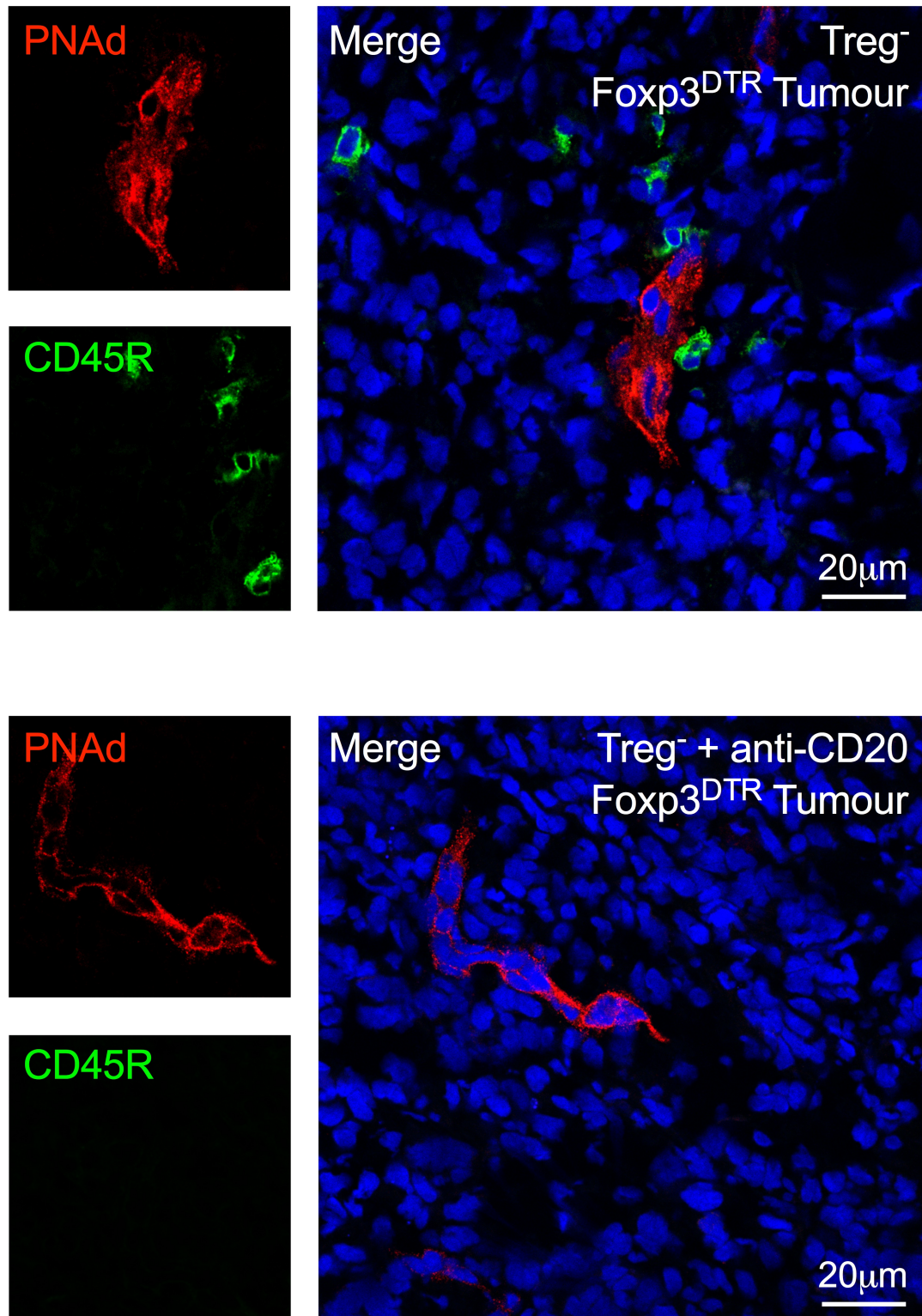
Figure 4.9 | High Endothelial Venules are found in tumours in the absence of CD45R^{+} B cells. Confocal images of High Endothelial Venules (HEV) within tumours of Treg depleted (top) and anti-CD20 treated, Treg depleted (bottom) Foxp3[DTR] animals. Endothelial cells of HEV were detected by immunofluorescence staining using a biotinylated rat anti-PNAd primary antibody (clone MECA-79) and streptavidin Alexa Fluor[®] 555 secondary antibody (red). Tumour sections were dual-stained for PNAd and B cells (rat anti-CD45R detected using donkey anti-rat Alexa Fluor[®] 488 secondary antibody; green). Merged images include the nuclear stain DAPI (blue). Scale bars are shown.

[1] Spearman's correlation [2] Mann Whitney non-parametric *t* test [3] Kruskal-Wallis One-Way ANOVA with Dunn's multiple comparisons test [4] Linear Regression
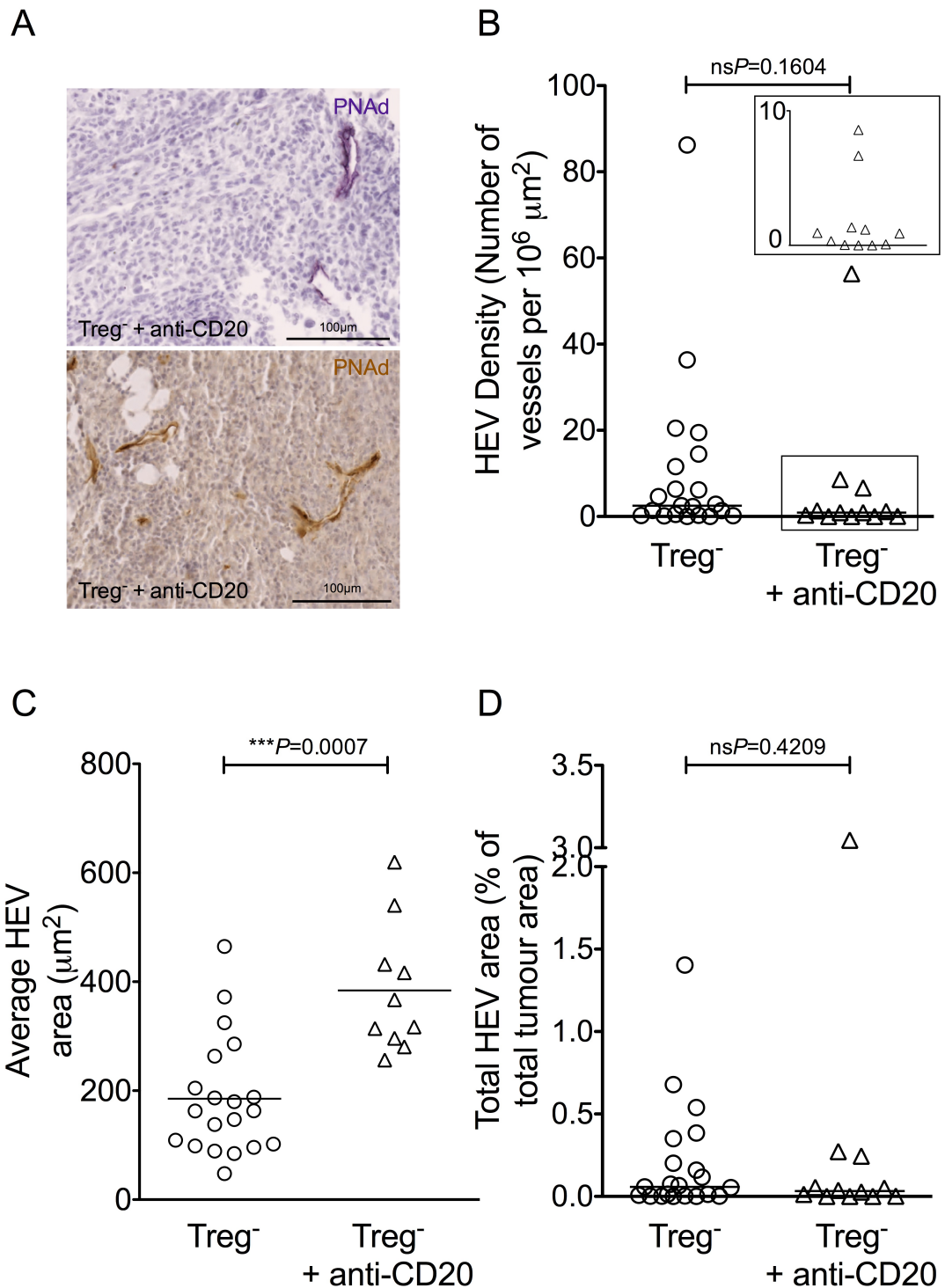
Figure 4.10 | Measures of High Endothelial Venule density and total area are not significantly altered in the absence of B cells.

Quantitative measures of High Endothelial Venules (HEV) in tumours of anti-CD20 treated, Treg depleted Foxp3[DTR] animals. (A) Representative microscope images of HEV in paraffin embedded tumours. The anti-PNAd antibody (clone MECA-79) was detected using either DAB chromogen (top; brown staining) or VIP chromogen (bottom; purple staining). Sections were counterstained using haematoxylin. Scale bars are shown. (B) HEV density was calculated per unit area of tumour (μm^2). The insert shows an enlarged version of the boxed area. (C) Average area of HEV vessels calculated in μm^2. (D) Total HEV area as a proportion of total tumour area, calculated as a percentage. Data are presented as individual datapoints plus median. Statistical significance was determined by Mann Whitney t tests. N = 12 anti-CD20 treated, Treg⁻ tumours (10 in C); N = 21 Treg⁻ tumours (20 in C).

[1] Spearman's correlation [2] Mann Whitney non-parametric t test [3] Kruskal-Wallis One-Way ANOVA with Dunn's multiple comparisons test [4] Linear Regression

To assess functionality of HEV in anti-CD20 treated Treg depleted tumours, I correlated HEV density or total HEV area with numbers of tumour infiltrating T cells and tumour growth rates (Figure 4.11). I found a weak positive correlation between HEV density and number of tumour infiltrating CD8^{+} T cells in anti-CD20 treated tumours (r = 0.6305, *P=0.0323[1]; Figure 4.11 A). The number of CD4^{+} T cells also appeared to correlate positively with HEV density, although statistical significance was not reached (r = 0.5639, nsP=0.0591[1]; Figure 4.11 B).

There was a weak negative correlation between numbers of CD4^{+} and CD8^{+} T cells and tumour growth rate, although this did not reach statistical significance for either type of T cell (r = -0.3217, nsP=0.3085 for CD4^{+} T cells[1]; r = -0.2657, nsP=0.4042 for CD8^{+} T cells[1]; Figure 4.11 C-D). Furthermore, there was a very weak correlation between measures of HEV density and total HEV area and tumour growth rate, which were far from reaching statistical significance (r = -0.1681, nsP=0.6039 for HEV density[1]; r = -0.0070, nsP=0.9910 for total HEV area[1]; Figure 4.11 E-F). These data suggested that despite no significant change in HEV density or total HEV area in anti-CD20 treated tumours relative to Treg depleted tumours, the functionality of HEV that developed during anti-CD20 treatment was significantly compromised relative to HEV in Treg depleted tumours, in terms of facilitating anti-tumour lymphocyte extravasation into tumours and subsequent tumour growth control.

Collectively, these data show that, whilst depletion of B cells results in a modest, insignificant decrease in HEV density in tumours, there is no difference in total HEV area in tumours. Therefore, HEV neogenesis can proceed uninterrupted in the absence of these cells. These data suggest that B cells do not represent a key LTi-like 'HEV-initiator' cell type in this system. However, the average size of HEV was significantly increased in the absence of B cells. Furthermore, the data suggest a function of B cells in the maintenance of a fully functional HEV phenotype in tumours, as the infiltration of high numbers of T cells via HEV and an association with reduced tumour growth rate was abrogated in the absence of B cells.

[1] Spearman's correlation [2] Mann Whitney non-parametric *t* test [3] Kruskal-Wallis One-Way ANOVA with Dunn's multiple comparisons test [4] Linear Regression
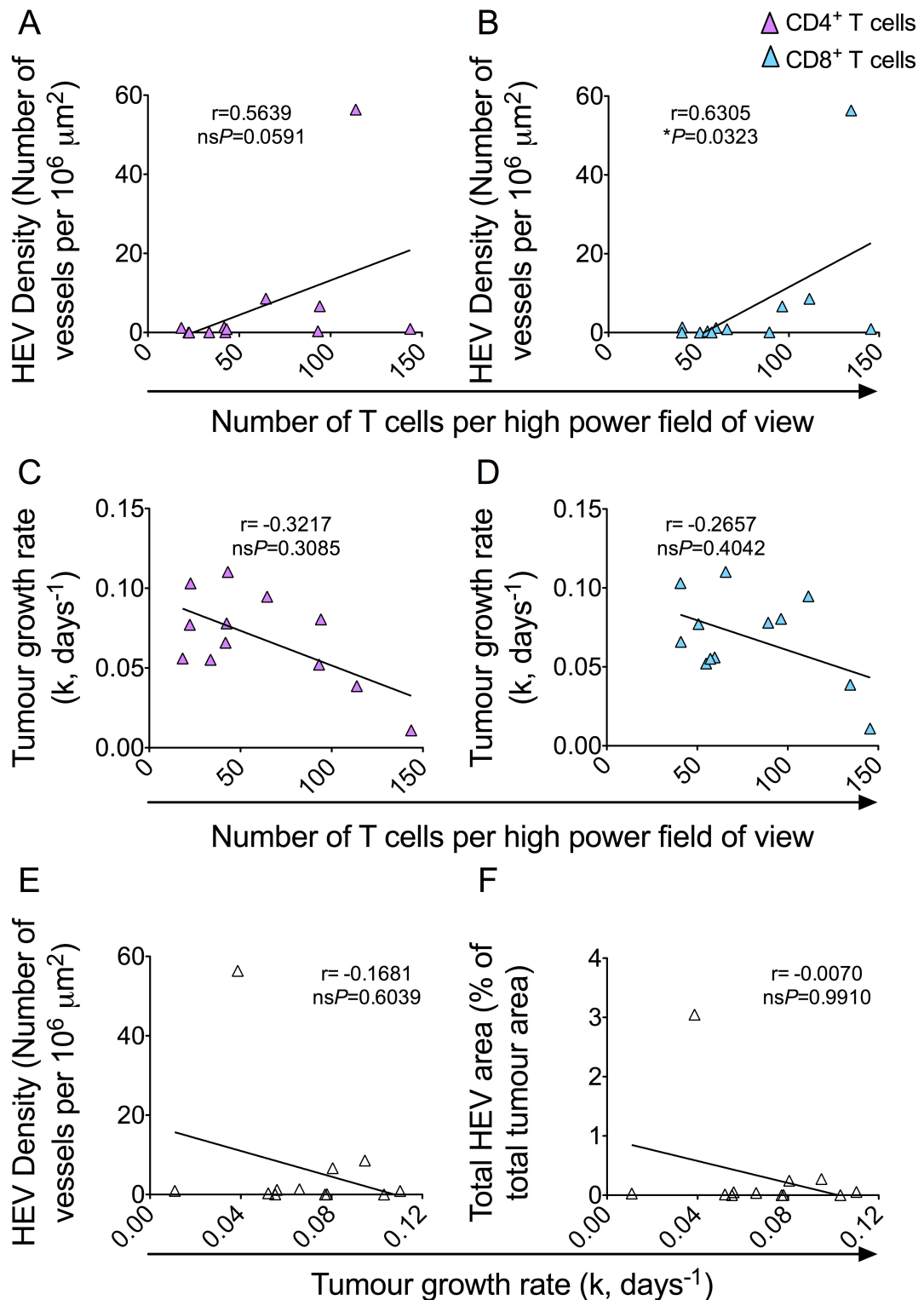
Figure 4.11 | Functionality of High Endothelial Venules in B cell-depleted tumours is significantly compromised.

Correlations between number of intra-tumoural CD4^{+} and CD8^{+} T cells, High Endothelial Venule (HEV) density and total HEV area, and tumour growth rates for anti-CD20 treated, Treg depleted Foxp3[DTR] animals. (A-B) Numbers of intra-tumoural CD4^{+} and CD8^{+} T cells plotted against tumour HEV density; CD4^{+} T cells (A; purple); CD8^{+} T cells (B; blue). (C-D) Numbers of intra-tumoural CD4^{+} and CD8^{+} T cells plotted against tumour growth rates (k, days[-1]); CD4^{+} T cells (C; purple); CD8^{+} T cells (D; blue). (E-F) HEV density (E) and total HEV area (as proportion of total tumour area; F) plotted against tumour growth rate (k, days[-1]). Statistical significance was determined by the non-parametric Spearman's correlation coefficient test, and the r statistic and P values are shown. N = 12.

[1] Spearman's correlation [2] Mann Whitney non-parametric t test [3] Kruskal-Wallis One-Way ANOVA with Dunn's multiple comparisons test [4] Linear Regression

4.5 Results: Depletion of Both CD4^{+} and CD8^{+} T cells Significantly Abrogates HEV Neogenesis in Tumours

Depletion of Tregs in Foxp3[DTR] animals results in a significant increase in number, proliferation and activation of both CD4^{+} and CD8^{+} T cells (Kim et al. 2007; Hindley et al. 2012). Furthermore, there is a highly significant increase in numbers of tumour-infiltrating CD4^{+} and CD8^{+} T cells following Treg depletion, which confer a significant reduction in tumour growth rate (Hindley et al. 2012). Our hypothesis states that neogenesis of HEV in tumours facilitates high numbers of both CD4^{+} and CD8^{+} T cells to infiltrate the tumour mass, which then ensure an effective anti-tumour immune response, resulting in tumour growth control. It is entirely possible that T cells themselves, which are highly activated following Treg depletion, also represent the initiator cell type in the process of HEV neogenesis.

T cells, like B cells, are prolific producers of TNF Superfamily cytokines involved in organogenesis of HEV-containing lymphoid organs (Ware 2005). T cells could therefore form part of a positive feedback loop, in which they produce cytokines necessary for development of HEV in tumours, which, once formed, allow entry of vast numbers of activated T cells constituting a robust anti-tumour immune response. I aimed to first establish whether *either* CD4^{+} or CD8^{+} T cells were required for HEV neogenesis in tumours by injecting tumour-bearing Treg depleted Foxp3[DTR] animals with a cocktail of anti-CD4 and anti-CD8 antibodies, according to the protocol in Chapter Two, and analysing tumour sections for HEV by immunohistochemistry. To deplete T cells, I used a combination of two different anti-CD4 monoclonal antibody clones (YTS-191 & YTA-3), and a combination of two different anti-CD8 monoclonal antibody clones (YTS-169 & YTS-156); each pair of antibodies has been shown to synergize *in vivo*, resulting in more efficient CD4^{+} or CD8^{+} T cell depletion, respectively, than when a single clone is administered alone (Qin et al. 1987; Qin et al. 1989; Cobbold et al. 1984).

Efficacy of the anti-CD4/ anti-CD8 antibody cocktail was examined by flow cytometric analysis of CD4^{+} and CD8^{+} T cell proportions and numbers in spleen, NDLN

[1] Spearman's correlation [2] Mann Whitney non-parametric *t* test [3] Kruskal-Wallis One-Way ANOVA with Dunn's multiple comparisons test [4] Linear Regression

and DLN, and tumour, as well as counting of T cells in immunofluorescently stained tumour sections. These analyses confirmed that the antibody cocktail resulted in a significant reduction in both the proportion and absolute number of both CD4^{+} and CD8^{+} T cells in spleen, LNs and tumour (Figure 4.12). Of note, the antibody cocktail resulted in the loss of the majority but not all T cells; absolute depletion of CD4^{+} T cells was particularly difficult to achieve.

PNAd^{+} staining could be found on occasion in frozen tumour sections (Figure 4.13). However, the vast majority of tumours from anti-CD4/CD8 treated animals contained no PNAd[+] staining. Where it could be found, PNAd staining co-localised with CD31 (data not shown).

PNAd[+] vessels were also incredibly scarce in paraffin embedded tumour sections from anti-CD4/CD8 treated animals (Figure 4.14 A). Those vessels that were present in anti-CD4/CD8 treated tumours appeared more fragile, with weaker PNAd[+] staining, and the endothelial cells even less plump than those in Treg depleted tumours. When PNAd[+] vessels in anti-CD4/CD8 treated tumours were quantified, I found a striking difference; despite incomplete depletion of T cells from tumours (Figure 4.12), anti-CD4/CD8 treated tumours contained significantly lower numbers of PNAd[+] HEV per unit tumour area than Treg depleted tumours (***P=0.0007[2]; Figure 4.14 B). There was no significant difference in average HEV area that formed in anti-CD4/CD8 treated tumours and Treg depleted tumours (ns$P$=0.4109[2], Figure 4.14 C). In corroboration of the striking reduction in HEV density, there was also a highly significant decrease in the total HEV area of anti-CD4/CD8 treated tumours relative to Treg depleted tumours (**P=0.0031[2]; Figure 4.14 D). These data show that even a partial reduction in T cell numbers in tumours severely abrogates the process of HEV neogenesis.

[1] Spearman's correlation [2] Mann Whitney non-parametric t test [3] Kruskal-Wallis One-Way ANOVA with Dunn's multiple comparisons test [4] Linear Regression
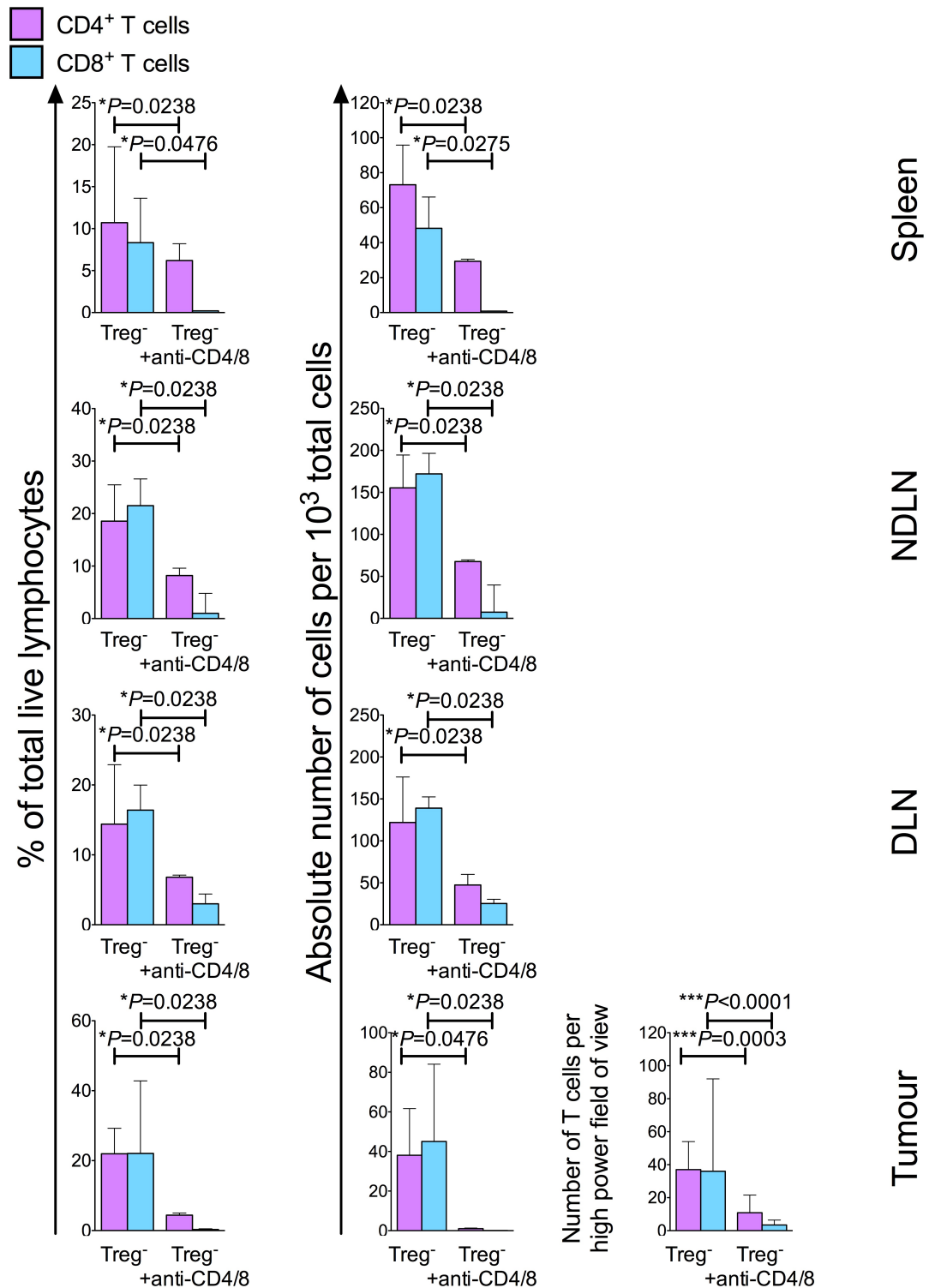
Figure 4.12 | Treatment with a cocktail of anti-CD4 and anti-CD8 monoclonal antibodies depletes CD4^{+} and CD8^{+} T cells from lymphoid organs and tumour.
Proportion and absolute number of T cells in spleen, non tumour-draining lymph node (NDLN), tumour-draining lymph node (DLN) and tumour, determined by flow cytometry or counting of immunofluorescently stained tumour sections, in Treg depleted and anti-CD4/CD8 treated, Treg depleted Foxp3[DTR] animals, at the end of treatment. Data shown are: proportion of total live lymphocytes expressing CD4 or CD8 (left), absolute number of CD4^{+} or CD8^{+} T cells (middle) or counts of CD4^{+} or CD8^{+} T cell per high power field of view in tumour (bottom right). CD4^{+} T cells (purple); CD8^{+} T cells (blue). Data are presented as median ± Interquartile range. Statistical significance was determined by Mann Whitney t tests. N = 3 for anti-CD4/CD8 treated Treg depleted, N = 6 for Treg depleted Foxp3[DTR] animals (proportion and absolute number by flow cytometry); N = 16 for anti-CD4/CD8 treated Treg depleted, N = 21 for Treg depleted Foxp3[DTR] animals (counting of immunofluorescently stained tumour sections).

[1] Spearman's correlation [2] Mann Whitney non-parametric t test [3] Kruskal-Wallis One-Way ANOVA with Dunn's multiple comparisons test [4] Linear Regression
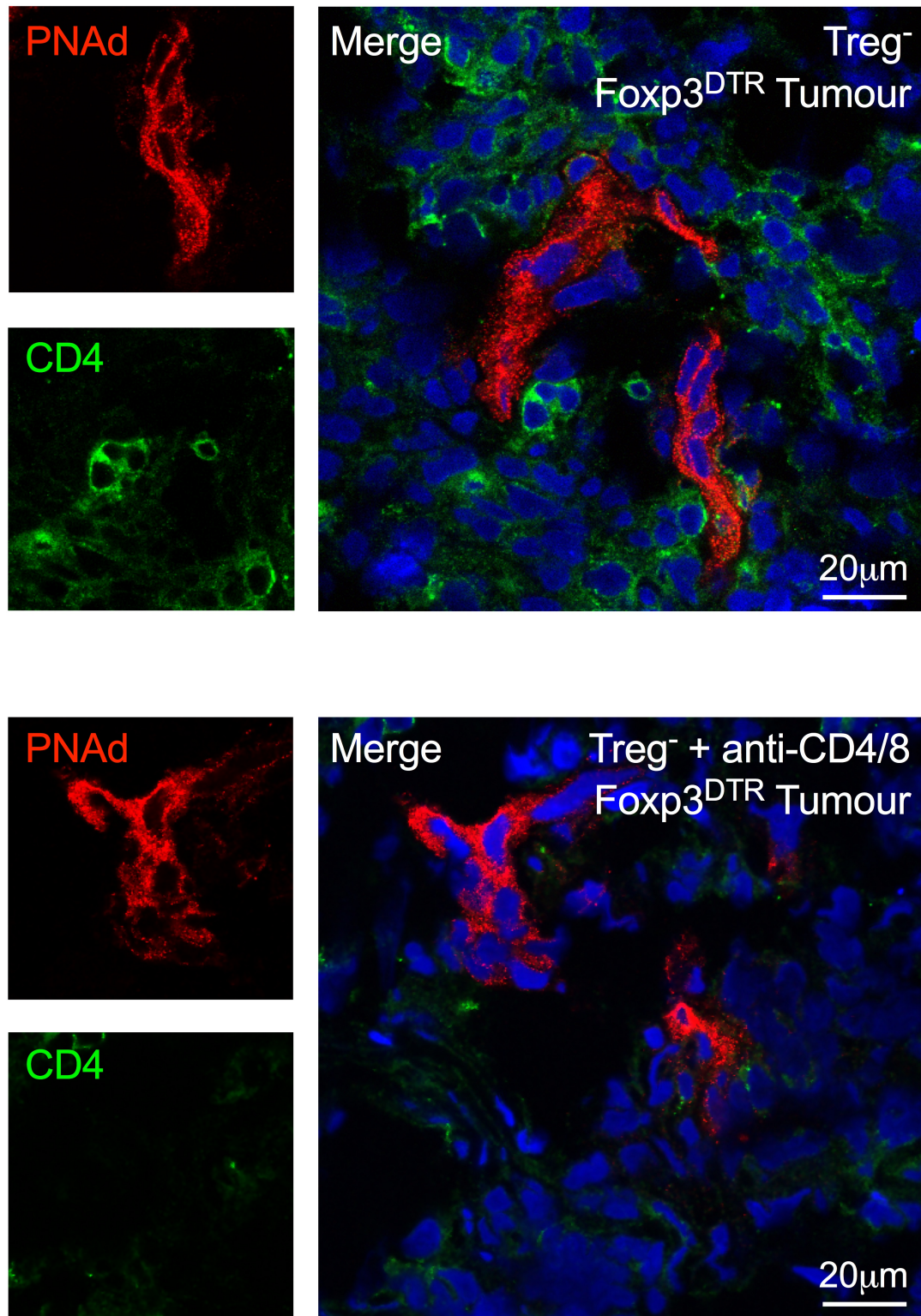
Figure 4.13 | High Endothelial Venules are found in tumours in the absence of T cells.
Confocal images of High Endothelial Venules (HEV) within tumours of Treg depleted (top) and anti-CD4/CD8 treated, Treg depleted (bottom) Foxp3^{DTR} animals. Endothelial cells of HEV were detected by immunofluorescence staining using a biotinylated rat anti-PNAd primary antibody (clone MECA-79) and streptavidin Alexa Fluor® 555 secondary antibody (red). Tumour sections were dual-stained for PNAd and CD4^{+} T cells (rat anti-CD4 detected using donkey anti-rat Alexa Fluor® 488 secondary antibody; green). Merged images include the nuclear stain DAPI (blue). Scale bars are shown.

[1] Spearman's correlation [2] Mann Whitney non-parametric *t* test [3] Kruskal-Wallis One-Way ANOVA with Dunn's multiple comparisons test [4] Linear Regression

Figure 4.14 | Measures of High Endothelial Venule density and total area are significantly decreased in the absence of T cells.

Quantitative measures of High Endothelial Venules (HEV) in tumours of anti-CD4/CD8 treated, Treg depleted Foxp3[DTR] animals. (A) Representative microscope images of HEV in paraffin embedded tumours. The anti-PNAd antibody (clone MECA-79) was detected using VIP chromogen (purple staining). Sections were counterstained using haematoxylin. Scale bars are shown. (B) HEV density was calculated per unit area of tumour (μm^2). The insert shows an enlarged version of the boxed area. (C) Average area of HEV vessels calculated in μm^2. (D) Total HEV area as a proportion of total tumour area, calculated as a percentage. Data are presented as individual datapoints plus median. Statistical significance was determined by Mann Whitney t tests. N = 16 anti-CD4/CD8 treated, Treg- tumours (14 in C); N = 21 Treg- tumours (20 in C).

[1] Spearman's correlation [2] Mann Whitney non-parametric t test [3] Kruskal-Wallis One-Way ANOVA with Dunn's multiple comparisons test [4] Linear Regression

A weak positive correlation between numbers of CD4^{+} T cells and HEV density was observed for anti-CD4/CD8 treated tumours; the association between numbers of CD8^{+} T cells and HEV density was stronger than that for CD4^{+} T cells, but neither association reached statistical significance (r = 0.2246, ns$P$=0.4030 for CD4^{+} T cells[1]; r = 0.4580, ns$P$=0.0744 for CD8^{+} T cells[1]; Figure 4.15 A-B). These data could indicate that either 1) HEV that develop in anti-CD4/CD8 treated tumours are at least partially functional in allowing T cell entry, or 2) HEV can *only* form in tumours in which CD4/CD8 depletion is not absolute. These data do not distinguish between these two possibilities, as it is impossible to delineate cause from effect here.

There was a weak positive correlation between numbers of CD4^{+} T cells and tumour growth rate that did not reach statistical significance (r = 0.3870, ns$P$=0.1386[1]), and no association between numbers of CD8^{+} T cells and tumour growth rate for anti-CD4/CD8 treated tumours (r = -0.0250, ns$P$=0.9267[1]; Figure 4.15 C-D). These data suggest the existence of a threshold of number of intra-tumoural T cells, which must be reached before an association with tumour growth rate can be recognised. In this case, there are too few T cells within the tumour to confer a reduction in growth rate. In corroboration of these data, the observed association between both HEV density and total HEV area and tumour growth rate in Treg depleted tumours is completely lost upon CD4/CD8 depletion (r = 0.0191, ns$P$=0.9439 for HEV density[1]; r = 0.0133, ns$P$=0.9612 for total HEV area[1]; Figure 4.15 E-F). These data support my hypothesis that HEV neogenesis confers a reduction in tumour growth via facilitating infiltration of high numbers of anti-tumour T cells: in the case of CD4/CD8 T cell depleted tumours described here, any residual HEV can no longer confer a reduction in growth due to the absence of such T cell populations.

Collectively, these data indicate that the mechanism of HEV neogenesis in tumours following Treg depletion is reliant on CD4^{+} and / or CD8^{+} T cells. The finding that HEV neogenesis is severely abrogated in the absence of T cells suggests that T cells could represent an LTi-like 'HEV-initiator' cell type in the tumours studied here.

[1] Spearman's correlation [2] Mann Whitney non-parametric *t* test [3] Kruskal-Wallis One-Way ANOVA with Dunn's multiple comparisons test [4] Linear Regression
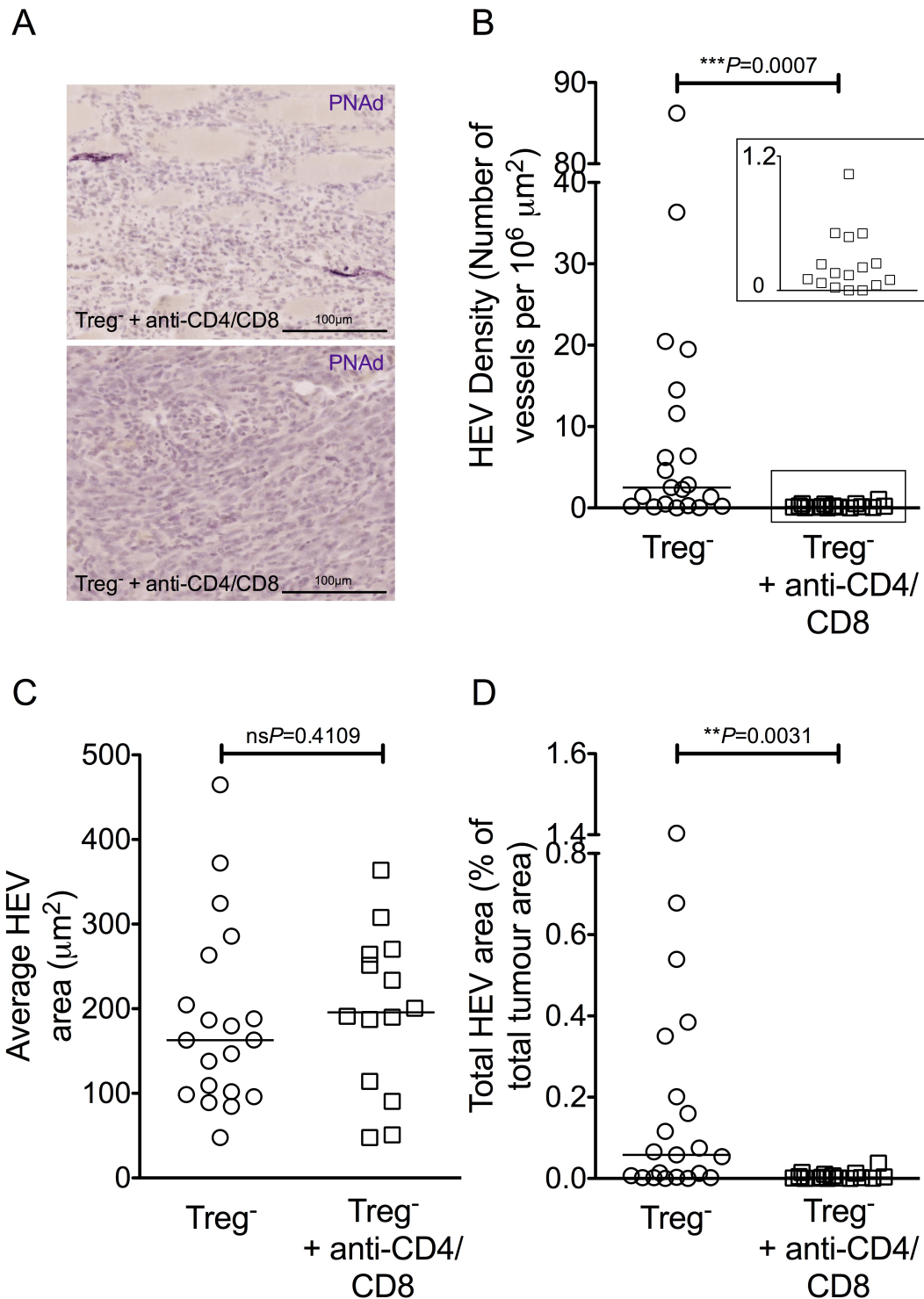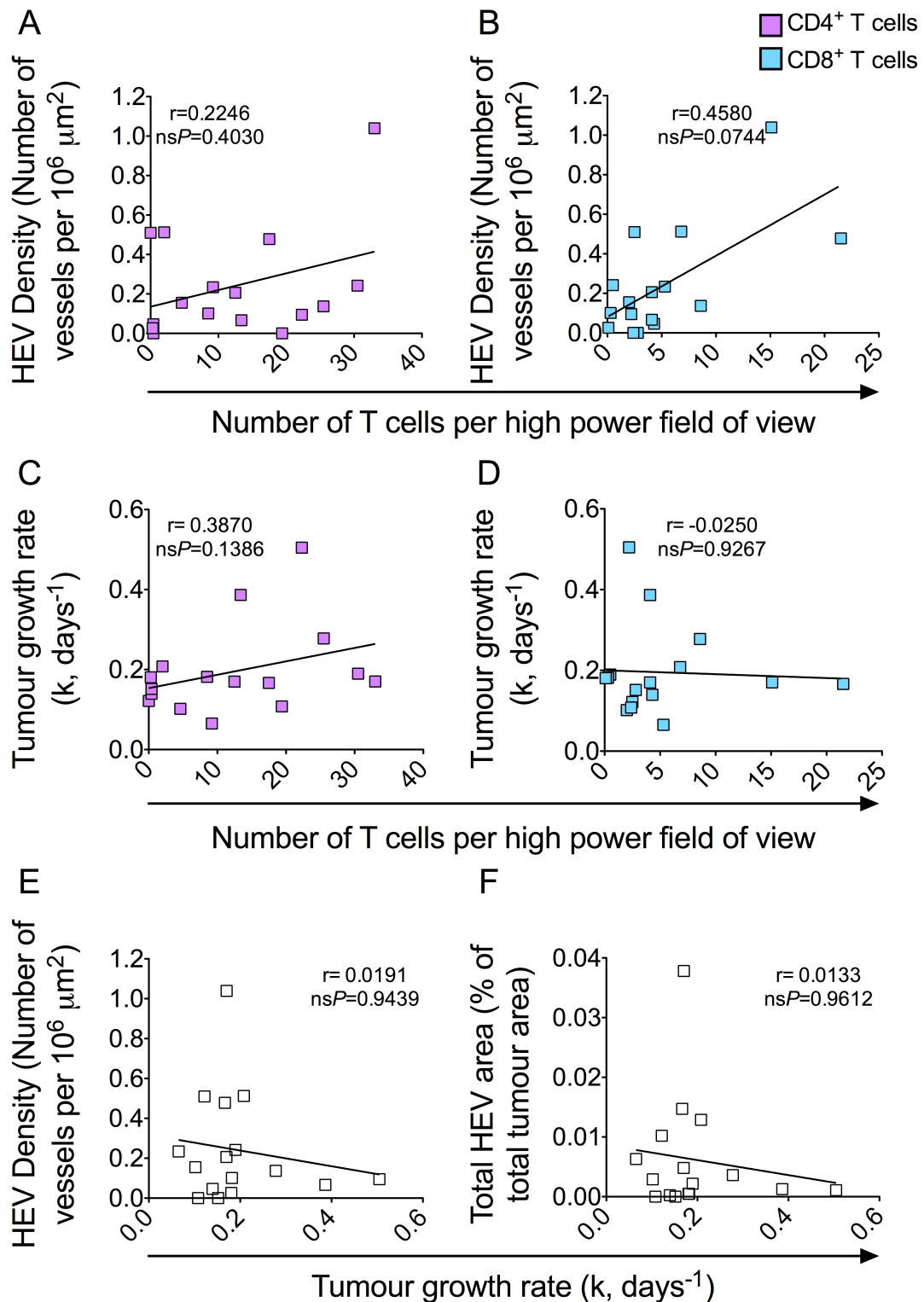
Figure 4.15 | Functionality of High Endothelial Venules in T cell-depleted tumours is significantly compromised.
Correlations between number of intra-tumoural CD4^{+} and CD8^{+} T cells, High Endothelial Venule (HEV) density and total HEV area, and tumour growth rates for anti-CD4/CD8 treated, Treg depleted Foxp3[DTR] animals. (A-B) Numbers of intra-tumoural CD4^{+} and CD8^{+} T cells plotted against tumour HEV density; CD4^{+} T cells (A; purple); CD8^{+} T cells (B; blue). (C-D) Numbers of intra-tumoural CD4^{+} and CD8^{+} T cells plotted against tumour growth rates (k, days[-1]); CD4^{+} T cells (C; purple); CD8^{+} T cells (D; blue). (E-F) HEV density (E) and total HEV area (as proportion of total tumour area; F) plotted against tumour growth rate (k, days[-1]). Statistical significance was determined by the non-parametric Spearman's correlation coefficient test, and the r statistic and P values are shown. N = 16.

[1] Spearman's correlation [2] Mann Whitney non-parametric t test [3] Kruskal-Wallis One-Way ANOVA with Dunn's multiple comparisons test [4] Linear Regression

4.6 Results: Depletion of CD4^{+} T cells Modestly Abrogates HEV Neogenesis in Tumours

Considering the striking findings described in Section 4.5 above, it was important to establish whether one or the other, or both of these two populations of T cells were instrumental in HEV neogenesis. To address this aim, I injected tumour-bearing Treg depleted Foxp3[DTR] animals with either anti-CD4 or anti-CD8 antibodies, as described in Chapter Two. The results of the anti-CD4 experiments are detailed here: for the results of the anti-CD8 experiments, see Section 4.7 below.

Efficacy of the anti-CD4 antibody was examined by flow cytometric analysis of T cell proportions and numbers in spleen, NDLN and DLN, and tumour, as well as counting of T cells in immunofluorescently stained tumour sections. These analyses confirmed that the anti-CD4 antibody resulted in a significant reduction in both the proportion and absolute number of CD4^{+} T cells in spleen, LNs and tumour (Figure 4.16). As for the experiments in which both CD4^{+} and CD8^{+} T cells were depleted, the anti-CD4 antibody resulted in the loss of the majority but not all T cells in all compartments.

Interestingly, depletion of CD4^{+} T cells resulted in a significant increase in not only the proportion (in LNs) but also the absolute number of CD8^{+} T cells in spleen and LNs (Figure 4.16). This affect of CD4^{+} T cell depletion on CD8^{+} T cell numbers using these specific monoclonal antibodies has been previously reported (Cobbold et al. 1992)(S. Cobbold communication). The underlying mechanism remains unknown, although it has been suggested that this affect is a result of compensatory homeostatic repopulation of the naïve T cell pool: naïve T cell homeostasis does not discriminate between CD4 and CD8 T cell populations and due to the considerably higher numbers of CD4^{+} than CD8^{+} T cells in normal animals, CD8 depletion allows little room for repopulation by CD4 but CD4 depletion creates significant room for repopulation by CD8 T cells (S. Cobbold communication).

[1] Spearman's correlation [2] Mann Whitney non-parametric *t* test [3] Kruskal-Wallis One-Way ANOVA with Dunn's multiple comparisons test [4] Linear Regression
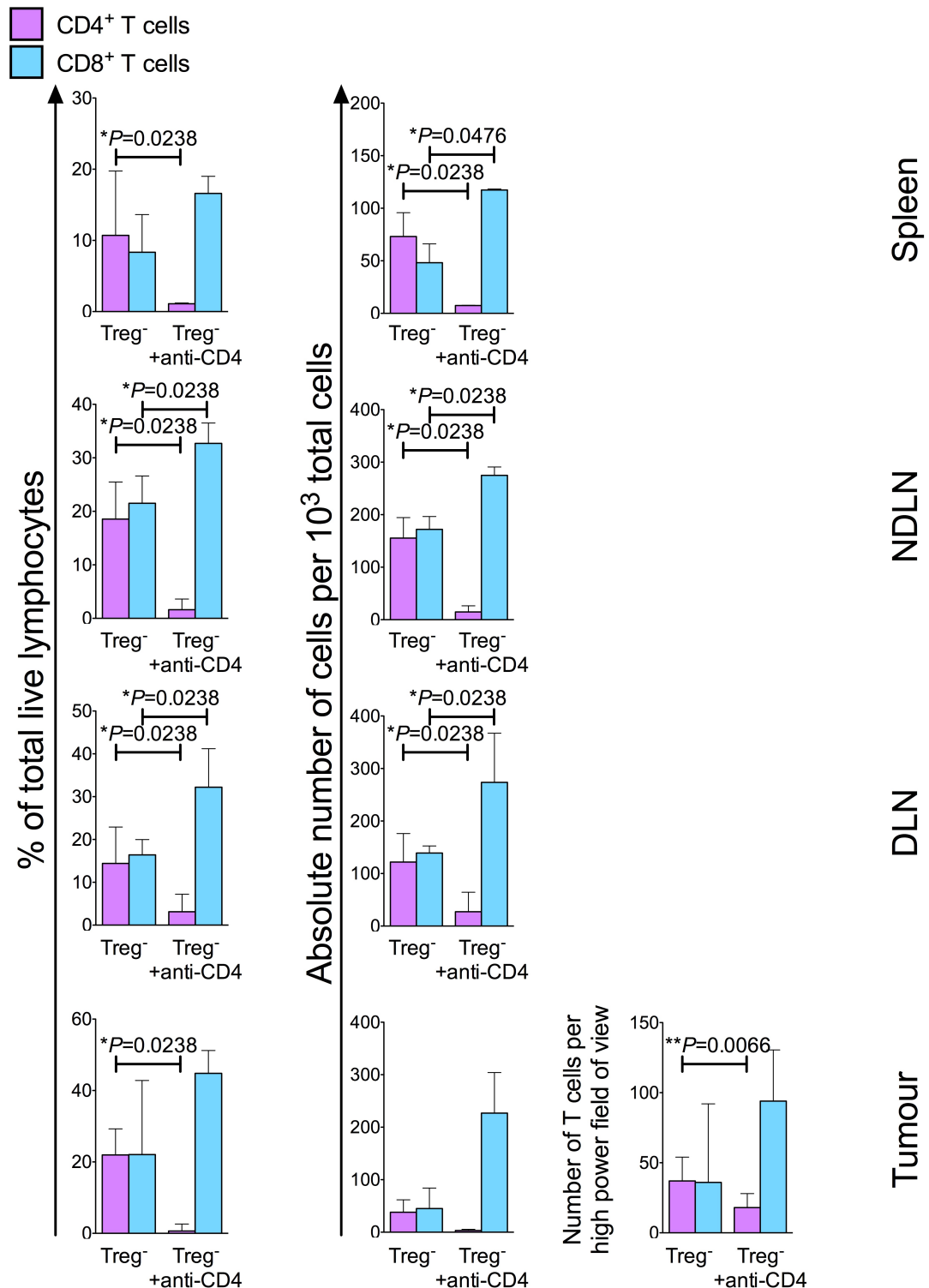
Figure 4.16 | Treatment with an anti-CD4 monoclonal antibody depletes CD4$^+$ T cells from lymphoid organs and tumour.

Proportion and absolute number of T cells in spleen, non tumour-draining lymph node (NDLN), tumour-draining lymph node (DLN) and tumour, determined by flow cytometry or counting of immunofluorescently stained tumour sections, in Treg depleted and anti-CD4 treated, Treg depleted Foxp3^{DTR} animals, at the end of treatment. Data shown are: proportion of total live lymphocytes expressing CD4 or CD8 (left), absolute number of CD4$^+$ or CD8$^+$ T cells (middle) or counts of CD4$^+$ or CD8$^+$ T cell per high power field of view in tumour (bottom right). CD4$^+$ T cells (purple); CD8$^+$ T cells (blue). Data are presented as median ± Interquartile range. Statistical significance was determined by Mann Whitney t tests. N = 3 for anti-CD4 treated Treg depleted, N = 6 for Treg depleted Foxp3^{DTR} animals (proportion and absolute number by flow cytometry); N = 11 for anti-CD4 treated Treg depleted, N = 21 for Treg depleted Foxp3^{DTR} animals (counting of immunofluorescently stained tumour sections).

[1] Spearman's correlation [2] Mann Whitney non-parametric t test [3] Kruskal-Wallis One-Way ANOVA with Dunn's multiple comparisons test [4] Linear Regression

PNAd[+] staining could be found in frozen tumour sections of some anti-CD4 treated animals (Figure 4.17), but, similarly to the anti-CD4/CD8 treated cohort, the majority of tumours from anti-CD4 treated animals contained no PNAd[+] staining. Where it could be found, PNAd staining again co-localised with CD31 (data not shown).

PNAd[+] vessels were also relatively scarce in paraffin embedded tumour sections from anti-CD4 treated animals (Figure 4.18 A). Anti-CD4 treated tumours demonstrated a modestly reduced HEV density relative to Treg depleted tumours (*P=0.0469[2]; Figure 4.18 B). The difference between anti-CD4 treated tumours and Treg depleted tumours was not as striking as that between anti-CD4/CD8 treated tumours and Treg depleted tumours, as described in Section 4.5. There was a highly significant increase in average HEV area in anti-CD4 treated tumours relative to Treg depleted tumours (***P=0.0005[2]; Figure 4.18 C). In line with the slight reduction in HEV density, total HEV area demonstrated a modest, statistically insignificant decrease in tumours of anti-CD4 treated tumours relative to Treg depleted tumours (ns$P$=0.2331[2]; Figure 4.18 D).

---

[1] Spearman's correlation [2] Mann Whitney non-parametric t test [3] Kruskal-Wallis One-Way ANOVA with Dunn's multiple comparisons test [4] Linear Regression
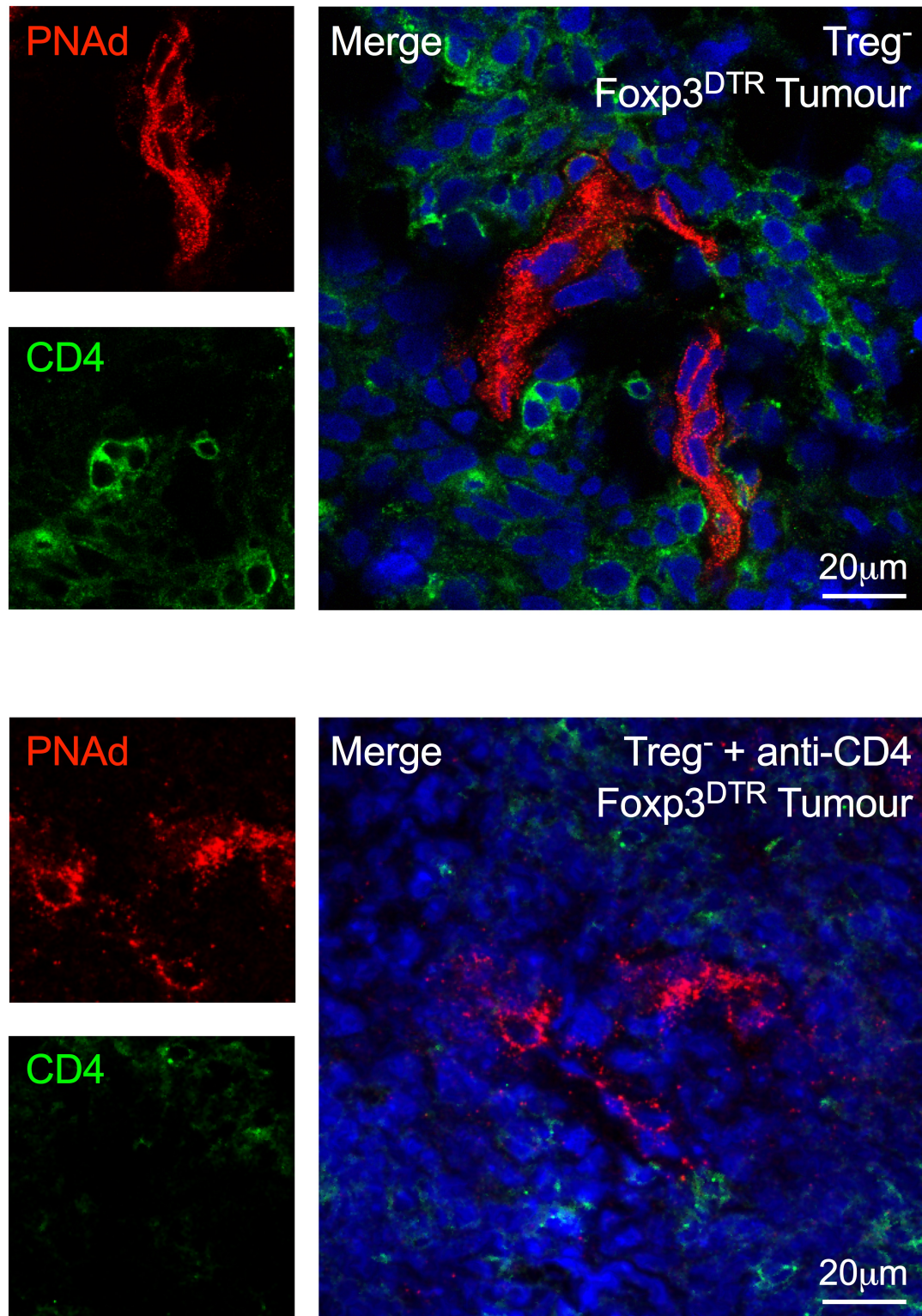
Figure 4.17 | High Endothelial Venules are found in tumours in the absence of CD4^{+} T cells. Confocal images of High Endothelial Venules (HEV) within tumours of Treg depleted (top) and anti-CD4 treated, Treg depleted (bottom) Foxp3[DTR] animals. Endothelial cells of HEV were detected by immunofluorescence staining using a biotinylated rat anti-PNAd primary antibody (clone MECA-79) and streptavidin Alexa Fluor® 555 secondary antibody (red). Tumour sections were dual-stained for PNAd and CD4^{+} T cells (rat anti-CD4 detected using donkey anti-rat Alexa Fluor® 488 secondary antibody; green). Merged images include the nuclear stain DAPI (blue). Scale bars are shown.

[1] Spearman's correlation [2] Mann Whitney non-parametric *t* test [3] Kruskal-Wallis One-Way ANOVA with Dunn's multiple comparisons test [4] Linear Regression
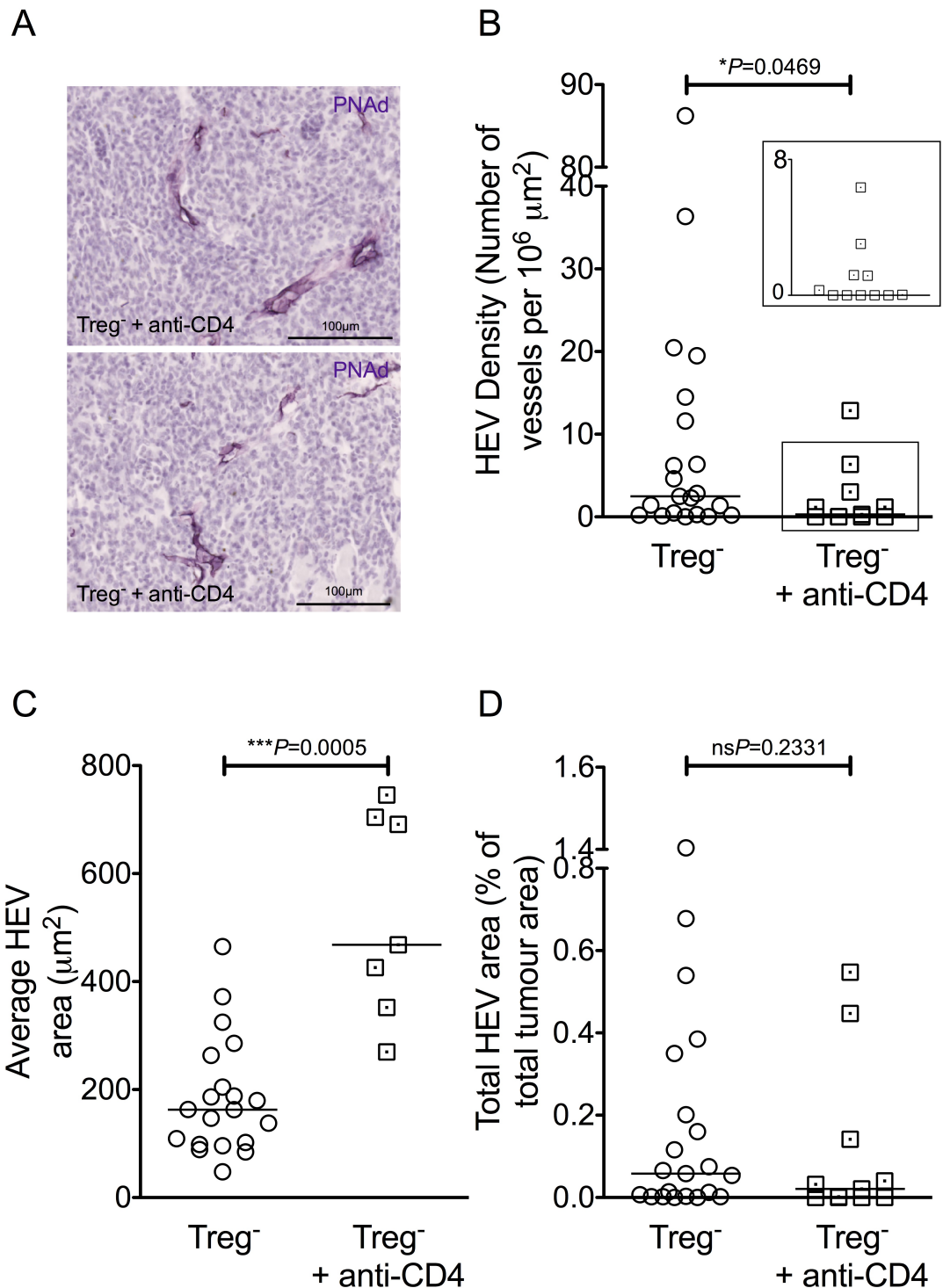
Figure 4.18 | Measures of High Endothelial Venule density and total area are modestly decreased in the absence of CD4$^+$ T cells.

Quantitative measures of High Endothelial Venules (HEV) in tumours of anti-CD4 treated, Treg depleted Foxp3^{DTR} animals. (A) Representative microscope images of HEV in paraffin embedded tumours. The anti-PNAd antibody (clone MECA-79) was detected using VIP chromogen (purple staining). Sections were counterstained using haematoxylin. Scale bars are shown. (B) HEV density was calculated per unit area of tumour (µm^2). The insert shows an enlarged version of the boxed area. (C) Average area of HEV vessels calculated in µm^2. (D) Total HEV area as a proportion of total tumour area, calculated as a percentage. Data are presented as individual datapoints plus median. Statistical significance was determined by Mann Whitney t tests. N = 11 anti-CD4/CD8 treated, Treg$^-$ tumours (7 in C); N = 21 Treg$^-$ tumours (20 in C).

[1] Spearman's correlation [2] Mann Whitney non-parametric t test [3] Kruskal-Wallis One-Way ANOVA with Dunn's multiple comparisons test [4] Linear Regression

Plotting HEV density as a function of the number of remaining CD4^{+} T cells in tumours of anti-CD4 treated animals revealed that, in contrast to Treg depleted control tumours, HEV density only weakly correlated with numbers of CD4^{+} T cells (r = 0.5583, ns*P*=0.0761[1]; Figure 4.19 A). These data could suggest that HEV that form in the absence of CD4^{+} T cells are dysfunctional in their ability to allow infiltration of residual CD4^{+} T cells into tumours. This scenario is unlikely, considering the weak but significant positive correlation between HEV density and numbers of infiltrating CD8^{+} T cells (r = 0.7118, *P*=0.0162[1]; Figure 4.19 B). Thus, HEV that form in the absence of CD4^{+} T cells are at least partly functional in facilitating T cell trafficking into tumours.

Number of tumour infiltrating CD4^{+} T cells demonstrated a weak negative correlation with tumour growth rate, suggesting residual CD4^{+} T cells were efficient in conferring a degree of anti-tumour efficacy (r = -0.6000, ns*P*=0.0968[1]; Figure 4.19 C). Number of tumour infiltrating CD8^{+} T cells demonstrated a statistically significant negative correlation with tumour growth rate, corroborating the idea that HEV in CD4-depleted tumours were functional in terms of supporting CD8^{+} T cell trafficking (r = -0.7500, *P*=0.0255[1]; Figure 4.19 D). Furthermore, there was a weak negative correlation between both HEV density and total HEV area and tumour growth rate, despite neither association reaching statistical significance (r = -0.4686, ns*P*=0.2125 for HEV density[1]; r = -0.3849, ns*P*=0.3125 for total HEV area[1]; Figure 4.19 E-F).

Collectively, these data suggest CD4^{+} T cells play a minor role in HEV neogenesis, as HEV formation is modestly abrogated after loss of these cells. However, development of HEV in tumours in which depletion of CD4^{+} T cells was almost absolute suggests the presence of other cell types capable of directing HEV neogenesis. The difference in HEV density and total HEV area between tumours of anti-CD4/CD8 treated and anti-CD4 treated tumours suggests CD8^{+} T cells may play an important role in this process. The slight decrease in functionality of HEV that formed in the absence of CD4^{+} T cells relative to HEV in control Treg depleted tumours could reflect a requirement for CD4^{+} T cell help by anti-tumour CD8^{+} T cells.

[1] Spearman's correlation [2] Mann Whitney non-parametric *t* test [3] Kruskal-Wallis One-Way ANOVA with Dunn's multiple comparisons test [4] Linear Regression
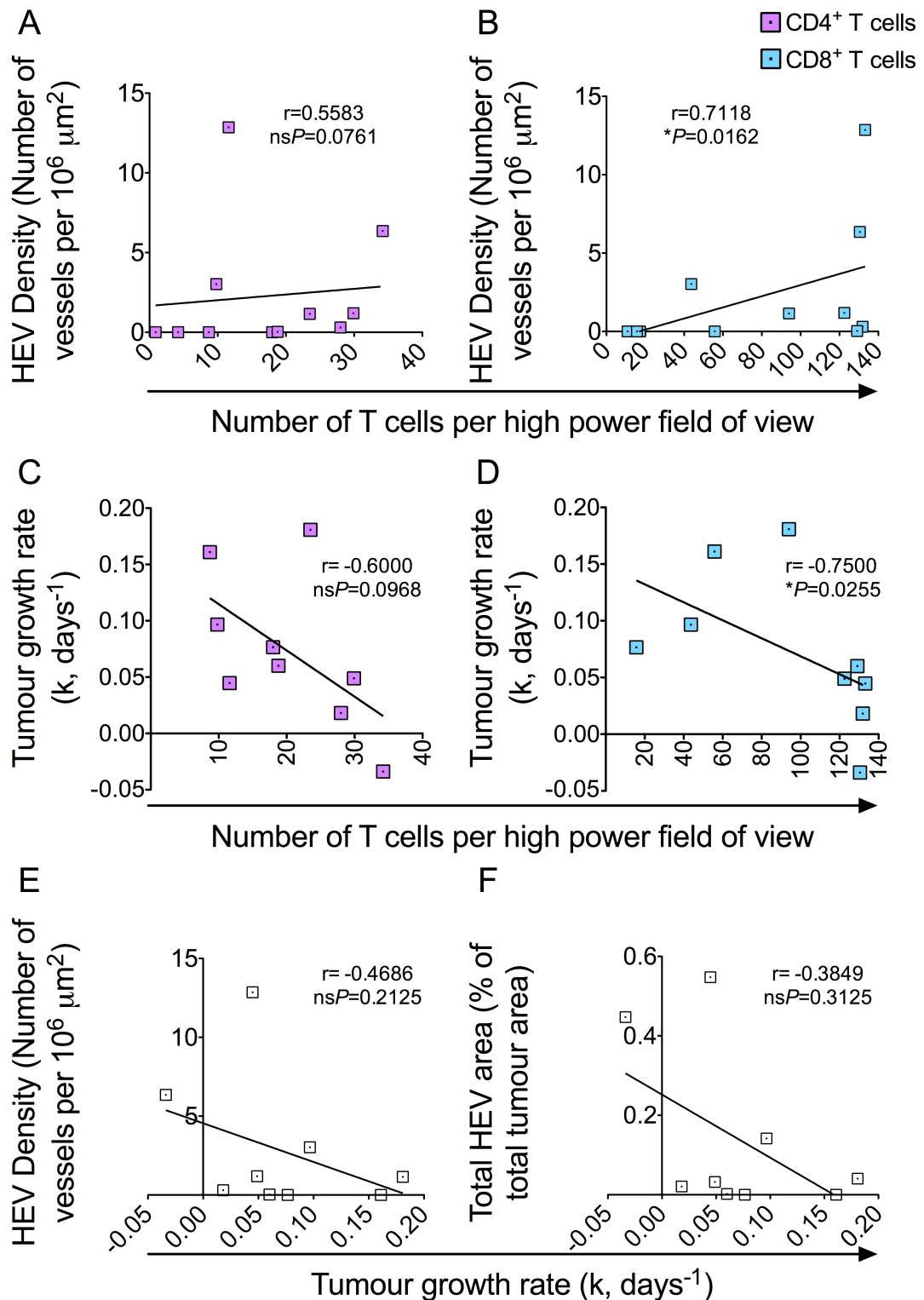
Figure 4.19 | Functionality of High Endothelial Venules in CD4^{+} T cell-depleted tumours is modestly compromised.
Correlations between number of intra-tumoural CD4^{+} and CD8^{+} T cells, High Endothelial Venule (HEV) density and total HEV area, and tumour growth rates for anti-CD4 treated, Treg depleted Foxp3[DTR] animals. (A-B) Numbers of intra-tumoural CD4^{+} and CD8^{+} T cells plotted against tumour HEV density; CD4^{+} T cells (A; purple); CD8^{+} T cells (B; blue). (C-D) Numbers of intra-tumoural CD4^{+} and CD8^{+} T cells plotted against tumour growth rates (k, days[-1]); CD4^{+} T cells (C; purple); CD8^{+} T cells (D; blue). (E-F) HEV density (E) and total HEV area (as proportion of total tumour area; F) plotted against tumour growth rate (k, days[-1]). Statistical significance was determined by the non-parametric Spearman's correlation coefficient test, and the r statistic and P values are shown. N = 11 (9 C-F).

[1] Spearman's correlation [2] Mann Whitney non-parametric t test [3] Kruskal-Wallis One-Way ANOVA with Dunn's multiple comparisons test [4] Linear Regression

4.7 Results: Depletion of CD8^{+} T cells Phenocopies Depletion of Both CD4^{+} and CD8^{+} T cells in Severely Abrogating HEV Neogenesis

In parallel to treating tumour-bearing Foxp3[DTR] animals with anti-CD4 depleting antibodies, I treated a separate group of animals with the anti-CD8 antibody alone. The anti-CD8 antibody resulted in a significant reduction in both the proportion and absolute number of CD8^{+} T cells in spleen and LNs, and absolute number in tumour (Figure 4.20). The anti-CD8 antibody resulted in the loss of the majority but not all T cells in all compartments. In support of previous reports, the anti-CD8 antibody resulted in a selective effect upon CD8^{+} T cells only, with no reciprocal increase in numbers of CD4^{+} T cells (Figure 4.20) (Cobbold et al. 1992)(S. Cobbold communication).

Reminiscent of tumours of anti-CD4/CD8 treated animals, PNAd^{+} HEV could on occasion be found in tumours of anti-CD8 treated animals, but were extremely scarce (Figure 4.21). The infrequent PNAd[+] staining once again colocalised with CD31 (data not shown). Paraffin embedded tumour sections of anti-CD8 treated animals also contained very few PNAd[+] HEV: the majority of tumours contained no vessels whatsoever, in a similar manner to tumours of anti-CD4/CD8 treated animals (Figure 4.22 A). Indeed, there was a highly significant reduction in HEV density in treated tumours relative to Treg depleted tumours (**P=0.0054[2]; Figure 4.22 B). The few HEV within CD8 depleted tumours demonstrated a slightly significant increase in average area (*P=0.0229[2]; Figure 4.22 C). Total HEV area was also significantly reduced in tumours of anti-CD8 treated tumours relative to Treg depleted tumours (*P=0.0146[2]; Figure 4.22 D). These data combined with those from the anti-CD4/CD8 and anti-CD4 experiments described above collectively suggest that CD8^{+} T cells are crucial in the process of intra-tumoural HEV neogenesis.

---

[1] Spearman's correlation [2] Mann Whitney non-parametric t test [3] Kruskal-Wallis One-Way ANOVA with Dunn's multiple comparisons test [4] Linear Regression
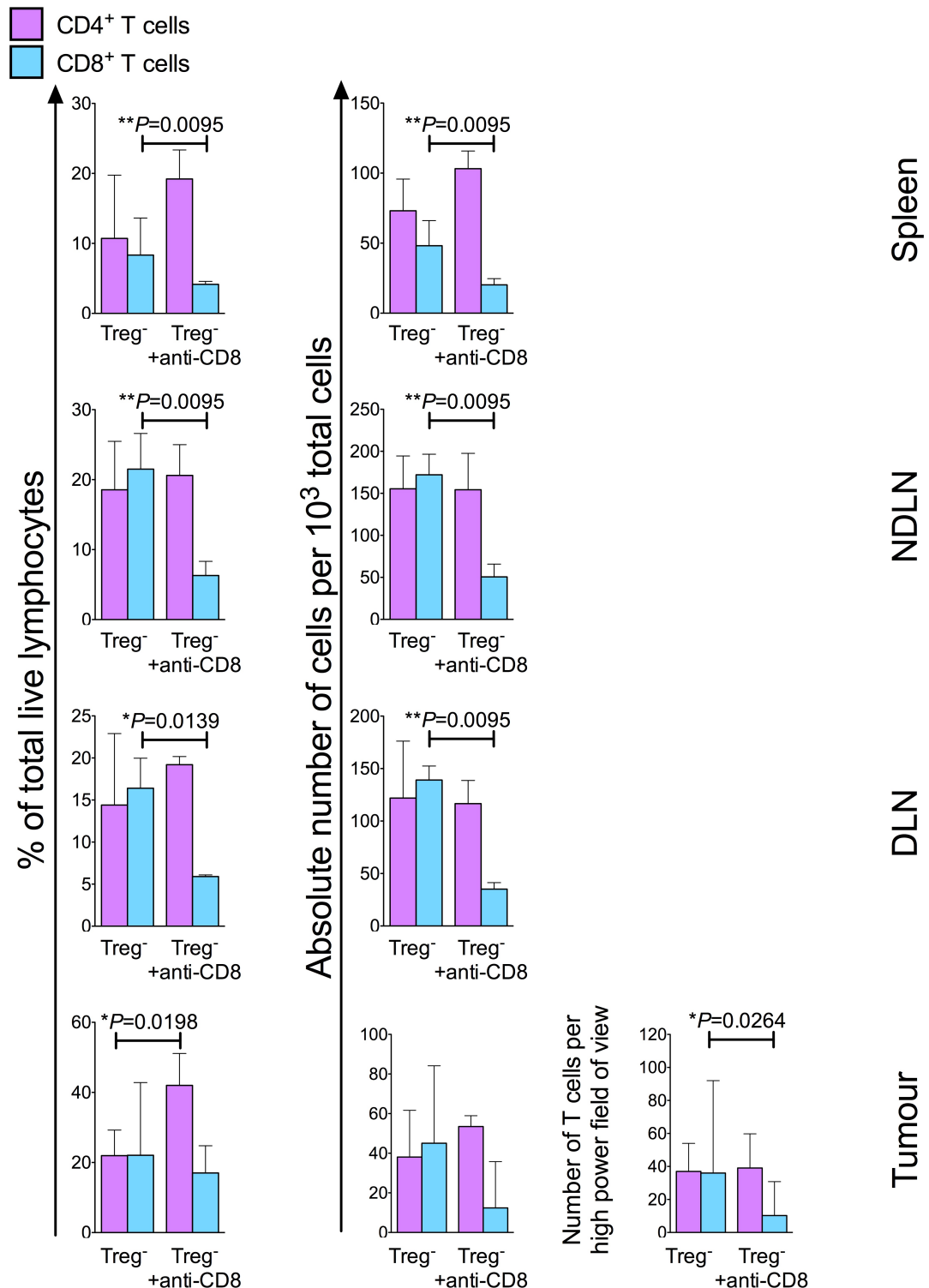
Figure 4.20 | Treatment with an anti-CD8 monoclonal antibody depletes CD8^{+} T cells from lymphoid organs and tumour.

Proportion and absolute number of T cells in spleen, non tumour-draining lymph node (NDLN), tumour-draining lymph node (DLN) and tumour, determined by flow cytometry or counting of immunofluorescently stained tumour sections, in Treg depleted and anti-CD8 treated, Treg depleted Foxp3[DTR] animals, at the end of treatment. Data shown are: proportion of total live lymphocytes expressing CD4 or CD8 (left), absolute number of CD4^{+} or CD8^{+} T cells (middle) or counts of CD4^{+} or CD8^{+} T cell per high power field of view in tumour (bottom right). CD4^{+} T cells (purple); CD8^{+} T cells (blue). Data are presented as median ± Interquartile range. Statistical significance was determined by Mann Whitney t tests. N = 4 for anti-CD8 treated Treg depleted, N = 6 for Treg depleted Foxp3[DTR] animals (proportion and absolute number by flow cytometry); N = 8 for anti-CD8 treated Treg depleted, N = 21 for Treg depleted Foxp3[DTR] animals (counting of immunofluorescently stained tumour sections).

[1] Spearman's correlation [2] Mann Whitney non-parametric t test [3] Kruskal-Wallis One-Way ANOVA with Dunn's multiple comparisons test [4] Linear Regression
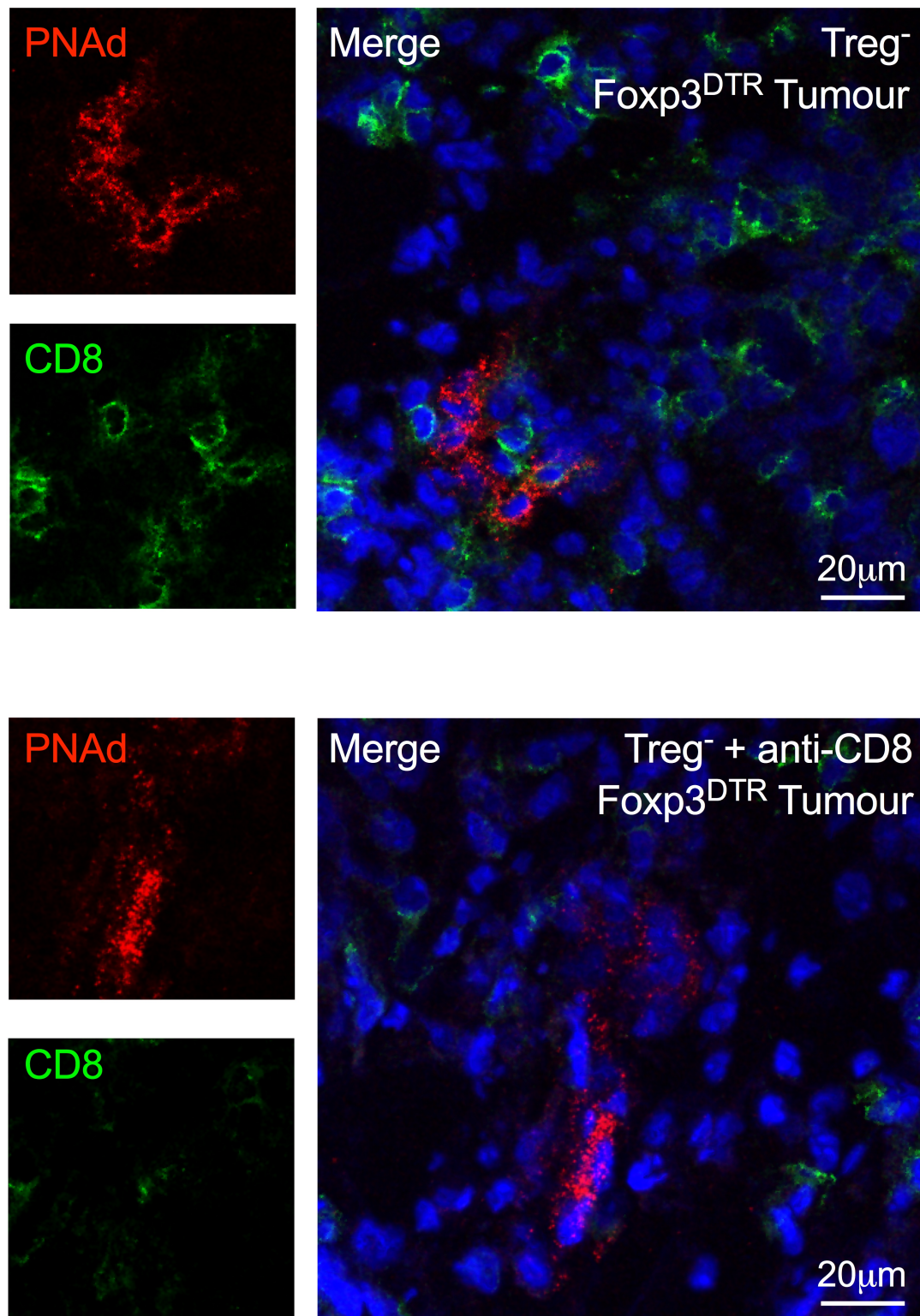
Figure 4.21 | High Endothelial Venules are found in tumours in the absence of CD8^{+} T cells. Confocal images of High Endothelial Venules (HEV) within tumours of Treg depleted (top) and anti-CD8 treated, Treg depleted (bottom) Foxp3[DTR] animals. Endothelial cells of HEV were detected by immunofluorescence staining using a biotinylated rat anti-PNAd primary antibody (clone MECA-79) and streptavidin Alexa Fluor[®] 555 secondary antibody (red). Tumour sections were dual-stained for PNAd and CD8^{+} T cells (rat anti-CD8 detected using donkey anti-rat Alexa Fluor[®] 488 secondary antibody; green). Merged images include the nuclear stain DAPI (blue). Scale bars are shown.

[1] Spearman's correlation [2] Mann Whitney non-parametric *t* test [3] Kruskal-Wallis One-Way ANOVA with Dunn's multiple comparisons test [4] Linear Regression
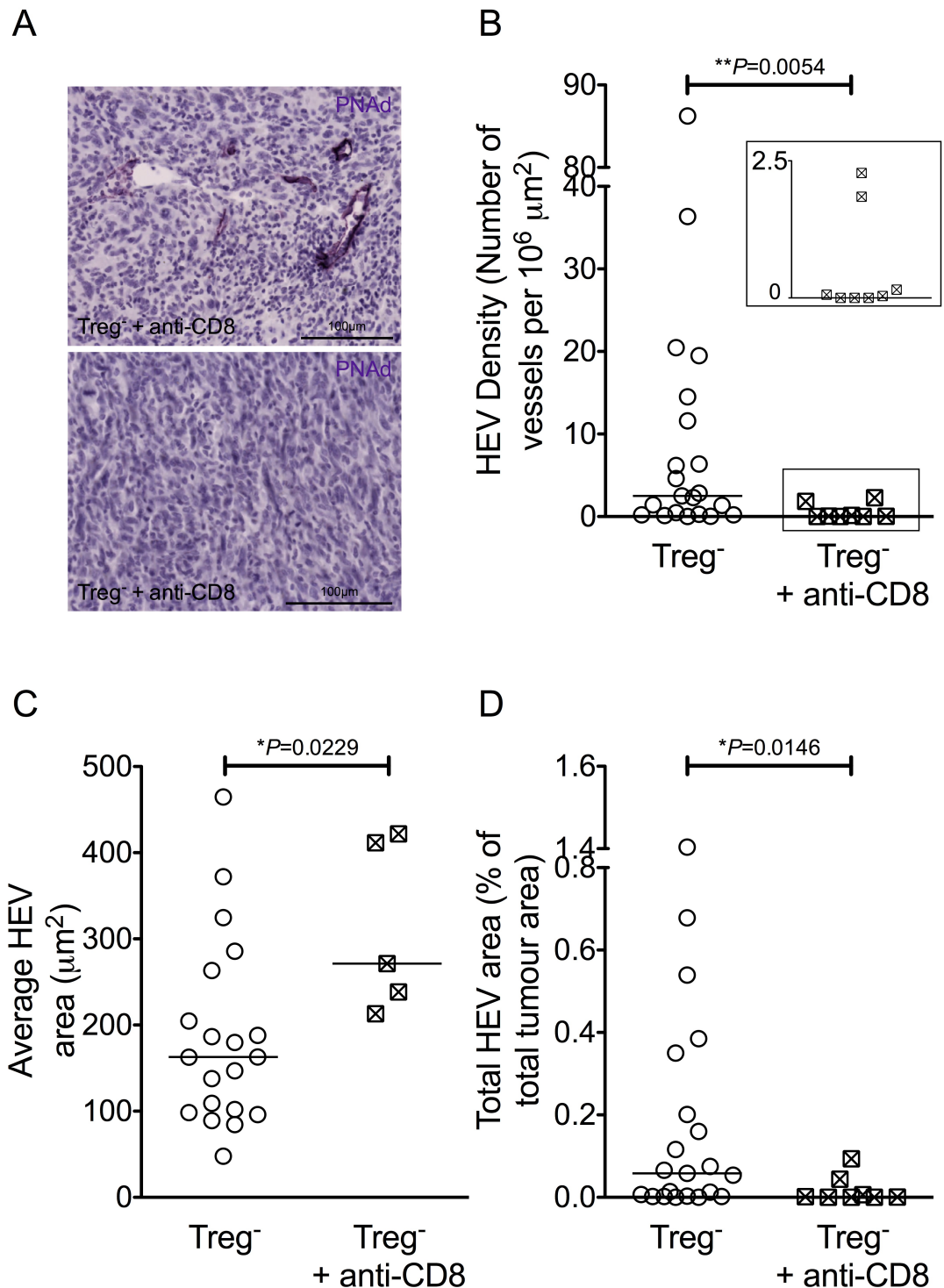
Figure 4.22 | Measures of High Endothelial Venule density and total area are significantly decreased in the absence of CD8^{+} T cells.

Quantitative measures of High Endothelial Venules (HEV) in tumours of anti-CD8 treated, Treg depleted Foxp3[DTR] animals. (A) Representative microscope images of HEV in paraffin embedded tumours. The anti-PNAd antibody (clone MECA-79) was detected using VIP chromogen (purple staining). Sections were counterstained using haematoxylin. Scale bars are shown. (B) HEV density was calculated per unit area of tumour (μm^2). The insert shows an enlarged version of the boxed area. (C) Average area of HEV vessels calculated in μm^2. (D) Total HEV area as a proportion of total tumour area, calculated as a percentage. Data are presented as individual datapoints plus median. Statistical significance was determined by Mann Whitney t tests. N = 8 anti-CD8 treated, Treg[-] tumours (5 in C); N = 21 Treg[-] tumours (20 in C).

[1] Spearman's correlation [2] Mann Whitney non-parametric t test [3] Kruskal-Wallis One-Way ANOVA with Dunn's multiple comparisons test [4] Linear Regression

I found a weak positive correlation between HEV density and both CD4^{+} and CD8^{+} T cells in tumours of anti-CD8 treated animals, although neither association reached statistical significance (r = 0.1464, ns$P$=0.7520 for CD4^{+} T cells[1]; r = 0.4636, ns$P$=0.2431 for CD8^{+} T cells[1]; Figure 4.23 A-B). These data suggest that HEV that form during anti-CD8 treatment are functional in terms of facilitating high numbers of T cells to enter the tumour. These data could also be interpreted to suggest that HEV density is a function of the number of CD8^{+} T cells present in the tumour, as HEV are only present in those tumours containing higher numbers of CD8^{+} T cells.

There was no significant correlation between either numbers of CD4^{+} T cells or CD8^{+} T cells and tumour growth rate for anti-CD8 treated animals (r = 0.0476, ns$P$=0.9349 for CD4^{+} T cells[1]; r = -0.0952, ns$P$=0.8401 for CD8^{+} T cells[1]; Figure 4.23 C-D). These data support the idea of the existence of a threshold of number of intra-tumoural T cells, which must be reached before an association with tumour growth rate is observed. As is the case in anti-CD4/CD8 treated tumours, there are too few T cells within the tumour mass of anti-CD8 treated animals to confer a reduction in tumour growth rate. However, there remains a slight negative correlation between both measures of HEV density and total HEV area and tumour growth rate for anti-CD8 treated animals, suggesting maintenance of HEV functionality to a degree (r = -0.5855, ns$P$=0.1323 for HEV density and total HEV area[1]; Figure 4.23 E-F).

Collectively these data imply a significant role for CD8^{+} T cells in HEV neogenesis in tumours, as this process is severely abrogated in the absence of these cells. However, the phenotype is less absolute than that observed in tumours of anti-CD4/CD8 treated animals, supporting the data in Section 4.6 showing a partial phenotype after depletion of only CD4^{+} T cells. In contrast to the anti-CD4 treated tumours, tumours of CD8^{+} T cell depleted animals demonstrated HEV neogenesis only in the situation where a residual number of CD8^{+} T cells remained, highlighting a superior requirement for CD8^{+} T cells over CD4^{+} T cells in the process of HEV formation.

[1] Spearman's correlation [2] Mann Whitney non-parametric t test [3] Kruskal-Wallis One-Way ANOVA with Dunn's multiple comparisons test [4] Linear Regression
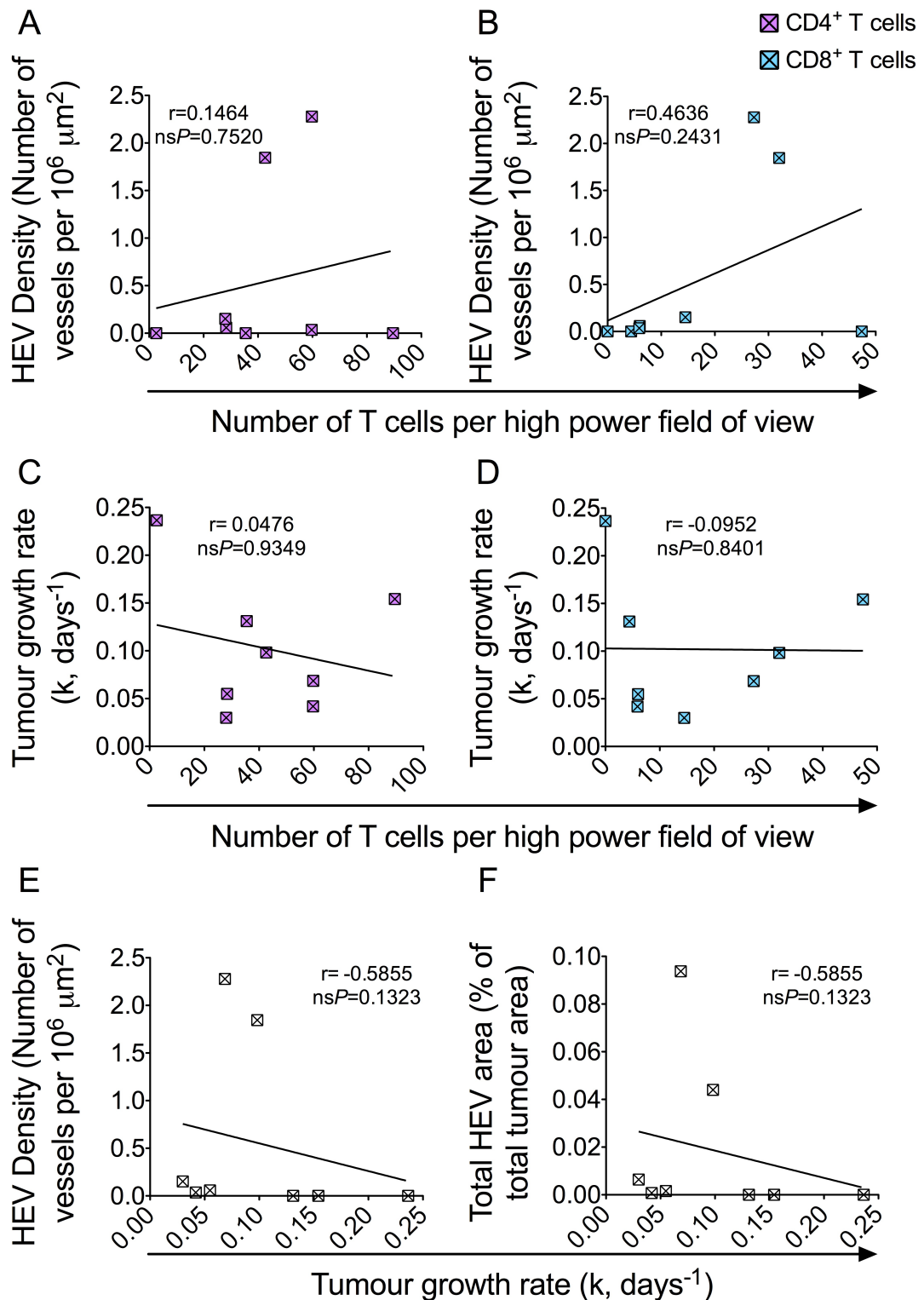
Figure 4.23 | Functionality of High Endothelial Venules in CD8^{+} T cell-depleted tumours is compromised.
Correlations between number of intra-tumoural CD4^{+} and CD8^{+} T cells, High Endothelial Venule (HEV) density and total HEV area, and tumour growth rates for anti-CD8 treated, Treg depleted Foxp3[DTR] animals. (A-B) Numbers of intra-tumoural CD4^{+} and CD8^{+} T cells plotted against tumour HEV density; CD4^{+} T cells (A; purple); CD8^{+} T cells (B; blue). (C-D) Numbers of intra-tumoural CD4^{+} and CD8^{+} T cells plotted against tumour growth rates (k, days[-1]); CD4^{+} T cells (C; purple); CD8^{+} T cells (D; blue). (E-F) HEV density (E) and total HEV area (as proportion of total tumour area; F) plotted against tumour growth rate (k, days[-1]). Statistical significance was determined by the non-parametric Spearman's correlation coefficient test, and the r statistic and P values are shown. N = 8.

[1] Spearman's correlation [2] Mann Whitney non-parametric t test [3] Kruskal-Wallis One-Way ANOVA with Dunn's multiple comparisons test [4] Linear Regression

4.8 Results: Comparison of T cell Infiltration, HEV Neogenesis and Tumour Growth across all Cell Depletion Treatments

To compare the impact of different cell depletion treatments on T cell infiltration and HEV neogenesis in the tumour, and overall tumour growth, I plotted these data altogether (Figures 4.24-4.26). To compare parameters for each treatment group to Treg depleted control tumours that contain either high or low densities of HEV, I separated the Treg depleted control tumours into "HEV[lo]" and "HEV[hi]" categories, by selecting 6 Treg depleted tumours with the lowest HEV density and 6 Treg deleted tumours with the highest HEV density. Plotting numbers of intra-tumoural CD4^{+} or CD8^{+} T cells for each treatment group once again demonstrated the efficacy of the T cell depleting antibodies, and highlighted the previously observed slight increase in CD8^{+} T cells in tumours of anti-CD4 treated animals (Figure 4.24). As the number of intra-tumoural CD8^{+} T cells function as a surrogate marker of HEV neogenesis, these data corroborate the data illustrating no change in total HEV area in these tumours, signifying functional HEV are able to form in the absence of CD4^{+} T cells (Figure 4.24).

Indeed, when HEV density and total HEV area were plotted for all treatments, only treatments in which T cells were depleted resulted in a significant decrease in HEV density relative to HEV^{hi} controls, with treatments in which CD8^{+} T cells were depleted having the most significant effect on HEV density[3] (Figure 4.25 A). Furthermore, only the treatments in which CD8^{+} T cells were depleted resulted in a significant decrease in total HEV area, relative to HEV^{hi} controls[3] (Figure 4.25 B). These data support the conclusion that CD8^{+} T cells are an essential cell population in the process of HEV neogenesis in tumours following Treg depletion, in which CD4^{+} T cells also play a minor role; CD20^{+} B cells play no role in HEV neogenesis following Treg depletion.

Simultaneous depletion of CD4+ and CD8^{+} T cells resulted in a significant increase in tumour growth rate, relative to Treg depleted controls (Figure 4.26 A). Moreover, simultaneous loss of both populations of T cells resulted in a significant increase in tumour growth rate relative to HEV[hi] Treg depleted controls, but not HEV[lo]

Treg depleted controls, suggesting a causal link between intra-tumoural HEV, T cell infiltration and tumour control (Figure 4.26 B). The significant increase in tumour growth rate in anti-CD4/CD8 treated animals relative to anti-CD4 treated animals signifies the importance of CD8^{+} CTLs in the anti-tumour immune response to MCA-induced fibrosarcomas following Treg depletion, supporting previous data (Betts et al. 2007; Ondondo et al. 2013; Teng et al. 2010; Koebel et al. 2007). The difference in tumour growth rate between anti-CD4/CD8 treated and anti-CD8 treated mice could signify either a requirement for CD4^{+} T cells for effective tumour control, or simply reflect the observed less efficient depletion of CD8^{+} T cells in the single depletion group. The lack of a difference in tumour growth rate between Treg depleted controls and anti-CD4 treated animals supports the latter hypothesis, in suggesting that CD4^{+} T cells are not required for tumour control.

To determine whether tumour growth could be explained by HEV density and / or treatment regime, I used a linear model with fixed effects to analyse the relationship between tumour growth and each independent variable one-by-one, by statistically controlling for the variation introduced by each independent variable. These analyses revealed that while treatment had a far more profound effect on tumour growth (***P<0.001), HEV density, as an independent variable, indeed had a significant impact on tumour growth (*P=0.0111). These data emphasize that while treatment could be having an overall impact on tumour growth rate via multiple various mechanisms, HEV density alone is a significant biological variable that influences the growth of tumours.
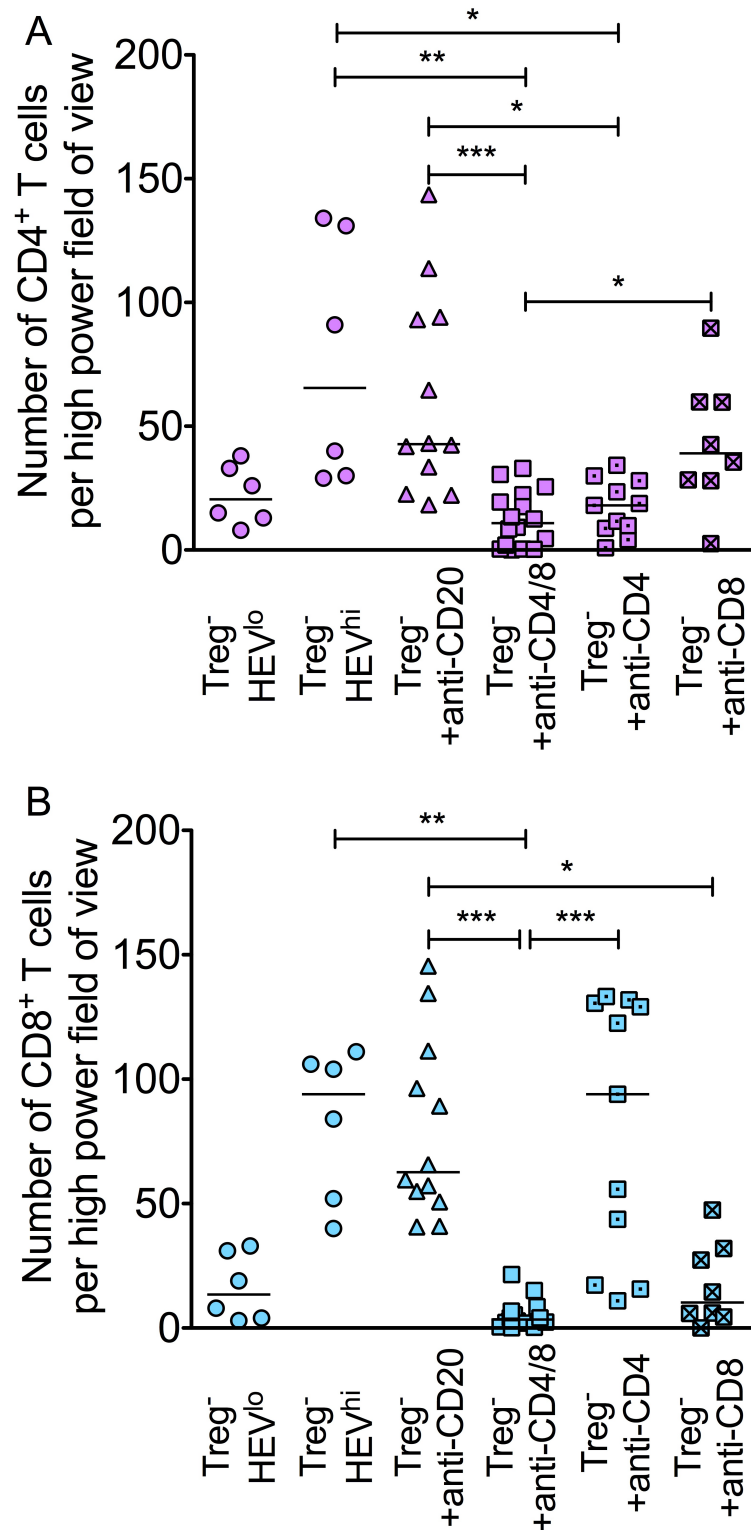
Figure 4.24 | Immune cell depletion treatments did or did not alter absolute numbers of CD4^{+} and / or CD8^{+} T cells inside tumours.

Number of intra-tumoural CD4^{+} (A) and CD8^{+} (B) T cells for each of the following treatment groups: Treg depleted (Treg^{-}) HEV^{lo}, N = 6; Treg^{-} HEV^{hi}, N = 6; anti-CD20 treated, Treg^{-}, N = 12; anti-CD4/CD8 treated, Treg[-], N = 16; anti-CD4 treated, Treg[-], N = 11; and anti-CD8 treated, Treg[-], N = 8. Data are presented as individual datapoints plus median. Statistical significance was determined by Kruskal-Wallis One-Way ANOVA and Dunn's multiple comparisons tests (* = $P \leq 0.05$, ** = $P \leq 0.01$, *** = $P \leq 0.001$).

[1] Spearman's correlation [2] Mann Whitney non-parametric *t* test [3] Kruskal-Wallis One-Way ANOVA with Dunn's multiple comparisons test [4] Linear Regression

Figure 4.25 | Immune cell depletion treatments did or did not alter High Endothelial Venule density and / or total area inside tumours.

HEV density (A) and total HEV area (B) for each of the following treatment groups: Treg depleted (Treg⁻) HEV^{lo}, N = 6; Treg⁻ HEV^{hi}, N = 6; anti-CD20 treated, Treg⁻, N = 12; anti-CD4/CD8 treated, Treg⁻, N = 16; anti-CD4 treated, Treg⁻, N = 11; and anti-CD8 treated, Treg⁻, N = 8. HEV density was calculated per unit area of tumour (µm^2) and total HEV area was calculated as a percentage of total tumour area. Data are presented as individual datapoints plus median. Statistical significance was determined by Kruskal-Wallis One-Way ANOVA and Dunn's multiple comparisons tests (* = $P \le 0.05$, ** = $P \le 0.01$).

[1] Spearman's correlation [2] Mann Whitney non-parametric t test [3] Kruskal-Wallis One-Way ANOVA with Dunn's multiple comparisons test [4] Linear Regression
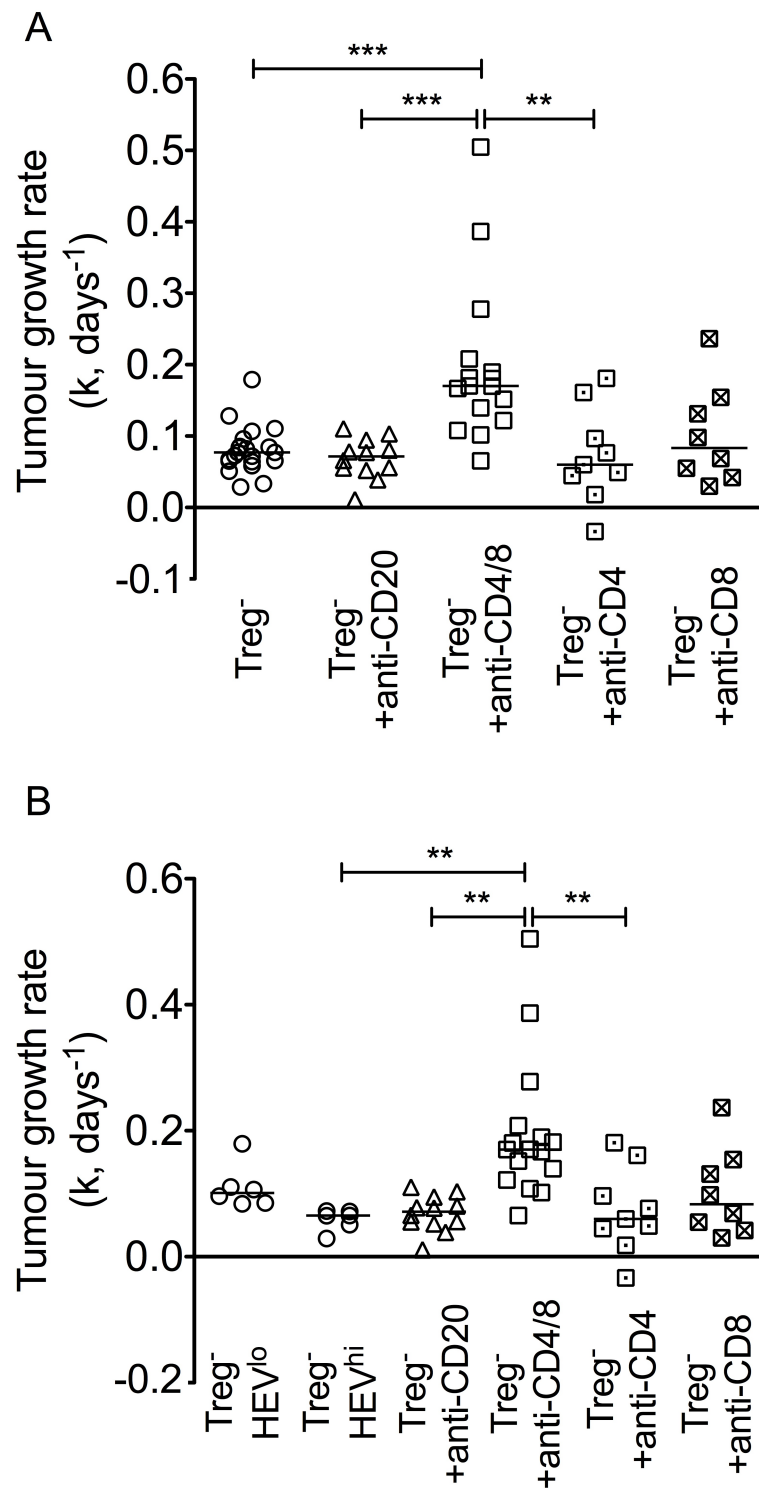
Figure 4.26 | Immune cell depletion treatments did or did not alter growth rate of tumours. Tumour growth rate (k, days^{-1}) data for each of the following treatment groups: Treg depleted control group (Treg$^-$; N = 21 (A); Treg$^-$ HEV^{lo}; N = 6; Treg$^-$ HEV^{hi}; N = 6 (B)), anti-CD20 treated, Treg$^-$, N = 12; anti-CD4/CD8 treated, Treg$^-$, N = 16; anti-CD4 treated, Treg$^-$, N = 9; and anti-CD8 treated, Treg$^-$, N = 8. Data are presented as individual datapoints plus median. Statistical significance was determined by Kruskal-Wallis One-Way ANOVA and Dunn's multiple comparisons tests (** = $P \leq 0.01$, *** = $P \leq 0.001$).

[1] Spearman's correlation [2] Mann Whitney non-parametric t test [3] Kruskal-Wallis One-Way ANOVA with Dunn's multiple comparisons test [4] Linear Regression
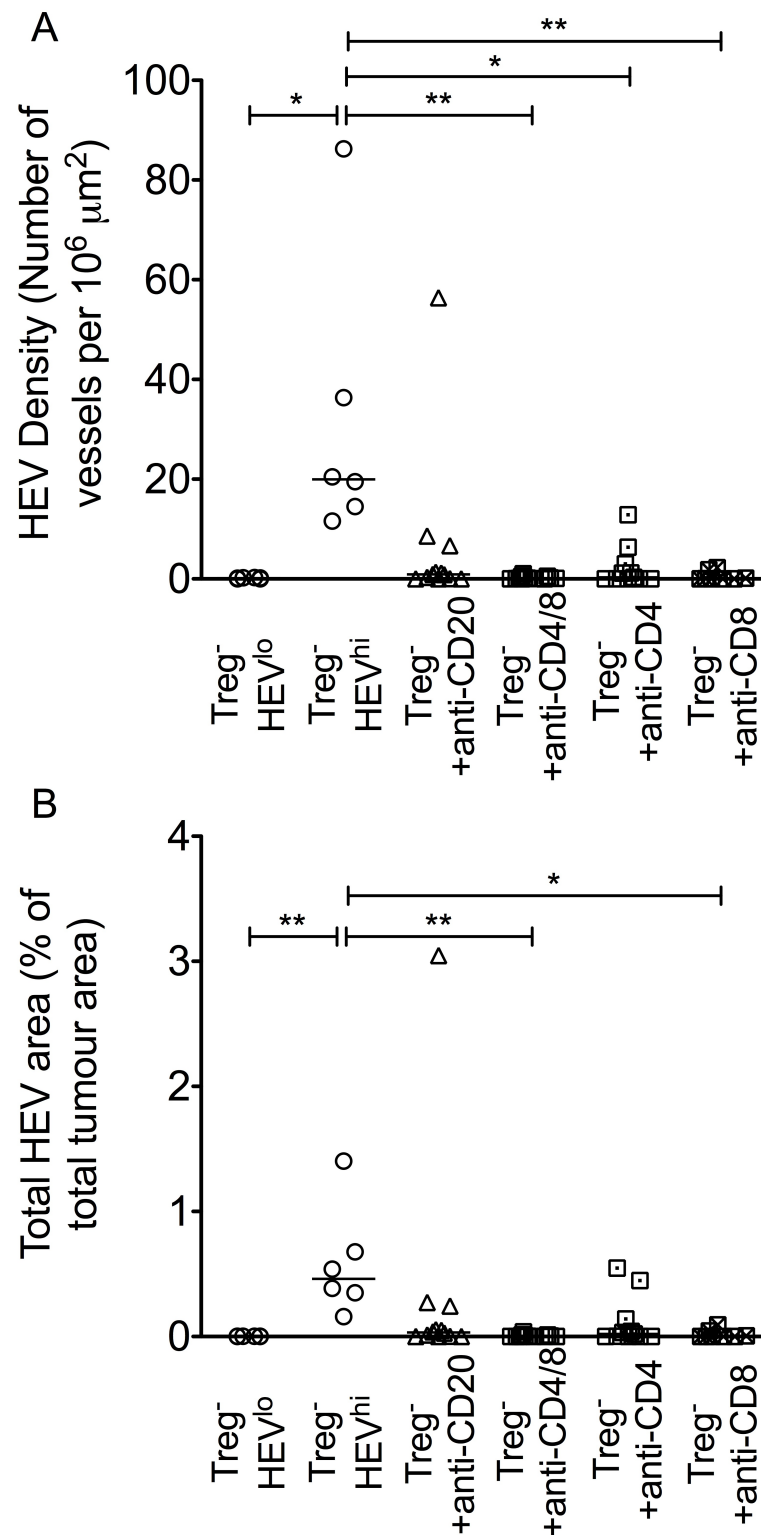
4.9 Discussion

The data presented here show no role for B lymphocytes in neogenesis of PNAd[+] HEV in tumours following Treg depletion. Instead, density and total area of HEV are significantly reduced following depletion of T cells. Thus, T lymphocytes play an essential role in development of PNAd^{+} HEV in tumours (Figure 4.27).

My data further define that CD8^{+} T lymphocytes are required for HEV neogenesis: this process is severely compromised in the absence of CD8^{+} T cells. The difference in HEV measures between tumours of anti-CD4/CD8 and anti-CD8 treated animals suggests a role for CD4^{+} T cells also. This difference could be explained by the less efficient CD8^{+} T cell depletion in anti-CD8 treated animals relative to anti-CD4/CD8 treated animals. However, depletion of CD4^{+} T cells alone results in a modest abrogation in HEV neogenesis, implying a minor role for CD4^{+} T cells. This could be a direct role for CD4^{+} T cells in HEV neogenesis, or an indirect, accessory role via CD8^{+} T cell support.

While initial formation of HEV structure and abluminal PNAd expression on HEV endothelium during lymphoid organ formation proceeds in the absence of T or B cells, the development of a fully mature HEV phenotype requires lymphocytes (Liao & Ruddle 2006). While this study implies a degree of lymphocyte dependency for development of a mature HEV phenotype, a separate study demonstrated unimpaired L-selectin-dependent lymphocyte trafficking to peripheral LNs in RAG-1 deficient mice (Galkina et al. 2003). Our model of HEV neogenesis in Treg depleted MCA tumours could therefore represent a significant departure from normal LN HEV development, which seems to proceed mostly uninterrupted in the absence of lymphocytes.

HEV neogenesis in tumours in the context Treg depletion can perhaps instead be likened to HEV formation during chronic inflammation. DCs have been implicated in regulation of PNAd[+] HEV in TLOs of inflamed lungs in mouse models (GeurtsvanKessel et al. 2009; Halle et al. 2009). However, a series of studies have instead implicated lymphocytes in HEV neogenesis and / or TLO development during inflammation. HEV in chronic inflammation-associated TLOs in the RIP-LTα mouse

display only abluminal PNAd expression, presumably due to the lack of LTβ overexpression (Kratz et al. 1996). However, RIP-LTα RAG2 deficient littermates lack all PNAd expression on TLO-associated HEV, suggesting that lymphocyte-derived factors in addition to LTα are required for basal abluminal PNAd expression on HEV endothelium (Kratz et al. 1996).

Marinkovic and colleagues demonstrated the absolute requirement for CD3^{+} CD4^{+} T lymphocytes, rather than canonical RORγt^{+} LTi cells, in TLO generation in the thyroid driven by CCL21 over-expression (Marinkovic et al. 2006). Furthermore, T_H17 cells are responsible for inducing CXCL13 expression that drives iBALT development following inflammatory insult in the lung (Rangel-Moreno et al. 2011). A recent study strongly implicated T_H17 cells in the formation of synovial ELS in both experimental and clinical rheumatoid arthritis (RA) (Jones et al. 2015). This study identified IL-27, a cytokine often elevated in serum and synovia of patients, as a key regulator of T_H17 cells and thereby inhibitor of ectopic lymphoid neogenesis. Interestingly, the T_H17 cells associated with organised ELS development in the absence of IL-27 signalling appeared to be gp38-expressing, Tfh-cell like cells, which have been implicated in ELS formation in autoimmunity elsewhere (Jones et al. 2015; Peters et al. 2011). Perhaps, in the context of the chronic autoimmunity induced by Treg depletion and tumour immunity as described herein, effector T lymphocytes compensate for the lack of canonical LTi-like cells to induce the formation of isolated PNAd-expressing HEV, much as for TLO induction in other inflammatory models.

The cells involved in driving HEV neogenesis specifically in tumours remain to be defined. Martinet and colleagues suggested that LTβ-producing DCs initiate HEV development in breast tumours (Martinet et al. 2013; Martinet & Girard 2013). However, a direct functional link between DCs and PNAd[+] vasculature in tumours has yet to be defined. In corroboration of my data, a recently published study described that development of "LN-like" PNAd^{+} vasculature in tumours of both melanoma and lung carcinoma mouse models is reliant upon endogenous effector CD8^{+} T cells (Peske et al. 2015). Peske and colleagues noted the presence of PNAd^{+} HEV expressing CCL21

located within organised aggregates of B lymphocytes and gp38-expressing stromal cells, within tumours of WT animals. In contrast, there was a distinctive lack of PNAd^{+} tumour vasculature in gene-targeted animals specifically devoid of CD8^{+} T cells, and RAG2 deficient animals. Furthermore, PNAd-expressing vessels were restored to levels observed in WT animals upon adoptive transfer of CD8^{+} T cells to RAG2 deficient mice. The authors suggested that although NK cells could induce PNAd^{+} vasculature in some tumour settings in a redundant fashion, CD8^{+} T lymphocytes were primarily responsible for HEV induction in tumours (Peske et al. 2015).

My hypothesis states that T cell infiltration represents a significant bottleneck in control of tumour growth following Treg depletion: this bottleneck can be overcome by formation of HEV (Hindley et al. 2012). However, my data shown here indicate an early role for T lymphocytes in development of HEV, which poses some important questions: are T cells acting locally to induce HEV in tumours, and if so, how do 'HEV-initiator' T cells reach the tumour site without HEV? Considering LN HEV are induced by physical interactions between LTαβ-expressing LTi cells and LTβR-expressing vascular endothelial cells (Onder et al. 2013), I hypothesise that similar proximal signals are required for HEV development in tumours. The phenotype of 'HEV-initiator' T cells could mean they do not require HEV to infiltrate tumours (i.e. L-selectin[lo]), and can instead access tumour via endothelium, which is highly activated following Treg depletion (Li et al. 2010). It is also possible that 'HEV-initiator' T cells access tumour by use of chemokine aided migration (Ondondo et al. 2014[a]). These 'HEV-initiator' T cells then provide signals to kick-start HEV neogenesis, which then facilitate entry of anti-tumour T cells: these could also act as further HEV-initiator cells, thereby establishing a self-amplifying loop to underpin effective tumour control. It will be important to define the specific phenotype of CD8^{+} T lymphocytes capable of initiating HEV neogenesis, if therapies aimed at promoting HEV development in tumours are to be designed.

The data presented in this Chapter pose an important question: What factors could T lymphocytes be producing that are capable of directing HEV neogenesis in tumours after Treg depletion? I address this question in the following results chapter.

[1] Spearman's correlation [2] Mann Whitney non-parametric *t* test [3] Kruskal-Wallis One-Way ANOVA with Dunn's multiple comparisons test [4] Linear Regression

Figure 4.27 | Updated hypothesis of HEV Neogenesis in Carcinogen-Induced Tumours after Treg Depletion.
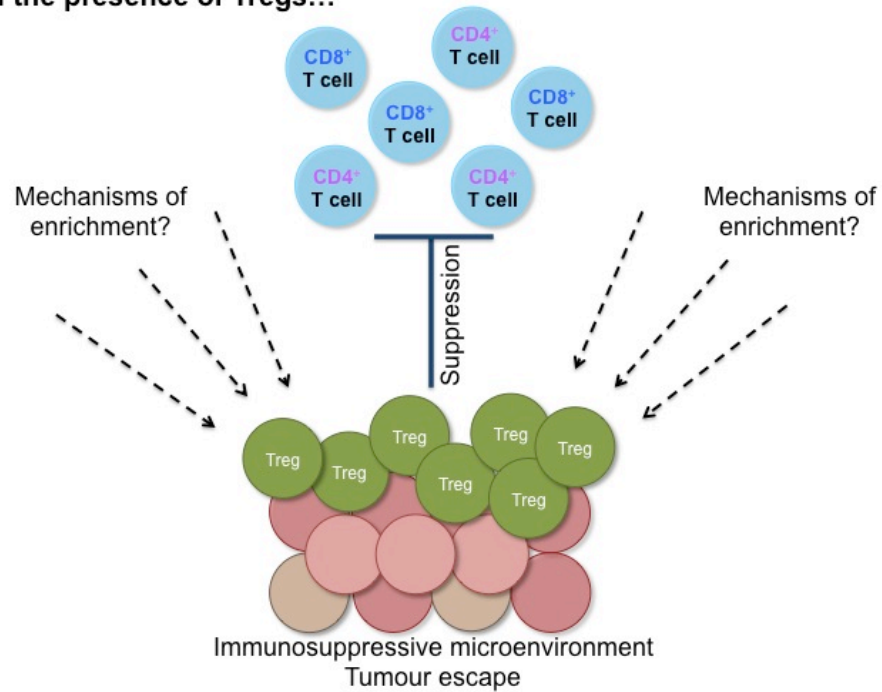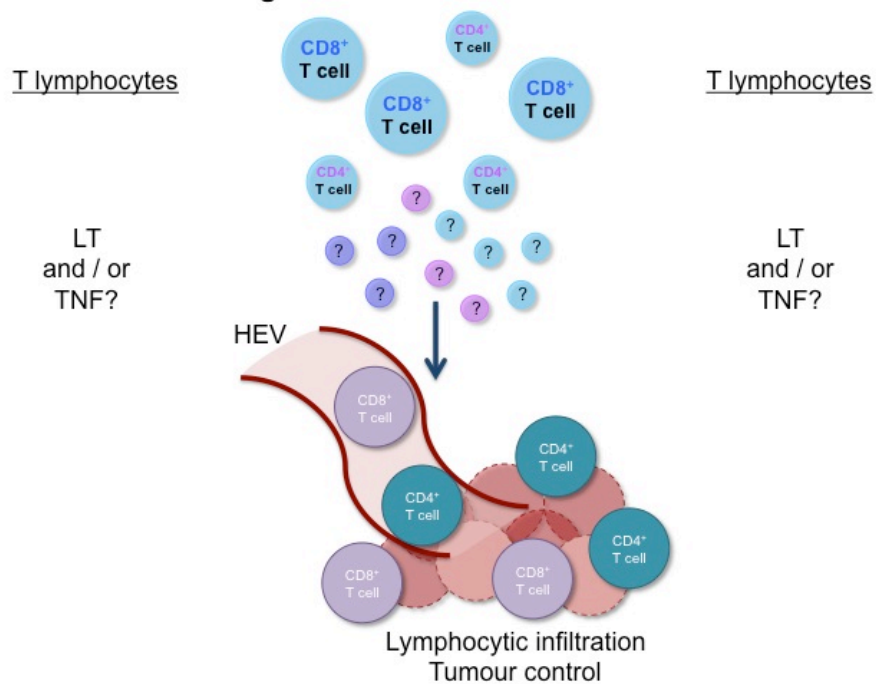
Chapter Five

5 Results: Cytokines and signalling pathways involved in High Endothelial Venule neogenesis in tumours

5.1 Introduction

The nature of the communication between LTi and LTo cells that directs lymphoid organ development is firmly established: $LT\alpha_1\beta_2$ expressing LTi cells interact with LTβR expressing LTo cells (Mebius 2003). LTβR signalling is also required for maintenance of HEV structure and function in adult lymphoid organs (Browning et al. 2005; Liao & Ruddle 2006; Lu & Browning 2014). LTβR expression by vascular endothelial cells also seems necessary specifically for HEV development within lymphoid organs (Onder et al. 2013). However, there remains a considerable gap in our knowledge surrounding HEV development during ontogeny.

TNFR signalling has also been implicated in LN development. Mice genetically deficient for TNFα, TNFRI or TNFRII demonstrate relatively normal development of most LN, except PP (Pfeffer et al. 1993; Neumann et al. 1996; Pasparakis et al. 1996; Pasparakis et al. 1997; Körner et al. 1997; Erickson et al. 1994; Kuprash et al. 2005). However, while in utero treatment with an LTβR.Ig fusion protein was permissive for mesenteric, sacral, cervical and lumbar LN development, administration of a TNFRI.Ig fusion protein or anti-TNFα antibody in combination with LTβR.Ig treatment, resulted in complete blockade of all LN development. This key study suggested a contribution by TNFα-TNFRI signalling to LN development, even if in a redundant fashion to LTβR signalling (Rennert et al. 1998).

Additionally, animals deficient in both LTβ and TNFRI lack all LN and PP in contrast to $LT\beta^{-/-}$ mice, which retain some LNs (Koni & Flavell 1998; Koni et al. 1997; Alimzhanov et al. 1997; Kuprash et al. 1999). Furthermore, TNFα over-expression can compensate for the lack of LTi cells in LN and TLO development to a certain degree, as $TNF/Rorc(\gamma t)^{-/-}$ mice develop TLOs and several SLOs. Within LNs of $TNF/Rorc(\gamma t)^{-/-}$ mice, $PNAd^+$ HEV were present and indistinguishable from those in wild-type LNs

[1] One-Way ANOVA with Tukey's multiple comparison test [2] Paired t test [3] Mann Whitney test [4] Spearman's correlation [5] Welch's unequal variance t test [6] Kruskal-Wallis One-Way ANOVA with Dunn's multiple comparisons test [7] Linear Regression

(Furtado et al. 2014). These data lend support to the idea that TNFR signalling also plays an important role in normal development of HEV-containing lymphoid organs.

Martinet and colleagues have proposed that LTβR signalling, initiated by LTβ-expressing DCs, drives HEV neogenesis in human breast tumours (Martinet et al. 2013; Martinet & Girard 2013). The mechanisms driving HEV neogenesis in the context of chronic autoimmunity induced by the depletion of Tregs could represent a significant departure from any of the above scenarios. If novel immunotherapeutic approaches to drive intra-tumoural HEV neogenesis are to be designed, it is absolutely necessary to first delineate the molecular mechanisms underpinning HEV formation in tumours.

I therefore aimed to establish the role of:

- LTβR signalling, and

- TNFR signalling

in HEV neogenesis in tumours following Treg depletion.

---

[1] One-Way ANOVA with Tukey's multiple comparison test [2] Paired *t* test [3] Mann Whitney test [4] Spearman's correlation [5] Welch's unequal variance *t* test [6] Kruskal-Wallis One-Way ANOVA with Dunn's multiple comparisons test [7] Linear Regression

5.2 Results: TNF Superfamily members are differentially regulated in HEV containing Treg depleted MCA tumours

To ascertain whether mechanisms underpinning HEV neogenesis in tumours relied upon similar signalling pathways and cytokines as development of HEV-containing SLOs, I analysed genetic data previously acquired in my host lab. Microarray analyses had been performed on RNA extracted from whole tumour tissue of either Treg replete animals (whose tumours are consistently HEV negative), Treg depleted animals whose tumours contained HEV, or Treg depleted animals whose tumours were HEV negative. I focused my analysis on the immediate TNF Superfamily genes, as ligands and receptors of this family play a crucial role in development of HEV-containing LNs during ontogeny and therefore represented strong candidates for controlling HEV neogenesis in tumours (Mebius 2003; van de Pavert & Mebius 2014; van de Pavert & Mebius 2010).

Several ligands and receptors of the immediate TNF Superfamily were significantly differentially expressed in tumour tissue of HEV positive, Treg depleted tumours relative to HEV negative, Treg depleted tumours and HEV negative, Treg replete tumours (Figure 5.1). Of particular interest, gene expression of LTβ but not LTα or LTβR, was significantly increased in HEV positive tumours relative to HEV negative tumours and tumours of Treg replete animals[1]. Interestingly, gene expression of TNFα and TNFR2 was also significantly increased in HEV positive tumours relative to the two other groups; TNFR1 expression, on the other hand, was significantly down-regulated in HEV positive tumours[1]. Expression of LIGHT, another ligand capable of signalling via the LTβR, was significantly upregulated in HEV positive tumours, relative to other groups, whilst no change was observed in HVEM expression[1]. Collectively, these data indicate involvement of immediate TNFSF members in HEV neogenesis in tumours, as for normal development of HEV-containing LNs.

---

[1] One-Way ANOVA with Tukey's multiple comparison test [2] Paired *t* test [3] Mann Whitney test [4] Spearman's correlation [5] Welch's unequal variance *t* test [6] Kruskal-Wallis One-Way ANOVA with Dunn's multiple comparisons test [7] Linear Regression
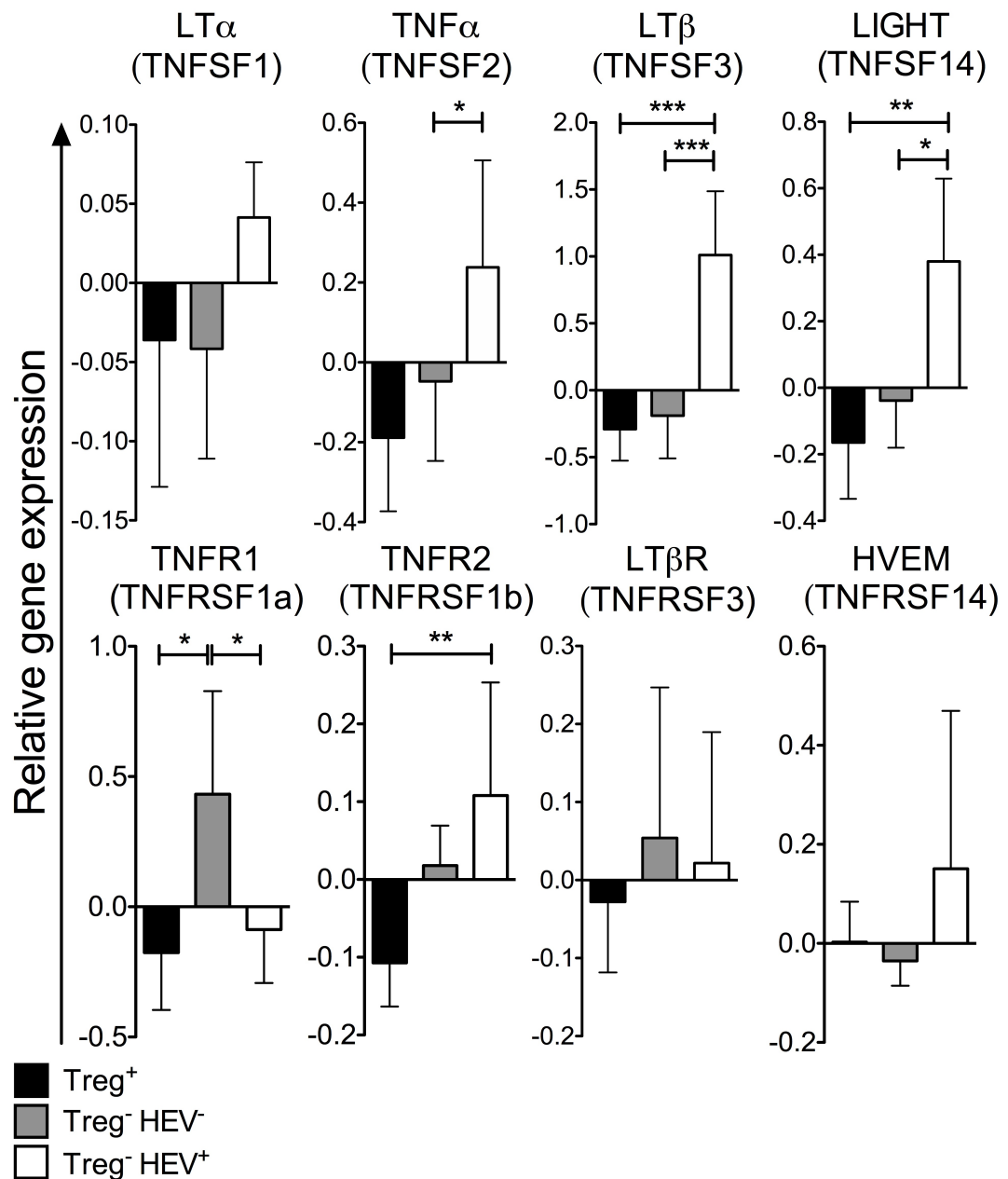
Figure 5.1 | Several members of the Tumour Necrosis Superfamily of ligands and receptors are differentially regulated in HEV⁺ tumours of Treg depleted animals relative to HEV⁻ tumours of Treg depleted and Treg replete tumours.

Bar charts showing relative gene expression of ligands and receptors of the immediate TNFSF in tumours of Treg replete animals (black bars), HEV negative tumours of Treg depleted animals (grey bars), and HEV positive tumours of Treg depleted animals (white bars), as determined by microarray analysis. N = 5 per group. Data are presented as mean ± Standard Deviation (SD). Relative gene expression was calculated following normalisation to internal control house-keeping genes. Statistical significance was determined by One-Way ANOVA with Tukey's multiple comparison tests to compare pairs of means (* = $P \leq 0.05$, ** = $P \leq 0.01$, *** = $P \leq 0.001$). HEV, High Endothelial Venule; TNFSF, Tumour Necrosis Factor Superfamily.

[1] One-Way ANOVA with Tukey's multiple comparison test [2] Paired *t* test [3] Mann Whitney test [4] Spearman's correlation [5] Welch's unequal variance *t* test [6] Kruskal-Wallis One-Way ANOVA with Dunn's multiple comparisons test [7] Linear Regression

5.3 Results: Lymphotoxin β Receptor antagonism does not prevent HEV neogenesis in tumours

Given the crucial role of the $LT\alpha_1\beta_2$-LTβR signalling pathway in development of HEV-containing SLOs (Mebius 2003; van de Pavert & Mebius 2014; van de Pavert & Mebius 2010), the implied role for this pathway specifically in formation of HEV within LNs (Onder et al. 2013), and the increased expression of the gene encoding LTβ in HEV positive tumours of our model (Figure 5.1), I explored the relevance of LTαβ-LTβR signalling for intra-tumoural HEV formation. I treated tumour-bearing Foxp3[DTR] animals with DT and an LTβR.Ig fusion protein, according to the protocol in Chapter 2. My primary readouts for these experiments were HEV presence and morphology in tumours, T cell numbers in tumours and tumour growth rates.

Efficacy of LTβR.Ig treatment was confirmed by examination of CD45R^{+} CD19^{+} CD21^{hi} CD23^{lo} Marginal Zone (MZ) B cells in the spleen by flow cytometry. MZ B cell development and maintenance is reliant upon both LT and TNF signalling (Fu & Chaplin 1999; Mackay & Browning 1998) and a reduction in the proportion of splenic MZ B cells is a hallmark of LTβR antagonism (Mackay et al. 1997). I observed a significant decrease in both the proportion and absolute number of splenic MZ B cells following LTβR.Ig treatment, in both Treg replete and Treg depleted animals[2] (Figure 5.2).

Interestingly, I observed a significant decrease in the proportion and absolute number of MZ B cells upon Treg depletion alone, even in the absence of LTβR.Ig treatment[1] (Supplemental Figure 5.1 A-B). This effect was also observed in LTβR.Ig-treated animals, so that Treg depletion and LTβR.Ig treatment synergised to further decrease the proportion and number of MZ B cells. There was no significant difference in the proportion or absolute number of splenic MZ B cells between Wild-Type C57BL/6 animals and C57BL/6 animals treated with DT[2]: these data confirm that the observed reduction in MZ B cells is a direct consequence of the loss of Tregs rather than a result of DT administration (Supplemental Figure 5.1 C-D).

[1] One-Way ANOVA with Tukey's multiple comparison test [2] Paired *t* test [3] Mann Whitney test [4] Spearman's correlation [5] Welch's unequal variance *t* test [6] Kruskal-Wallis One-Way ANOVA with Dunn's multiple comparisons test [7] Linear Regression

Figure 5.2 | Antagonism of LTβ Receptor signalling results in a significant reduction in proportions and absolute numbers of Marginal Zone B cells in the Spleen.
Efficacy of the LTβR.Ig reagent, as assessed by a decrease in Marginal Zone (MZ) B cells in spleen of Treg replete or Treg depleted Foxp3[DTR] animals. (A) Representative flow cytometry plots showing the proportion of CD19^{+} CD45R^{+} B cells that are CD21^{hi} CD23^{lo} MZ B cells, in the spleen of Treg replete (top), Treg replete LTβR.Ig treated (second down), Treg depleted (third down) and Treg depleted LTβR.Ig treated (bottom) Foxp3[DTR] animals. Cells are gated on CD19^{+}, CD45R^{+}. Numbers represent MZ B cells (gated), as a proportion of live CD19^{+} CD45R^{+} B cells. Expression of CD23 is shown on the y axis; expression of CD21 is shown on the x axis. (B-C) Proportion of CD19^{+} CD45R^{+} B cells that are CD21^{hi} CD23^{lo} MZ B cells (left hand graphs) and absolute number of CD21^{hi} CD23^{lo} MZ B cells per 100 total live cells (right hand graphs) in spleen of Treg replete and Treg replete LTβR.Ig treated Foxp3[DTR] animals (B) or Treg depleted and Treg depleted LTβR.Ig treated Foxp3[DTR] animals (C). Data are presented as individual datapoints and mean ± Standard Deviation (SD). Statistical significance was determined by unpaired *t* tests. N = 3 per group.

[1] One-Way ANOVA with Tukey's multiple comparison test [2] Paired *t* test [3] Mann Whitney test [4] Spearman's correlation [5] Welch's unequal variance *t* test [6] Kruskal-Wallis One-Way ANOVA with Dunn's multiple comparisons test [7] Linear Regression

FDCs, a unique population of stromal cells located in the centre of B cell follicles in SLOs, require both LT and TNF signalling via B cells for their maturation and maintenance. FDCs are characterised by high expression of surface complement receptors CR1 (CD35) and CR2 (CD21) (Heesters et al. 2014; Allen & Cyster 2008). Loss of splenic FDC upon LTβR.Ig treatment is well documented (Mackay & Browning 1998; Chiang et al. 2009).

By immunofluorescence staining using CD45R, MAdCAM-1 and CD35/CD21 specific antibodies, I noticed a profound loss of splenic FDC upon LTβR.Ig treatment in both Treg replete and Treg depleted animals (Figures 5.3-5.4). Blockade of LTβR signalling using LTβR.Ig also results in overall disruption to normal stromal cell networks in the spleen, including decreased or absent MAdCAM-1 expression by marginal sinus-lining stromal cells (Fu & Chaplin 1999; Ware 2005; Mackay et al. 1997). A loss of MAdCAM-1 staining of sinus-lining cells was observable in spleen sections of Treg replete and Treg depleted animals following LTβR.Ig treatment (Figures 5.3-5.4). Of note, the affect of LTβR.Ig treatment on FDCs was not always easily detectable by visual inspection of immunofluorescently stained spleen sections from Treg depleted animals: Treg depletion alone often resulted in significant disruption to overall splenic microarchitecture, including loss of FDCs and sometimes MAdCAM-1 staining of sinus-lining cells (Supplemental Figure 5.2). Furthermore, some Splenic B cell follicles of animals treated with the combined therapy (LTβR.Ig and DT) maintained relatively normal FDC cell compartments and MAdCAM-1 staining of sinus-lining cells (Supplemental Figure 5.3).

[1] One-Way ANOVA with Tukey's multiple comparison test [2] Paired *t* test [3] Mann Whitney test [4] Spearman's correlation [5] Welch's unequal variance *t* test [6] Kruskal-Wallis One-Way ANOVA with Dunn's multiple comparisons test [7] Linear Regression
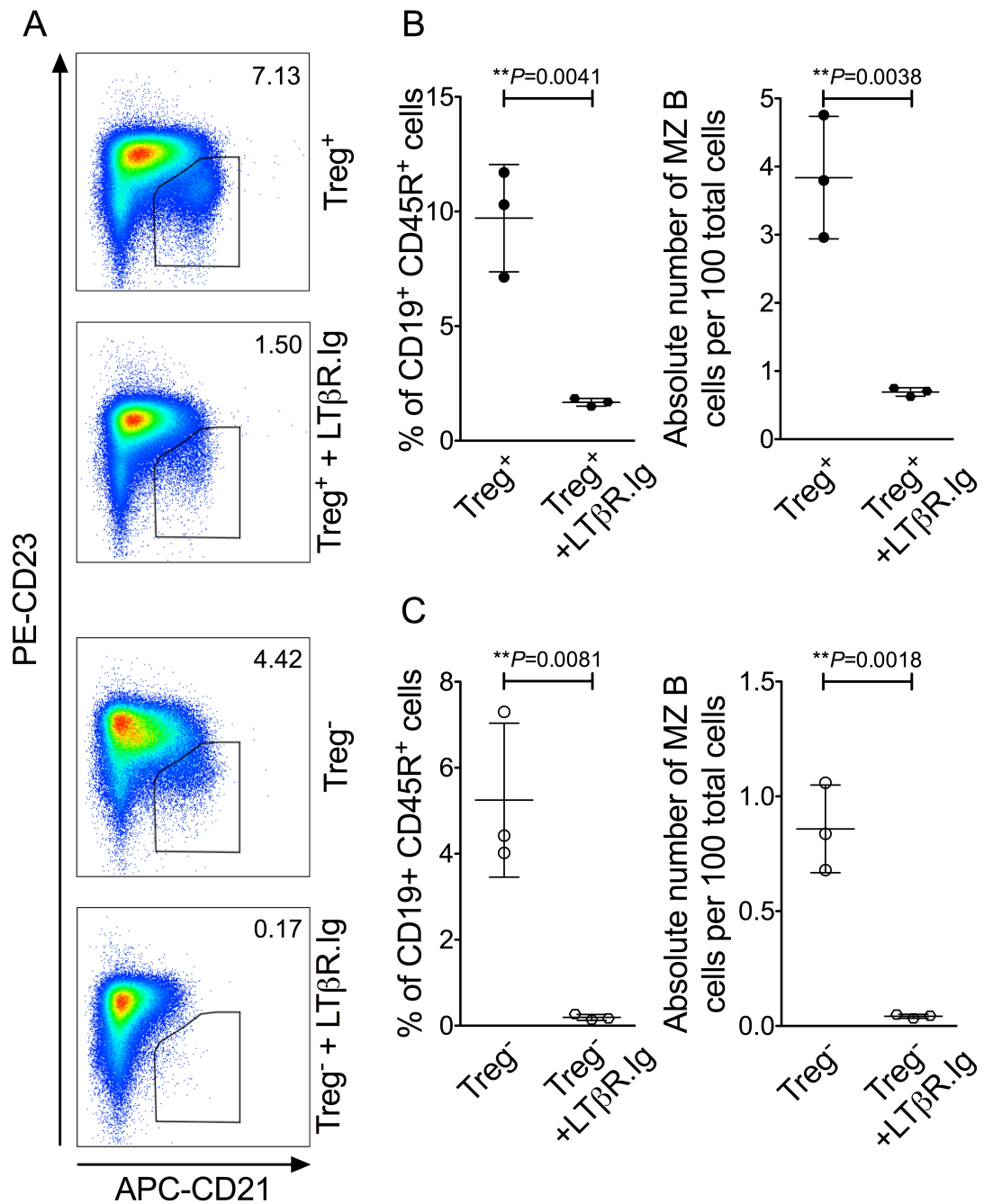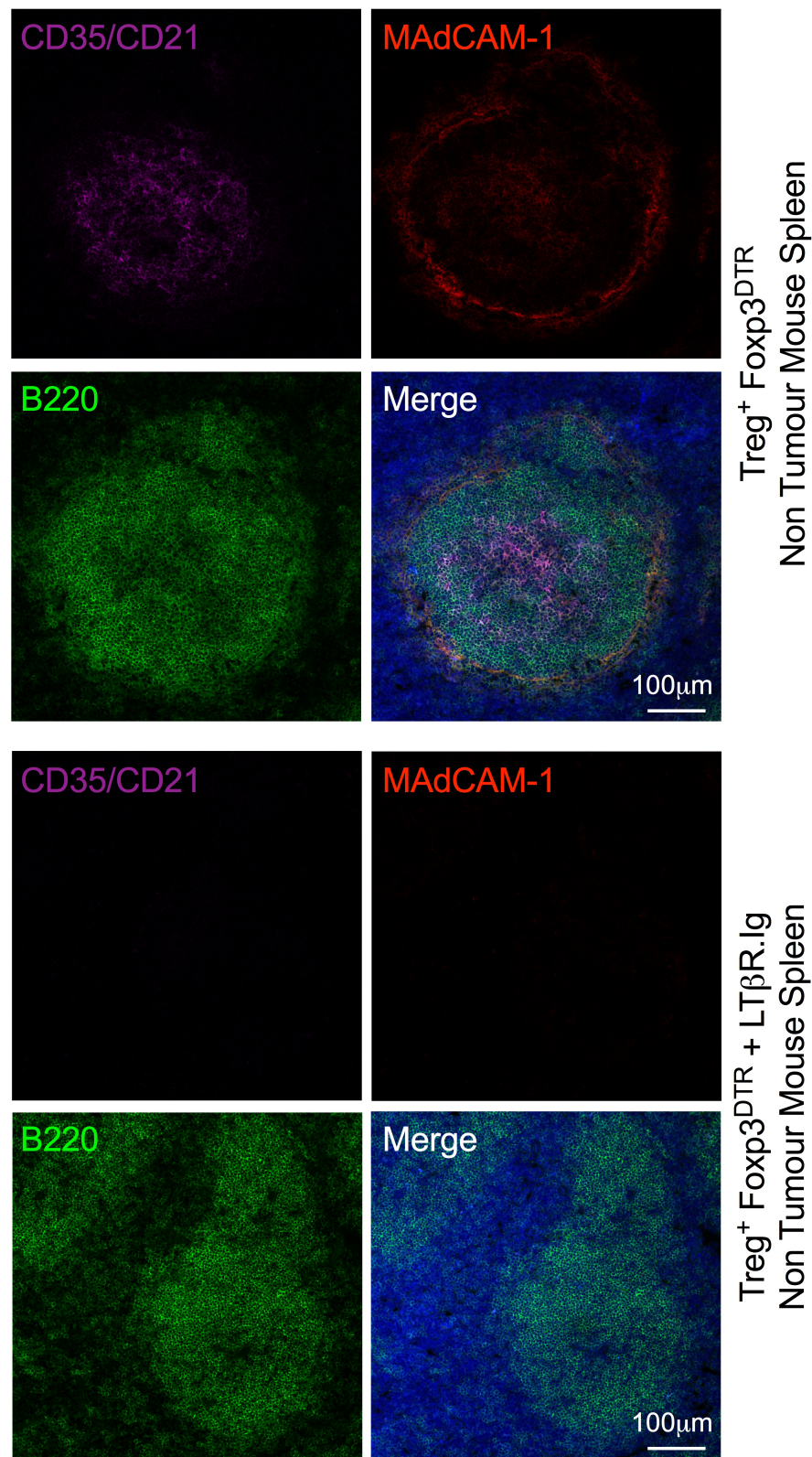
Figure 5.3 | Antagonism of LTβ Receptor signalling results in a profound loss of CD35/CD21^{+} Follicular Dendritic Cells and MAdCAM-1^{+} marginal zone sinus lining cells in Treg^{+} Spleen. Representative confocal high power images showing loss of CD35/CD21^{+} Follicular Dendritic Cells (FDC) and MAdCAM-1^{+} staining of marginal sinus lining cells in spleen of Treg replete Foxp3[DTR] animals following treatment with LTβR.Ig. Images of a spleen from a Treg replete animal (top) and from an LTβR.Ig treated, Treg replete animal (bottom) are shown. Sections were co-stained using a rat anti-CD35/CD21-APC antibody (purple), a rat anti-MAdCAM-1 antibody followed by goat anti-rat AlexaFluor-568 secondary antibody (red) and a biotinylated rat anti-CD45R antibody followed by streptaviding-FITC secondary antibody (green). Merged images include the nuclear stain DAPI (blue). Scale bars are shown.

[1] One-Way ANOVA with Tukey's multiple comparison test [2] Paired *t* test [3] Mann Whitney test [4] Spearman's correlation [5] Welch's unequal variance *t* test [6] Kruskal-Wallis One-Way ANOVA with Dunn's multiple comparisons test [7] Linear Regression

Figure 5.4 | Antagonism of LTβ Receptor signalling results in a profound loss of CD35/CD21^{+} Follicular Dendritic Cells and MAdCAM-1^{+} marginal zone sinus lining cells in Treg^{-} Spleen. Representative confocal high power images showing loss of CD35/CD21^{+} Follicular Dendritic Cells (FDC) and MAdCAM-1^{+} staining of marginal sinus lining cells in spleen of Treg depleted Foxp3[DTR] animals following treatment with LTβR.Ig. Images of a spleen from a Treg depleted animal (top) and from an LTβR.Ig treated, Treg depleted animal (bottom) are shown. Sections were co-stained using a rat anti-CD35/CD21-APC antibody (purple), a rat anti-MAdCAM-1 antibody followed by goat anti-rat AlexaFluor-568 secondary antibody (red) and a biotinylated rat anti-CD45R antibody followed by streptaviding-FITC secondary antibody (green). Merged images include the nuclear stain DAPI (blue). Scale bars are shown.

[1] One-Way ANOVA with Tukey's multiple comparison test [2] Paired *t* test [3] Mann Whitney test [4] Spearman's correlation [5] Welch's unequal variance *t* test [6] Kruskal-Wallis One-Way ANOVA with Dunn's multiple comparisons test [7] Linear Regression

Whilst PNAd[+] HEV were detectable in Inguinal LNs of LTβR.Ig treated animals, vessel morphology was significantly disrupted in a high proportion of samples: vessel distribution within the LN appeared less organised, and vessels appeared larger, often with more open lumen than those in LNs of Treg depleted Foxp3[DTR] animals (Figure 5.5). Of note, not all LN HEV were disrupted following LTβR.Ig treatment: some HEV were indiscernible from those in LNs of Treg depleted animals. However, these data indicated a reduction in the fully differentiated status of HEV in LNs, a well-described consequence of LTβR.Ig treatment (Browning et al. 2005).

LTβR.Ig treatment reduces PLN cellularity as a result of impaired lymphocyte trafficking via HEV due to dedifferentiation of vessels (Browning et al. 2005). The morphological disruption to HEV of inguinal LNs in LTβR.Ig treated Treg depleted animals was reflected by a significant reduction in inguinal LN cellularity[1] (Figure 5.6 A). The same trend, albeit not statistically significant, was observed for Treg replete animals (Figure 5.6 A). The profound lymphadenopathy induced by Treg depletion (Kim et al. 2007) (Figure 5.6 A & B), made the observed reduction in inguinal LN cellularity of Treg depleted mice upon LTβR.Ig treatment even more striking.

Lymphocyte homing to mucosal lymphoid organs is dependent on the integrin $\alpha_4\beta_7$–MAdCAM-1 adhesion cascade as well as the L-selectin–PNAd adhesion cascade (Butcher et al. 1999). Despite reports of reduced PNAd and MAdCAM-1 expression on HEV and decreased mesenteric LN cellularity upon LTβR.Ig treatment (Browning et al. 2005), I observed no change in mesenteric LN cellularity after LTβR.Ig treatment of Treg replete or Treg depleted animals[1], perhaps reflecting maintained MAdCAM-1 expression and dominance of $\alpha_4\beta_7$–MAdCAM-1 interactions for homing to mesenteric LN (Figure 5.6 B; data not shown). In line with reports of inhibited lymphocyte entry into LNs resulting in increased numbers of lymphocytes in spleen, I observed an increase in splenic cellularity following LTβR.Ig treatment in Treg replete animals (Browning et al. 2005): the profound splenomegaly induced by Treg loss masked this affect of LTβR.Ig treatment in Treg depleted animals (Kim et al. 2007) (Figure 5.6 C).

[1] One-Way ANOVA with Tukey's multiple comparison test [2] Paired *t* test [3] Mann Whitney test [4] Spearman's correlation [5] Welch's unequal variance *t* test [6] Kruskal-Wallis One-Way ANOVA with Dunn's multiple comparisons test [7] Linear Regression
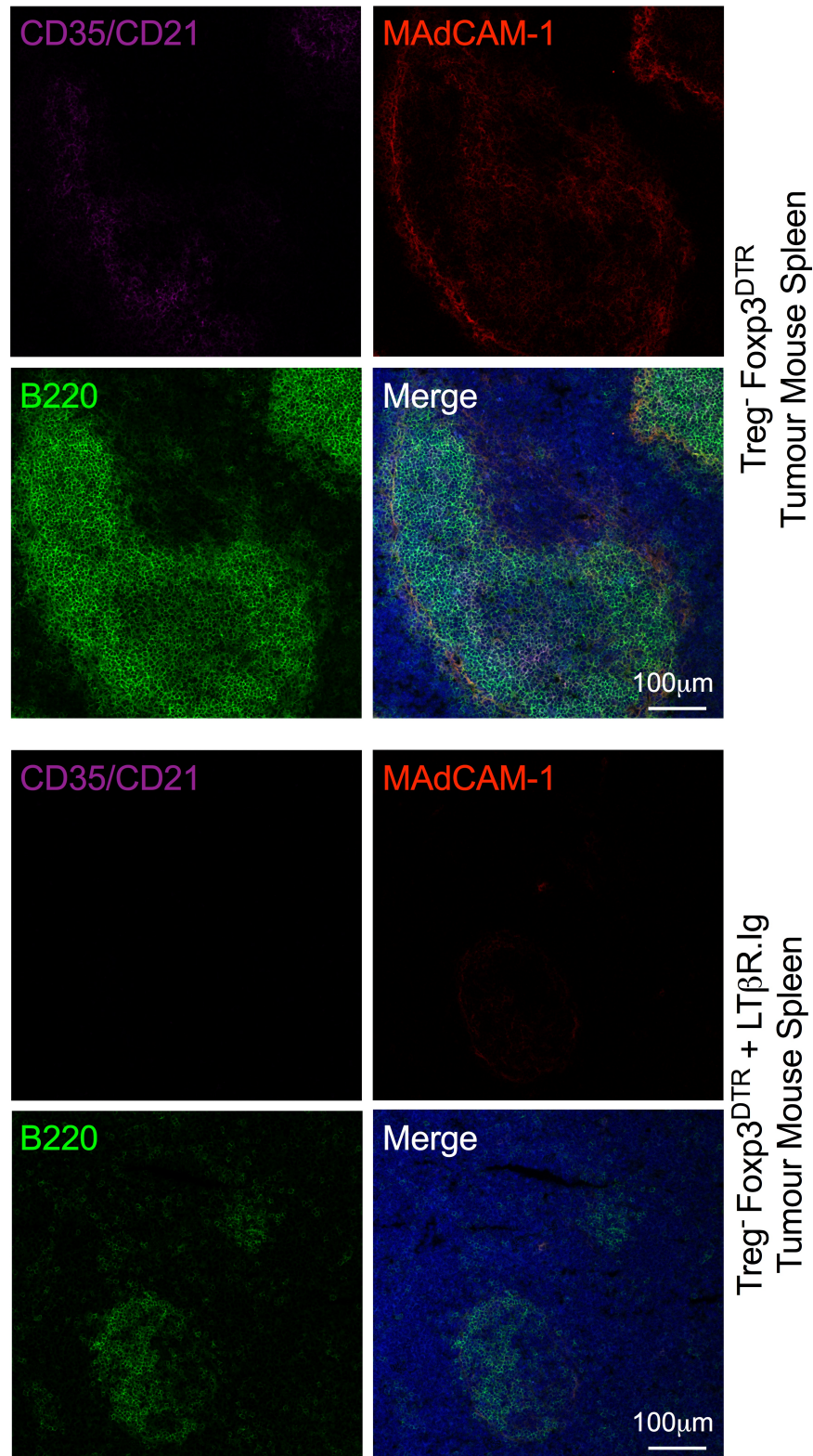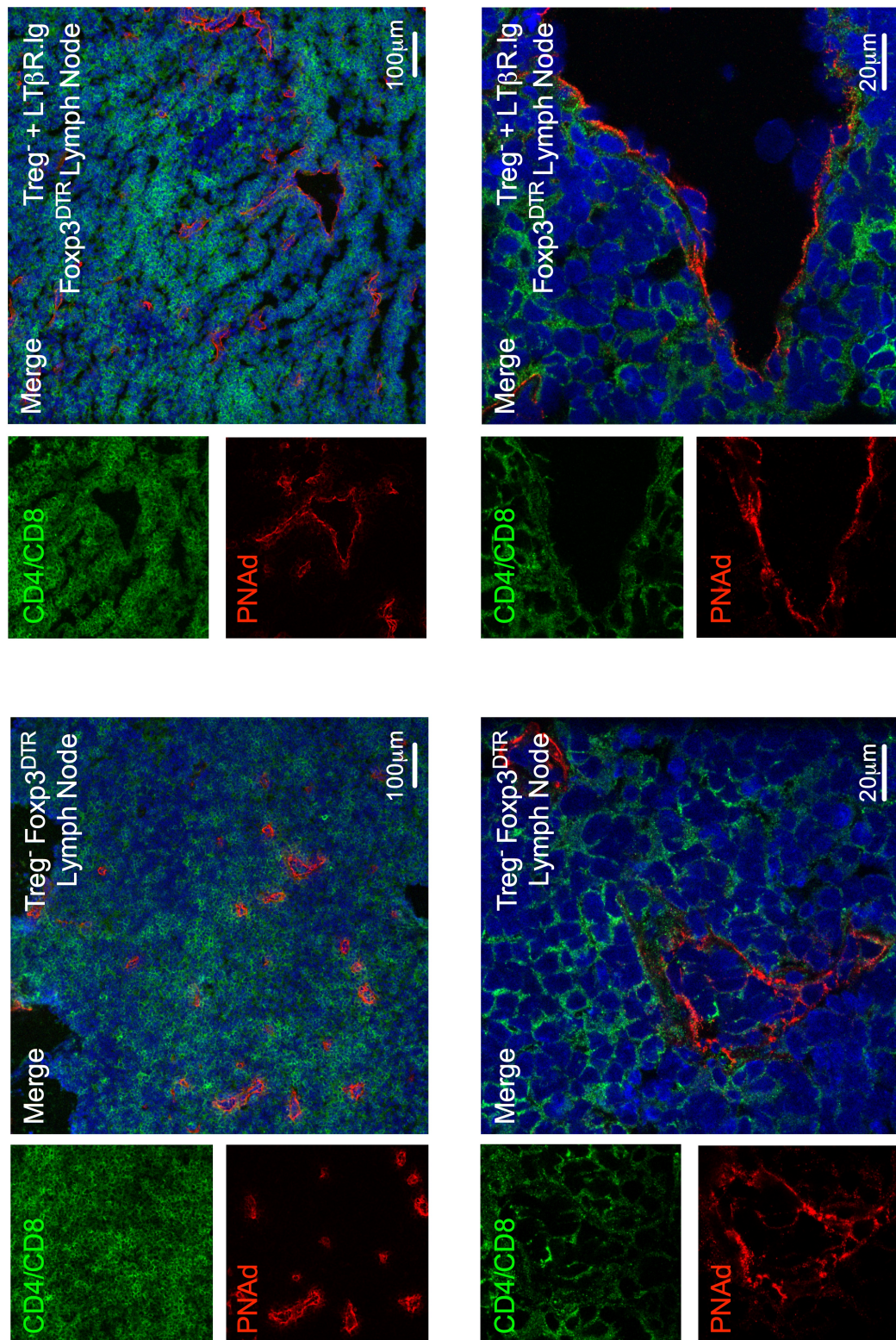
Figure 5.5 | Antagonism of LTβ Receptor signalling results in a profound disruption to Lymph Node High Endothelial Venule morphology.

Representative confocal microscope images showing disruption to PNAd$^+$ HEV of lymph nodes in Treg depleted Foxp3^{DTR} animals following treatment with LTβR.Ig. Low power (top) and high power (bottom) images of lymph node sections from a Treg depleted Foxp3^{DTR} animal (left) and from an LTβR.Ig treated, Treg depleted Foxp3^{DTR} animal (right) are shown. Sections were immunofluorescently co-stained using a biotinylated rat anti-PNAd primary antibody (clone MECA-79), which was detected using a streptavidin-555 secondary antibody (red), and rat anti-CD4 and rat anti-CD8a primary antibodies, which were detected using an anti-rat donkey AlexFluor 488 secondary antibody (green). Merged images include the nuclear stain DAPI (blue). Scale bars are shown.

[1] One-Way ANOVA with Tukey's multiple comparison test [2] Paired *t* test [3] Mann Whitney test [4] Spearman's correlation [5] Welch's unequal variance *t* test [6] Kruskal-Wallis One-Way ANOVA with Dunn's multiple comparisons test [7] Linear Regression

Figure 5.6 | Antagonism of LTβ Receptor signalling results in a reduction in Inguinal Lymph Node cellularity with a concurrent increase in Splenic cellularity.
Absolute numbers of cells in lymphoid organs of Treg replete and Treg depleted Foxp3[DTR] animals treated with or without LTβR.Ig, as assessed by haemocytometer count. Numbers of cells per 10^6 total cells are shown for Inguinal lymph node (A), Mesenteric lymph node (B) and Spleen (C), of Treg replete (closed shapes) Foxp3[DTR] animals treated with or without LTβR.Ig, and Treg depleted (open shapes) Foxp3[DTR] animals treated with or without LTβR.Ig. Statistical significance was determined by One-way ANOVA with Tukey's multiple comparison tests to compare pairs of means (* = $P \le 0.05$, ** = $P \le 0.01$, *** = $P \le 0.001$). N = 3 per group.

[1] One-Way ANOVA with Tukey's multiple comparison test [2] Paired *t* test [3] Mann Whitney test [4] Spearman's correlation [5] Welch's unequal variance *t* test [6] Kruskal-Wallis One-Way ANOVA with Dunn's multiple comparisons test [7] Linear Regression

To determine the affect of LTβR.Ig treatment on intra-tumoural HEV neogenesis, tumour sections were examined by immunohistochemistry. PNAd[+] HEV were present in LTβR.Ig-treated Treg depleted frozen tumour sections (Figure 5.7). PNAd co-localised with CD31, as in control Treg depleted tumours, confirming the detection of vascular endothelial cells (Figure 5.7). PNAd[+] HEV were also readily detectable in paraffin embedded tumour sections of LTβR.Ig-treated Treg depleted animals (Figure 5.8 A). Quantification of PNAd[+] vessels in paraffin embedded tumour sections revealed no significant difference in HEV density of LTβR.Ig-treated Treg depleted tumours relative to control Treg depleted tumours (ns*P*=0.0825[3]; Figure 5.8 B). However, there was a noticeable trend towards an increase in HEV density in LTβR.Ig-treated tumours. Interestingly, the average HEV area in LTβR.Ig-treated Treg depleted tumours was significantly greater than that in control Treg depleted tumours (****P*=0.0005[3]; Figure 5.8 C). These findings were corroborated by the visual observation that HEV in LTβR.Ig-treated tumours often appeared larger, with more open lumen, than HEV of Treg depleted tumours (Figure 5.8 A). In support of the observed trend towards an increase in HEV density in LTβR.Ig-treated tumours, there was a modest increase in the total HEV area in LTβR.Ig-treated tumours relative to Treg depleted tumours (**P*=0.0306[3]; Figure 5.8 D).

To assess functionality of intra-tumoural HEV in LTβR.Ig treated Treg depleted animals, I correlated measures of HEV density or total HEV area with numbers of tumour infiltrating T cells and tumour growth rates (Figure 5.9). There was a significant positive correlation between HEV density and number of tumour infiltrating T cells (r = 0.8901, ****P*<0.0001 for CD4^{+} T cells[4]; r = 0.6777, **P*=0.0109 for CD8^{+} T cells[4]; Figure 5.9 A-B). These data indicated that intra-tumoural HEV that developed following Treg depletion, during LTβR.Ig treatment, were functional in terms of facilitating lymphocyte trafficking into the tumour mass. Furthermore, numbers of tumour infiltrating T cells appeared to correlate negatively with tumour growth rate in LTβR.Ig-treated animals, as observed for the control Treg depleted group, although in this case, the trend did not reach statistical significance (r = -0.4121, ns*P*=0.1618 for CD4^{+} T cells[4]; r = -0.4904,

ns$P$=0.0889 for CD8^{+} T cells[4]; Figure 5.9 C-D). Similarly, both HEV density and total HEV area seemed to correlate negatively with tumour growth rate following LTβR.Ig treatment, although, again, statistical significance was not reached (r = -0.3022, ns$P$=0.3156 for HEV Density[4]; r = -0.3297, ns$P$=0.2713 for HEV Area[4]; Figure 5.9 E-F). The observed loss of a statistically significant correlation between HEV density or total HEV area and tumour growth rate in LTβR.Ig-treated animals relative to control Treg depleted animals indicates that LTβR.Ig treatment could be having some effect on HEV integrity or functionality.

Collectively, these data indicate that LTβR antagonism does not interrupt HEV neogenesis in tumours following Treg depletion. These data suggest that signalling via the LTβR is not required for intra-tumoural HEV formation in this model, and that an alternative signalling circuitry drives this biological process. Interruption of LTβR signalling did however seem to have a partial effect upon functionality of tumour HEV, in terms of conferring a degree of tumour growth control. Collectively, these data imply that HEV neogenesis in tumours of Treg depleted animals represents a distinct molecular mechanism to that underpinning normal development of HEV-containing LNs in wild-type animals, which is critically dependent upon LTβR signalling.

[1] One-Way ANOVA with Tukey's multiple comparison test [2] Paired t test [3] Mann Whitney test [4] Spearman's correlation [5] Welch's unequal variance t test [6] Kruskal-Wallis One-Way ANOVA with Dunn's multiple comparisons test [7] Linear Regression
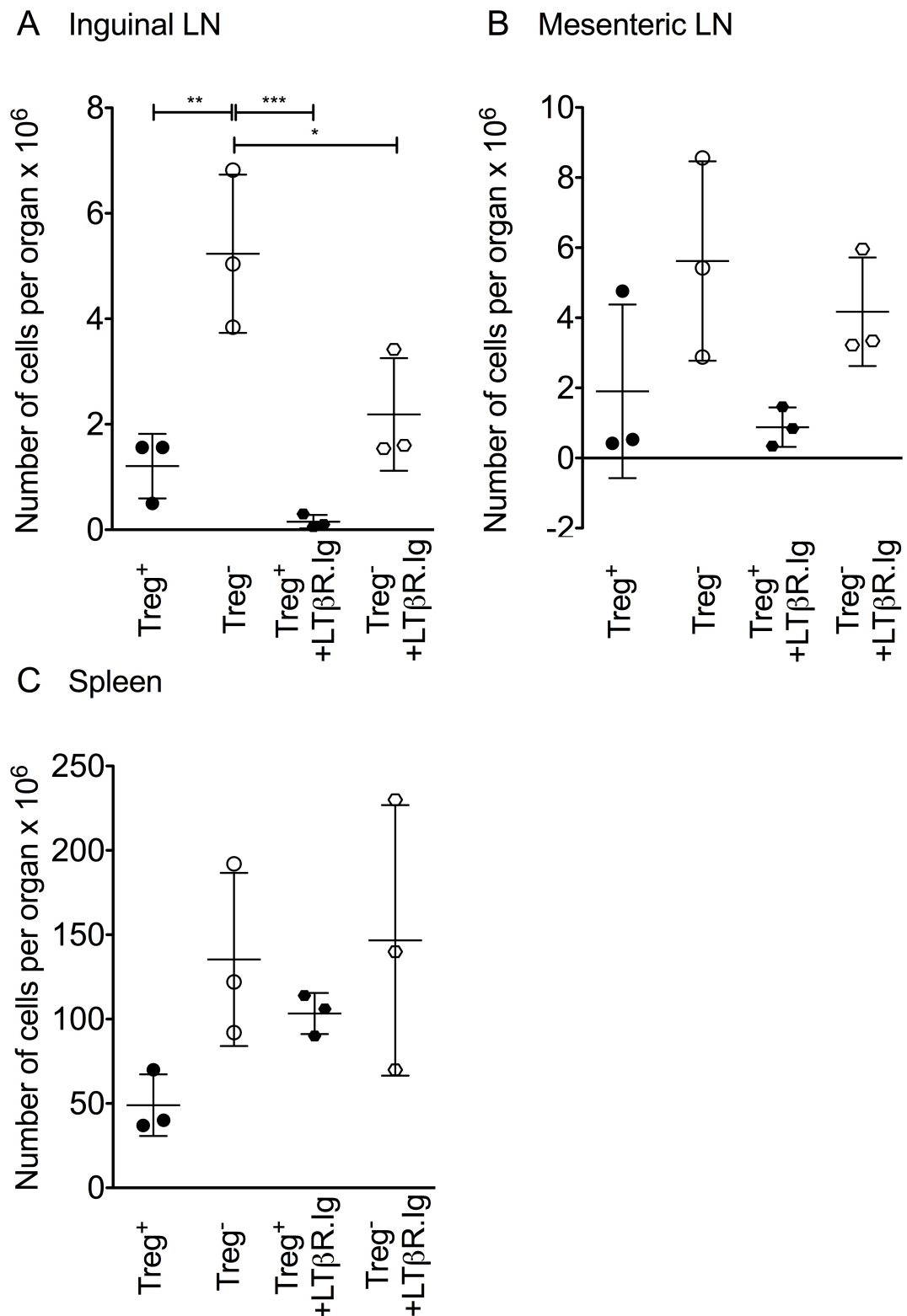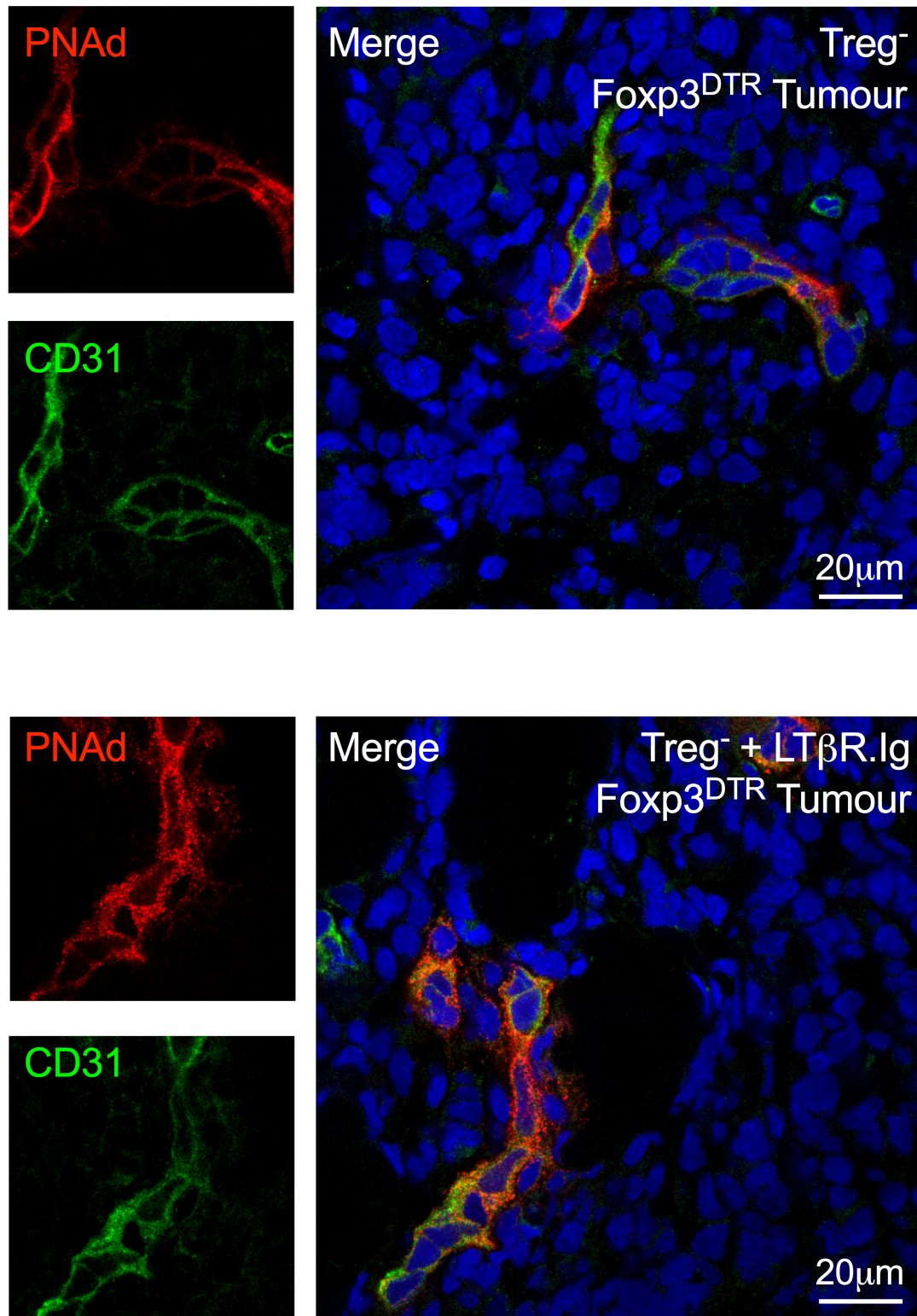
Figure 5.7 | High Endothelial Venules are found in tumours following LTβ Receptor antagonism. Confocal images of High Endothelial Venules (HEV) within tumours of Treg depleted (top) and LTβR.Ig treated, Treg depleted (bottom) Foxp3^{DTR} animals. Endothelial cells of HEV were detected by immunofluorescence staining using a biotinylated rat anti-PNAd primary antibody (clone MECA-79) and streptavidin Alexa Fluor® 555 secondary antibody (red). Tumour sections were dual-stained for PNAd and CD31 (rat anti-CD31-FITC; green). Merged images include the nuclear stain DAPI (blue). Scale bars are shown.

[1] One-Way ANOVA with Tukey's multiple comparison test [2] Paired *t* test [3] Mann Whitney test [4] Spearman's correlation [5] Welch's unequal variance *t* test [6] Kruskal-Wallis One-Way ANOVA with Dunn's multiple comparisons test [7] Linear Regression

Figure 5.8 | Measures of High Endothelial Venule density and total area are modestly increased when LTβ Receptor signalling is antagonised.

Quantitative measures of High Endothelial Venules (HEV) in tumours of LTβR.Ig treated, Treg depleted Foxp3[DTR] animals. (A) Representative microscope images of HEV in paraffin embedded tumours. The anti-PNAd antibody (clone MECA-79) was detected using DAB chromogen (brown staining). Sections were counterstained using haematoxylin. Scale bars are shown. (B) HEV density was calculated per unit area of tumour (μm^2). (C) Average area of HEV vessels calculated in μm^2. (D) Total HEV area as a proportion of total tumour area, calculated as a percentage. Data are presented as individual datapoints plus median. Statistical significance was determined by Mann Whitney t tests. N = 13 LTβR.Ig treated, Treg⁻ tumours; N = 21 Treg⁻ tumours (20 in C).

[1] One-Way ANOVA with Tukey's multiple comparison test [2] Paired t test [3] Mann Whitney test [4] Spearman's correlation [5] Welch's unequal variance t test [6] Kruskal-Wallis One-Way ANOVA with Dunn's multiple comparisons test [7] Linear Regression
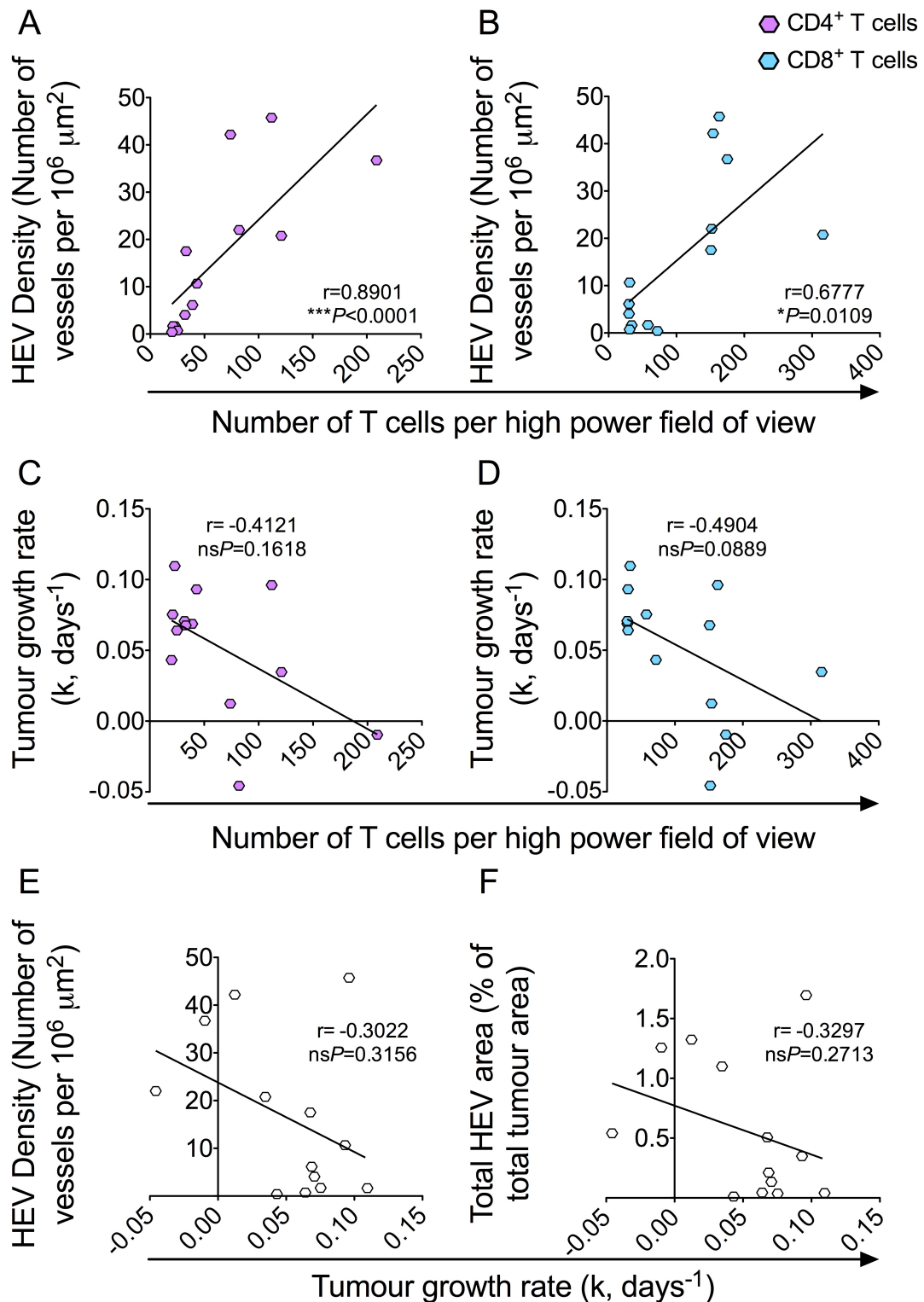
Figure 5.9 | Functionality of High Endothelial Venules in tumours in which LTβ Receptor signalling is blocked seems partially compromised.

Correlations between number of intra-tumoural CD4^{+} and CD8^{+} T cells, High Ednothelial Venule (HEV) density and total HEV area, and tumour growth rates for LTβR.Ig treated, Treg depleted Foxp3[DTR] animals. (A-B) Numbers of intra-tumoural CD4^{+} and CD8^{+} T cells plotted against tumour HEV density; CD4^{+} T cells (A; purple); CD8^{+} T cells (B; blue). (C-D) Numbers of intra-tumoural CD4^{+} and CD8^{+} T cells plotted against tumour growth rates (k, days[-1]); CD4^{+} T cells (C; purple); CD8^{+} T cells (D; blue). (E-F) HEV density (E) and total HEV area (as proportion of total tumour area; F) plotted against tumour growth rate (k, days[-1]). Statistical significance was determined by the non-parametric Spearman's correlation coefficient test, and the r statistic and P values are shown. N = 13.

[1] One-Way ANOVA with Tukey's multiple comparison test [2] Paired t test [3] Mann Whitney test [4] Spearman's correlation [5] Welch's unequal variance t test [6] Kruskal-Wallis One-Way ANOVA with Dunn's multiple comparisons test [7] Linear Regression

5.4 Results: TNFR antagonism using a TNFRII.Ig fusion protein reduces HEV density, total HEV area and average HEV area in tumours

Having eliminated a role for LTβR signalling, I investigated a role for TNFR signalling in HEV neogenesis in our tumour model. In addition to an implied role in SLO development (Rennert et al. 1998), genes encoding TNFα and TNFR2 were significantly upregulated in HEV positive tumours of Treg depleted animals relative to HEV negative tumours of Treg depleted animals, and Treg replete animals (Figure 5.1). I therefore treated tumour-bearing Foxp3[DTR] animals with DT and a TNFRII fusion protein (Enbrel® (Etanercept)), according to the protocol in Chapter 2.

Blockade of TNFR signalling using TNFRII.Ig results in similar splenic architectural disruption as observed following LTβR antagonism, including a loss of MAdCAM-1 staining on marginal sinus lining cells and splenic FDCs (Chiang et al. 2009). Successful antagonism of TNFR signalling was confirmed by a profound loss of FDC and MAdCAM-1 staining following TNFRII.Ig treatment (Figure 5.10). The degree of disruption varied; some samples demonstrated maintained MAdCAM-1 expression (Supplemental Figure 5.4). However, loss of FDCs was a reliable, consistent surrogate marker of TNFR antagonism by TNFRII.Ig.

Inguinal LNs of some TNFRII.Ig treated animals contained fewer PNAd[+] HEV, and / or PNAd staining appeared weaker (Figure 5.11). These data are in contrast to a report where murine TNFRII.Ig failed to disrupt LN HEV (Browning et al. 2005). However, the disruption to LN architecture following Treg depletion signifies the magnitude of baseline systemic alterations in this system (Figures 4.2-4.4). As for LTβR.Ig, TNFRII.Ig treatment also disrupted LN HEV morphology: vessel distribution was less uniform, and vessels often had more open lumen than those in LNs of Treg depleted animals (Figure 5.11). Again, the degree of disruption varied, and some LN HEV of TNFRII.Ig treated mice were indiscernible from those of Treg depleted animals. However, these data indicated a reduction in the fully differentiated status of HEV in LNs, in a similar manner to that following LTβR.Ig treatment.

[1] One-Way ANOVA with Tukey's multiple comparison test [2] Paired *t* test [3] Mann Whitney test [4] Spearman's correlation [5] Welch's unequal variance *t* test [6] Kruskal-Wallis One-Way ANOVA with Dunn's multiple comparisons test [7] Linear Regression
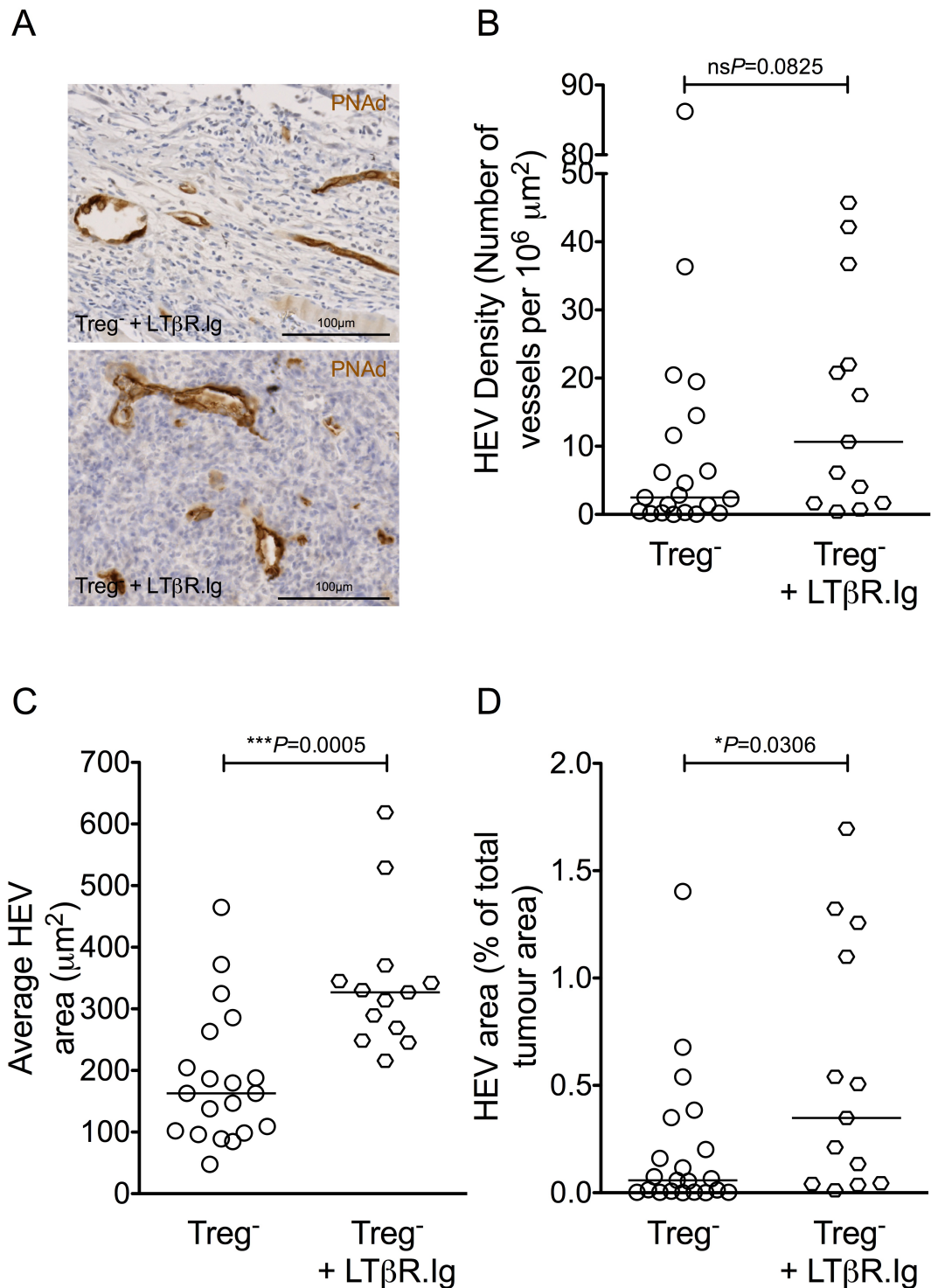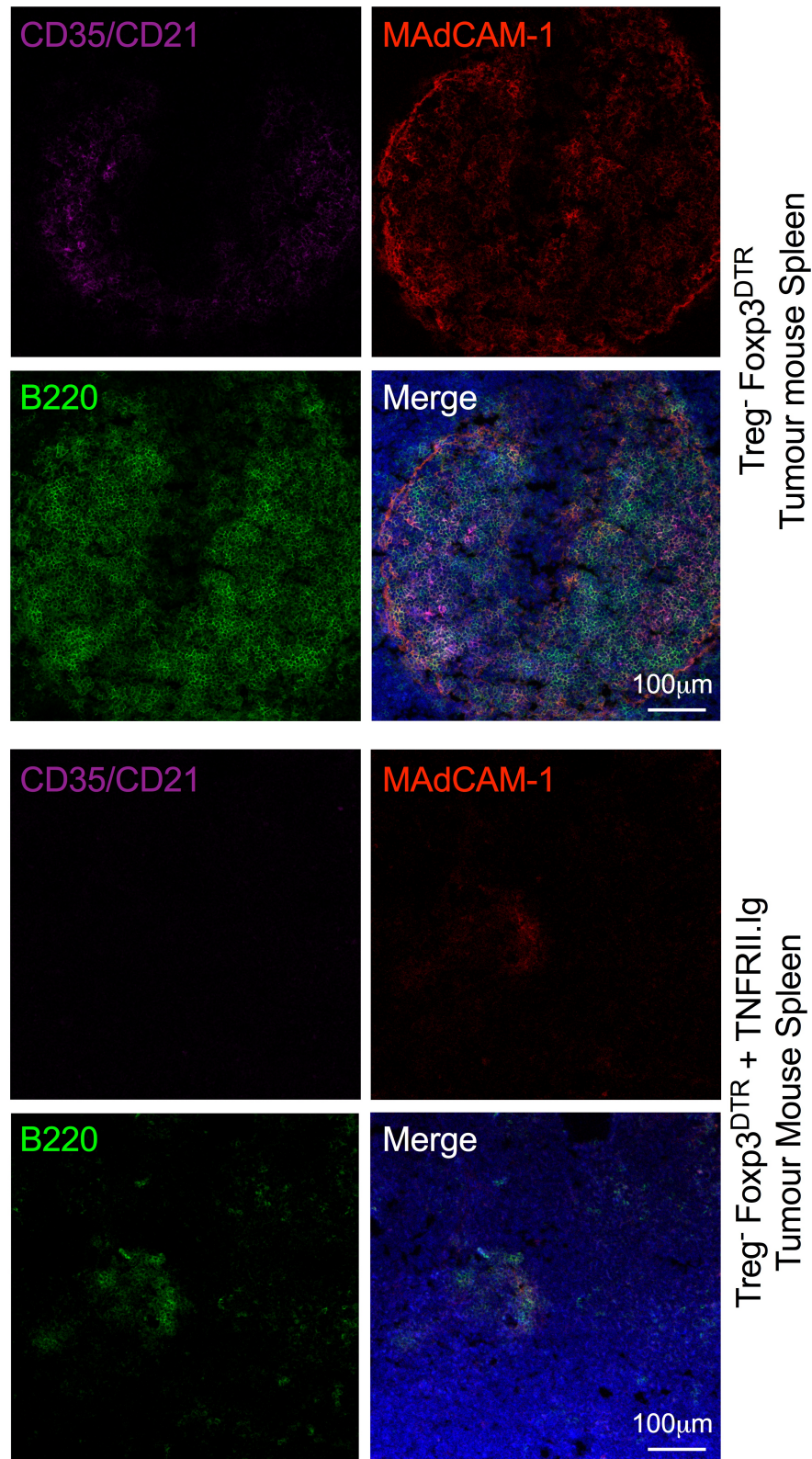
Figure 5.10 | Antagonism of TNF Receptor signalling results in a profound loss of CD35/CD21^{+} Follicular Dendritic Cells and MAdCAM-1^{+} marginal zone sinus lining cells in Treg^{-} Spleen. Representative confocal high power images showing loss of CD35/CD21^{+} Follicular Dendritic Cells (FDC) and MAdCAM-1^{+} staining of marginal sinus lining cells in spleen of Treg depleted Foxp3[DTR] animals following treatment with TNFRII.Ig. Images of a spleen from a Treg depleted animal (top) and from an TNFRII.Ig treated, Treg depleted animal (bottom) are shown. Sections were co-stained using a rat anti-CD35/CD21-APC antibody (purple), a rat anti-MAdCAM-1 antibody followed by goat anti-rat AlexaFluor-568 secondary antibody (red) and a biotinylated rat anti-CD45R antibody followed by streptaviding-FITC secondary antibody (green). Merged images include the nuclear stain DAPI (blue). Scale bars are shown.

[1] One-Way ANOVA with Tukey's multiple comparison test [2] Paired *t* test [3] Mann Whitney test [4] Spearman's correlation [5] Welch's unequal variance *t* test [6] Kruskal-Wallis One-Way ANOVA with Dunn's multiple comparisons test [7] Linear Regression

Figure 5.11 | Antagonism of TNF Receptor signalling results in a profound disruption to Lymph Node High Endothelial Venule morphology.

Representative confocal microscope images showing disruption to PNAd[+] HEV of lymph nodes in Treg depleted Foxp3[DTR] animals following treatment with TNFRII.Ig. Low power (top) and high power (bottom) images of lymph node sections from a Treg depleted Foxp3[DTR] animal (left) and from an TNFRII.Ig treated, Treg depleted Foxp3[DTR] animal (right) are shown. Sections were immunofluorescently co-stained using a biotinylated rat anti-PNAd primary antibody (clone MECA-79), which was detected using a streptavidin-555 secondary antibody (red), and rat anti-CD4 and rat anti-CD8a primary antibodies, which were detected using an anti-rat donkey AlexFluor 488 secondary antibody (green). Merged images include the nuclear stain DAPI (blue). Scale bars are shown.

[1] One-Way ANOVA with Tukey's multiple comparison test [2] Paired *t* test [3] Mann Whitney test [4] Spearman's correlation [5] Welch's unequal variance *t* test [6] Kruskal-Wallis One-Way ANOVA with Dunn's multiple comparisons test [7] Linear Regression

PNAd^{+} CD31^{+} HEV were present in tumours of Treg depleted, TNFRII.Ig treated animals (Figure 5.12). However, PNAd staining of HEV appeared weaker in the majority of TNFRII.Ig treated tumours and the morphology of the endothelial cells lining HEV appeared deflated relative to Treg depleted control samples (Figure 5.12 & 5.13 A). Furthermore, HEV appeared fewer in number and smaller in size, relative to vessels found in Treg depleted control tumours (Figure 5.13 A). Indeed, when HEV were quantified, there was a noticeable decrease in HEV density in Treg depleted, TNFRII.Ig treated tumours relative to control Treg depleted tumours, despite not reaching statistical significance (ns$P$=0.3946[3]; Figure 5.13 B). In line with these data, there was a reduction in total HEV area in TNFRII.Ig treated tumours relative to control Treg depleted tumours, despite not reaching statistical significance (ns$P$=0.3326[3]; Figure 5.13 D). Lastly, in support of observations, there was a decrease in average HEV area in TNFRII.Ig treated tumours, despite once again not reaching statistical significance (ns$P$=0.1394[3]; Figure 5.13 C).

There was a weak positive correlation between HEV density and number of tumour infiltrating CD4^{+} T cells in TNFRII.Ig treated tumours (r = 0.6016, *P=0.0106[4]; Figure 5.14 A). The number of CD8^{+} T cells also appeared to correlate positively with HEV density, although statistical significance was not reached (r = 0.4491, ns$P$=0.0706[4]; Figure 5.14 B). However, numbers of tumour infiltrating T cells did not correlate with tumour growth rate in TNFRII.Ig-treated animals, in contrast to the control Treg depleted group (r = -0.05770, ns$P$=0.8259 for CD4^{+} T cells[4]; r = -0.2074, ns$P$=0.4245 for CD8^{+} T cells[4]; Figure 5.14 C-D). In agreement with these data, both HEV density and total HEV area displayed very weak negative correlations with tumour growth rate following TNFRII.Ig treatment, which were far from reaching statistical significance (r = -0.3235, ns$P$=0.2052 for HEV Density[4]; r = -0.2304, ns$P$=0.3737 for HEV Area[4]; Figure 5.14 E-F). These data suggest that intra-tumoural HEV that developed during TNFRII.Ig treatment were compromised in terms of their ability to facilitate infiltration of lymphocytes capable of supporting an effective anti-tumour immune response.

[1] One-Way ANOVA with Tukey's multiple comparison test [2] Paired t test [3] Mann Whitney test [4] Spearman's correlation [5] Welch's unequal variance t test [6] Kruskal-Wallis One-Way ANOVA with Dunn's multiple comparisons test [7] Linear Regression
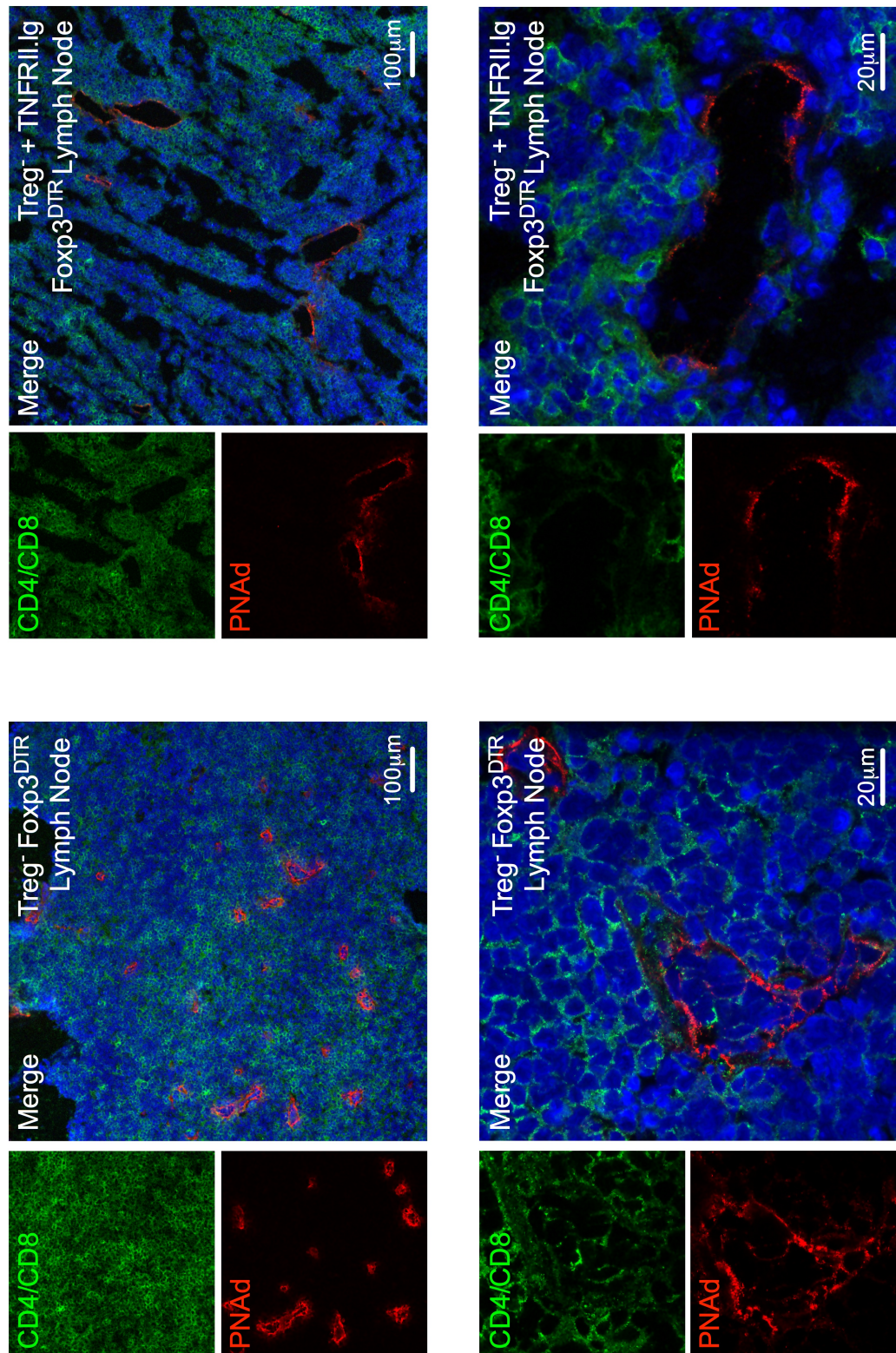
Collectively, these data show that, whilst HEV neogenesis was not completely ablated in tumours of Treg depleted TNFRII.Ig treated animals, HEV density, total HEV area and average HEV area appear reduced. Furthermore, HEV functionality seems diminished, as correlation between HEV density and infiltrating T cells or tumour growth rate are mostly lost after TNFRII.Ig treatment. Therefore, HEV neogenesis in tumours following Treg depletion appears to be at least partially reliant upon TNFR signalling.

[1] One-Way ANOVA with Tukey's multiple comparison test [2] Paired *t* test [3] Mann Whitney test [4] Spearman's correlation [5] Welch's unequal variance *t* test [6] Kruskal-Wallis One-Way ANOVA with Dunn's multiple comparisons test [7] Linear Regression
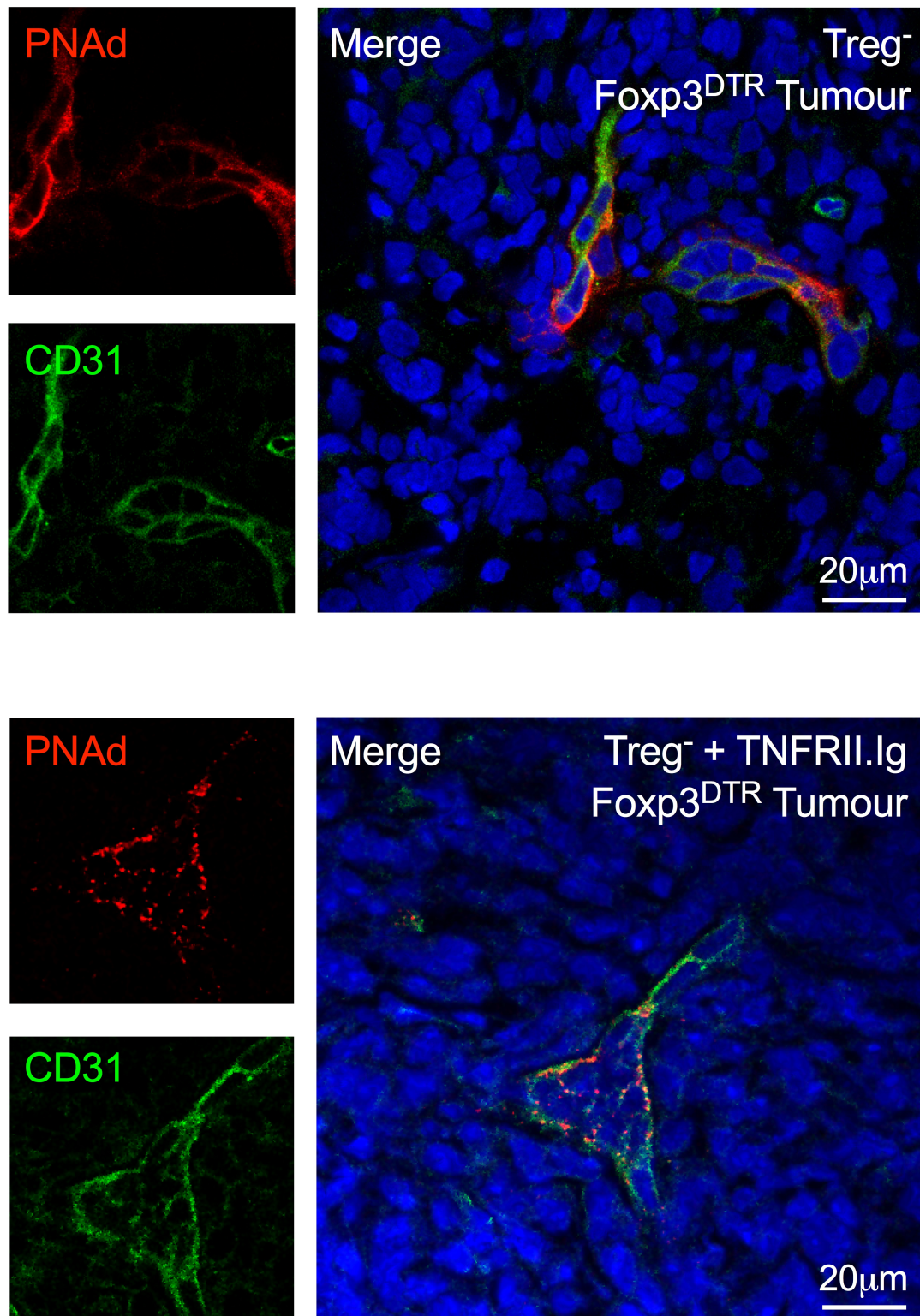
Figure 5.12 | High Endothelial Venules are found in tumours following TNF Receptor antagonism.
Confocal images of High Endothelial Venules (HEV) within tumours of Treg depleted (top) and TNFRII.Ig treated, Treg depleted (bottom) Foxp3^{DTR} animals. Endothelial cells of HEV were detected by immunofluorescence staining using a biotinylated rat anti-PNAd primary antibody (clone MECA-79) and streptavidin Alexa Fluor® 555 secondary antibody (red). Tumour sections were dual-stained for PNAd and CD31 (rat anti-CD31-FITC; green). Merged images include the nuclear stain DAPI (blue). Scale bars are shown.

[1] One-Way ANOVA with Tukey's multiple comparison test [2] Paired *t* test [3] Mann Whitney test [4] Spearman's correlation [5] Welch's unequal variance *t* test [6] Kruskal-Wallis One-Way ANOVA with Dunn's multiple comparisons test [7] Linear Regression

Figure 5.13 | Measures of High Endothelial Venule density and total area are profoundly decreased when TNF Receptor signalling is antagonised.

Quantitative measures of High Endothelial Venules (HEV) in tumours of TNFRII.Ig treated, Treg depleted Foxp3^{DTR} animals. (A) Representative microscope images of HEV in paraffin embedded tumours. The anti-PNAd antibody (clone MECA-79) was detected using DAB chromogen (brown staining). Sections were counterstained using haematoxylin. Scale bars are shown. (B) HEV density was calculated per unit area of tumour (μm^2). The insert shows an enlarged version of the boxed area. (C) Average area of HEV vessels calculated in μm^2. (D) Total HEV area as a proportion of total tumour area, calculated as a percentage. Data are presented as individual datapoints plus median. Statistical significance was determined by Mann Whitney t tests. N = 17 TNFII.Ig treated, Treg$^-$ tumours; N = 21 Treg$^-$ tumours (20 in C).

[1] One-Way ANOVA with Tukey's multiple comparison test [2] Paired t test [3] Mann Whitney test [4] Spearman's correlation [5] Welch's unequal variance t test [6] Kruskal-Wallis One-Way ANOVA with Dunn's multiple comparisons test [7] Linear Regression
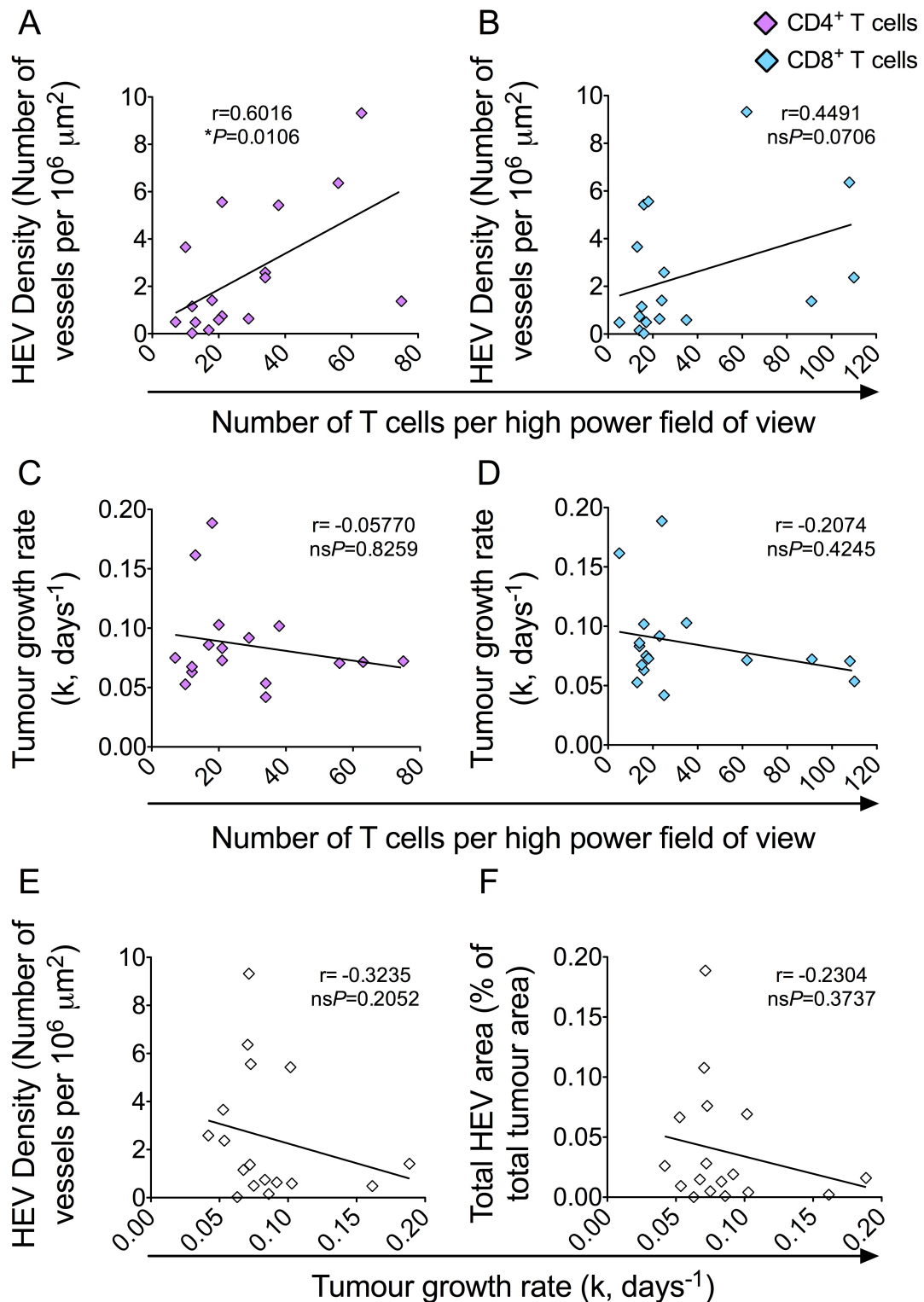
Figure 5.14 | Functionality of High Endothelial Venules in tumours in which TNF Receptor signalling is blocked seems severely compromised.
Correlations between number of intra-tumoural CD4$^+$ and CD8$^+$ T cells, High Endothelial Venule (HEV) density and total HEV area, and tumour growth rates for TNFRII.Ig treated, Treg depleted Foxp3^{DTR} animals. (A-B) Numbers of intra-tumoural CD4$^+$ and CD8$^+$ T cells plotted against tumour HEV density; CD4$^+$ T cells (A; purple); CD8$^+$ T cells (B; blue). (C-D) Numbers of intra-tumoural CD4$^+$ and CD8$^+$ T cells plotted against tumour growth rates (k, days^{-1}); CD4$^+$ T cells (C; purple); CD8$^+$ T cells (D; blue). (E-F) HEV density (E) and total HEV area (as proportion of total tumour area; F) plotted against tumour growth rate (k, days^{-1}). Statistical significance was determined by the non-parametric Spearman's correlation coefficient test, and the r statistic and P values are shown. N = 17.

[1] One-Way ANOVA with Tukey's multiple comparison test [2] Paired t test [3] Mann Whitney test [4] Spearman's correlation [5] Welch's unequal variance t test [6] Kruskal-Wallis One-Way ANOVA with Dunn's multiple comparisons test [7] Linear Regression
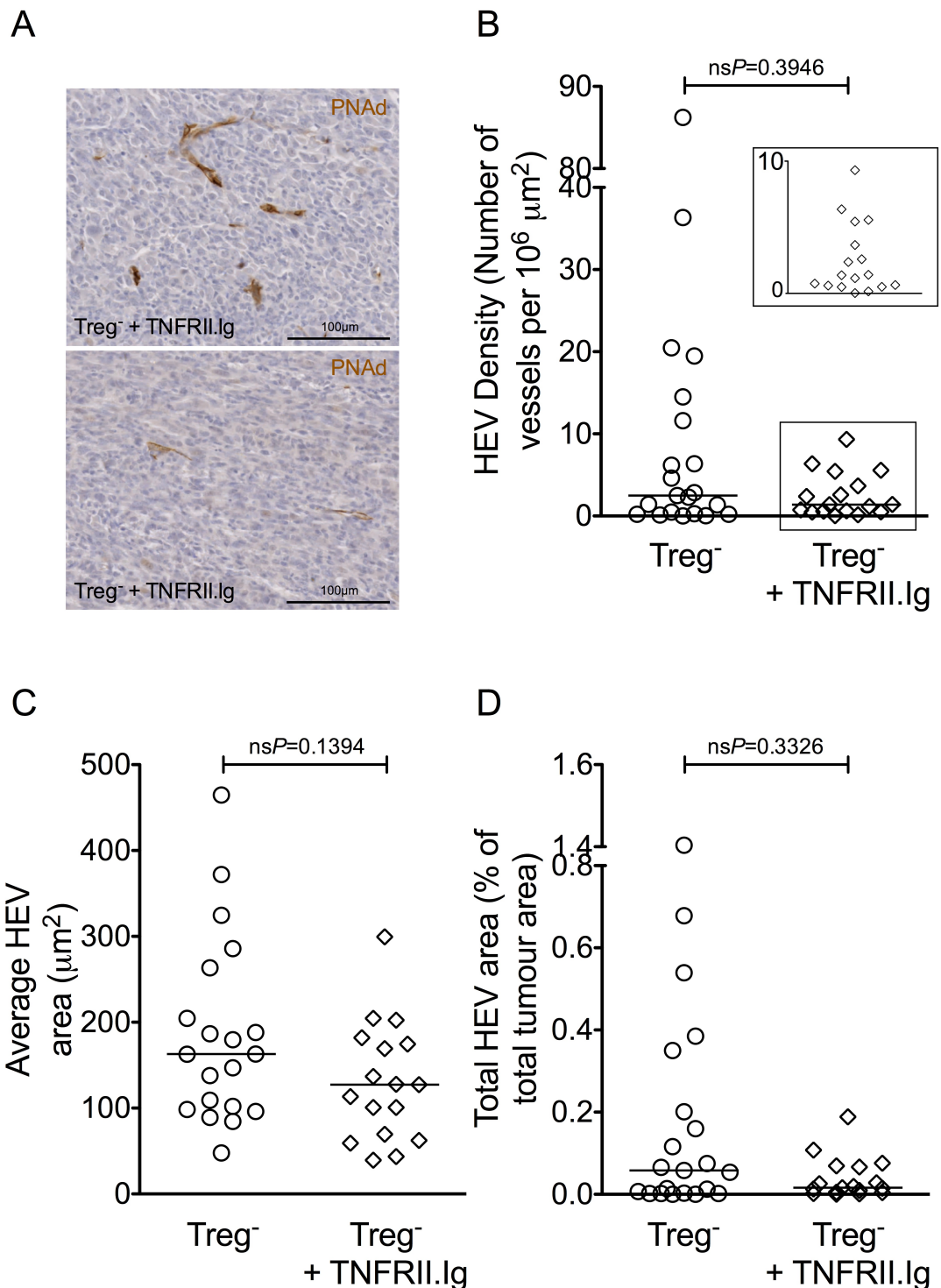
5.5 Results: TNFR antagonism using an anti-TNFα antibody reduces HEV density and total HEV area but increases average HEV area in tumours

Having identified a putative role for TNFR signalling in HEV neogenesis in tumours, I investigated the affect of another method of TNFR signalling blockade on intra-tumoural HEV neogenesis. I treated tumour-bearing Foxp3^DTR animals with DT together with an anti-TNFα monoclonal antibody (clone XT22-MP6), according to the protocol in Chapter 2.

As for both LTβR.Ig and TNFRII.Ig treatments, efficacy of anti-TNFα treatment was confirmed by immunohistochemical staining of spleen sections using CD45R, MAdCAM-1 and CD21/CD35 specific antibodies. As for TNFRII.Ig treatment, Treg depleted animals displayed a profound loss of FDCs and a partial loss of MAdCAM-1 staining following anti-TNFα treatment (Figure 5.15). As for previous treatments, the degree of disruption to splenic stromal cell compartments varied, mainly with regard to expression of MAdCAM-1 on sinus lining cells (Supplemental Figure 5.5). However, as for TNFRII.Ig treatment, marked loss of FDCs following anti-TNFα treatment was a consistent surrogate marker of TNFR signalling blockade.

As for LNs of TNFRII.Ig treated animals, LNs of anti-TNFα treated animals seemed to contain fewer HEV, and / or PNAd staining of HEV appeared weaker (Figure 5.16). Reminiscent of previous treatments, anti-TNFα resulted in less organised vessel distribution, and vessels appeared to have more open lumen than those in LNs of Treg depleted Foxp3^DTR animals (Figure 5.16). Again, although the degree of disruption varied between samples, these data indicated a degree of dedifferentiation of LN HEV, in a similar manner to that following either LTβR.Ig or TNFRII.Ig treatments.
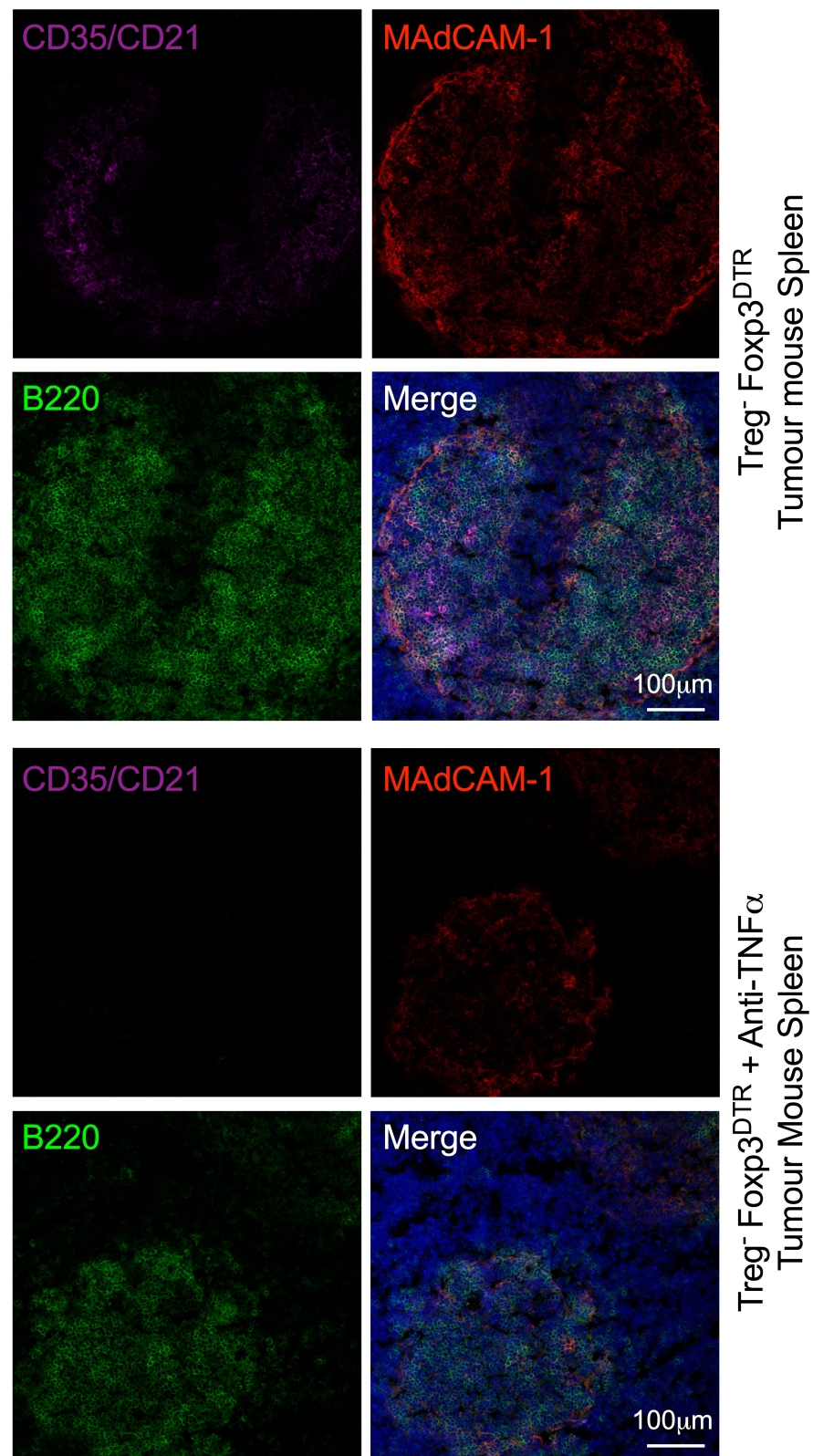
Figure 5.15 | Neutralisation of TNFα results in a profound loss of CD35/CD21^{+} Follicular Dendritic Cells and MAdCAM-1^{+} marginal zone sinus lining cells in Treg^{-} Spleen.

Representative confocal high power images showing loss of CD35/CD21^{+} Follicular Dendritic Cells (FDC) and MAdCAM-1^{+} staining of marginal sinus lining cells in spleen of Treg depleted Foxp3[DTR] animals following treatment with anti-TNFα. Images of a spleen from a Treg depleted animal (top) and from an anti-TNFα treated, Treg depleted animal (bottom) are shown. Sections were co-stained using a rat anti-CD35/CD21-APC antibody (purple), a rat anti-MAdCAM-1 antibody followed by goat anti-rat AlexaFluor-568 secondary antibody (red) and a biotinylated rat anti-CD45R antibody followed by streptavidin-FITC secondary antibody (green). Merged images include the nuclear stain DAPI (blue). Scale bars are shown.

[1] One-Way ANOVA with Tukey's multiple comparison test [2] Paired t test [3] Mann Whitney test [4] Spearman's correlation [5] Welch's unequal variance t test [6] Kruskal-Wallis One-Way ANOVA with Dunn's multiple comparisons test [7] Linear Regression
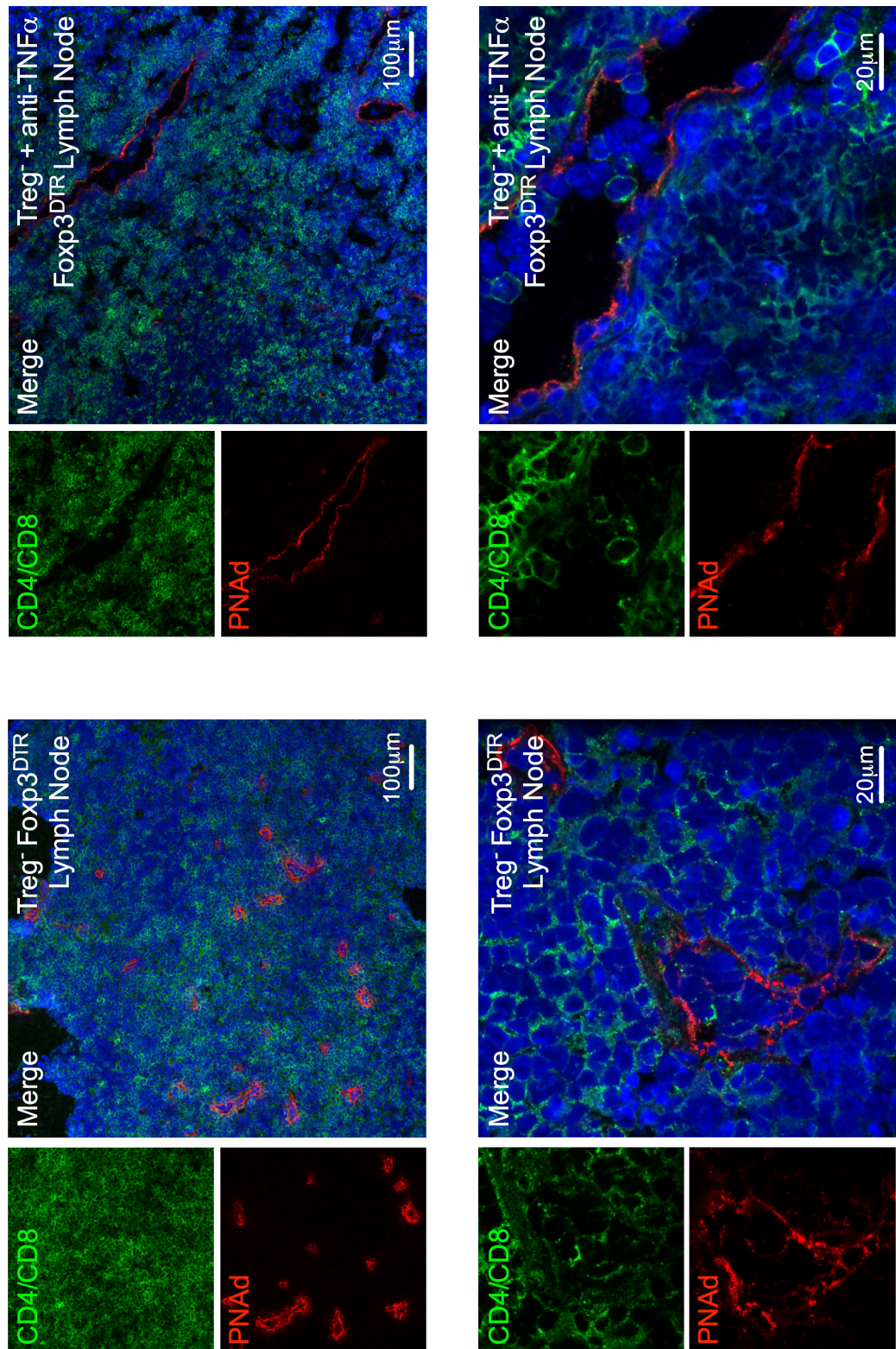
Figure 5.16 | Neutralisation of TNFα results in a profound disruption to Lymph Node High Endothelial Venule morphology.

Representative confocal microscope images showing disruption to PNAd[+] HEV of lymph nodes in Treg depleted Foxp3[DTR] animals following treatment with anti-TNFα. Low power (top) and high power (bottom) images of lymph node sections from a Treg depleted Foxp3[DTR] animal (left) and from an anti-TNFα treated, Treg depleted Foxp3[DTR] animal (right) are shown. Sections were immunofluorescently co-stained using a biotinylated rat anti-PNAd primary antibody (clone MECA-79), which was detected using a streptavidin-555 secondary antibody (red), and rat anti-CD4 and rat anti-CD8a primary antibodies, which were detected using an anti-rat donkey AlexFluor 488 secondary antibody (green). Merged images include the nuclear stain DAPI (blue). Scale bars are shown.

[1] One-Way ANOVA with Tukey's multiple comparison test [2] Paired *t* test [3] Mann Whitney test [4] Spearman's correlation [5] Welch's unequal variance *t* test [6] Kruskal-Wallis One-Way ANOVA with Dunn's multiple comparisons test [7] Linear Regression

PNAd^{+} CD31^{+} HEV were also present in tumours of Treg depleted anti-TNFα treated animals (Figure 5.17). However, similarly to TNFRII.Ig treated tumours, PNAd staining of HEV appeared weaker in some anti-TNFα treated tumours relative to Treg depleted control samples, and HEV endothelial cell morphology often appeared severely deflated (Figure 5.17 and 5.18 A). However, whilst anti-TNFα treatment resulted in an apparent reduction in intra-tumoural HEV number, HEV often appeared larger and with more open lumen relative to vessels of Treg depleted control tumours, reminiscent of HEV in LTβR.Ig treated tumours (Figure 5.18 A).

These visual observations were corroborated by quantitative measures of intra-tumoural HEV. There was a marked decrease in HEV density in Treg depleted tumours following anti-TNFα treatment, despite not reaching statistical significance (ns$P$=0.1037[3]; Figure 5.18 B). Furthermore, in line with the visual observation that many of the HEV appeared larger with more open lumen, average HEV area was significantly greater following anti-TNFα treatment (***P=0.0002[3]; Figure 5.18 C). There was a reduction in total HEV area in Treg depleted tumours following anti-TNFα treatment, again, despite not reaching statistical significance (ns$P$=0.6059[3]; Figure 5.18 D). This subtle change in total HEV area could reflect a combined affect of the overall reduction in number of vessels per unit area, but the significant increase in average vessel area.

As for TNFRII.Ig treated tumours, there was a weak positive correlation between HEV density and number of tumour infiltrating CD4^{+} T cells in anti-TNFα treated tumours (r = 0.7472, *P=0.0112[4]; Figure 5.19 A). The number of CD8^{+} T cells also appeared to correlate positively with HEV density, although statistical significance was not reached (r = 0.1458, ns$P$=0.6731[4]; Figure 5.19 B). However, as for TNFRII.Ig treated tumours, numbers of tumour infiltrating T cells did not correlate with tumour growth rate in anti-TNFα-treated animals, in contrast to the control Treg depleted group (r = -0.2000, ns$P$=0.5574 for CD4^{+} T cells[4]; r = -0.04545, ns$P$=0.9033 for CD8^{+} T cells[4]; Figure 5.19 C-D). In agreement with these data, neither HEV density nor total HEV area showed any correlation with tumour growth rate following anti-TNFα treatment (r =

[1] One-Way ANOVA with Tukey's multiple comparison test [2] Paired t test [3] Mann Whitney test [4] Spearman's correlation [5] Welch's unequal variance t test [6] Kruskal-Wallis One-Way ANOVA with Dunn's multiple comparisons test [7] Linear Regression

0.07745, ns$P$=0.8179 for HEV Density[4]; r = 0.1503, ns$P$=0.6538 for HEV Area[4]; Figure 5.19 E-F). These data suggest that intra-tumoural HEV that develop during anti-TNFα treatment are severely compromised in terms of their ability to facilitate lymphocytic infiltration, and indirectly a reduction in tumour growth rate.

Collectively, these data show that HEV neogenesis can occur in tumours of Treg depleted, anti-TNFα treated animals, but HEV density and total HEV area appear reduced, whilst average HEV area is increased. Furthermore, HEV functionality seems significantly diminished, as correlations between HEV density and infiltrating T cells are weak, and correlations between HEV density or total HEV area and tumour growth rate are completely lost after anti-TNFα treatment. These data corroborate the findings of Section 5.4, in suggesting that HEV neogenesis in tumours following Treg depletion appears to be at least partially reliant upon TNFR signalling.
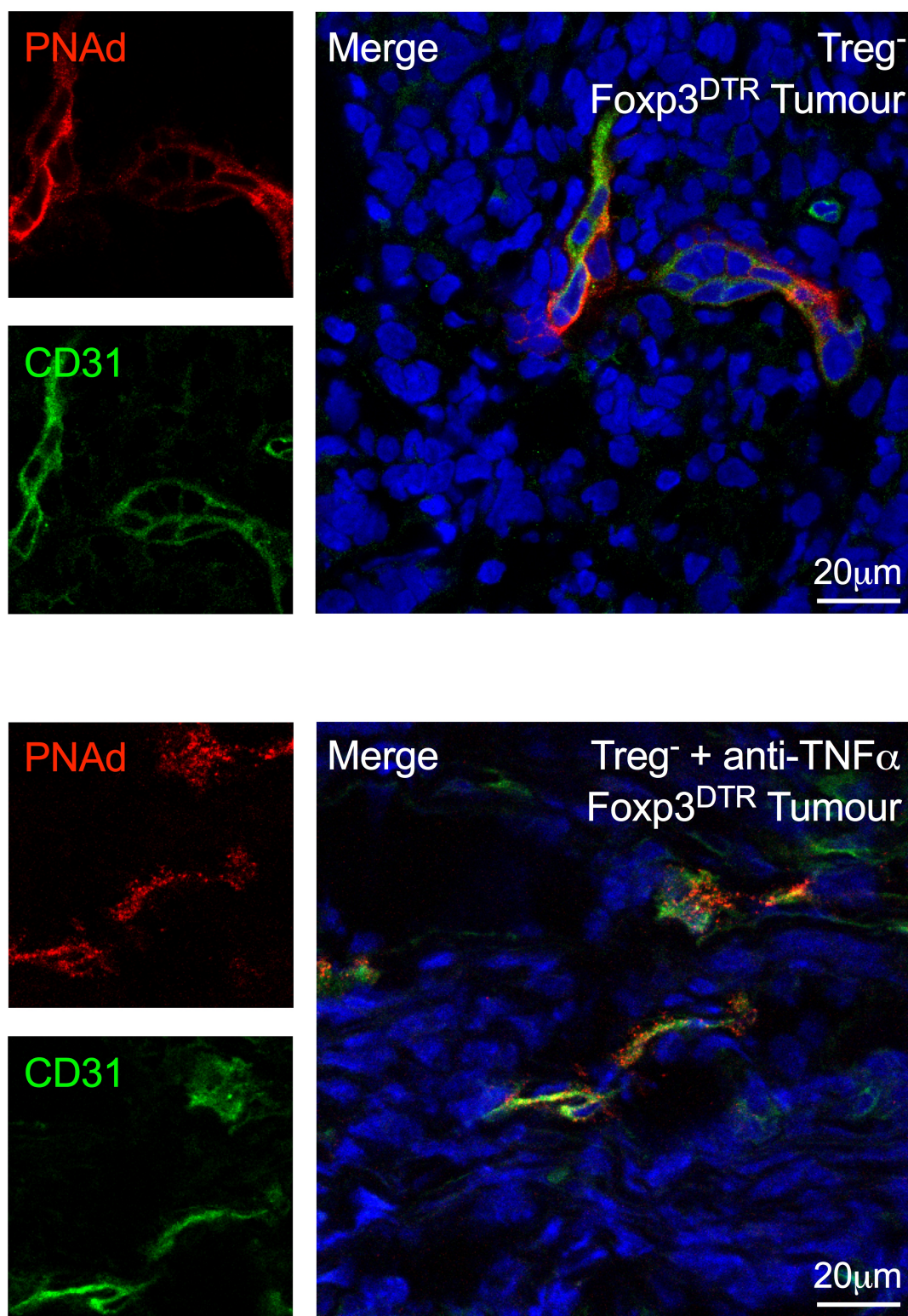
Figure 5.17 | High Endothelial Venules are found in tumours following TNFα neutralisation. Confocal images of High Endothelial Venules (HEV) within tumours of Treg depleted (top) and anti-TNFα treated, Treg depleted (bottom) Foxp3^{DTR} animals. Endothelial cells of HEV were detected by immunofluorescence staining using a biotinylated rat anti-PNAd primary antibody (clone MECA-79) and streptavidin Alexa Fluor® 555 secondary antibody (red). Tumour sections were dual-stained for PNAd and CD31 (rat anti-CD31-FITC; green). Merged images include the nuclear stain DAPI (blue). Scale bars are shown.

[1] One-Way ANOVA with Tukey's multiple comparison test [2] Paired *t* test [3] Mann Whitney test [4] Spearman's correlation [5] Welch's unequal variance *t* test [6] Kruskal-Wallis One-Way ANOVA with Dunn's multiple comparisons test [7] Linear Regression

Figure 5.18 | Measures of High Endothelial Venule density and total area are decreased when TNFα is neutralised.

Quantitative measures of High Endothelial Venules (HEV) in tumours of anti-TNFα treated, Treg depleted Foxp3^{DTR} animals. (A) Representative microscope images of HEV in paraffin embedded tumours. The anti-PNAd antibody (clone MECA-79) was detected using VIP chromogen (purple staining). Sections were counterstained using haematoxylin. Scale bars are shown. (B) HEV density was calculated per unit area of tumour (μm^2). The insert shows an enlarged version of the boxed area. (C) Average area of HEV vessels calculated in μm^2. (D) Total HEV area as a proportion of total tumour area, calculated as a percentage. Data are presented as individual datapoints plus median. Statistical significance was determined by Mann Whitney t tests. N = 11 anti-TNFα treated, Treg$^-$ tumours (9 in C); N = 21 Treg$^-$ tumours (20 in C).

[1] One-Way ANOVA with Tukey's multiple comparison test [2] Paired t test [3] Mann Whitney test [4] Spearman's correlation [5] Welch's unequal variance t test [6] Kruskal-Wallis One-Way ANOVA with Dunn's multiple comparisons test [7] Linear Regression
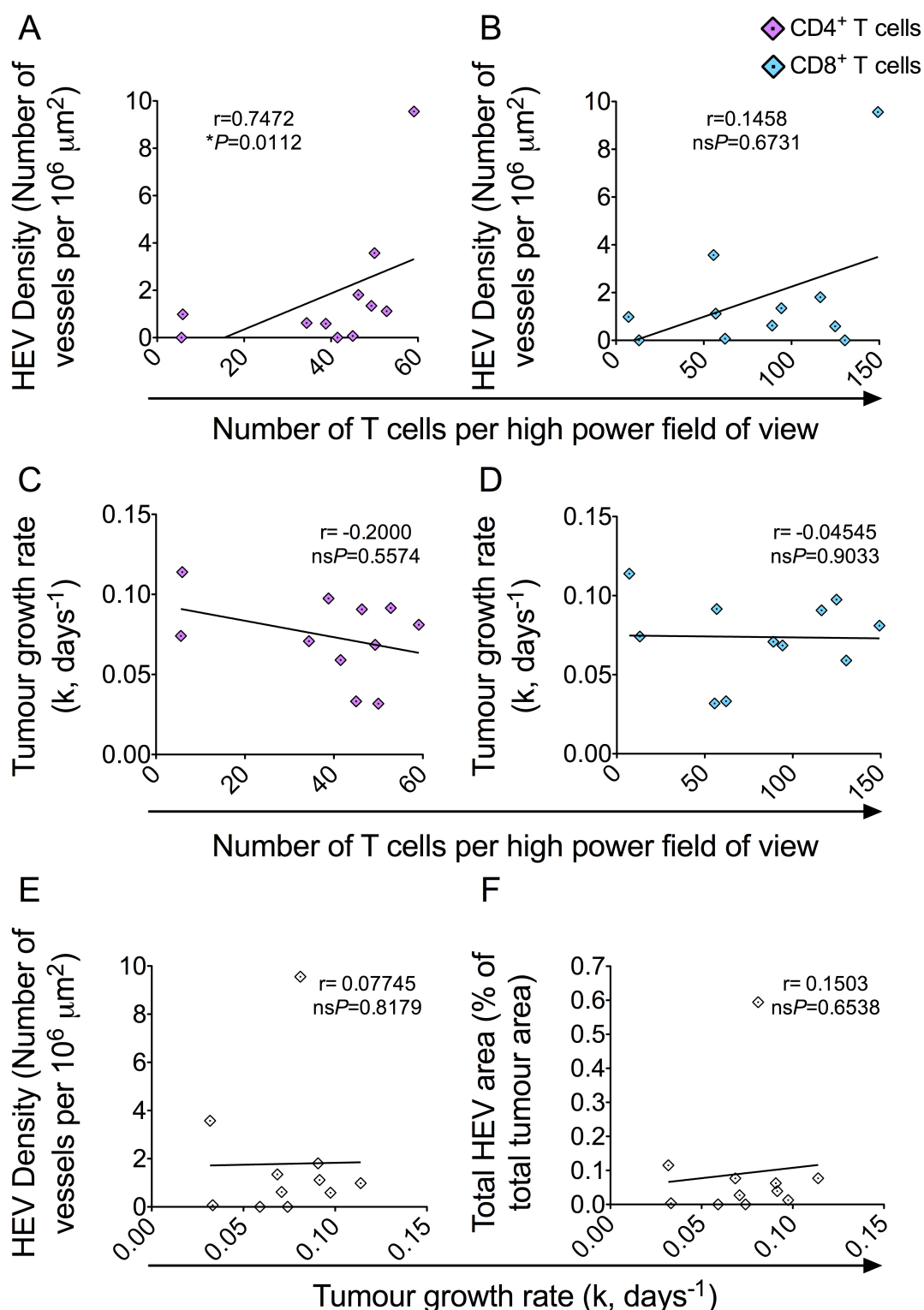
Figure 5.19 | Functionality of High Endothelial Venules in tumours in which TNFα is neutralised seems severely compromised.
Correlations between number of intra-tumoural CD4^{+} and CD8^{+} T cells, High Endothelial Venule (HEV) density and total HEV area, and tumour growth rates for anti-TNFα treated, Treg depleted Foxp3[DTR] animals. (A-B) Numbers of intra-tumoural CD4^{+} and CD8^{+} T cells plotted against tumour HEV density; CD4^{+} T cells (A; purple); CD8^{+} T cells (B; blue). (C-D) Numbers of intra-tumoural CD4^{+} and CD8^{+} T cells plotted against tumour growth rates (k, days[-1]); CD4^{+} T cells (C; purple); CD8^{+} T cells (D; blue). (E-F) HEV density (E) and total HEV area (as proportion of total tumour area; F) plotted against tumour growth rate (k, days[-1]). Statistical significance was determined by the non-parametric Spearman's correlation coefficient test, and the r statistic and P values are shown. N = 11.

[1] One-Way ANOVA with Tukey's multiple comparison test [2] Paired t test [3] Mann Whitney test [4] Spearman's correlation [5] Welch's unequal variance t test [6] Kruskal-Wallis One-Way ANOVA with Dunn's multiple comparisons test [7] Linear Regression

5.6 Results: The proportion of TNFα-producing T cells in the tumour correlates with HEV density

Having identified a role for CD4^{+} and CD8^{+} T cells (Chapter Four), and a putative role for TNFα (above) in HEV neogenesis, I investigated whether a link existed between T cells and TNFα. I first analysed serum from Treg replete and Treg depleted animals to establish whether circulating levels of soluble TNFα were altered following Treg loss. I found higher levels of soluble TNFα in serum of Treg depleted animals relative to Treg replete animals (ns$P$=0.0504[5]; Figure 5.20). Despite not reaching statistical significance, the heavy skewing of the 95% confidence intervals (CI) of the mean away from zero indicate the existence of a biological difference between Treg replete and Treg depleted groups in terms of levels of TNFα in the serum (upper 95% CI: 31.2932; lower 95% CI: -0.0366). These data showing an increase in this pro-inflammatory cytokine are not surprising, considering the systemic autoimmunity induced by Treg depletion in Foxp3[DTR] animals (Kim et al. 2007). Heightened levels of systemic TNFα allow for the speculation that this cytokine could be involved in HEV neogenesis in tumours following loss of Tregs.

I next analysed proportions of intra-tumoral T cells or T cells in lymphoid organs expressing intracellular TNFα by flow cytometry, and correlated this measure with HEV density in tumours. I found a highly significant, striking positive correlation between the proportion of intra-tumoural CD4^{+} or CD8^{+} T cells producing TNFα and HEV density in tumours (r = +0.7500, *P=0.0255 for both CD4^{+} and CD8^{+} T cells[4]; Figure 5.21). In contrast, there was no correlation between proportion of T cells expressing TNFα in lymphoid organs and HEV density in tumour. Instead, a negative correlation existed between the proportion of CD8^{+} T cells producing TNFα in LNs and HEV density in tumour (r = -0.6833, ns$P$=0.0503 for NDLN[4]; r = -0.3000, ns$P$=0.4366 for DLN[4]; Figure 5.21). These data directly index HEV density of tumours to TNFα production by T cells *in the tumour*, and strongly support the developing hypothesis that TNFα-producing T cells are key drivers of HEV neogenesis in tumours.

[1] One-Way ANOVA with Tukey's multiple comparison test [2] Paired *t* test [3] Mann Whitney test [4] Spearman's correlation [5] Welch's unequal variance *t* test [6] Kruskal-Wallis One-Way ANOVA with Dunn's multiple comparisons test [7] Linear Regression
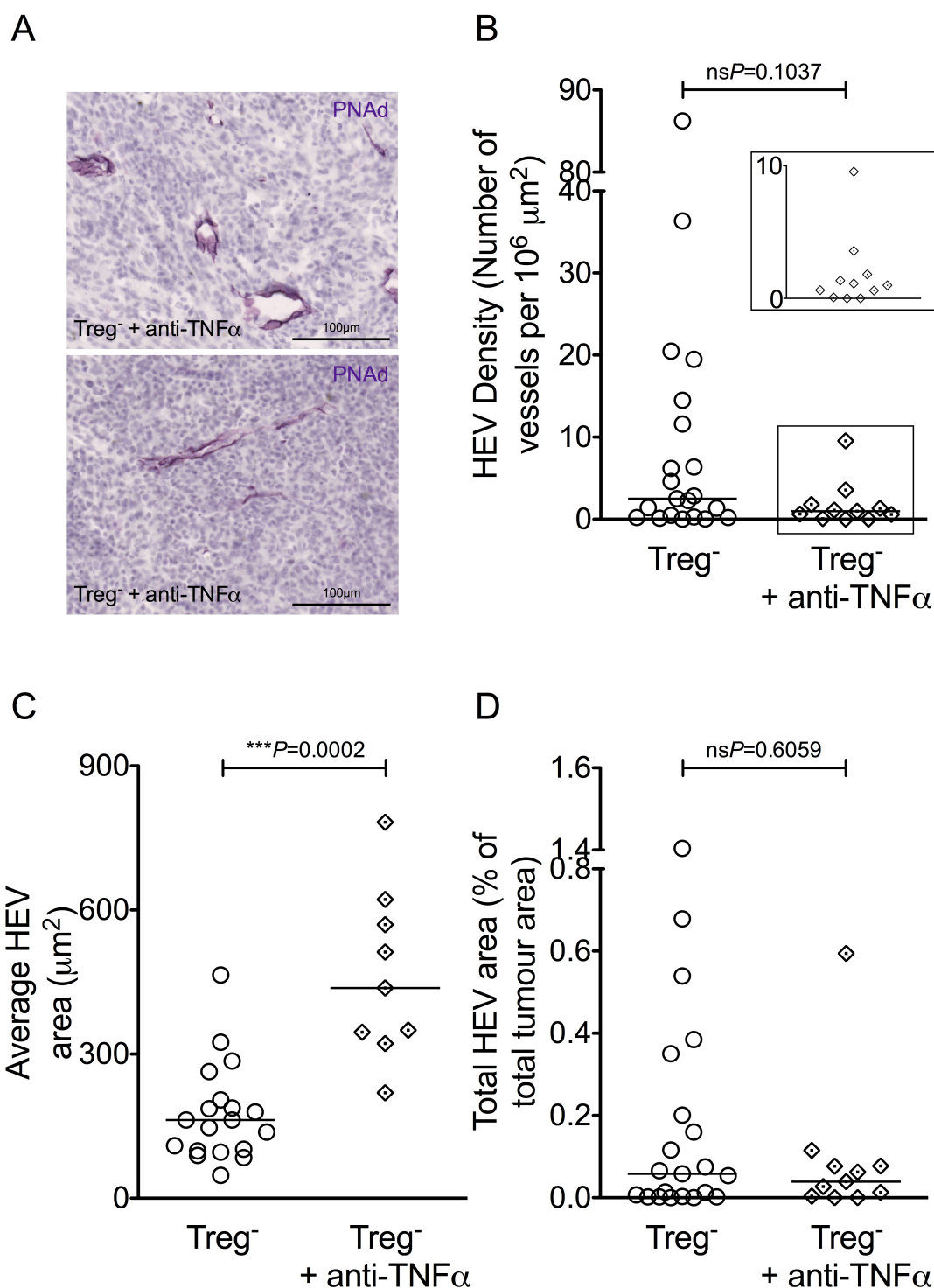
Figure 5.20 | Treg depleted animals have higher circulating levels of TNFα than Treg replete animals.

Quantity of soluble TNFα (pg/ml) detected by Enzyme Linked ImmunoSorbent Assay (ELISA) in serum of Treg replete (Treg[+]; closed circles) and Treg depleted (Treg[-]; open circles) Foxp3[DTR] animals. Data are represented as individual datapoints plus mean. Sensitivity limit of the ELISA is shown by the dotted line. Statistical significance was determined by Welch's unequal variance *t* test. N = 6.

Figure 5.21 | Density of intra-tumoural High Endothelial Venules correlates with the proportion of T cells producing TNFα in the tumour.
Correlations between High Endothelial Venule (HEV) density, calculated per unit area of tumour (μm^2), and proportion (%) of CD4^{+} (purple circles) or CD8^{+} (blue circles) T cells expressing intra-cellular TNFα, in Spleen, non-tumour draining lymph node (NDLN), tumour-draining lymph node (DLN), and Tumour. Statistical significance was determined by the non-parametric Spearman's correlation coefficient test, and the r statistic and *P* values are shown. N = 9.

[1] One-Way ANOVA with Tukey's multiple comparison test [2] Paired *t* test [3] Mann Whitney test [4] Spearman's correlation [5] Welch's unequal variance *t* test [6] Kruskal-Wallis One-Way ANOVA with Dunn's multiple comparisons test [7] Linear Regression

5.7 Results: Comparison of T cell infiltration, HEV neogenesis and tumour growth across all cytokine blockade treatments

As for the data described in Chapter Four, I wished to compare the impact of different treatments on T cell infiltration, HEV neogenesis and growth rates of tumours collectively (Figures 5.22-5.24). Again, I separated the control Treg depleted group into "HEV[lo]" and "HEV[hi]" categories. Despite no statistically significant differences, tumours of LTβR.Ig treated animals and anti-TNFα treated animals most closely resembled the HEV[hi] control group and tumours of TNFRII.Ig treated animals most closely resembled the HEV^{lo} control group, in terms of numbers of tumour infiltrating CD4^{+} T cells[6] (Figure 5.22 A). A similar pattern was observed for numbers of tumour infiltrating CD8^{+} T cells (Figure 5.22 B). Here, there was a statistically significant increase in the number of intra-tumoural CD8^{+} T cells in LTβR.Ig treated animals relative to both the HEV^{lo} control group and TNFRII.Ig treated animals[6]. As my hypothesis states that intra-tumoural HEV dictate T cell infiltration into tumours, these data indicate that TNFRII.Ig treatment in particular significantly impacts HEV neogenesis in tumours, as frequencies of CD4^{+} and CD8^{+} T cells in the tumours are profoundly reduced in this treatment group relative to HEV^{hi} Treg depleted tumours.

Both HEV density and total HEV area of tumours of LTβR.Ig treated animals were statistically significantly greater than tumours of the HEV[lo] control Treg depleted group, as was the case for HEV[hi] control Treg depleted tumours[6] (Figure 5.23A-B). Tumours of TNFRII.Ig, and anti-TNFα treated animals contained a statistically significantly lower density of HEV relative to HEV[hi] control Treg depleted tumours[6] (Figure 5.23A). Interestingly, in line with previous observations, only TNFRII.Ig treatment, and not anti-TNFα treatment, resulted in a statistically significant decrease in total HEV area, relative to HEV[hi] control Treg depleted tumours[6] (Figure 5.23B). These data underpin my conclusion that blockade of TNFR signalling, particularly via use of TNFRII.Ig, has a profound impact on the development of intra-tumoural HEV in this model.

There were no statistically significant differences in tumour growth rate between treatment groups[6] (Figure 5.24 A-B). However, there was a noticeable trend towards a decrease in tumour growth rate following LTβR.Ig treatment: this group more closely resembled the HEV[hi] control group than the HEV[lo] control group (Figure 5.24 B), and contained several samples with negative growth rates (i.e. tumours that were regressing). In contrast, the TNFRII.Ig treated group more closely resembled the HEV[lo] control group than the HEV[hi] control group (Figure 5.24 B), and contained several samples with high tumour growth rates (i.e. tumours that were progressing). These tumour growth data are in line with the hypothesis that blockade of TNFR signalling, particularly via use of the TNFRII.Ig protein, impedes HEV neogenesis in tumours, resulting in diminished intra-tumoural T cell infiltration and accelerated tumour growth. In contrast, blockade of LTβR signalling does not prevent HEV neogenesis in tumours, allowing these vessels to form and facilitate infiltration of high numbers of T cells, conferring a degree of tumour growth control.

As in Chapter Four, I used a linear model with fixed effects to determine whether tumour growth could be explained by HEV density and / or treatment regime. While treatment had a more profound effect on tumour growth (***P<0.001), HEV density, as an independent variable, significantly influenced tumour growth (*P=0.0105). Once again, these data emphasize that while treatment can influence tumour growth rate via a plethora of mechanisms, HEV density stands alone as an independent variable that significantly impacts upon the growth rate of tumorus.

[1] One-Way ANOVA with Tukey's multiple comparison test [2] Paired t test [3] Mann Whitney test [4] Spearman's correlation [5] Welch's unequal variance t test [6] Kruskal-Wallis One-Way ANOVA with Dunn's multiple comparisons test [7] Linear Regression
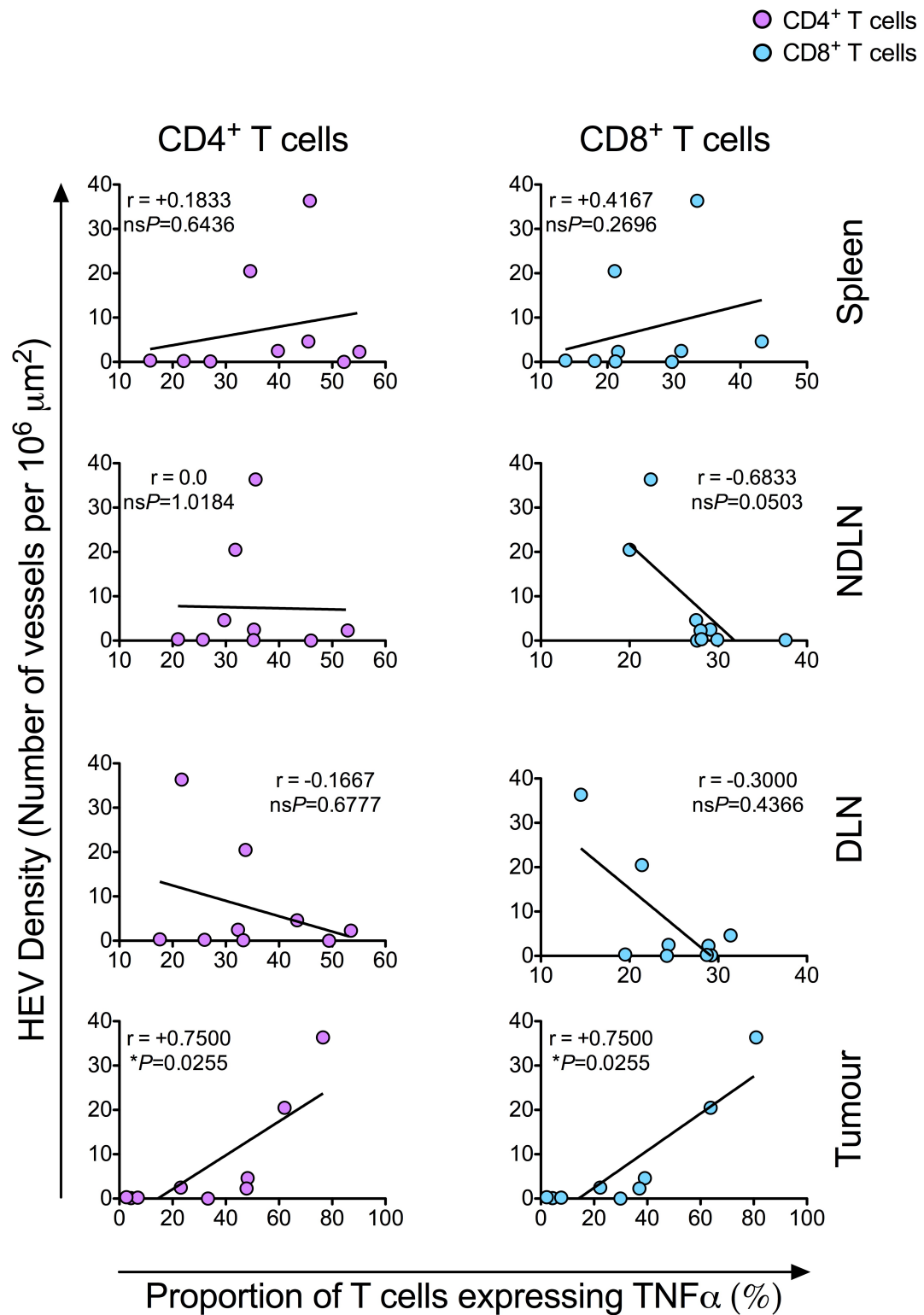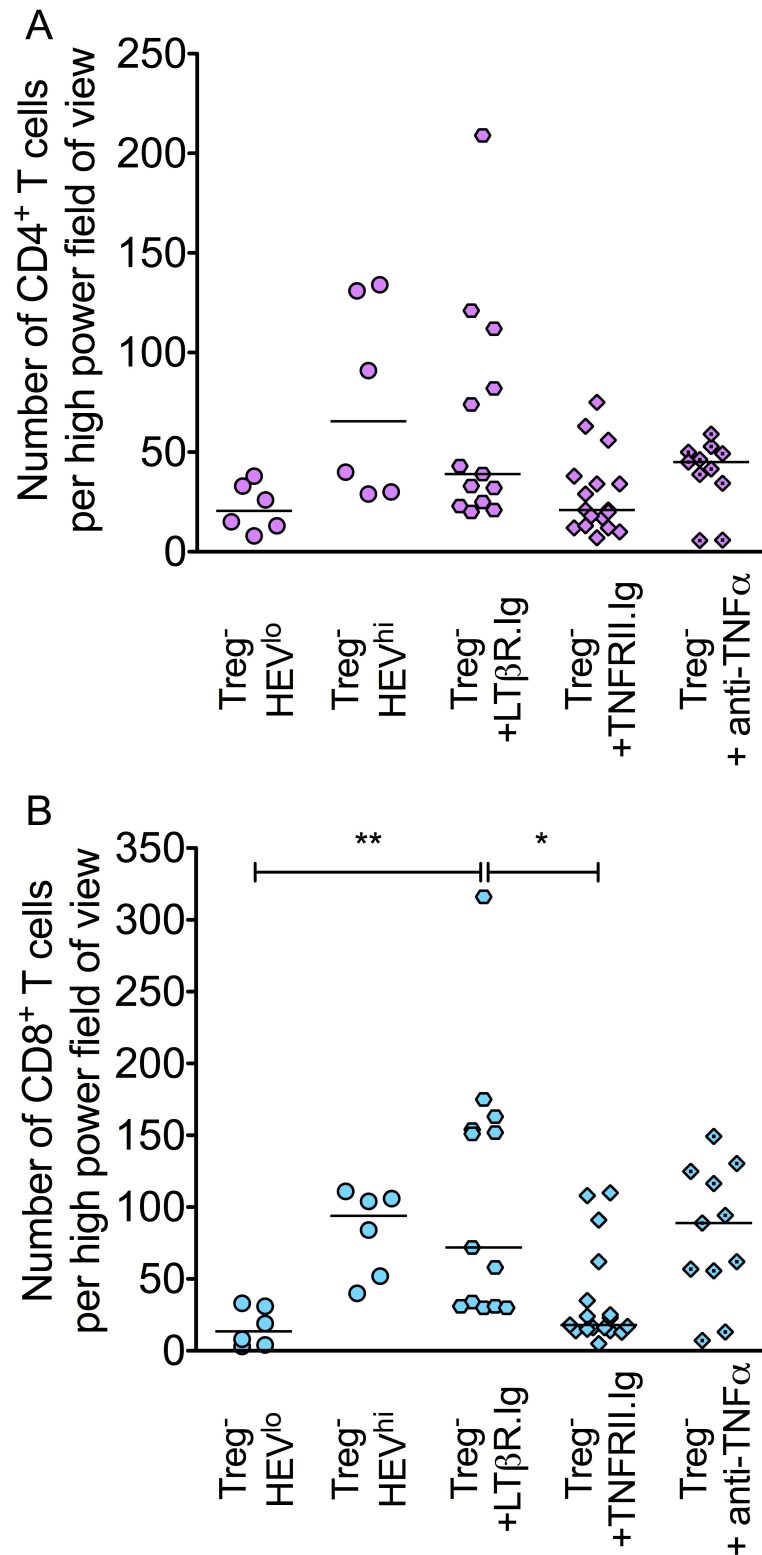
Figure 5.22 | Signalling blockade or cytokine neutralisation treatments did or did not alter absolute numbers of CD4$^+$ and / or CD8$^+$ T cells inside tumours.
Number of intra-tumoural CD4$^+$ (A) and CD8$^+$ (B) T cells for each of the following treatment groups: Treg depleted (Treg$^-$) HEV^{lo}, N = 6; Treg$^-$ HEV^{hi}, N = 6; LTβR.Ig treated, Treg$^-$, N = 13; TNFRII.Ig treated, Treg$^-$, N = 17; and anti-TNFα treated, Treg$^-$, N = 11. Data are presented as individual datapoints plus median. Statistical significance was determined by Kruskal-Wallis One-Way ANOVA and Dunn's multiple comparisons tests (* = $P\leq0.05$, ** = $P\leq0.01$, *** = $P\leq0.001$).

[1] One-Way ANOVA with Tukey's multiple comparison test [2] Paired *t* test [3] Mann Whitney test [4] Spearman's correlation [5] Welch's unequal variance *t* test [6] Kruskal-Wallis One-Way ANOVA with Dunn's multiple comparisons test [7] Linear Regression

Figure 5.23 | Signalling blockade or cytokine neutralisation treatments did or did not alter High Endothelial Venule density and / or total area inside tumours.

HEV density (A) and total HEV area (B) for each of the following treatment groups: Treg depleted (Treg⁻) HEV^{lo}, N = 6; Treg⁻ HEV^{hi}, N = 6; LTβR.Ig treated, Treg⁻, N = 13; TNFRII.Ig treated, Treg⁻, N = 17; and anti-TNFα treated, Treg⁻, N = 11. Data are presented as individual datapoints plus median. Statistical significance was determined by Kruskal-Wallis One-Way ANOVA and Dunn's multiple comparisons tests (* = $P \leq 0.05$, ** = $P \leq 0.01$, *** = $P \leq 0.001$).

Figure 5.24 | Signalling blockade or cytokine neutralisation treatments did or did not alter growth rate of tumours.

Tumour growth rate (k, days^{-1}) data for each of the following treatment groups: Treg depleted (Treg$^-$) HEV^{lo}, N = 6; Treg$^-$ HEV^{hi}, N = 6; LTβR.Ig treated, Treg$^-$, N = 13; TNFRII.Ig treated, Treg$^-$, N = 17; and anti-TNFα treated, Treg$^-$, N = 11. Data are presented as individual datapoints plus median. Statistical significance was determined by Kruskal-Wallis One-Way ANOVA and Dunn's multiple comparisons tests (* = $P \leq 0.05$, ** = $P \leq 0.01$, *** = $P \leq 0.001$).

[1] One-Way ANOVA with Tukey's multiple comparison test [2] Paired t test [3] Mann Whitney test [4] Spearman's correlation [5] Welch's unequal variance t test [6] Kruskal-Wallis One-Way ANOVA with Dunn's multiple comparisons test [7] Linear Regression

5.8 Discussion

LTβR signalling is essential for normal development of HEV-containing LN during ontogeny (Mebius 2003), and blockade of LTβR signalling results in loss of PNAd-expressing HEV in TLOs associated with chronic inflammation (Gatumu et al. 2009; Gräbner et al. 2009; Motallebzadeh et al. 2012; Rangel-Moreno et al. 2011). Furthermore, LTβR signalling has recently been implicated in the process of HEV neogenesis in tumours (Martinet et al. 2013; Martinet & Girard 2013). Here, I have shown that HEV neogenesis in MCA tumours following Treg depletion occurs entirely independently of LTβR signalling. The development of HEV in tumours of Treg depleted Foxp3^{DTR} animals could represent a significant deviation from these other systems, as Treg depletion results in extensive systemic immune activation and disruption to lymphoid organ architecture. Indeed the results of Chapter Four suggest the existence of a distinct mechanism of HEV development, due to the absolute reliance on T lymphocytes.

Instead, my data point to a role for an alternative signalling circuitry, TNFα-TNFR signalling, in driving HEV neogenesis in Treg depleted tumours (Figure 5.25). Blockade of TNFR signalling via two independent treatments (TNFRII.Ig fusion protein and anti-TNFα antibody) resulted in a decrease in the HEV density and total HEV area of Treg depleted tumours. Despite not reaching statistical significance, these measures were clearly altered following these treatments.

Some studies have shown that abluminal expression of PNAd in LN HEV can be independent of LTβR signalling. In LTβ$^{-/-}$ animals or those treated with antagonist LTβR.Ig fusion protein, LN HEV maintain residual abluminal expression of PNAd (Drayton et al. 2003; Browning et al. 2005; Liao & Ruddle 2006). Furthermore, despite the loss of the characteristic morphology of HEV endothelial cells upon ablation of LTβR in vascular endothelial cells, PNAd expression remains (Onder et al. 2013). The recently published study by Peske and colleagues confirmed that PNAd expression on HEV vessels in tumours of melanoma and lung carcinoma mouse models is also LTβR-independent (Peske et al. 2015). Instead, the authors demonstrate the reliance

[1] One-Way ANOVA with Tukey's multiple comparison test [2] Paired *t* test [3] Mann Whitney test [4] Spearman's correlation [5] Welch's unequal variance *t* test [6] Kruskal-Wallis One-Way ANOVA with Dunn's multiple comparisons test [7] Linear Regression
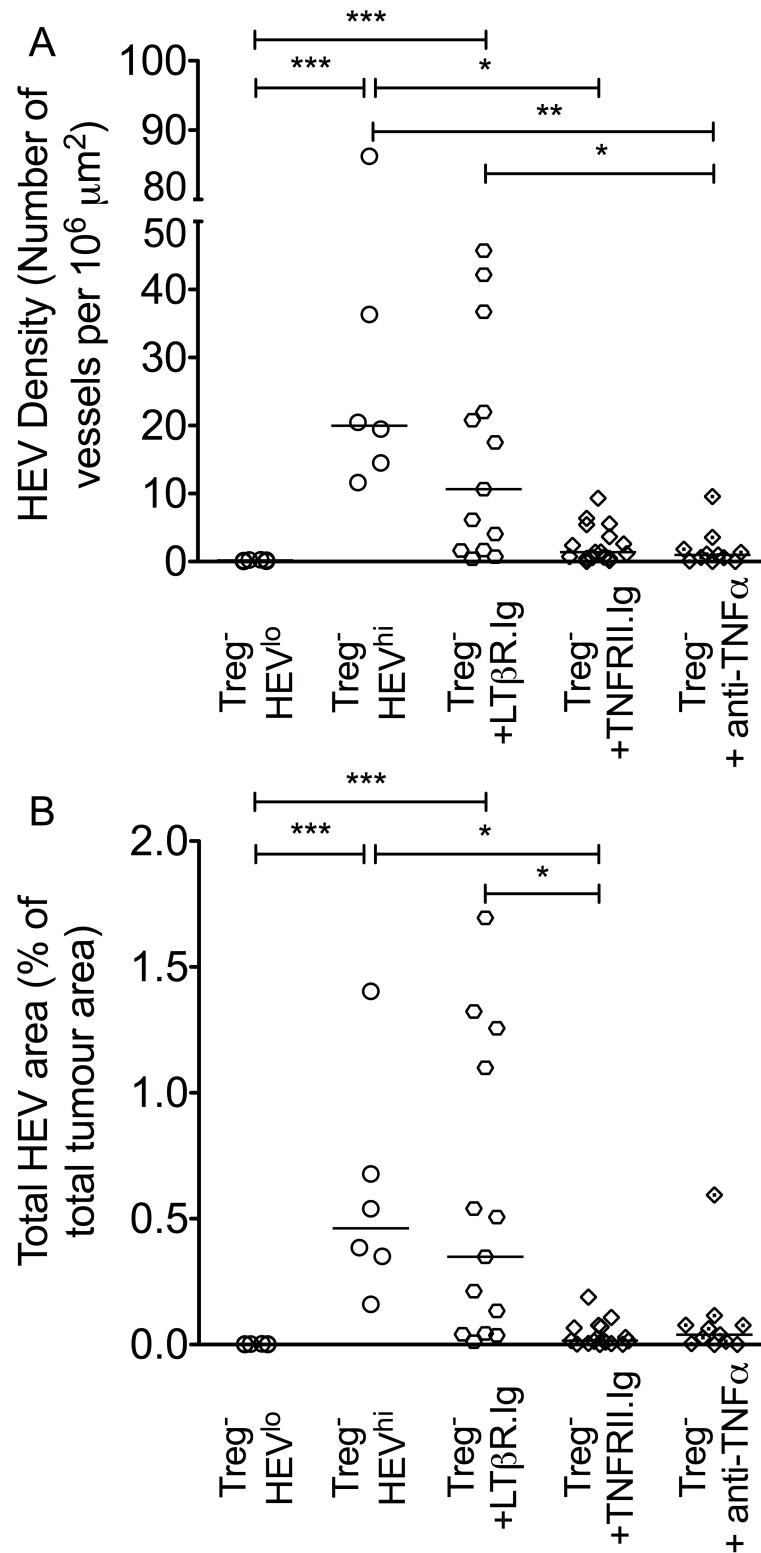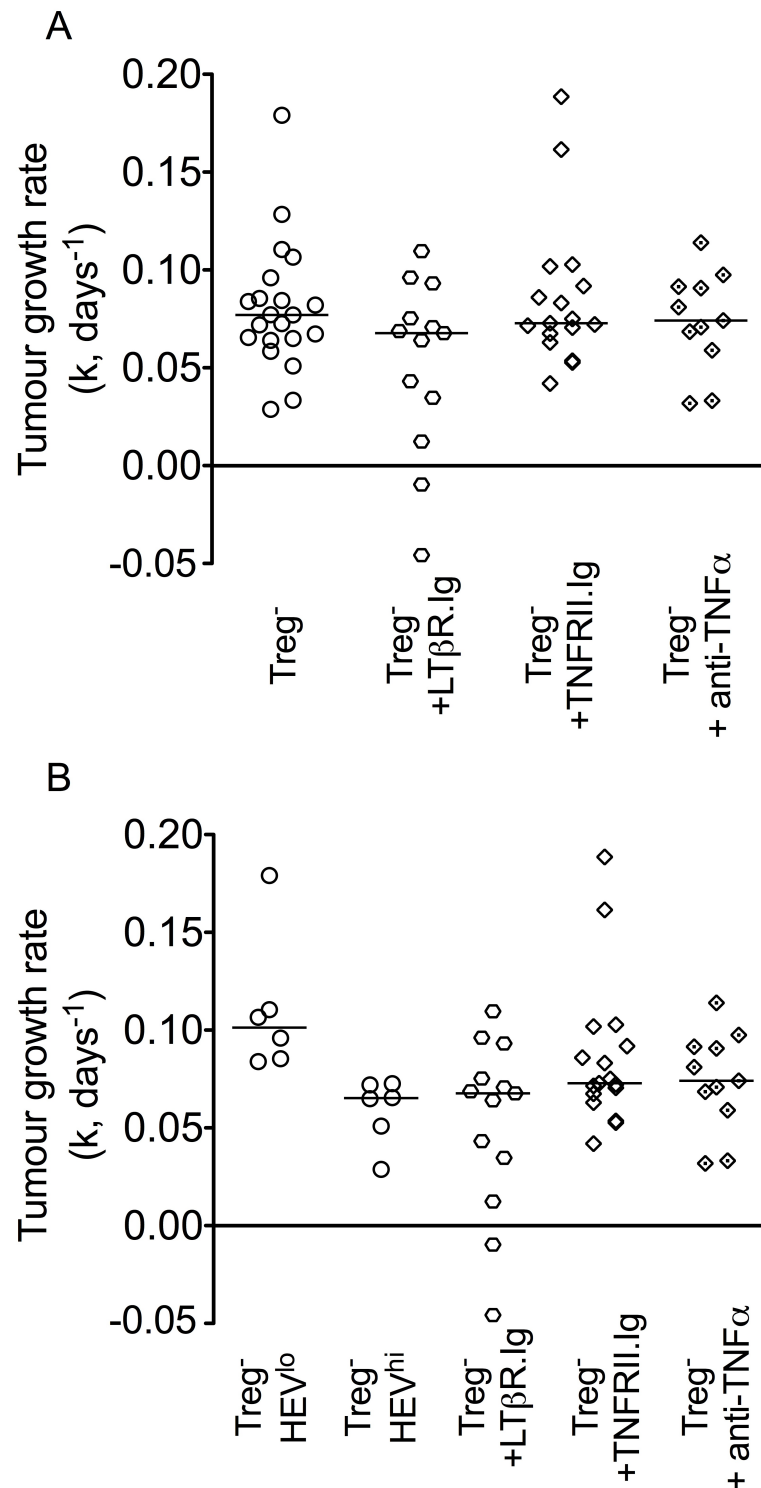
on CD8^{+} T lymphocytes and LTα$_3$-TNFR signalling for development of PNAd^{+} vasculature in the tumour.

Both HEV density and total HEV area datasets for the Treg depleted control group fit a bifurcated pattern of distribution, whereby one group of datapoints remain close to zero and another display significant departure from zero. In complete contrast, HEV density and total HEV area datasets for both TNFRII.Ig treated and anti-TNFα treated groups demonstrate significant departure from this bifurcated pattern of distribution, with all datapoints remaining close to zero or at least below a certain threshold. These data indicate that, while some PNAd[+] HEV can indeed be found in tumours following either TNFRII.Ig or anti-TNFα treatment, signalling blockade prevented all tumours from reaching a high density or total area observed for some tumours in Treg depleted controls.

The development of HEV in some tumours following TNFRII.Ig or anti-TNFα treatments (i.e. the partial rather than absolute phenotype) could represent either insufficient blockade of signalling using these agents, or the activity of an alternative signalling circuitry, which can compensate for the loss of TNFR signalling to a certain degree, but not entirely. The first explanation is unlikely: efficacy of treatment was confirmed in each case by analysis of MZ B cells and FDCs in the spleen, which displayed significant disruption in most animals, relative to Treg depleted controls. Therefore it seems likely that a distinct signalling circuitry can partially compensate for the loss of TNFR signalling in some cases. However, the data show that intact TNFR signalling is what is required to achieve HEV neogenesis to the extent observed in the Treg depleted control group of animals.

TNFα is a pleiotropic cytokine with multiple roles in both inflammation and immunity. The pro-inflammatory effects of TNFα are well known; TNFR2 acts as a co-stimulatory molecule for effector T cell activation, in a TCR-dependent manner. However, TNFα also contributes to anti-inflammatory and immunosuppressive processes of the immune system, via activation of Tregs through TNFR2, which is expressed at high levels by the vast majority of both mouse and human Tregs. The

effects of blocking signalling via the TNFRs on intra-tumoural T cell accumulation in the MCA tumours studied here could be reflective of a direct affect of signalling blockade on effector T cells, rather than an indirect affect of prohibiting HEV neogenesis (Chen & Oppenheim 2011).

TNFα is also a vasoactive agent (Chen et al. 2003). Targeting TNFα to tumour blood vessels can upregulate adhesion molecule expression on the surface of endothelial cells and subsequently enhance CD8$^+$ cytotoxic T cell infiltration (Calcinotto et al. 2012). Blockade of TNFR signalling in my studies could therefore result in fewer T cells within the tumour due to induction of 'endothelial cell anergy' of the general tumour vasculature in the absence of TNFR signalling, thereby precluding effector T cell infiltration.

TNFα was originally identified for its anti-tumour activity via its ability to induce rapid haemorrhagic necrosis of cancers (Carswell et al. 1975). In light of the potent systemic pro-inflammatory activity *in vivo*, use of a new technique termed isolated limb perfusion (ILP) has enabled successful treatment of cancers growing in the extremities by local, isolated administration of TNFα (Aggarwal et al. 2012). TNFα can induce major destruction of tumour-associated vasculature, and has also been implicated in the T cell driven anti-tumour immune response (Balkwill 2009). Therefore, in the study described here, blockade of TNFα could have a multitude of effects, influencing T cell effector function or activation, tumour vasculature, and / or HEV neogenesis, all of which could culminate in changes in tumour growth.

The blocking activities of TNFRII.Ig (Etanercept) and anti-TNFα (MP6-XT22) differ slightly: Etanercept binds soluble TNFα and soluble LTα$_3$ but forms only unstable associations with membrane-bound TNFα, from which it dissociates rapidly. In contrast, MP6-XT22 binds both soluble TNFα and membrane-bound TNFα, but not soluble LTα$_3$ (Ware 2005; Taylor 2010; Tracey et al. 2008; Scallon et al. 2002; Grattendick et al. 2008). In each case, therefore, there remains at least one active ligand that can still stimulate signalling via the TNFRs; membrane-bound TNFα, in the case of Etanercept, and soluble LTα$_3$, in the case of MP6-XT22. Therefore, this

[1] One-Way ANOVA with Tukey's multiple comparison test [2] Paired *t* test [3] Mann Whitney test [4] Spearman's correlation [5] Welch's unequal variance *t* test [6] Kruskal-Wallis One-Way ANOVA with Dunn's multiple comparisons test [7] Linear Regression

incomplete blockade of signalling via the TNFRs could account for incomplete abolishment of HEV neogenesis in tumours. Indeed, a recent study of HEV neogenesis in the mouse B16 melanoma model strongly implicated $LT\alpha_3$-TNFR signalling in this process (Peske et al. 2015). Future studies will be required to definitively determine the role this signalling circuitry may play in HEV neogenesis in our MCA model following Treg depletion. Blockade of $LT\alpha_3$ by use of a monoclonal antibody, and administration of both TNFRII.Ig and anti-TNFα reagents simultaneously are possibilities to confirm the signalling pathway responsible for HEV development.

Figure 5.25 | Updated hypothesis of HEV Neogenesis in Carcinogen-Induced Tumours after Treg Depletion.
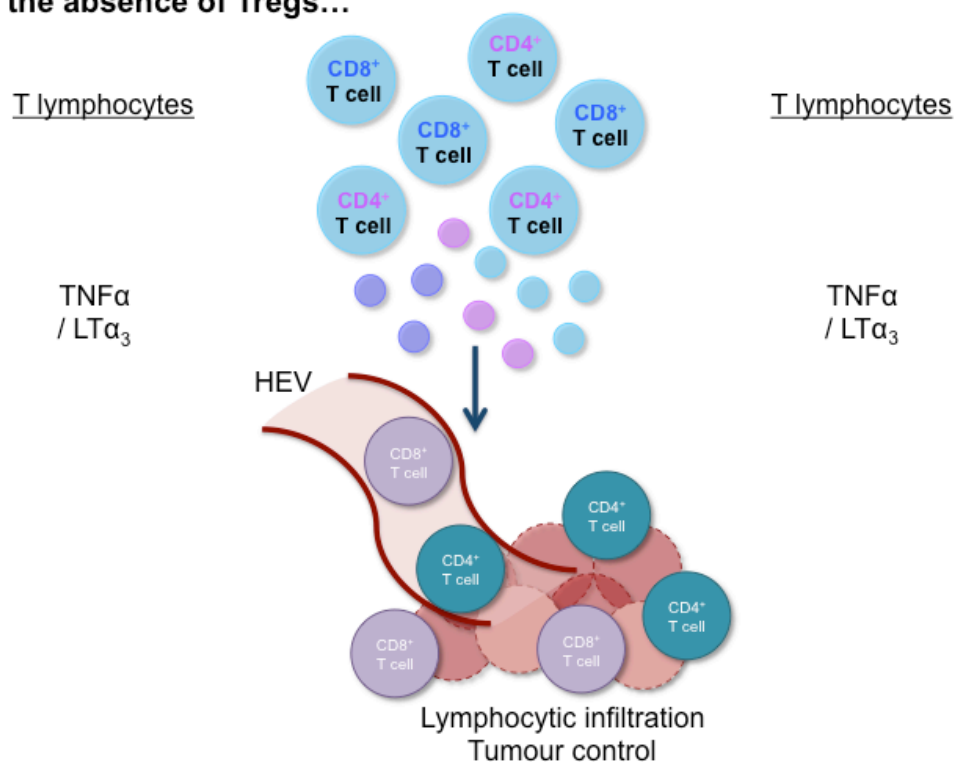
Chapter Six

6 Final Discussion

6.1 Enrichment of CD69$^+$ Foxp3$^+$ Regulatory T cells in Tumours

Foxp3$^+$ Tregs are enriched in mouse and human tumours (Curiel et al. 2004; Bates et al. 2006; Betts et al. 2007; Betts et al. 2006). Intra-tumoural Tregs facilitate establishment of an immunosuppressive microenvironment, impinging on anti-tumour immune responses (Nishikawa & Sakaguchi 2010; Gallimore & Godkin 2008). Modalities aimed at circumventing accumulation of Tregs in tumours could substantially improve efficacy of cancer immunotherapies in the future.

My data show that while a large proportion of intra-tumoural Tregs express the T_H1-lineage transcription factor T-bet, T-bet-expressing Tregs were dispensable for control of tumour development. Sequestration of IL-2 in the TME did not represent a mechanism by which Tregs exert dominance at this site. More importantly, a large proportion of intra-tumoural Tregs expressed CD69. Furthermore, CD69 expression conferred a superior suppressive capacity on Tregs relative to those not expressing this marker. CD69 could therefore represent a potential biomarker of super-suppressive Tregs in the TME, and also a therapeutic target. Indeed, treatment of CD69-expressing Tregs with an anti-CD69 monoclonal antibody downregulated CD69 expression and blocked suppressive function (Sancho et al. 2006; Cortés et al. 2014).

Selective targeting of CD69-expressing Tregs in the tumour would be challenging, as this marker is upregulated on recently activated T cells, ablation of which would hinder an anti-tumour immune response (González-Amaro et al. 2013). Therapeutic use of antagonistic mAbs to selectively decrease number or function of CD69-bearing Tregs within the tumour requires further understanding of the specific functional role of this receptor on different immune cells. Selectively targeting an antagonistic anti-CD69 antibody to intra-tumoural Tregs to simultaneously counteract their retention and accumulation, and modify their suppressive function, represents a potential clinical translation of the data presented in this thesis.

6.2 The function of Intra-Tumoural High Endothelial Venules

HEV in lymphoid organs facilitate infiltration of naïve and central memory lymphocytes (Girard et al. 2012). I hypothesised that ectopically formed HEV within MCA-induced tumours of Treg depleted Foxp3^{DTR} animals served to allow infiltration of high frequencies of T cells. My data establish that HEV density in tumours of Treg depleted animals significantly and positively correlates with numbers of infiltrating CD8$^+$ and CD4$^+$ T cells.

Despite this correlation, a causative link between HEV and intra-tumoural T cells has not yet been established in the model described here. In fact, considering the data presented here documenting a prominent role for T cells in the process of HEV neogenesis, it is entirely possible that the high numbers of T cells inside HEV-containing tumours is a cause rather than an effect of HEV neogenesis. To resolve this, *in vivo* T cell trafficking studies will be performed, during which the Mel-14 anti-L-selectin monoclonal antibody, which precludes interactions between L-selectin and PNAd ligands, will be used to block lymphocyte trafficking via HEV (Hou et al. 1995; Lepault et al. 1994; Ondondo et al. 2014[b]). By comparing numbers of TIL in relation to HEV density in animals treated with Mel-14 or control antibodies, we will determine whether interactions between L-selectin^{hi} lymphocytes and PNAd on HEV endothelium are responsible for increased numbers of lymphocytes in HEV containing tumours. Importantly, considering my data describing a key role for T lymphocytes in the process of HEV neogenesis in tumours, the Mel-14 antibody must be administered after HEV have been allowed to form in tumours, as systemic blockade of L-selectin-PNAd interactions would inhibit lymphocytic recirculation and priming in LNs, which may be essential for conferring their HEV inducing capabilities. Due to our limited knowledge surrounding kinetics of HEV development in MCA tumours, this experiment may be technically challenging. Alternatively, short-term competitive homing studies using labelled L-selectin knockout and wild-type T cells could be performed, allowing assessment of intra-tumoural HEV functionality by analysing relative frequencies of differently labelled T cells that home to tumours by flow cytometry.

It is plausible that, due to selective recruitment of L-selectin[hi] lymphocytes (i.e. central memory and naïve T lymphocytes), HEV may alter the specific composition of the tumour infiltrating T cell pool. Future experiments will seek to determine the degree of overlap of TCR repertoires of naïve (CD44^{lo} L-selectin^{hi}), central memory (CD44^{hi} L-selectin^{hi}) and effector memory (CD44^{hi} L-selectin^{lo}) T cells isolated from HEV positive or HEV null tumours of Treg depleted animals. These data will help to establish whether intra-tumoural HEV facilitate infiltration of central memory and / or naïve T lymphocytes, and will indicate whether antigen-specific priming of naïve lymphocytes occurs at the tumour site. These data will help to identify immunological requirements for supporting an effective anti-tumour response following induction of HEV in tumours.

Currently the evidence for intra-tumoural HEV supporting increased T cell infiltration into MCA-induced tumours in our model is largely anecdotal, based on their highly specialised function in lymphoid organs. It is important to consider that intra-tumoural HEV are not the only means by which effector T cells can access the TME: the activation status of the existing tumour vasculature is likely to play a significant role in this process. Indeed, tumours of anti-TNFα treated animals contained large numbers of T cells in the absence of ectopic HEV, suggesting other prominent mechanisms by which effector immune cells can access the tumour to mount an attack. However, the robust reduction in tumour growth rate conferred by HEV strongly supports the idea that these vessels mediate a distinctly potent anti-tumour activity.

6.3 The mechanism of High Endothelial Venule formation in tumours

My data presented here elucidate a primary role for CD8^{+}, and to a lesser extent, CD4^{+} T cells in HEV neogenesis in tumours following Treg depletion. The data also eliminate a role for signalling via the LTβ receptor, and instead strongly implicate signalling via the TNF receptor(s) by one of the cognate ligands, TNFα and / or $LT\alpha_3$, in HEV neogenesis. From these data, a new hypothesis has been formulated, stating that HEV neogenesis in tumours in the absence of Tregs is driven by T cell derived TNFα and / or $LT\alpha_3$ acting directly on tumour endothelium.

To test this hypothesis, a series of studies will be performed in the near future. Firstly, a series of *in vivo* studies will be initiated, during which an antagonistic anti-LTα antibody will be administered alongside DT treatment of tumour bearing Foxp3^{DTR} animals (Chiang et al. 2009). Analysis of tumours for HEV presence will ascertain the contribution of the LTα$_3$ ligand to HEV neogenesis, in a similar manner to the cytokine blockade studies described in this thesis. In another set of experiments, the ability of purified, activated T cells from Treg depleted animals to induce HEV in tumours of Treg replete hosts will be tested. In preliminary studies, splenic CD3$^+$ T cells were isolated from Treg depleted animals and injected into the base of the tumour-bearing leg of Treg replete hosts, a route known to drain to tumour via lymphatic vasculature (Ondondo et al. 2014[b]). HEV were absent from all 5 tumours analysed, indicating the inability of highly activated T cells to overcome the dominant immunosuppression enforced by Tregs within the tumour and induce HEV (unpublished observations). In future studies, T cells isolated by the same process will be administered by intravenous injection to tumour bearing Treg replete hosts, to investigate the possibility that activated T cells must directly access the tumour endothelium to induce a program of HEV differentiation in the presence of Tregs. If activated T cells are capable of inducing HEV in Treg replete tumours in this manner, these experiments will be repeated, and a cohort of animals will additionally be subjected to TNFα or LTα$_3$ blockade by administration of blocking antibodies previously mentioned. Analysis of HEV presence in tumours will indicate whether blockade of either signalling molecule precludes the ability of T cells to induce HEV. In longer-term studies, and for definitive proof that T cell derived TNFα and / or LTα$_3$ drives HEV neogenesis in tumours by direct contact with the endothelium, endothelial cell-TNFR conditional knockout animals, and T-TNF knockout and T-LTα knockout animals (in which the gene encoding TNFα or LTα is specifically ablated in T cells, respectively), will be crossed with Foxp3^{DTR} animals (Grivennikov et al. 2005). In the resultant offspring, tumours will be induced by MCA injection, Tregs will be depleted by DT administration and tumours subsequently

analysed for HEV. These studies should collectively demonstrate that T cell derived TNFα or LTα$_3$ is responsible for inducing a program of HEV neogenesis in tumours.

6.4 The role of Foxp3^{+} Regulatory T cells in Prohibition of High Endothelial Venule Formation

An intriguing observation in the model of MCA-induced carcinogenesis is that intra-tumoural HEV form in animals devoid of Tregs: PNAd[+] vessels are completely absent from tumours of Treg replete mice (Hindley et al. 2012). These data imply that Tregs inhibit neogenesis of HEV in tumours. Considering the profound paucity in numbers and / or functional impairment of Tregs in numerous autoimmune diseases (Lahl et al. 2007; Kim et al. 2007; Brunkow et al. 2001; Wildin et al. 2001; Bennett et al. 2001), it could be logical to hypothesise that Tregs could play a regulatory role in development of ectopic lymphoid tissue (Carragher et al. 2008).

Kocks and colleagues observed spontaneous development of highly organised iBALT containing PNAd[+] HEV, which normally only develop in response to inflammatory insult in wild-type animals, in lung tissue of germ-free CCR7^{-/-} mice (Kocks et al. 2007). CCR7 is essential for maintenance of Tregs and Treg-mediated peripheral immune regulation, evident from the dramatic decrease in Treg abundance and enhanced immunity in CCR7 deficient animals (Kocks et al. 2007; Schneider et al. 2007). Adoptive transfer of wild-type but not CCR7^{-/-} Tregs into CCR7-deficient hosts largely interrupted iBALT formation, and homing of Tregs to peripheral lymphoid organs was essential for their prevention of iBALT formation. Surprisingly, CCR7^{-/-} animals had elevated numbers of Treg in peripheral tissues including the lung, suggesting LNs are the site of Treg-mediated regulation of iBALT manifestation (Kocks et al. 2007). A separate study reported the development of spontaneous iBALT in IL-2-deficient animals, which are devoid of Tregs (Contractor et al. 1998). Such studies imply a crucial regulatory role for Tregs in prevention of ectopic lymphoid neogenesis (Carragher et al. 2008).

It will be important to define the mechanism by which Tregs impinge on intra-tumoural HEV neogenesis in the MCA model if therapies aimed at encouraging HEV development are to be designed. Although Tregs can impinge on endothelial cell activation (He et al. 2010; Matrougui et al. 2011), Tregs could play an indirect role in the control of HEV neogenesis in tumours, via limitation of accumulation and / or effector activities of immune cell populations (Peske et al. 2015). Tregs limit DC activation and function (Shevach 2009; Schmidt et al. 2012; Vignali 2012), and considering recent data implicating DCs in orchestration of HEV formation in tumours (Martinet et al. 2013; Martinet & Girard 2013), some may speculate that Tregs could prohibit HEV neogenesis via suppression of DC activation or production of HEV-inducing cytokines by DC (Gallimore et al. 2013). In light of my data establishing a crucial role for CD8^{+}, and possibly CD4^{+}, T lymphocytes in HEV neogenesis in MCA-induced fibrosarcomas, however, I hypothesise that Tregs prevent HEV development in MCA tumours by actively suppressing the activation of and / or cytokine production by another immune cell subset: T lymphocytes. Indeed, there are multiple mechanisms by which Tregs suppress activation and proliferation of T lymphocytes (Shevach 2009; Schmidt et al. 2012; Vignali 2012), which could be co-opted to prevent HEV induction by T cells within the tumour. *In vitro* Treg suppression assays will be implemented in future studies to assess whether a direct or indirect mechanism of suppression exists between Tregs and conventional T lymphocytes in terms of T cell production of an HEV-inducing cytokine, putatively identified here as TNFα and / or LTα_3.

It is intriguing that a recently published study documented intra-tumoural HEV in several mouse models of cancer in the presence of normal proportions of Foxp3^{+} Tregs (Peske et al. 2015). The authors suggest that the fact that depletion of Foxp3^{+} Tregs was not required for HEV neogenesis in B16 tumour models engineered to express ovalbumin (OVA) likely reflects, at least in part, a difference in antigenic strength between OVA and neoantigens formed in carcinogen-induced tumours. Therefore, in the presence of a strong antigenic stimulus such as OVA, sufficiently robust effector activity can be generated in the presence of Tregs to enable HEV neogenesis to occur.

It is important to consider the fact that both B16-OVA and MCA induced tumour models may represent highly polarised systems in terms of high antigenic stimulus, relative to human cancers. The extremely high number of mutations induced by MCA lead to the formation of thousands of neoantigens, which can be considered a significant caveat of this model (Matsushita et al. 2012). However, although the high antigenic load of MCA tumours may lead to more robust HEV neogenesis following Treg depletion than might occur in human tumours, recent data from our lab documenting intra-tumoural HEV in the 4T1 mammary carcinoma model following Treg depletion imply the wide applicability of our data from the MCA tumour model. Whether antigenic stimulus plays a role in HEV neogenesis in tumours or not, Treg depletion appears to confer a robust amplification of the process of HEV neogenesis: both HEV in B16-OVA tumours (which required tyramide amplification protocols for visualisation) and tumour growth control were far inferior to that observed in our MCA model following Treg depletion (Peske et al. 2015). This is particularly relevant considering the plethora of clinical trials currently investigating Treg depletion as a prominent component of cancer immunotherapy regimes.

To translate our findings to a clinically relevant setting, investigations into therapies specifically targeting Tregs will be conducted. Currently, there are no clinical agents available that specifically target Tregs. CTX is an FDA approved agent, and is already being used in clinical trials to specifically ablate the Treg compartment (Le & Jaffee 2012). Future studies will investigate the feasibility of CTX treatment in pre-clinical mouse models to spontaneously induce HEV neogenesis in MCA-induced tumours of wild-type animals.

Inhibitors of phosphoinositide-3-OH kinase (PI(3)K) have recently been shown to override Treg-mediated suppression of immune responses and result in profound anti-tumour immunity. Inactivation of the p110δ isoform of PI(3)K in Tregs was both necessary and sufficient to confer immunological tumour resistance (Ali et al. 2014). This method of breaking immune tolerance to unleash an effective anti-tumour immune

response shall be investigated for the ability to also induce intra-tumoural HEV in our model in future studies.

Depletion of Tregs in the Foxp3^{DTR} MCA model of carcinogenesis using diphtheria toxin results in effective anti-tumour immune responses at the expense of profound systemic autoimmunity and morbidity (Kim et al. 2007). It could be highly challenging to control autoimmune reactions in patients following systemic depletion of Tregs. This concern highlights a requirement to design therapies for targeted Treg depletion locally at the tumour site. In this regard, agents such as some anti-CTLA-4 antibodies could be used to leverage the ability of the TME to selectively deplete Tregs *in situ*, thereby sparing host-protective peripheral Tregs (Simpson et al. 2013).

It is clear, however, that ectopic lymphoid tissue and / or HEV form in a multitude of settings in the presence of normal frequencies of functional Foxp3$^+$ Treg. NOD mice develop ectopic lymphoid tissue in lung and pancreas (Xu et al. 2003; Faveeuw et al. 1994), despite harbouring normal frequencies of Tregs (Mellanby et al. 2007). Moreover, the vast majority of clinical reports of ectopic lymphoid tissue and / or isolated HEV in human malignancies develop in the context of the profound enrichment of Tregs observed in cancers (Goc et al. 2013; Neyt et al. 2012; Pitzalis et al. 2014; Ager & May 2015).

A word of caution is issued by studies documenting intra-tumoural HEV formation in the presence of Treg, where HEV-containing TLO can paradoxically lead to immune tolerance and disease progression. Indeed, forced expression of CCL21 in B16 melanomas led to rapid recruitment of immunosuppressive Tregs and MDSCs, resulting in promotion of tumour progression (Shields et al. 2010). A study conducted in our lab documented the formation of extra-tumoural lymphoid aggregates containing HEV, which were associated with disease progression in CRC patients (Bento et al. 2015). It is possible that accumulation of Tregs in tumour associated TLOs is at least partly responsible for disease progression, by exertion of local suppression of anti-tumour immune responses. Indeed, Gobert and colleagues found that high frequencies of Tregs within tumour associated lymphoid tissue of breast cancer patients correlated

with poor survival (Gobert et al. 2009). Furthermore, a recently published study elegantly demonstrated the ability of tumour associated tertiary lymphoid structures (TA-TLS) to foster Treg-mediated suppression of endogenous anti-tumour T cell responses against lung adenocarcinomas (Joshi et al. 2015). Such studies illustrate that function of tumour associated TLOs is likely dictated by the immunological cellular composition of the TLO as well as the state of disease progression, and warrants further detailed investigations into specific immune responses harboured by TLOs prior to the development of strategies aimed at enhancing their development in tumours.

6.5 The Requirement for a HEV-Permissive Tumour Microenvironment?

Interestingly, HEV develop in MCA-induced tumours of only a fraction (approximately 50%) of Treg depleted animals (Hindley et al. 2012) (and data shown here). These data establish that while depletion of Tregs is an essential prerequisite for HEV neogenesis in tumours of this model, it is certainly not sufficient for this process (Hindley et al. 2012; Gallimore et al. 2013). The mechanism that accounts for this inconsistent response to Treg depletion could be immunological in nature: T lymphocytes of some Treg depleted animals could become highly activated and synthesise HEV-inducing cytokine(s), while T cells of other animals devoid of Tregs could be unable to produce the necessary cytokine(s). However, profound systemic activation of T cells is observed in all animals following Treg depletion, suggesting a consistent immune response to Treg depletion among animals (Hindley et al. 2012). Alternatively, the immunogenicity of an individual tumour may dictate whether an immune response stimulated by depletion of Tregs efficiently clears tumour or not. Highly immunogenic tumours could activate tumour-specific T lymphocytes, which then drive HEV neogenesis in the tumour, while tumours that have escaped immune attention via immunoediting could fail to induce and / or support the necessary immune response for the HEV developmental program. Indeed, outgrowth of MCA-induced sarcomas can occur when the tumour lacks expression of strongly immunogenic

antigens, by a mechanism of T cell-dependent immunoselection (Matsushita et al. 2012).

Instead, HEV development could be dictated by tumour-intrinsic factors. A multitude of features of the TME could influence HEV neogenesis, collectively contributing to the creation of an environment either hostile or conducive to HEV formation. A key component of the TME that could be intricately linked to neogenesis of HEV is the tumour vasculature. Interestingly, data generated in our lab from microarray analyses of whole tumours revealed a noticeable decrease in expression of genes associated with a defined "angiogenesis" signature in HEV-containing tumours relative to HEV null tumours, including genes such as *vegfa*, encoding VEGF-A, and *cadherin 5*, encoding vascular endothelial (VE)-cadherin (unpublished data). In agreement with these microarray data, immunofluorescent staining revealed that HEV containing tumours contain fewer CD31$^+$ vessels which appeared more ordered, relative to HEV null tumours that typically contained vast numbers of CD31$^+$ vessels that appeared unruly and chaotic in nature (unpublished data). In line with these data, I hypothesise that tumours of high angiogenic activity contain vast numbers of vessels but that these are chaotic and therefore result in poor perfusion and oxygenation of tumours: low infiltration of effector T lymphocytes into such tumours would prohibit productive interactions leading to HEV neogenesis. On the other hand, tumours of low angiogenic activity contain fewer CD31$^+$ vessels, which are better ordered and more mature and / or normal and / or activated and hence facilitate better perfusion and enable infiltration of T lymphocytes that can then initiate a HEV neogenic program. Furthermore, as tumours of Treg replete animals display a mixed angiogenic genetic signature, angiogenic activity prior to Treg depletion could determine and therefore predict whether HEV will form. Should the angiogenic signature of tumours prove to be a key predictor in HEV neogenesis following Treg depletion, anti-angiogenic modalities aimed at normalising tumour vasculature will be explored for efficacy to promote HEV neogenesis in *all* Treg depleted tumours.

In contrast to the endothelial cell extrinsic mechanisms discussed above, the ability of a tumour to support development of HEV following Treg depletion could instead be dictated by endothelial cell intrinsic mechanisms. HEV neogenesis could be determined by the ability of the endothelium of tumour vasculature to respond to HEV-inducing cytokine(s) secreted in the TME: the "responsiveness" of the endothelium. Tumour endothelium is known to be incredibly refractory to activation induced by pro-inflammatory cytokines (Chen et al. 2003). Variation in the responsiveness of the endothelium of different tumours, potentially determined by differential expression of various immunosuppressive molecules, could dictate the ability of the vasculature to differentiate into functional HEV-type vessels upon stimulation.

Endothelial cells of HEV in LNs are of vascular origin, suggesting that HEV form from pre-existing, newly formed post capillary vasculature in the LN parenchyma under the influence of as yet unidentified factors. Whether tumour associated HEV derive by differentiation of pre-existing tumour vasculature that forms during tumour angiogenesis, or are initiated by circulating endothelial progenitors during an alternative process of tumour vasculogenesis is unknown (Ager & May 2015). Endothelium-dependent vessel growth can be insufficient to sustain rapid growth of tumours, in which case tumours employ a mechanism of vasculogenic mimicry (VM), during which vascular networks form from non-endothelial, tumour cell origins (Maniotis et al. 1999; Zhang et al. 2007). Multiple other origins of tumour vasculature have been reported, including an epithelial derived origin via processes of epithelial-mesenchymal transition (EMT), and even a CD11b^{+} myeloid origin (Yang et al. 2004; Qiao et al. 2015). Vessels in MCA-induced tumours co-expressed CD31 and PNAd, supporting the hypothesis that HEV develop by differentiation of the endothelium belonging to existing tumour vasculature. Furthermore, I noted that only portions of CD31^{+} vessels expressed PNAd, rather than continuous colocalisation of the two markers along the entirety of individual vessels, suggesting that different areas of vessels could be at various stages of differentiation, perhaps in response to local signals released by

proximal HEV-initiator cells. A detailed characterisation of tumour derived vascular cells will be carried out in future, to identify the precise origins of tumour HEV cells.

The ability of tumour-associated HEV to aid disease progression by selective recruitment of immunosuppressive Tregs and MDSCs (Shields et al. 2010), indicates that neogenesis of HEV is unlikely to be sufficient to underpin an effective anti-tumour immune response capable of eradicating tumour. Whether an effective immune response is established following recruitment of T cells to tumour via HEV will significantly depend on the inherent immunogenicity of that individual tumour/ malignant cells within the tumour, and exposure to highly immunogenic tumour antigens for incoming T lymphocytes. Furthermore, local signals within the tumour must support priming of tumour antigen-specific T cells. It is attractive to speculate that by lowering the threshold for both HEV neogenesis in tumours and activation of immune cells via depletion of Tregs, it could be possible to elicit a robust anti-tumour immune response against even low immunogenicity tumours (Gallimore et al. 2013). If confirmation of my data could be obtained from independent studies in different models, an inviting prospect for future cancer immunotherapy would be that of disabling Tregs, either via blockade of their intra-tumoural accumulation or modification of Treg suppressive function in tumours, perhaps via targeting of retention-promoting, suppressive function-enhancing molecules such as CD69, together with therapies that specifically encourage intra-tumoural HEV neogenesis. Furthermore, if my hypothesis regarding the impact of a highly angiogenic TME on HEV neogenesis proves correct, anti-angiogenic agents will additionally be required in a multipronged combinatorial therapy to simultaneously inhibit angiogenic activity.

6.6 Final Conclusion

In conclusion, I have shown here that intra-tumoural Tregs express high levels of CD69, a molecule potentially involved in retaining Tregs at the site of antigen and promoting enhanced suppressive function, thereby contributing to their dominance within the tumour mass. In the absence of Tregs, HEV neogenesis within tumours is

associated with profound infiltration of CD4$^+$ and CD8$^+$ T lymphocytes, which underpin an effective anti-tumour immune response to exert tumour growth control. The process of HEV neogenesis critically relies upon CD8$^+$ T cells, with a potential accessory role for CD4$^+$ T lymphocytes. While signalling via the LTβR is dispensable for HEV neogenesis in Treg depleted tumours, TNFR mediated signalling is required, with TNFα and / or LTα$_3$ cytokines representing prime candidates for activation of TNFR(s) in this process (Figure 6.1). Further understanding of the molecular mechansims underpinning HEV neogenesis in MCA-induced tumours could facilitate clinical translation of the findings described here in the near future.

Figure 6.1 Schematic representing the final conclusion of the work of this thesis.
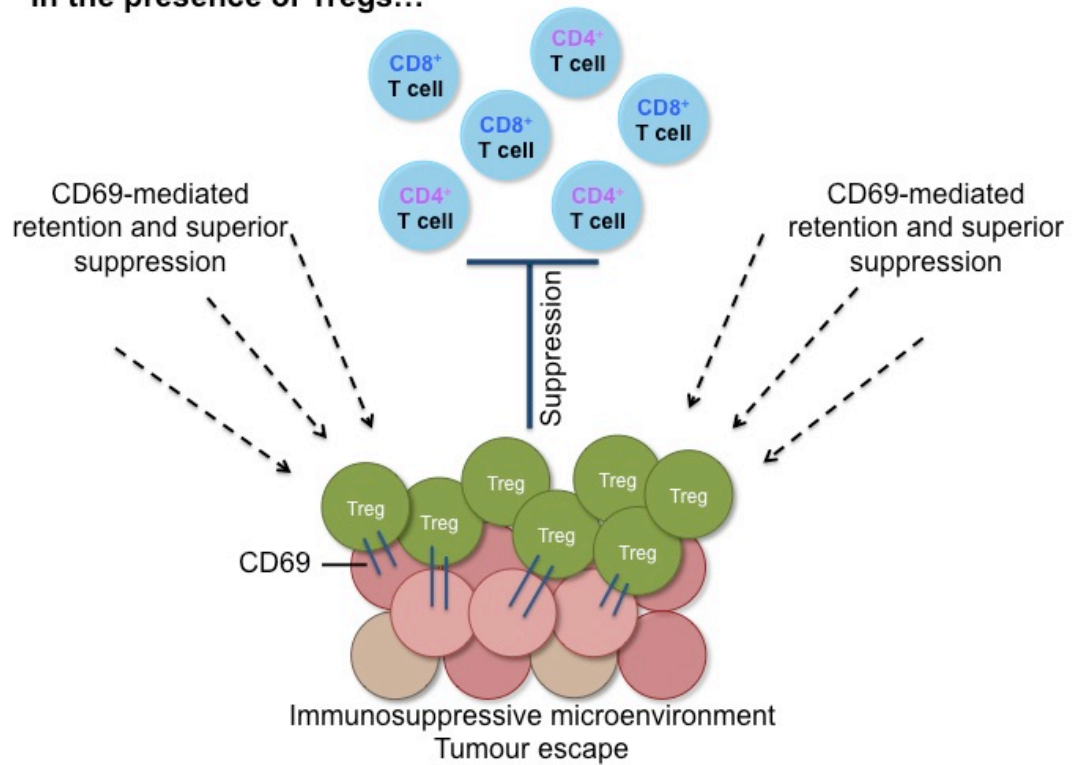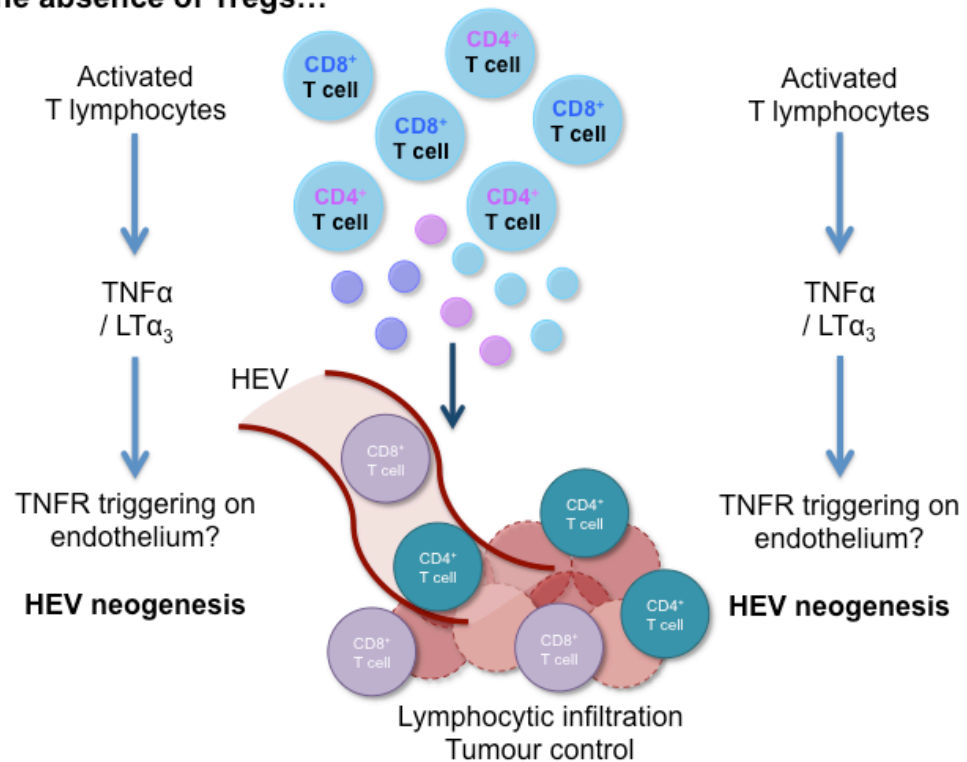
Appendix

Supplemental Figures
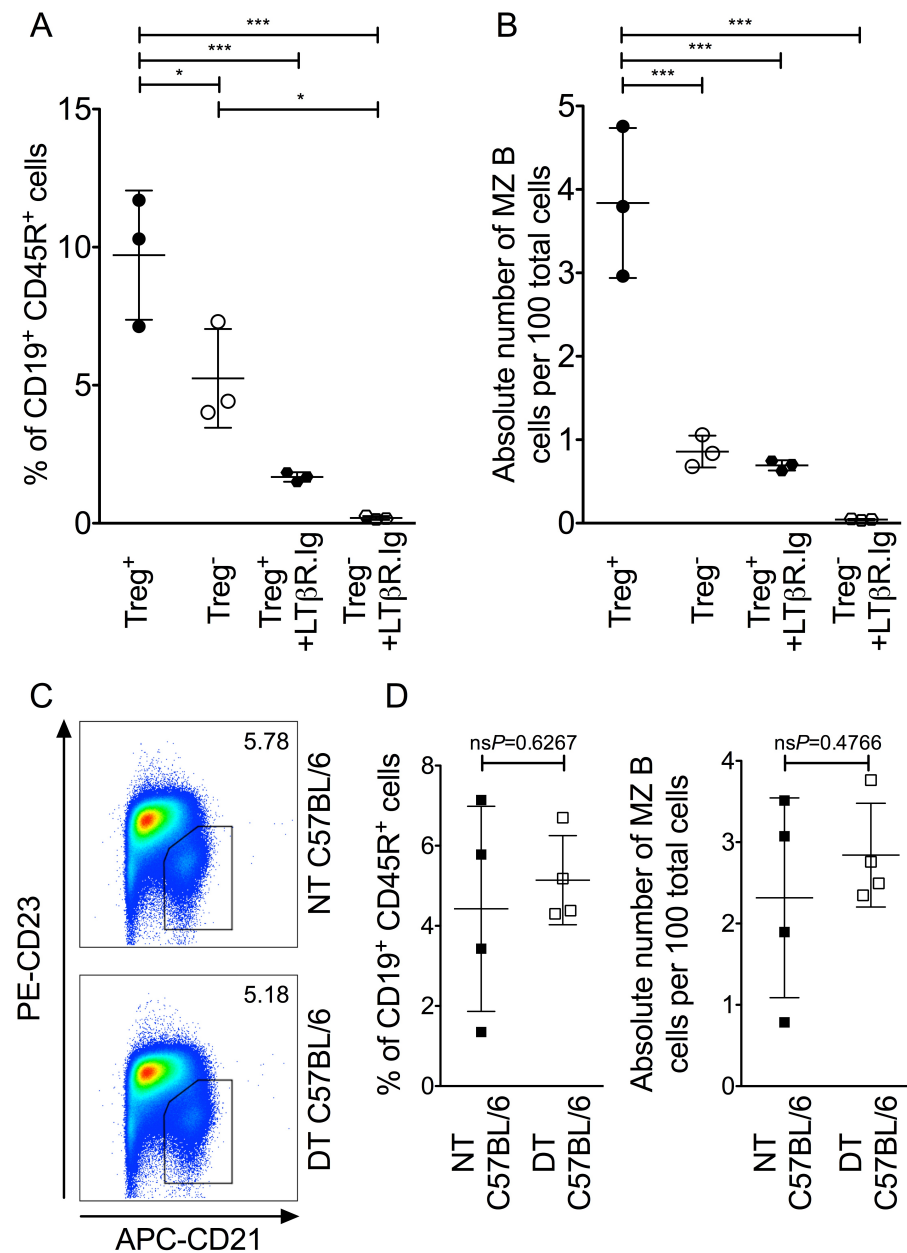
Supplementary Figure 5.1 | Efficacy of LTβR.Ig, as assessed by Marginal Zone (MZ) B cells in spleen of Treg replete or Treg depleted Foxp3[DTR] animals. (A-B) Proportion of CD19^{+} CD45R^{+} B cells that are CD21^{hi} CD23^{lo} MZ B cells (A) and absolute number of CD21^{hi} CD23^{lo} MZ B cells per 100 total live cells (B) in spleen of Treg replete and Treg replete LTβR.Ig treated Foxp3[DTR] animals (closed circles) or Treg depleted and Treg depleted LTβR.Ig treated Foxp3[DTR] animals (open circles), as shown in Figure 5.2. Data are presented as mean ± Standard Deviation (SD). Statistical significance was determined by One-way ANOVA with Tukey's multiple comparison tests to compare pairs of means (* = $P \leq 0.05$, ** = $P \leq 0.01$, *** = $P \leq 0.001$). N = 3 per group. **(C)** Representative flow cytometry plots showing proportion of CD19^{+} CD45R^{+} B cells that are CD21^{hi} CD23^{lo} MZ B cells, in the spleen of Non-treated C57BL/6 animals (top), and diphtheria toxin treated C57BL/6 animals (bottom). Cells are gated on CD19^{+}, CD45R^{+}. Numbers represent MZ B cells (gated), as a proportion of live CD19^{+} CD45R^{+} B cells. Expression of CD23 is shown on the y axis; expression of CD21 is shown on the x axis. **(D)** Proportion of CD19^{+} CD45R^{+} B cells that are CD21^{hi} CD23^{lo} MZ B cells (left hand graph) and absolute number of CD21^{hi} CD23^{lo} MZ B cells per 100 total live cells (right hand graph) in spleen of Non-treated C57BL/6 animals (closed squares), and diphtheria toxin treated C57BL/6 animals (open squares). Data are presented as individual datapoints with mean ± Standard Deviation (SD). Statistical significance was determined by unpaired *t* tests. N = 4 per group.
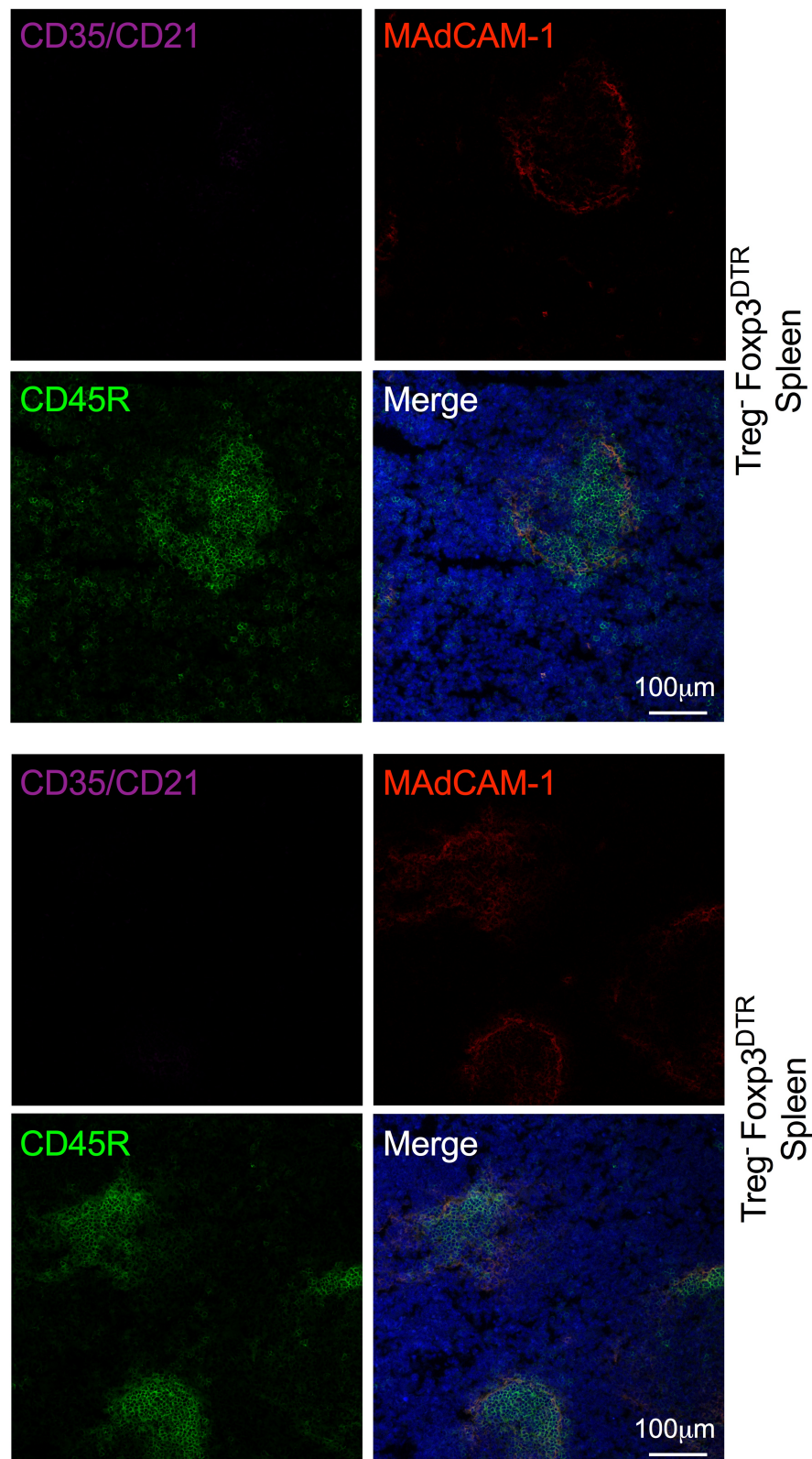
Supplementary Figure 5.2 | Two representative confocal high power microscope images showing CD35/CD21$^+$ Marginal Zone (MZ) B cells, MAdCAM-1$^+$ staining of marginal sinus lining cells and B cells in spleen of Treg depleted Foxp3^{DTR} animals. Sections were co-stained using the following antibodies: rat anti-CD35/CD21-APC (purple), rat anti-MAdCAM-1 detected using goat anti-rat IgG Alexa Fluor® 568 (red) and biotinylated rat anti-CD45R detected using Streptavidin-FITC (green). Merged images include the nuclear stain DAPI (blue). Scale bars are shown.
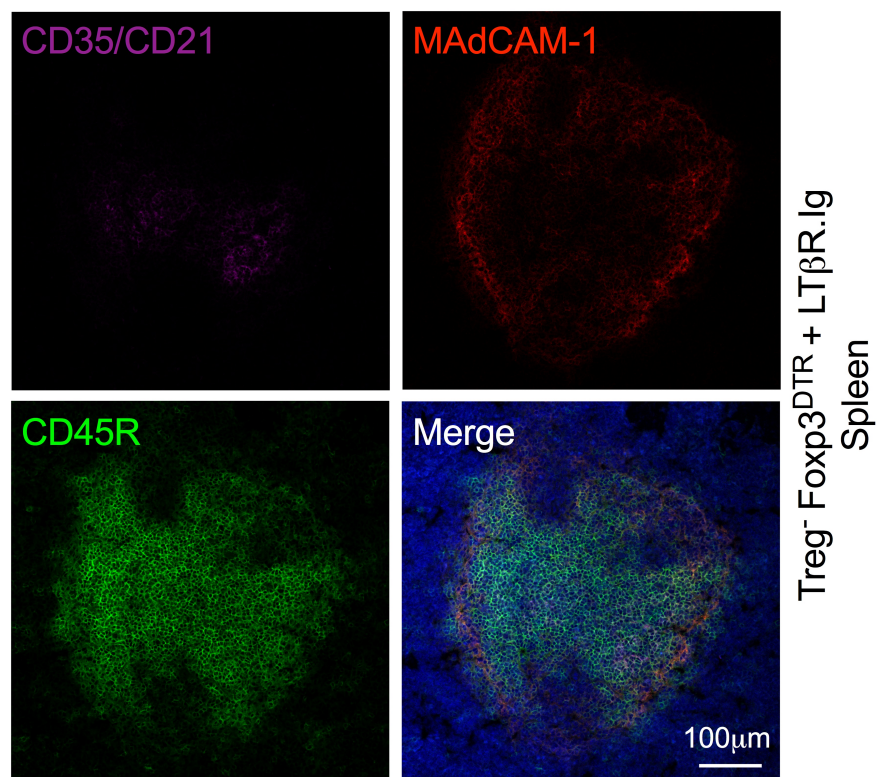
Supplementary Figure 5.3 | A representative confocal high power microscope image showing CD35/CD21^{+} Marginal Zone (MZ) B cells, MAdCAM-1^{+} staining of marginal sinus lining cells and B cells in spleen of a Treg depleted Foxp3[DTR] animal treated with LTβR.Ig. Sections were co-stained using the following antibodies: anti-CD35/CD21-APC (purple), anti-MAdCAM-1 detected using anti-rat IgG Alexa Fluor[®] 568 (red) and biotinylated-anti-CD45R detected using Streptavidin-FITC (green). Merged images include the nuclear stain DAPI (blue). Scale bars are shown.
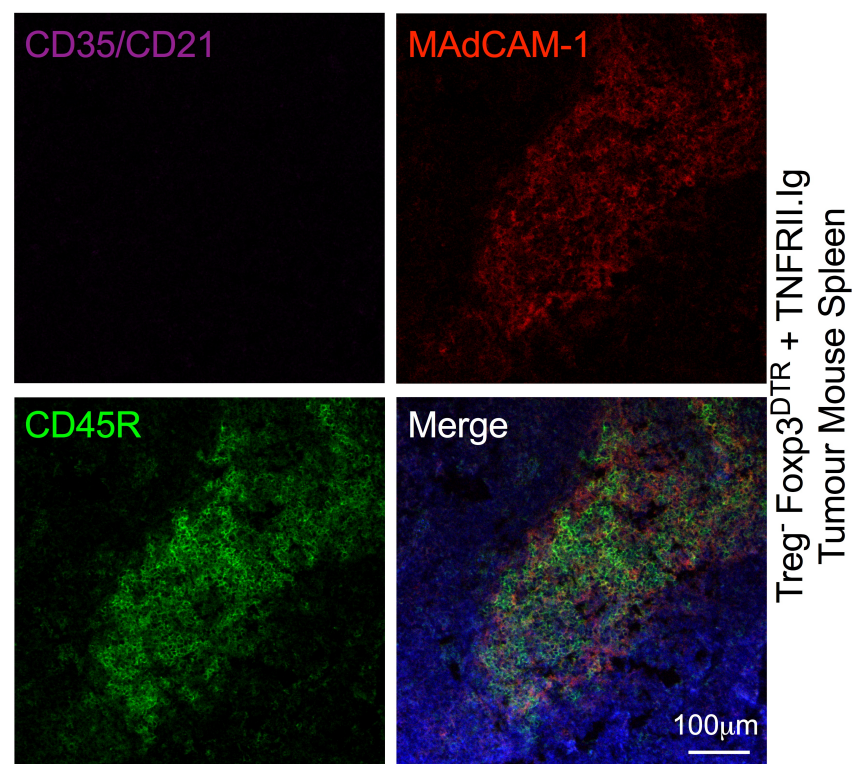
Supplementary Figure 5.4 | A representative confocal high power microscope image showing CD35/CD21^{+} Marginal Zone (MZ) B cells, MAdCAM-1^{+} staining of marginal sinus lining cells and B cells in spleen of a Treg depleted Foxp3[DTR] animal treated with TNFRII.Ig. Sections were co-stained using the following antibodies: anti-CD35/CD21-APC (purple), anti-MAdCAM-1 detected using anti-rat IgG Alexa Fluor® 568 (red) and biotinylated-anti-CD45R detected using Streptavidin-FITC (green). Merged images include the nuclear stain DAPI (blue). Scale bars are shown.
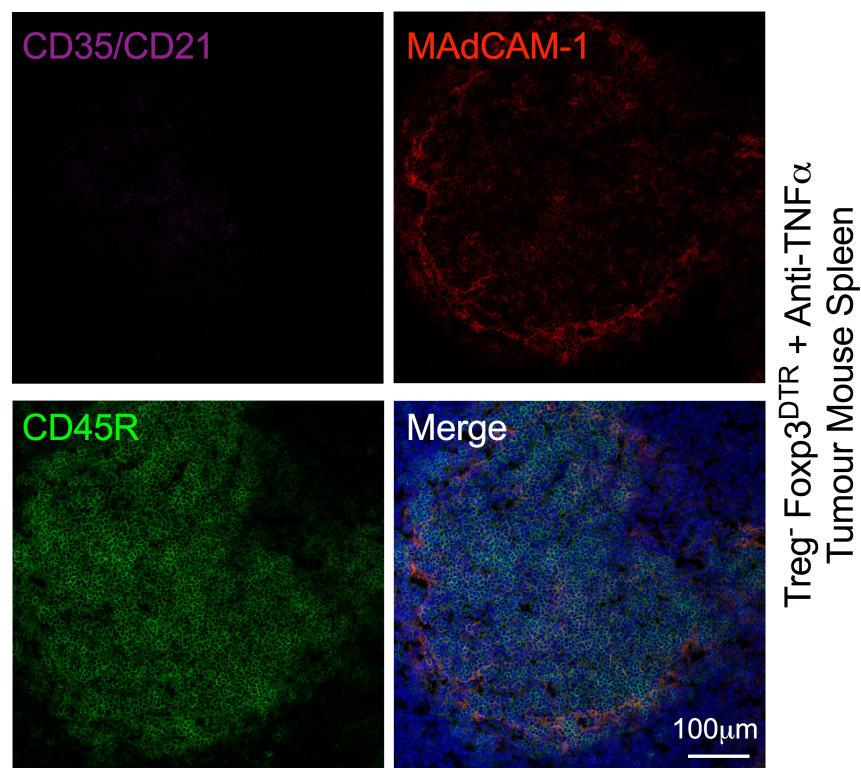
Supplementary Figure 5.5 | A representative confocal high power microscope image showing CD35/CD21^{+} Marginal Zone (MZ) B cells, MAdCAM-1^{+} staining of marginal sinus lining cells and B cells in spleen of a Treg depleted Foxp3[DTR] animal treated with Anti-TNFα (MP6-XT22). Sections were co-stained using the following antibodies: anti-CD35/CD21-APC (purple), anti-MAdCAM-1 detected using anti-rat IgG Alexa Fluor® 568 (red) and biotinylated-anti-CD45R detected using Streptavidin-FITC (green). Merged images include the nuclear stain DAPI (blue). Scale bars are shown.

Isotype and Fluorescence Minus One (FMO) controls
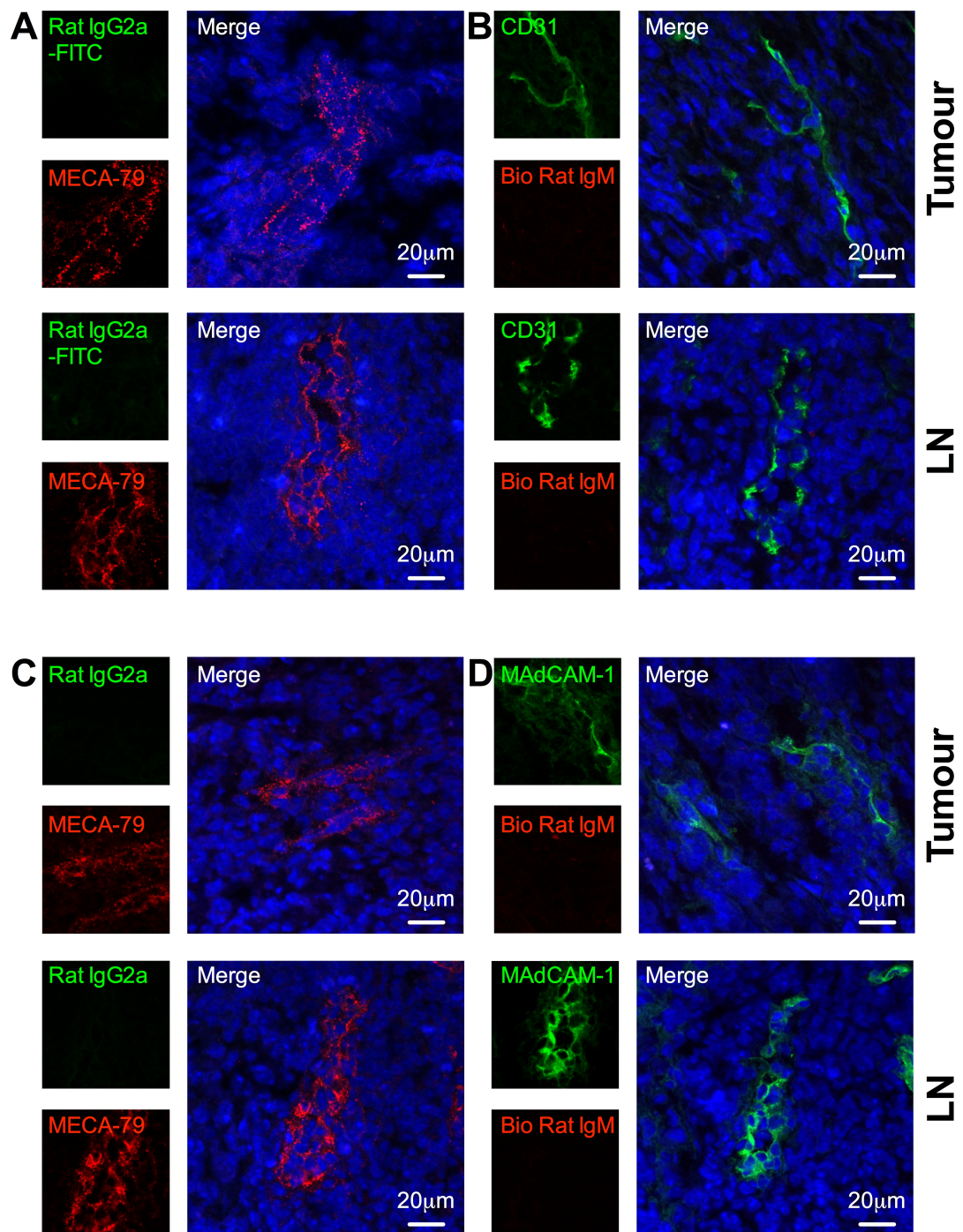
Figure A | High power confocal microscope images of immunofluorescently stained tumour and Lymph Node (LN) sections, showing the appropriate isotype controls for stains included in Results Sections. A) Sections were co-stained using a biotinylated rat anti-PNAd primary antibody (clone MECA-79) and streptavidin-555 secondary antibody (red) and Rat IgG2a-FITC isotype control antibody (green). B) Sections were co-stained using a biotinylated Rat IgM isotype control antibody and streptavidin-555 secondary antibody (red) and rat anti-CD31-FITC antibody (green). C) Sections were co-stained using a biotinylated rat anti-PNAd primary antibody (clone MECA-79) and streptavidin-555 secondary antibody (red) and Rat IgG2a isotype control antibody and donkey anti-rat AlexaFluor-488 secondary antibody (green). D) Sections were co-stained using a biotinylated Rat IgM isotype control antibody and streptavidin-555 secondary antibody (red) and rat anti-MAdCAM-1 antibody followed by donkey anti-rat AlexaFluor-488 secondary antibody (green). In each case, tumour sections are shown on top and LN sections are shown on bottom. Scale bars are shown.
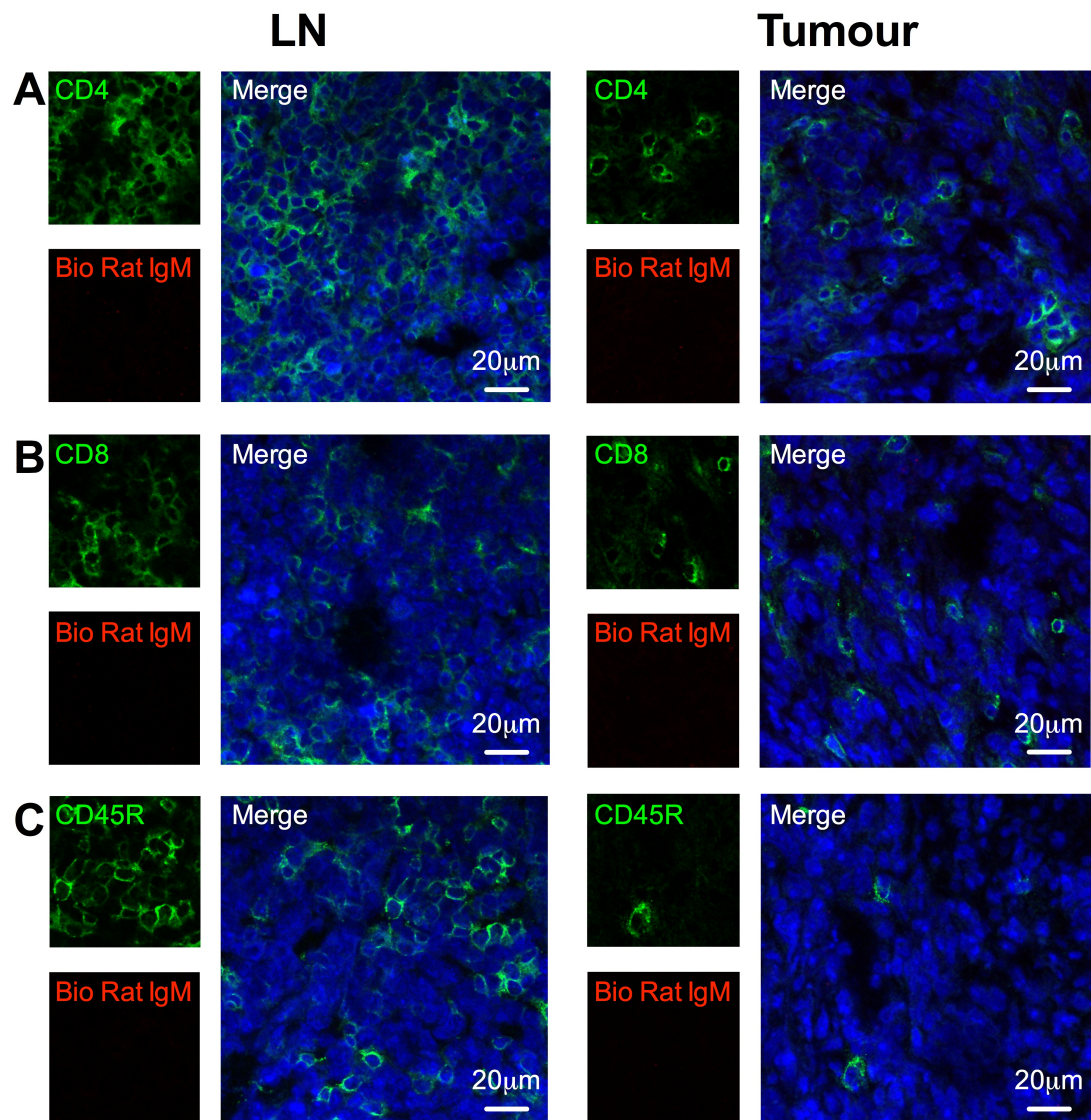
Figure B | High power confocal microscope images of sections of immunofluorescently stained tumour and Lymph Node (LN) sections, showing the appropriate isotype controls for stains included in Results Sections. Sections were co-stained using a biotinylated Rat IgM isotype control antibody and streptavidin-555 secondary antibody (red) and either a rat anti-CD4 antibody (A), a rat anti-CD8 antibody (B), or a rat anti-CD45R antibody (C), each detected using donkey anti-rat Alexa Fluor® 488 secondary antibody (green). In each case, LN sections are shown on the left and tumour sections are shown on the right. Scale bars are shown.
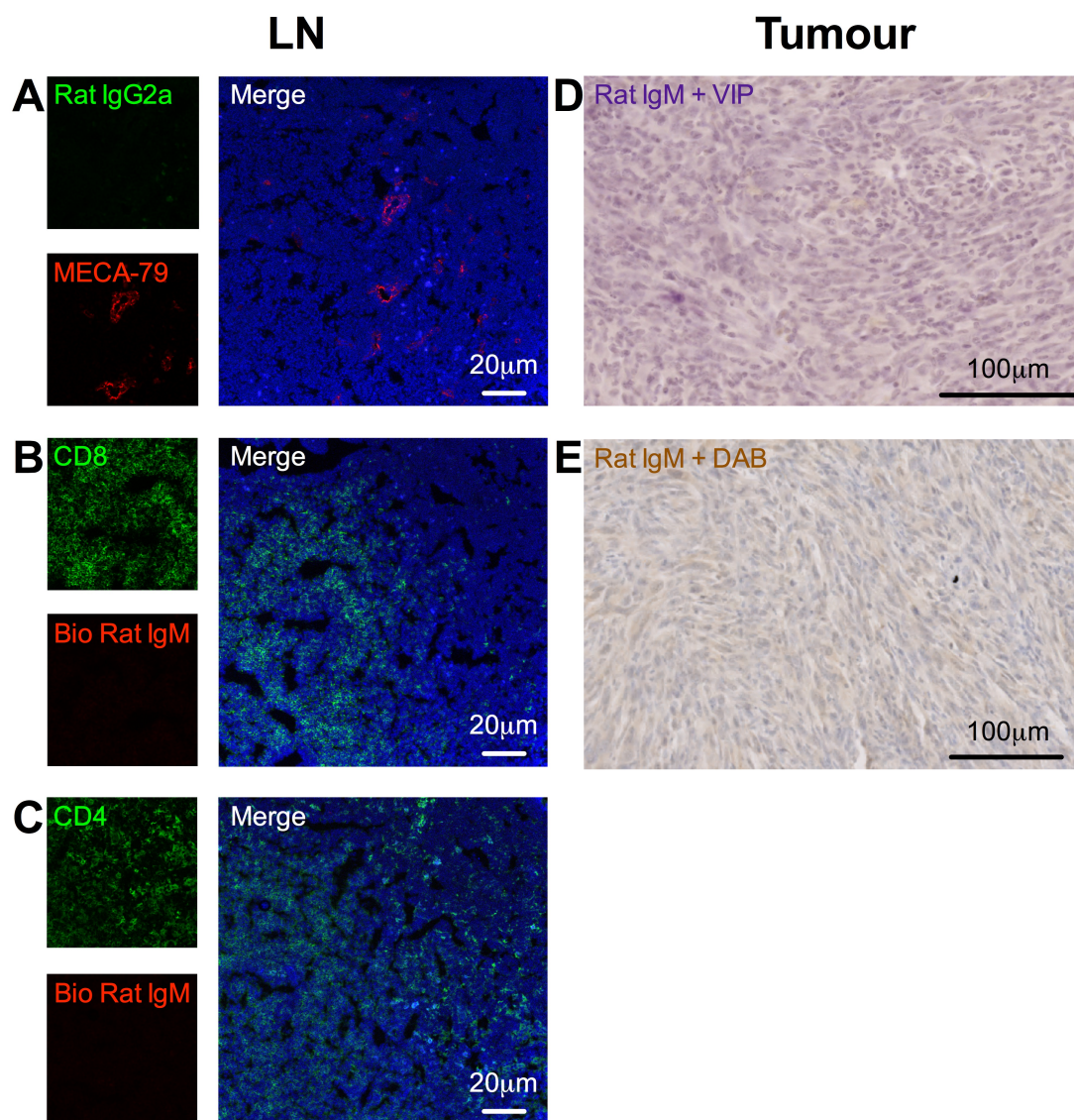
LN   **Tumour**

Figure C | Low power confocal microscope images of sections of immunofluorescently stained Lymph Node (LN) sections (A-C), and microscope images of paraffin embedded tumour sections (D-E), showing the appropriate isotype controls for stains included in Results Sections. A) LN sections were co-stained using a biotinylated rat anti-PNAd antibody (clone MECA-79) and streptavidin Alexa Fluor® 555 (red) and a Rat IgG2a isotype control antibody and donkey anti-rat AlexaFluor-488 secondary antibody (green). B-C) LN sections were co-stained using a biotinylated Rat IgM isotype control antibody and streptavidin-555 secondary antibody (red) and either a rat anti-CD8 antibody (B), or a rat anti-CD4 antibody (C), each detected using donkey anti-rat Alexa Fluor® 488 secondary antibody (green). D-E) Paraffin embedded tumour sections were stained using a Rat IgM isotype control antibody, detected using either VIP chromogen (purple; D) or DAB chromogen (brown; E). Scale bars are shown.
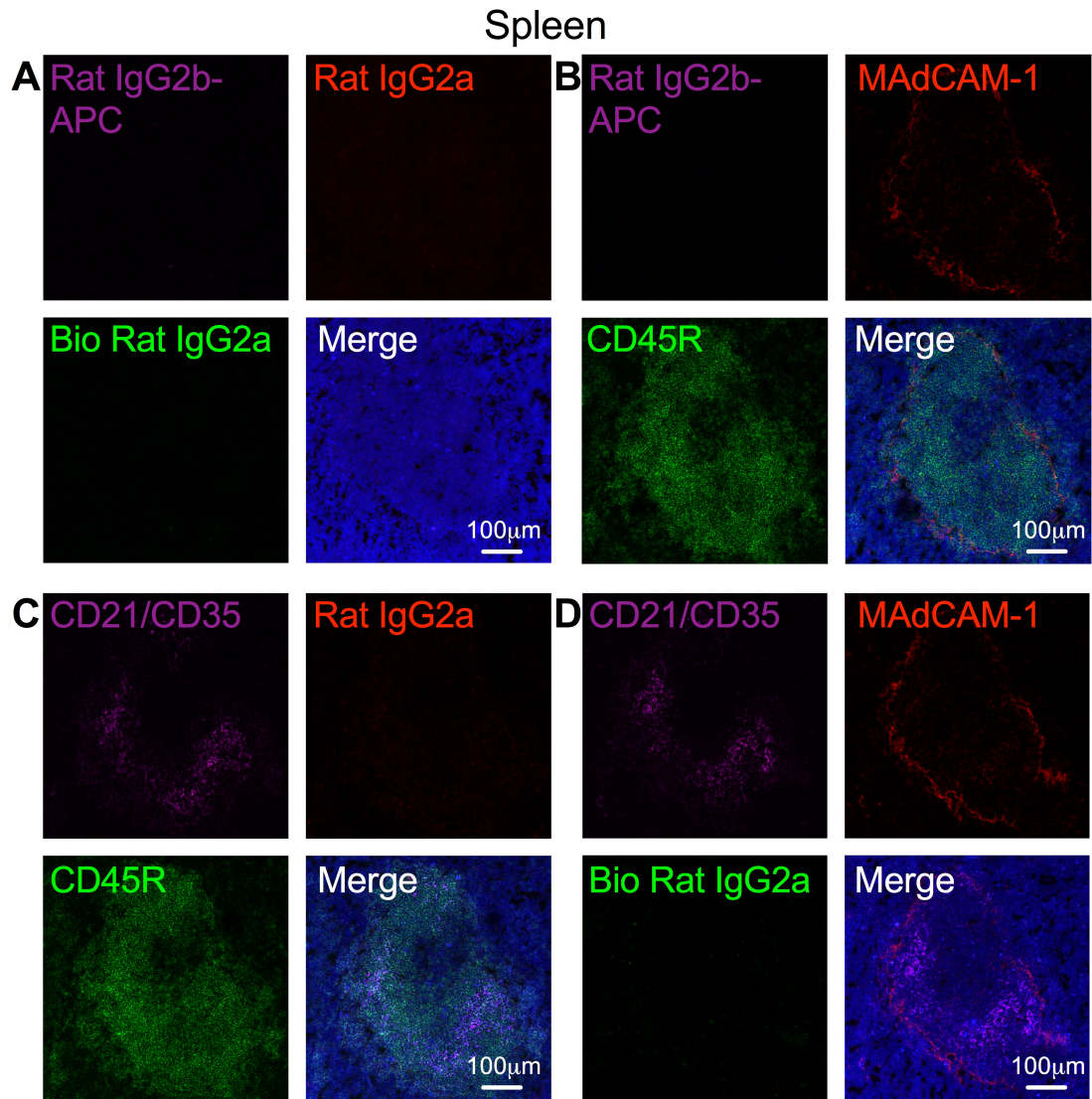
Spleen

Figure D | Low power confocal microscope images of sections of immunofluorescently stained Spleen sections, showing the appropriate isotype controls for Marginal Zone (MZ) B cell stains included in Results Sections. A) Sections were co-stained using a Rat IgG2b-APC isotype control antibody (purple), a Rat IgG2a isotype control antibody detected using a goat anti-rat Alexa Fluor® 568 secondary antibody (red), and a Rat IgG2a-FITC isotype control antibody (green). B) Sections were co-stained using a Rat IgG2b-APC isotype control antibody (purple), a rat anti-MAdCAM-1 antibody detected using a goat anti-rat Alexa Fluor® 568 secondary antibody (red), and a rat anti-CD45R-FITC antibody (green). C) Sections were co-stained using a rat anti-CD21/CD35-APC antibody (purple), a Rat IgG2a isotype control antibody detected using a goat anti-rat Alexa Fluor® 568 secondary antibody (red), and a rat anti-CD45R-FITC antibody (green). D) Sections were co-stained using a rat anti-CD21/CD35-APC antibody (purple), a rat anti-MAdCAM-1 antibody detected using a goat anti-rat Alexa Fluor® 568 secondary antibody (red), and a Rat IgG2a-FITC isotype control antibody (green). Scale bars are shown.
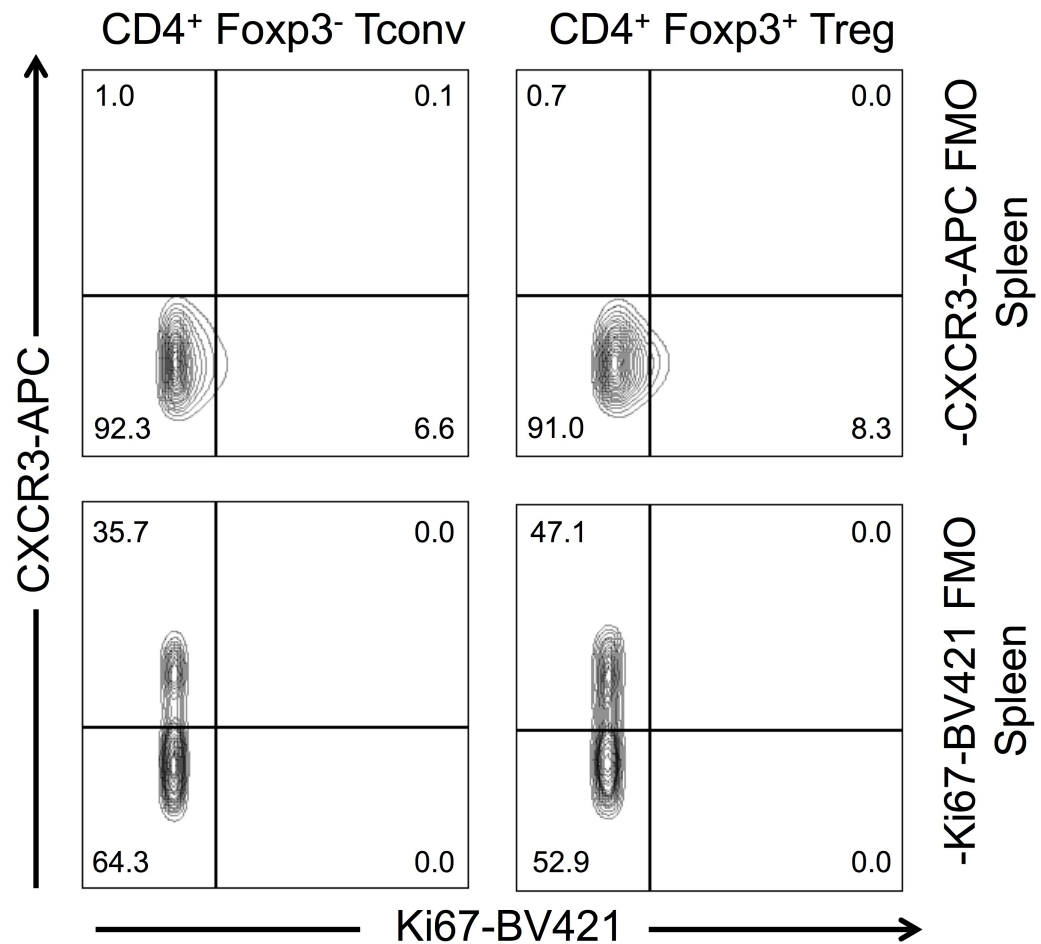
Figure E | Flow cytometry plots showing Fluorescence Minus One (FMO) controls for CXCR3-APC antibody (top) or Ki67-BV421 antibody (bottom) in stained Spleen single cell suspension samples. Cells are gated on live CD4$^+$ Foxp3$^-$ conventional T cells (Tconv; left column), or live CD4$^+$ Foxp3$^+$ regulatory T cells (Treg; right column). Numbers represent proportion of cells in each quadrant.

References

Abbas, A.K. et al., 2013. Regulatory T cells: recommendations to simplify the nomenclature. *Nature Immunology*, 14(4), pp.307–308.

Adachi, S. et al., 1997. Three distinctive steps in Peyer's patch formation of murine embryo. *International immunology*, 9(4), pp.507–514.

Ager, A. & May, M.J., 2015. Understanding high endothelial venules: Lessons for cancer immunology. *Oncoimmunology*, 4(6), p.e1008791.

Aggarwal, B.B., 2003. Signalling pathways of the TNF superfamily: a double-edged sword. *Nature Reviews Immunology*, 3(9), pp.745–756.

Aggarwal, B.B., Gupta, S.C. & Kim, J.H., 2012. Historical perspectives on tumor necrosis factor and its superfamily: 25 years later, a golden journey. *Blood*, 119(3), pp.651–665.

Ahmadzadeh, M. & Rosenberg, S.A., 2006. IL-2 administration increases CD4+ CD25(hi) Foxp3+ regulatory T cells in cancer patients. *Blood*, 107(6), pp.2409–2414.

Alcamo, E. et al., 2002. Requirement for the NF-kappaB family member RelA in the development of secondary lymphoid organs. *The Journal of experimental medicine*, 195(2), pp.233–244.

Ali, K. et al., 2014. Inactivation of PI(3)K p110δ breaks regulatory T-cell-mediated immune tolerance to cancer. *Nature*, 510(7505), pp.407–411.

Alimzhanov, M.B. et al., 1997. Abnormal development of secondary lymphoid tissues in lymphotoxin beta-deficient mice. *Proceedings of the National Academy of Sciences of the United States of America*, 94(17), pp.9302–9307.

Allen, C.D.C. & Cyster, J.G., 2008. Follicular dendritic cell networks of primary follicles and germinal centers: phenotype and function. *Seminars in immunology*, 20(1), pp.14–25.

Almeida, A.R.M., Zaragoza, B. & Freitas, A.A., 2006. Indexation as a novel mechanism of lymphocyte homeostasis: the number of CD4+CD25+ regulatory T cells is indexed to the number of IL-2-producing cells. *Journal of immunology (Baltimore, Md. : 1950)*, 177(1), pp.192–200.

Aloisi, F. & Pujol-Borrell, R., 2006. Lymphoid neogenesis in chronic inflammatory diseases. *Nature Reviews Immunology*, 6(3), pp.205–217.

Alvaro, T. et al., 2005. Outcome in Hodgkin's lymphoma can be predicted from the presence of accompanying cytotoxic and regulatory T cells. *Clinical cancer research : an official journal of the American Association for Cancer Research*, 11(4), pp.1467–1473.

Andrian, von, U.H. & Mempel, T.R., 2003. Homing and cellular traffic in lymph nodes. *Nature Reviews Immunology*, 3(11), pp.867–878.

Androlewicz, M.J., Browning, J.L. & Ware, C.F., 1992. Lymphotoxin is expressed as a heteromeric complex with a distinct 33-kDa glycoprotein on the surface of an activated human T cell hybridoma. *The Journal of biological chemistry*, 267(4), pp.2542–2547.

Annacker, O. et al., 2001. CD25+ CD4+ T cells regulate the expansion of peripheral CD4 T cells through the production of IL-10. *Journal of immunology (Baltimore, Md. : 1950)*, 166(5), pp.3008–3018.

Ansel, K.M. et al., 2000. A chemokine-driven positive feedback loop organizes lymphoid follicles. *Nature*, 406(6793), pp.309–314.

Ansel, K.M. et al., 2006. Regulation of Th2 differentiation and Il4 locus accessibility. *Annual Review of Immunology*, 24(1), pp.607–656.

Antony, P.A. et al., 2005. CD8+ T cell immunity against a tumor/self-antigen is augmented by CD4+ T helper cells and hindered by naturally occurring T regulatory cells. *Journal of immunology (Baltimore, Md. : 1950)*, 174(5), pp.2591–2601.

Attridge, K. & Walker, L.S.K., 2014. Homeostasis and function of regulatory T cells (Tregs) in vivo: lessons from TCR-transgenic Tregs. *Immunological reviews*, 259(1), pp.23–39.

Avram, G. et al., 2013. The density and type of MECA-79-positive high endothelial venules correlate with lymphocytic infiltration and tumour regression in primary cutaneous melanoma. *Histopathology*, 63(6), pp.852–861.

Awwad, M. & North, R.J., 1988. Immunologically mediated regression of a murine lymphoma after treatment with anti-L3T4 antibody. A consequence of removing L3T4+ suppressor T cells from a host generating predominantly Lyt-2+ T cell-mediated immunity. *The Journal of experimental medicine*, 168(6), pp.2193–2206.

Bachmann, M.F. et al., 1999. Cutting edge: lymphoproliferative disease in the absence of CTLA-4 is not T cell autonomous. *Journal of immunology (Baltimore, Md. : 1950)*, 163(3), pp.1128–1131.

Bajénoff, M. et al., 2006. Stromal cell networks regulate lymphocyte entry, migration, and territoriality in lymph nodes. *Immunity*, 25(6), pp.989–1001.

Balkwill, F., 2009. Tumour necrosis factor and cancer. *Nature reviews. Cancer*, 9(5), pp.361–371.

Bankovich, A.J., Shiow, L.R. & Cyster, J.G., 2010. CD69 suppresses sphingosine 1-phosophate receptor-1 (S1P1) function through interaction with membrane helix 4. *The Journal of biological chemistry*, 285(29), pp.22328–22337.

Banks, T.A. et al., 1995. Lymphotoxin-alpha-deficient mice. Effects on secondary lymphoid organ development and humoral immune responsiveness. *Journal of immunology (Baltimore, Md. : 1950)*, 155(4), pp.1685–1693.

Barone, F. et al., 2008. CXCL13, CCL21, and CXCL12 expression in salivary glands of patients with Sjogren's syndrome and MALT lymphoma: association with reactive and malignant areas of lymphoid organization. *Journal of immunology (Baltimore, Md. : 1950)*, 180(7), pp.5130–5140.

Barthlott, T. et al., 2005. CD25+ CD4+ T cells compete with naive CD4+ T cells for IL-2 and exploit it for the induction of IL-10 production. *International immunology*, 17(3), pp.279–288.

Bates, G.J. et al., 2006. Quantification of regulatory T cells enables the identification of high-risk breast cancer patients and those at risk of late relapse. *Journal of clinical oncology : official journal of the American Society of Clinical Oncology*, 24(34),

pp.5373–5380.

Belkaid, Y., 2007. Regulatory T cells and infection: a dangerous necessity. *Nature Publishing Group*, 7(11), pp.875–888.

Bell, D. et al., 1999. In breast carcinoma tissue, immature dendritic cells reside within the tumor, whereas mature dendritic cells are located in peritumoral areas. *The Journal of experimental medicine*, 190(10), pp.1417–1426.

Benedict, C.A. et al., 2001. Lymphotoxins and cytomegalovirus cooperatively induce interferon-beta, establishing host-virus détente. *Immunity*, 15(4), pp.617–626.

Bennett, C.L. et al., 2001. The immune dysregulation, polyendocrinopathy, enteropathy, X-linked syndrome (IPEX) is caused by mutations of FOXP3. *Nature genetics*, 27(1), pp.20–21.

Bento, D.C. et al., 2015. High endothelial venules are rare in colorectal cancers but accumulate in extra-tumoral areas with disease progression. *Oncoimmunology*, 4(3), p.e974374.

Bergomas, F. et al., 2011. Tertiary intratumor lymphoid tissue in colo-rectal cancer. *Cancers*, 4(1), pp.1–10.

Bettelli, E. et al., 2004. Loss of T-bet, but not STAT1, prevents the development of experimental autoimmune encephalomyelitis. *The Journal of experimental medicine*, 200(1), pp.79–87.

Betts, G. et al., 2012. Suppression of tumour-specific CD4+ T cells by regulatory T cells is associated with progression of human colorectal cancer. *Gut*, 61(8), pp.1163–1171.

Betts, G. et al., 2007. The impact of regulatory T cells on carcinogen-induced sarcogenesis. *British journal of cancer*, 96(12), pp.1849–1854.

Betts, G.J. et al., 2006. Regulating the immune response to tumours. *Advanced drug delivery reviews*, 58(8), pp.948–961.

Blankenstein, T. & Qin, Z., 2003. Chemical carcinogens as foreign bodies and some pitfalls regarding cancer immune surveillance. *Advances in cancer research*, 90, pp.179–207.

Boehmer, von, L. et al., 2013. NY-ESO-1-specific immunological pressure and escape in a patient with metastatic melanoma. *Cancer immunity*, 13, p.12.

Bohling, S.D. & Allison, K.H., 2008. Immunosuppressive regulatory T cells are associated with aggressive breast cancer phenotypes: a potential therapeutic target. *Modern pathology : an official journal of the United States and Canadian Academy of Pathology, Inc*, 21(12), pp.1527–1532.

Boissonnas, A. et al., 2010. Foxp3+ T cells induce perforin-dependent dendritic cell death in tumor-draining lymph nodes. *Immunity*, 32(2), pp.266–278.

Boitard, C. et al., 1989. T cell-mediated inhibition of the transfer of autoimmune diabetes in NOD mice. *The Journal of experimental medicine*, 169(5), pp.1669–1680.

Bombardieri, M. et al., 2007. Activation-induced cytidine deaminase expression in follicular dendritic cell networks and interfollicular large B cells supports

functionality of ectopic lymphoid neogenesis in autoimmune sialoadenitis and MALT lymphoma in Sjögren's syndrome. *Journal of immunology (Baltimore, Md. : 1950)*, 179(7), pp.4929–4938.

Bonertz, A. et al., 2009. Antigen-specific Tregs control T cell responses against a limited repertoire of tumor antigens in patients with colorectal carcinoma. *The Journal of clinical investigation*, 119(11), pp.3311–3321.

Borsellino, G. et al., 2007. Expression of ectonucleotidase CD39 by Foxp3+ Treg cells: hydrolysis of extracellular ATP and immune suppression. *Blood*, 110(4), pp.1225–1232.

Boyman, O. & Sprent, J., 2012. The role of interleukin-2 during homeostasis and activation of the immune system. *Nature Publishing Group*, 12(3), pp.180–190.

Boyman, O. et al., 2006. Selective stimulation of T cell subsets with antibody-cytokine immune complexes. *Science (New York, N.Y.)*, 311(5769), pp.1924–1927.

Browning, J.L. et al., 1993. Lymphotoxin beta, a novel member of the TNF family that forms a heteromeric complex with lymphotoxin on the cell surface. *Cell*, 72(6), pp.847–856.

Browning, J.L. et al., 2005. Lymphotoxin-beta receptor signaling is required for the homeostatic control of HEV differentiation and function. *Immunity*, 23(5), pp.539–550.

Bruder, D. et al., 2004. Neuropilin-1: a surface marker of regulatory T cells. *European journal of immunology*, 34(3), pp.623–630.

Brunkow, M.E. et al., 2001. Disruption of a new forkhead/winged-helix protein, scurfin, results in the fatal lymphoproliferative disorder of the scurfy mouse. *Nature genetics*, 27(1), pp.68–73.

Buckanovich, R.J. et al., 2008. Endothelin B receptor mediates the endothelial barrier to T cell homing to tumors and disables immune therapy. *Nature medicine*, 14(1), pp.28–36.

Bui, J.D. et al., 2006. Comparative analysis of regulatory and effector T cells in progressively growing versus rejecting tumors of similar origins. *Cancer research*, 66(14), pp.7301–7309.

Burnet, M., 1957. Cancer; a biological approach. I. The processes of control. *British medical journal*, 1(5022), pp.779–786.

Butcher, E.C. et al., 1999. Lymphocyte trafficking and regional immunity. *Advances in immunology*, 72, pp.209–253.

Calcinotto, A. et al., 2012. Targeting TNF-α to neoangiogenic vessels enhances lymphocyte infiltration in tumors and increases the therapeutic potential of immunotherapy. *Journal of immunology (Baltimore, Md. : 1950)*, 188(6), pp.2687–2694.

Campbell, D.J. & Koch, M.A., 2011. Phenotypical and functional specialization of FOXP3+ regulatory T cells. *Nature Publishing Group*, 11(2), pp.119–130.

Cancer Research UK, http://www.cancerresearchuk.org/about-cancer/what-is-cancer, Accessed September 2015

Cao, X. et al., 2007. Granzyme B and perforin are important for regulatory T cell-mediated suppression of tumor clearance. *Immunity*, 27(4), pp.635–646.

Carragher, D.M., Rangel-Moreno, J. & Randall, T.D., 2008. Ectopic lymphoid tissues and local immunity. *Seminars in immunology*, 20(1), pp.26–42.

Carretero, R. et al., 2015. Eosinophils orchestrate cancer rejection by normalizing tumor vessels and enhancing infiltration of CD8(+) T cells. *Nature Immunology*, 16(6), pp.609–617.

Carswell, E.A. et al., 1975. An endotoxin-induced serum factor that causes necrosis of tumors. *Proceedings of the National Academy of Sciences of the United States of America*, 72(9), pp.3666–3670.

Castle, J.C. et al., 2012. Exploiting the mutanome for tumor vaccination. *Cancer research*, 72(5), pp.1081–1091.

Cederbom, L., Hall, H. & Ivars, F., 2000. CD4+CD25+ regulatory T cells down-regulate co-stimulatory molecules on antigen-presenting cells. *European journal of immunology*, 30(6), pp.1538–1543.

Cesana, G.C. et al., 2006. Characterization of CD4+CD25+ regulatory T cells in patients treated with high-dose interleukin-2 for metastatic melanoma or renal cell carcinoma. *Journal of clinical oncology : official journal of the American Society of Clinical Oncology*, 24(7), pp.1169–1177.

Chatila, T.A. et al., 2000. JM2, encoding a fork head-related protein, is mutated in X-linked autoimmunity-allergic disregulation syndrome. *The Journal of clinical investigation*, 106(12), pp.R75–81.

Chaudhry, A. et al., 2009. CD4+ regulatory T cells control TH17 responses in a Stat3-dependent manner. *Science (New York, N.Y.)*, 326(5955), pp.986–991.

Chen, H. et al., 2009. Anti-CTLA-4 therapy results in higher CD4+ICOShi T cell frequency and IFN-gamma levels in both nonmalignant and malignant prostate tissues. *Proceedings of the National Academy of Sciences of the United States of America*, 106(8), pp.2729–2734.

Chen, Q., Wang, W.-C. & Evans, S.S., 2003. Tumor microvasculature as a barrier to antitumor immunity. *Cancer immunology, immunotherapy : CII*, 52(11), pp.670–679.

Chen, S.-C. et al., 2002. Ectopic expression of the murine chemokines CCL21a and CCL21b induces the formation of lymph node-like structures in pancreas, but not skin, of transgenic mice. *Journal of immunology (Baltimore, Md. : 1950)*, 168(3), pp.1001–1008.

Chen, W. et al., 2003. Conversion of peripheral CD4+CD25- naive T cells to CD4+CD25+ regulatory T cells by TGF-beta induction of transcription factor Foxp3. *The Journal of experimental medicine*, 198(12), pp.1875–1886.

Chen, X. & Oppenheim, J.J., 2011. Contrasting effects of TNF and anti-TNF on the activation of effector T cells and regulatory T cells in autoimmunity. *FEBS letters*, 585(23), pp.3611–3618.

Chen, Z., Laurence, A. & O'Shea, J.J., 2007. Signal transduction pathways and transcriptional regulation in the control of Th17 differentiation. *Seminars in immunology*, 19(6), pp.400–408.

Chiang, E.Y. et al., 2009. Targeted depletion of lymphotoxin-alpha-expressing TH1 and TH17 cells inhibits autoimmune disease. *Nature medicine*, 15(7), pp.766–773.

Chu, P. et al., 2003. Systematic identification of regulatory proteins critical for T-cell activation. *Journal of biology*, 2(3), p.21.

Chyou, S. et al., 2008. Fibroblast-type reticular stromal cells regulate the lymph node vasculature. *Journal of immunology (Baltimore, Md. : 1950)*, 181(6), pp.3887–3896.

Cipponi, A. et al., 2012. Neogenesis of lymphoid structures and antibody responses occur in human melanoma metastases. *Cancer research*, 72(16), pp.3997–4007.

Cobbold, S.P. et al., 1992. Reprogramming the Immune System for Peripheral Tolerance with CD4 and CD8 Monoclonal Antibodies. *Immunological reviews*, 129(1), pp.165–201.

Cobbold, S.P. et al., 1984. Therapy with monoclonal antibodies by elimination of T-cell subsets in vivo. *Nature*, 312(5994), pp.548–551.

Colbeck, E.J. et al., 2015. Eliminating roles for T-bet and IL-2 but revealing superior activation and proliferation as mechanisms underpinning dominance of regulatory T cells in tumors. *Oncotarget*, 6(28), pp.24649–24659.

Coley, W.B., 1891. II. Contribution to the Knowledge of Sarcoma. *Annals of surgery*, 14(3), pp.199–220.

Coley, W.B., 1910. The Treatment of Inoperable Sarcoma by Bacterial Toxins (the Mixed Toxins of the Streptococcus erysipelas and the Bacillus prodigiosus). *Proceedings of the Royal Society of Medicine*, 3(Surg Sect), pp.1–48.

Collison, L.W. et al., 2007. The inhibitory cytokine IL-35 contributes to regulatory T-cell function. *Nature*, 450(7169), pp.566–569.

Contractor, N.V. et al., 1998. Lymphoid hyperplasia, autoimmunity, and compromised intestinal intraepithelial lymphocyte development in colitis-free gnotobiotic IL-2-deficient mice. *Journal of immunology (Baltimore, Md. : 1950)*, 160(1), pp.385–394.

Coppola, D. et al., 2011. Unique ectopic lymph node-like structures present in human primary colorectal carcinoma are identified by immune gene array profiling. *The American journal of pathology*, 179(1), pp.37–45.

Coronella, J.A. et al., 2002. Antigen-driven oligoclonal expansion of tumor-infiltrating B cells in infiltrating ductal carcinoma of the breast. *Journal of immunology (Baltimore, Md. : 1950)*, 169(4), pp.1829–1836.

Cortés, J.R. et al., 2014. Maintenance of immune tolerance by Foxp3+ regulatory T cells requires CD69 expression. *Journal of autoimmunity*, 55, pp.51–62.

Corthay, A., 2009. How do regulatory T cells work? *Scandinavian journal of immunology*, 70(4), pp.326–336.

Crotty, S., 2014. T follicular helper cell differentiation, function, and roles in disease. *Immunity*, 41(4), pp.529–542.

Crowe, P.D. et al., 1994. A lymphotoxin-beta-specific receptor. *Science (New York, N.Y.)*, 264(5159), pp.707–710.

Cupedo, T. et al., 2004. Induction of secondary and tertiary lymphoid structures in the skin. *Immunity*, 21(5), pp.655–667.

Curiel, T.J. et al., 2004. Specific recruitment of regulatory T cells in ovarian carcinoma fosters immune privilege and predicts reduced survival. *Nature medicine*, 10(9), pp.942–949.

Curran, M.A. & Allison, J.P., 2009. Tumor vaccines expressing flt3 ligand synergize with ctla-4 blockade to reject preimplanted tumors. *Cancer research*, 69(19), pp.7747–7755.

Curran, M.A. et al., 2010. PD-1 and CTLA-4 combination blockade expands infiltrating T cells and reduces regulatory T and myeloid cells within B16 melanoma tumors. *Proceedings of the National Academy of Sciences of the United States of America*, 107(9), pp.4275–4280.

de Chaisemartin, L. et al., 2011. Characterization of chemokines and adhesion molecules associated with T cell presence in tertiary lymphoid structures in human lung cancer. *Cancer research*, 71(20), pp.6391–6399.

De Togni, P. et al., 1994. Abnormal development of peripheral lymphoid organs in mice deficient in lymphotoxin. *Science (New York, N.Y.)*, 264(5159), pp.703–707.

Deaglio, S. et al., 2007. Adenosine generation catalyzed by CD39 and CD73 expressed on regulatory T cells mediates immune suppression. *The Journal of experimental medicine*, 204(6), pp.1257–1265.

Deteix, C. et al., 2010. Intragraft Th17 infiltrate promotes lymphoid neogenesis and hastens clinical chronic rejection. *Journal of immunology (Baltimore, Md. : 1950)*, 184(9), pp.5344–5351.

Dieckmann, D. et al., 2001. Ex vivo isolation and characterization of CD4(+)CD25(+) T cells with regulatory properties from human blood. *The Journal of experimental medicine*, 193(11), pp.1303–1310.

Dieu-Nosjean, M.-C. et al., 2008. Long-term survival for patients with non-small-cell lung cancer with intratumoral lymphoid structures. *Journal of clinical oncology : official journal of the American Society of Clinical Oncology*, 26(27), pp.4410–4417.

Dong, H. et al., 2002. Tumor-associated B7-H1 promotes T-cell apoptosis: a potential mechanism of immune evasion. *Nature medicine*, 8(8), pp.793–800.

Dougan, M. & Dranoff, G., 2009. Immune therapy for cancer. *Annual Review of Immunology*, 27(1), pp.83–117.

Drayton, D.L. et al., 2003. Ectopic LT alpha beta directs lymphoid organ neogenesis with concomitant expression of peripheral node addressin and a HEV-restricted sulfotransferase. *The Journal of experimental medicine*, 197(9), pp.1153–1163.

Drayton, D.L. et al., 2004. I kappa B kinase complex alpha kinase activity controls chemokine and high endothelial venule gene expression in lymph nodes and nasal-associated lymphoid tissue. *Journal of immunology (Baltimore, Md. : 1950)*, 173(10), pp.6161–6168.

Drayton, D.L. et al., 2006. Lymphoid organ development: from ontogeny to neogenesis. *Nature Immunology*, 7(4), pp.344–353.

Dunn, G.P. et al., 2002. Cancer immunoediting: from immunosurveillance to tumor

escape. *Nature Immunology*, 3(11), pp.991–998.

Eberl, G. et al., 2004. An essential function for the nuclear receptor RORgamma(t) in the generation of fetal lymphoid tissue inducer cells. *Nature Immunology*, 5(1), pp.64–73.

Elkord, E. et al., 2011. Expanded subpopulation of FoxP3+ T regulatory cells in renal cell carcinoma co-express Helios, indicating they could be derived from natural but not induced Tregs. *Clinical immunology (Orlando, Fla.)*, 140(3), pp.218–222.

Ellis, L.M. & Hicklin, D.J., 2008. VEGF-targeted therapy: mechanisms of anti-tumour activity. *Nature reviews. Cancer*, 8(8), pp.579–591.

Erdman, S.E. et al., 2005. CD4+CD25+ regulatory lymphocytes induce regression of intestinal tumors in ApcMin/+ mice. *Cancer research*, 65(10), pp.3998–4004.

Erickson, S.L. et al., 1994. Decreased sensitivity to tumour-necrosis factor but normal T-cell development in TNF receptor-2-deficient mice. *Nature*, 372(6506), pp.560–563.

Ermann, J. et al., 2001. CD4(+)CD25(+) T cells facilitate the induction of T cell anergy. *Journal of immunology (Baltimore, Md. : 1950)*, 167(8), pp.4271–4275.

Esplugues, E. et al., 2003. Enhanced antitumor immunity in mice deficient in CD69. *The Journal of experimental medicine*, 197(9), pp.1093–1106.

Eyles, J. et al., 2010. Tumor cells disseminate early, but immunosurveillance limits metastatic outgrowth, in a mouse model of melanoma. *The Journal of clinical investigation*, 120(6), pp.2030–2039.

Facciabene, A. et al., 2011. Tumour hypoxia promotes tolerance and angiogenesis via CCL28 and T(reg) cells. *Nature*, 475(7355), pp.226–230.

Facciabene, A., Santoro, S. & Coukos, G., 2012. Know thy enemy: Why are tumor-infiltrating regulatory T cells so deleterious? *Oncoimmunology*, 1(4), pp.575–577.

Fahlén, L. et al., 2005. T cells that cannot respond to TGF-beta escape control by CD4(+)CD25(+) regulatory T cells. *The Journal of experimental medicine*, 201(5), pp.737–746.

Fallarino, F. et al., 2003. Modulation of tryptophan catabolism by regulatory T cells. *Nature Immunology*, 4(12), pp.1206–1212.

Fan, L. et al., 2000. Cutting edge: ectopic expression of the chemokine TCA4/SLC is sufficient to trigger lymphoid neogenesis. *Journal of immunology (Baltimore, Md. : 1950)*, 164(8), pp.3955–3959.

Fava, R.A. et al., 2011. Lymphotoxin-beta receptor blockade reduces CXCL13 in lacrimal glands and improves corneal integrity in the NOD model of Sjögren's syndrome. *Arthritis research & therapy*, 13(6), p.R182.

Faveeuw, C., Gagnerault, M.C. & Lepault, F., 1994. Expression of homing and adhesion molecules in infiltrated islets of Langerhans and salivary glands of nonobese diabetic mice. *Journal of immunology (Baltimore, Md. : 1950)*, 152(12), pp.5969–5978.

Fife, B.T. et al., 2009. Interactions between PD-1 and PD-L1 promote tolerance by blocking the TCR-induced stop signal. *Nature Immunology*, 10(11), pp.1185–1192.

Finotto, S. et al., 2005. Asthmatic changes in mice lacking T-bet are mediated by IL-13. *International immunology*, 17(8), pp.993–1007.

Fisher, D.T. et al., 2011. IL-6 trans-signaling licenses mouse and human tumor microvascular gateways for trafficking of cytotoxic T cells. *The Journal of clinical investigation*, 121(10), pp.3846–3859.

Fisson, S. et al., 2003. Continuous activation of autoreactive CD4+ CD25+ regulatory T cells in the steady state. *The Journal of experimental medicine*, 198(5), pp.737–746.

Fontenot, J.D. et al., 2005. A function for interleukin 2 in Foxp3-expressing regulatory T cells. *Nature Immunology*, 6(11), pp.1142–1151.

Fontenot, J.D., Gavin, M.A. & Rudensky, A.Y., 2003. Foxp3 programs the development and function of CD4+CD25+ regulatory T cells. *Nature Immunology*, 4(4), pp.330–336.

Förster, R. et al., 1996. A putative chemokine receptor, BLR1, directs B cell migration to defined lymphoid organs and specific anatomic compartments of the spleen. *Cell*, 87(6), pp.1037–1047.

Förster, R. et al., 1999. CCR7 coordinates the primary immune response by establishing functional microenvironments in secondary lymphoid organs. *Cell*, 99(1), pp.23–33.

Förster, R., Davalos-Misslitz, A.C. & Rot, A., 2008. CCR7 and its ligands: balancing immunity and tolerance. *Nature Publishing Group*, 8(5), pp.362–371.

Freeman, G.J. et al., 2000. Engagement of the PD-1 immunoinhibitory receptor by a novel B7 family member leads to negative regulation of lymphocyte activation. *The Journal of experimental medicine*, 192(7), pp.1027–1034.

Fu, Y.X. & Chaplin, D.D., 1999. Development and maturation of secondary lymphoid tissues. *Annual Review of Immunology*, 17(1), pp.399–433.

Furtado, G.C. et al., 2014. TNFα-dependent development of lymphoid tissue in the absence of RORγt+ lymphoid tissue inducer cells. *Mucosal immunology*, 7(3), pp.602–614.

Fütterer, A. et al., 1998. The lymphotoxin beta receptor controls organogenesis and affinity maturation in peripheral lymphoid tissues. *Immunity*, 9(1), pp.59–70.

Fyfe, G. et al., 1995. Results of treatment of 255 patients with metastatic renal cell carcinoma who received high-dose recombinant interleukin-2 therapy. *Journal of clinical oncology : official journal of the American Society of Clinical Oncology*, 13(3), pp.688–696.

Gabrilovich, D.I., Ostrand-Rosenberg, S. & Bronte, V., 2012. Coordinated regulation of myeloid cells by tumours. *Nature Publishing Group*, 12(4), pp.253–268.

Galkina, E. et al., 2003. L-selectin shedding does not regulate constitutive T cell trafficking but controls the migration pathways of antigen-activated T lymphocytes. *The Journal of experimental medicine*, 198(9), pp.1323–1335.

Gallimore, A. & Godkin, A., 2008. Regulatory T cells and tumour immunity - observations in mice and men. *Immunology*, 123(2), pp.157–163.

Gallimore, A., Godkin, A. & Ager, A., 2013. High endothelial venules: Help or hindrance in the quest for antitumor immunity? *Oncoimmunology*, 2(5), p.e24272.

Galon, J. et al., 2006. Type, density, and location of immune cells within human colorectal tumors predict clinical outcome. *Science (New York, N.Y.)*, 313(5795), pp.1960–1964.

Ganss, R. et al., 2002. Combination of T-cell therapy and trigger of inflammation induces remodeling of the vasculature and tumor eradication. *Cancer research*, 62(5), pp.1462–1470.

Gao, Q. et al., 2007. Intratumoral balance of regulatory and cytotoxic T cells is associated with prognosis of hepatocellular carcinoma after resection. *Journal of clinical oncology : official journal of the American Society of Clinical Oncology*, 25(18), pp.2586–2593.

Gasteiger, G. & Kastenmuller, W., 2012. Foxp3+ Regulatory T-cells and IL-2: The Moirai of T-cell Fates? *Frontiers in immunology*, 3, p.179.

Gatumu, M.K. et al., 2009. Blockade of lymphotoxin-beta receptor signaling reduces aspects of Sjögren's syndrome in salivary glands of non-obese diabetic mice. *Arthritis research & therapy*, 11(1), p.R24.

Gavin, M.A. et al., 2002. Homeostasis and anergy of CD4(+)CD25(+) suppressor T cells in vivo. *Nature Immunology*, 3(1), pp.33–41.

Gavin, M.A. et al., 2006. Single-cell analysis of normal and FOXP3-mutant human T cells: FOXP3 expression without regulatory T cell development. *Proceedings of the National Academy of Sciences of the United States of America*, 103(17), pp.6659–6664.

GeurtsvanKessel, C.H. et al., 2009. Dendritic cells are crucial for maintenance of tertiary lymphoid structures in the lung of influenza virus-infected mice. *The Journal of experimental medicine*, 206(11), pp.2339–2349.

Ghiringhelli, F. et al., 2005. Tumor cells convert immature myeloid dendritic cells into TGF-beta-secreting cells inducing CD4+CD25+ regulatory T cell proliferation. *The Journal of experimental medicine*, 202(7), pp.919–929.

Girard, J.-P., Moussion, C. & Förster, R., 2012. HEVs, lymphatics and homeostatic immune cell trafficking in lymph nodes. *Nature Publishing Group*, 12(11), pp.762–773.

Gobert, M. et al., 2009. Regulatory T cells recruited through CCL22/CCR4 are selectively activated in lymphoid infiltrates surrounding primary breast tumors and lead to an adverse clinical outcome. *Cancer research*, 69(5), pp.2000–2009.

Goc, J. et al., 2013. Characteristics of tertiary lymphoid structures in primary cancers. *Oncoimmunology*, 2(12), p.e26836.

Goc, J. et al., 2014. Dendritic cells in tumor-associated tertiary lymphoid structures signal a Th1 cytotoxic immune contexture and license the positive prognostic value of infiltrating CD8+ T cells. *Cancer research*, 74(3), pp.705–715.

Gondek, D.C. et al., 2005. Cutting edge: contact-mediated suppression by CD4+CD25+ regulatory cells involves a granzyme B-dependent, perforin-independent mechanism. *Journal of immunology (Baltimore, Md. : 1950)*, 174(4), pp.1783–1786.

Gondek, D.C. et al., 2008. Transplantation survival is maintained by granzyme B+ regulatory cells and adaptive regulatory T cells. *Journal of immunology (Baltimore, Md. : 1950)*, 181(7), pp.4752–4760.

González-Amaro, R. et al., 2013. Is CD69 an effective brake to control inflammatory diseases? *Trends in molecular medicine*, 19(10), pp.625–632.

Gowans, J.L. & Knight, E.J., 1964. THE ROUTE OF RE-CIRCULATION OF LYMPHOCYTES IN THE RAT. *Proceedings of the Royal Society of London. Series B, Biological sciences*, 159, pp.257–282.

Grattendick, K.J. et al., 2008. Effects of three anti-TNF-alpha drugs: etanercept, infliximab and pirfenidone on release of TNF-alpha in medium and TNF-alpha associated with the cell in vitro. *International immunopharmacology*, 8(5), pp.679–687.

Gräbner, R. et al., 2009. Lymphotoxin beta receptor signaling promotes tertiary lymphoid organogenesis in the aorta adventitia of aged ApoE-/- mice. *The Journal of experimental medicine*, 206(1), pp.233–248.

Greenwald, R.J., Freeman, G.J. & Sharpe, A.H., 2005. The B7 family revisited. *Annual Review of Immunology*, 23(1), pp.515–548.

Greiner, D.L. et al., 1987. Depletion of RT6.1+ T lymphocytes induces diabetes in resistant biobreeding/Worcester (BB/W) rats. *The Journal of experimental medicine*, 166(2), pp.461–475.

Grell, M. et al., 1995. The transmembrane form of tumor necrosis factor is the prime activating ligand of the 80 kDa tumor necrosis factor receptor. *Cell*, 83(5), pp.793–802.

Grell, M. et al., 1998. The type 1 receptor (CD120a) is the high-affinity receptor for soluble tumor necrosis factor. *Proceedings of the National Academy of Sciences of the United States of America*, 95(2), pp.570–575.

Grivennikov, S.I. et al., 2005. Distinct and nonredundant in vivo functions of TNF produced by t cells and macrophages/neutrophils: protective and deleterious effects. *Immunity*, 22(1), pp.93–104.

Grivennikov, S.I., Greten, F.R. & Karin, M., 2010. Immunity, inflammation, and cancer. *Cell*, 140(6), pp.883–899.

Grohmann, U. et al., 2002. CTLA-4-Ig regulates tryptophan catabolism in vivo. *Nature Immunology*, 3(11), pp.1097–1101.

Grossman, W.J. et al., 2004. Human T regulatory cells can use the perforin pathway to cause autologous target cell death. *Immunity*, 21(4), pp.589–601.

Gu-Trantien, C. et al., 2013. CD4^{+} follicular helper T cell infiltration predicts breast cancer survival. *The Journal of clinical investigation*, 123(7), pp.2873–2892.

Hagen, ten, T.L.M., Seynhaeve, A.L.B. & Eggermont, A.M.M., 2008. Tumor necrosis factor-mediated interactions between inflammatory response and tumor vascular bed. *Immunological reviews*, 222(1), pp.299–315.

Halle, S. et al., 2009. Induced bronchus-associated lymphoid tissue serves as a general priming site for T cells and is maintained by dendritic cells. *The Journal of experimental medicine*, 206(12), pp.2593–2601.

Hamid, O. et al., 2013. Safety and tumor responses with lambrolizumab (anti-PD-1) in melanoma. *The New England journal of medicine*, 369(2), pp.134–144.

Hamzah, J. et al., 2008. Vascular normalization in Rgs5-deficient tumours promotes immune destruction. *Nature*, 453(7193), pp.410–414.

Hanahan, D. & Weinberg, R.A., 2011. Hallmarks of cancer: the next generation. *Cell*, 144(5), pp.646–674.

Hanahan, D. & Weinberg, R.A., 2000. The hallmarks of cancer. *Cell*, 100(1), pp.57–70.

Hansen, W. et al., 2012. Neuropilin 1 deficiency on CD4+Foxp3+ regulatory T cells impairs mouse melanoma growth. *The Journal of experimental medicine*, 209(11), pp.2001–2016.

Hayden, M.S. & Ghosh, S., 2014. Regulation of NF-κB by TNF family cytokines. *Seminars in immunology*, 26(3), pp.253–266.

He, S. et al., 2010. CD4+CD25+Foxp3+ regulatory T cells protect the proinflammatory activation of human umbilical vein endothelial cells. *Arteriosclerosis, thrombosis, and vascular biology*, 30(12), pp.2621–2630.

Heesters, B.A., Myers, R.C. & Carroll, M.C., 2014. Follicular dendritic cells: dynamic antigen libraries. *Nature Publishing Group*, 14(7), pp.495–504.

Hemmerich, S. et al., 2001. Sulfation of L-selectin ligands by an HEV-restricted sulfotransferase regulates lymphocyte homing to lymph nodes. *Immunity*, 15(2), pp.237–247.

Herzog, B.H. et al., 2013. Podoplanin maintains high endothelial venule integrity by interacting with platelet CLEC-2. *Nature*, 502(7469), pp.105–109.

Higano, C.S. et al., 2009. Integrated data from 2 randomized, double-blind, placebo-controlled, phase 3 trials of active cellular immunotherapy with sipuleucel-T in advanced prostate cancer. *Cancer*, 115(16), pp.3670–3679.

Hindley, J.P. et al., 2011. Analysis of the T-cell receptor repertoires of tumor-infiltrating conventional and regulatory T cells reveals no evidence for conversion in carcinogen-induced tumors. *Cancer research*, 71(3), pp.736–746.

Hindley, J.P. et al., 2012. T-cell trafficking facilitated by high endothelial venules is required for tumor control after regulatory T-cell depletion. *Cancer research*, 72(21), pp.5473–5482.

Hinrichs, C.S. & Rosenberg, S.A., 2014. Exploiting the curative potential of adoptive T-cell therapy for cancer. *Immunological reviews*, 257(1), pp.56–71.

Hjelmström, P. et al., 2000. Lymphoid tissue homing chemokines are expressed in chronic inflammation. *The American journal of pathology*, 156(4), pp.1133–1138.

Hodi, F.S. et al., 2010. Improved survival with ipilimumab in patients with metastatic melanoma. *The New England journal of medicine*, 363(8), pp.711–723.

Honda, K. et al., 2001. Molecular basis for hematopoietic/mesenchymal interaction during initiation of Peyer's patch organogenesis. *The Journal of experimental medicine*, 193(5), pp.621–630.

Hori, S. et al., 2002. Peripheral expansion of thymus-derived regulatory cells in anti-

myelin basic protein T cell receptor transgenic mice. *European journal of immunology*, 32(12), pp.3729–3735.

Hori, S., Nomura, T. & Sakaguchi, S., 2003. Control of regulatory T cell development by the transcription factor Foxp3. *Science (New York, N.Y.)*, 299(5609), pp.1057–1061.

Hou, S. et al., 1995. Subverting lymph node trafficking by treatment with the Mel-14 monoclonal antibody to L-selectin does not prevent an effective host response to Sendai virus. *Journal of immunology (Baltimore, Md. : 1950)*, 155(1), pp.252–258.

Hoves, S., Trapani, J.A. & Voskoboinik, I., 2010. The battlefield of perforin/granzyme cell death pathways. *Journal of leukocyte biology*, 87(2), pp.237–243.

Hsieh, C.-S., Lee, H.-M. & Lio, C.-W.J., 2012. Selection of regulatory T cells in the thymus. *Nature Publishing Group*, 12(3), pp.157–167.

Huang, Y. et al., 2013. Vascular normalization as an emerging strategy to enhance cancer immunotherapy. *Cancer research*, 73(10), pp.2943–2948.

Huang, Y. et al., 2012. Vascular normalizing doses of antiangiogenic treatment reprogram the immunosuppressive tumor microenvironment and enhance immunotherapy. *Proceedings of the National Academy of Sciences of the United States of America*, 109(43), pp.17561–17566.

Huehn, J. & Beyer, M., 2015. Epigenetic and transcriptional control of Foxp3+ regulatory T cells. *Seminars in immunology*, 27(1), pp.10–18.

Itoh, M. et al., 1999. Thymus and autoimmunity: production of CD25+CD4+ naturally anergic and suppressive T cells as a key function of the thymus in maintaining immunologic self-tolerance. *Journal of immunology (Baltimore, Md. : 1950)*, 162(9), pp.5317–5326.

Ivanov, I.I. et al., 2006. The orphan nuclear receptor RORgammat directs the differentiation program of proinflammatory IL-17+ T helper cells. *Cell*, 126(6), pp.1121–1133.

Iwai, Y. et al., 2002. Involvement of PD-L1 on tumor cells in the escape from host immune system and tumor immunotherapy by PD-L1 blockade. *Proceedings of the National Academy of Sciences of the United States of America*, 99(19), pp.12293–12297.

Izcue, A., Coombes, J.L. & Powrie, F., 2009. Regulatory lymphocytes and intestinal inflammation. *Annual Review of Immunology*, 27(1), pp.313–338.

Jaafar, F. et al., 2009. Correlation of CXCL12 expression and FoxP3+ cell infiltration with human papillomavirus infection and clinicopathological progression of cervical cancer. *The American journal of pathology*, 175(4), pp.1525–1535.

Jain, R.K., 2005. Normalization of tumor vasculature: an emerging concept in antiangiogenic therapy. *Science (New York, N.Y.)*, 307(5706), pp.58–62.

Johnson, L.A. et al., 2009. Gene therapy with human and mouse T-cell receptors mediates cancer regression and targets normal tissues expressing cognate antigen. *Blood*, 114(3), pp.535–546.

Jones, E., 2002. Cancer Immunity 2:1 (2002) - ARTICLE. pp.1–12.

Jones, E. et al., 2002. Depletion of CD25+ regulatory cells results in suppression of melanoma growth and induction of autoreactivity in mice. *Cancer immunity*, 2, p.1.

Jones, G.W. et al., 2015. Interleukin-27 inhibits ectopic lymphoid-like structure development in early inflammatory arthritis. *The Journal of experimental medicine*, 196(7), pp.979–10.

Jordan, M.S. et al., 2001. Thymic selection of CD4+CD25+ regulatory T cells induced by an agonist self-peptide. *Nature Immunology*, 2(4), pp.301–306.

Josefowicz, S.Z., Lu, L.-F. & Rudensky, A.Y., 2012. Regulatory T cells: mechanisms of differentiation and function. *Annual Review of Immunology*, 30(1), pp.531–564.

Joshi, N.S. et al., 2015. Regulatory T Cells in Tumor-Associated Tertiary Lymphoid Structures Suppress Anti-tumor T Cell Responses. *Immunity*, 43(3), pp.579–590.

Joyce, J.A. & Fearon, D.T., 2015. T cell exclusion, immune privilege, and the tumor microenvironment. *Science (New York, N.Y.)*, 348(6230), pp.74–80.

Kantoff, P.W. et al., 2010. Sipuleucel-T immunotherapy for castration-resistant prostate cancer. *The New England journal of medicine*, 363(5), pp.411–422.

Kavanagh, B. et al., 2008. CTLA4 blockade expands FoxP3+ regulatory and activated effector CD4+ T cells in a dose-dependent fashion. *Blood*, 112(4), pp.1175–1183.

Kawashima, H. et al., 2005. N-acetylglucosamine-6-O-sulfotransferases 1 and 2 cooperatively control lymphocyte homing through L-selectin ligand biosynthesis in high endothelial venules. *Nature Immunology*, 6(11), pp.1096–1104.

Khattri, R. et al., 2003. An essential role for Scurfin in CD4+CD25+ T regulatory cells. *Nature Immunology*, 4(4), pp.337–342.

Kim, H.P., Kelly, J. & Leonard, W.J., 2001. The basis for IL-2-induced IL-2 receptor alpha chain gene regulation: importance of two widely separated IL-2 response elements. *Immunity*, 15(1), pp.159–172.

Kim, J.M., Rasmussen, J.P. & Rudensky, A.Y., 2007. Regulatory T cells prevent catastrophic autoimmunity throughout the lifespan of mice. *Nature Immunology*, 8(2), pp.191–197.

Kissick, H.T. & Sanda, M.G., 2015. The role of active vaccination in cancer immunotherapy: lessons from clinical trials. *Current opinion in immunology*, 35, pp.15–22.

Klages, K. et al., 2010. Selective depletion of Foxp3+ regulatory T cells improves effective therapeutic vaccination against established melanoma. *Cancer research*, 70(20), pp.7788–7799.

Klein, G. et al., 1960. Demonstration of resistance against methylcholanthrene-induced sarcomas in the primary autochthonous host. *Cancer research*, 20, pp.1561–1572.

Klein, L. et al., 2014. Positive and negative selection of the T cell repertoire: what thymocytes see (and don't see). *Nature Publishing Group*, 14(6), pp.377–391.

Klein, L., Khazaie, K. & Boehmer, von, H., 2003. In vivo dynamics of antigen-specific regulatory T cells not predicted from behavior in vitro. *Proceedings of the National Academy of Sciences of the United States of America*, 100(15), pp.8886–8891.

Ko, K. et al., 2005. Treatment of advanced tumors with agonistic anti-GITR mAb and its effects on tumor-infiltrating Foxp3+CD25+CD4+ regulatory T cells. *The Journal of experimental medicine*, 202(7), pp.885–891.

Kobayashi, M. et al., 2011. Prominent expression of sialyl Lewis X-capped core 2-branched O-glycans on high endothelial venule-like vessels in gastric MALT lymphoma. *The Journal of pathology*, 224(1), pp.67–77.

Koch, M.A. et al., 2009. The transcription factor T-bet controls regulatory T cell homeostasis and function during type 1 inflammation. *Nature Immunology*, 10(6), pp.595–602.

Kochenderfer, J.N. et al., 2010. Eradication of B-lineage cells and regression of lymphoma in a patient treated with autologous T cells genetically engineered to recognize CD19. *Blood*, 116(20), pp.4099–4102.

Kocks, J.R. et al., 2007. Regulatory T cells interfere with the development of bronchus-associated lymphoid tissue. *The Journal of experimental medicine*, 204(4), pp.723–734.

Koebel, C.M. et al., 2007. Adaptive immunity maintains occult cancer in an equilibrium state. *Nature*, 450(7171), pp.903–907.

Koni, P.A. & Flavell, R.A., 1998. A role for tumor necrosis factor receptor type 1 in gut-associated lymphoid tissue development: genetic evidence of synergism with lymphotoxin beta. *The Journal of experimental medicine*, 187(12), pp.1977–1983.

Koni, P.A. et al., 1997. Distinct roles in lymphoid organogenesis for lymphotoxins alpha and beta revealed in lymphotoxin beta-deficient mice. *Immunity*, 6(4), pp.491–500.

Körner, H. et al., 1997. Distinct roles for lymphotoxin-alpha and tumor necrosis factor in organogenesis and spatial organization of lymphoid tissue. *European journal of immunology*, 27(10), pp.2600–2609.

Kratz, A. et al., 1996. Chronic inflammation caused by lymphotoxin is lymphoid neogenesis. *The Journal of experimental medicine*, 183(4), pp.1461–1472.

Krummel, M.F. & Allison, J.P., 1995. CD28 and CTLA-4 have opposing effects on the response of T cells to stimulation. *The Journal of experimental medicine*, 182(2), pp.459–465.

Krummel, M.F. & Allison, J.P., 1996. CTLA-4 engagement inhibits IL-2 accumulation and cell cycle progression upon activation of resting T cells. *The Journal of experimental medicine*, 183(6), pp.2533–2540.

Kumar, V. et al., 2012. Optical projection tomography reveals dynamics of HEV growth after immunization with protein plus CFA and features shared with HEVs in acute autoinflammatory lymphadenopathy. *Frontiers in immunology*, 3, p.282.

Kuniyasu, Y. et al., 2000. Naturally anergic and suppressive CD25(+)CD4(+) T cells as a functionally and phenotypically distinct immunoregulatory T cell subpopulation. *International immunology*, 12(8), pp.1145–1155.

Kuprash, D.V. et al., 2005. Novel tumor necrosis factor-knockout mice that lack Peyer's patches. *European journal of immunology*, 35(5), pp.1592–1600.

Kuprash, D.V. et al., 1999. TNF and lymphotoxin beta cooperate in the maintenance of secondary lymphoid tissue microarchitecture but not in the development of lymph

nodes. *Journal of immunology (Baltimore, Md. : 1950)*, 163(12), pp.6575–6580.

Ladányi, A. et al., 2007. Density of DC-LAMP(+) mature dendritic cells in combination with activated T lymphocytes infiltrating primary cutaneous melanoma is a strong independent prognostic factor. *Cancer immunology, immunotherapy : CII*, 56(9), pp.1459–1469.

Lahl, K. et al., 2007. Selective depletion of Foxp3+ regulatory T cells induces a scurfy-like disease. *The Journal of experimental medicine*, 204(1), pp.57–63.

Lane, P.J.L., Gaspal, F.M., McConnell, F.M., Kim, M.Y., et al., 2012. Lymphoid tissue inducer cells: innate cells critical for CD4+ T cell memory responses? *Annals of the New York Academy of Sciences*, 1247(1), pp.1–15.

Lane, P.J.L., Gaspal, F.M., McConnell, F.M., Withers, D.R., et al., 2012. Lymphoid tissue inducer cells: pivotal cells in the evolution of CD4 immunity and tolerance? *Frontiers in immunology*, 3, p.24.

Le, D.T. & Jaffee, E.M., 2012. Regulatory T-cell modulation using cyclophosphamide in vaccine approaches: a current perspective. *Cancer research*, 72(14), pp.3439–3444.

Leach, D.R., Krummel, M.F. & Allison, J.P., 1996. Enhancement of antitumor immunity by CTLA-4 blockade. *Science (New York, N.Y.)*, 271(5256), pp.1734–1736.

Lepault, F. et al., 1994. Recirculation, phenotype and functions of lymphocytes in mice treated with monoclonal antibody MEL-14. *European journal of immunology*, 24(12), pp.3106–3112.

Li, Betty et al., 2006. Vascular endothelial growth factor blockade reduces intratumoral regulatory T cells and enhances the efficacy of a GM-CSF-secreting cancer immunotherapy. *Clinical cancer research : an official journal of the American Association for Cancer Research*, 12(22), pp.6808–6816.

Li, Jiali et al., 2003. Complete regression of experimental solid tumors by combination LEC/chTNT-3 immunotherapy and CD25(+) T-cell depletion. *Cancer research*, 63(23), pp.8384–8392.

Li, Xingrui et al., 2010. Efficient Treg depletion induces T-cell infiltration and rejection of large tumors. *European journal of immunology*, 40(12), pp.3325–3335.

Li, Xudong & Zheng, Y., 2015. Regulatory T cell identity: formation and maintenance. *Trends in immunology*, 36(6), pp.344–353.

Liakou, C.I. et al., 2008. CTLA-4 blockade increases IFNgamma-producing CD4+ICOShi cells to shift the ratio of effector to regulatory T cells in cancer patients. *Proceedings of the National Academy of Sciences of the United States of America*, 105(39), pp.14987–14992.

Liang, B. et al., 2008. Regulatory T cells inhibit dendritic cells by lymphocyte activation gene-3 engagement of MHC class II. *Journal of immunology (Baltimore, Md. : 1950)*, 180(9), pp.5916–5926.

Liao, S. & Ruddle, N.H., 2006. Synchrony of high endothelial venules and lymphatic vessels revealed by immunization. *Journal of immunology (Baltimore, Md. : 1950)*, 177(5), pp.3369–3379.

Lim, H.W. et al., 2005. Cutting edge: direct suppression of B cells by CD4+ CD25+

regulatory T cells. *Journal of immunology (Baltimore, Md. : 1950)*, 175(7), pp.4180–4183.

Linterman, M.A. et al., 2011. Foxp3+ follicular regulatory T cells control the germinal center response. *Nature medicine*, 17(8), pp.975–982.

Liu, G. et al., 2009. The receptor S1P1 overrides regulatory T cell-mediated immune suppression through Akt-mTOR. *Nature Immunology*, 10(7), pp.769–777.

Liu, V.C. et al., 2007. Tumor evasion of the immune system by converting CD4+CD25- T cells into CD4+CD25+ T regulatory cells: role of tumor-derived TGF-beta. *Journal of immunology (Baltimore, Md. : 1950)*, 178(5), pp.2883–2892.

Liu, W. et al., 2006. CD127 expression inversely correlates with FoxP3 and suppressive function of human CD4+ T reg cells. *The Journal of experimental medicine*, 203(7), pp.1701–1711.

Liu, Y. et al., 2008. A critical function for TGF-beta signaling in the development of natural CD4+CD25+Foxp3+ regulatory T cells. *Nature Immunology*, 9(6), pp.632–640.

Lochner, M. et al., 2011. Microbiota-induced tertiary lymphoid tissues aggravate inflammatory disease in the absence of RORgamma t and LTi cells. *The Journal of experimental medicine*, 208(1), pp.125–134.

Loeser, S. et al., 2007. Spontaneous tumor rejection by cbl-b-deficient CD8+ T cells. *The Journal of experimental medicine*, 204(4), pp.879–891.

Lu, T.T. & Browning, J.L., 2014. Role of the Lymphotoxin/LIGHT System in the Development and Maintenance of Reticular Networks and Vasculature in Lymphoid Tissues. *Frontiers in immunology*, 5, p.47.

Luther, S.A. et al., 2000. BLC expression in pancreatic islets causes B cell recruitment and lymphotoxin-dependent lymphoid neogenesis. *Immunity*, 12(5), pp.471–481.

Luther, S.A. et al., 2002. Differing activities of homeostatic chemokines CCL19, CCL21, and CXCL12 in lymphocyte and dendritic cell recruitment and lymphoid neogenesis. *Journal of immunology (Baltimore, Md. : 1950)*, 169(1), pp.424–433.

Luther, S.A., Ansel, K.M. & Cyster, J.G., 2003. Overlapping roles of CXCL13, interleukin 7 receptor alpha, and CCR7 ligands in lymph node development. *The Journal of experimental medicine*, 197(9), pp.1191–1198.

Mackay, F. & Browning, J.L., 1998. Turning off follicular dendritic cells. *Nature*, 395(6697), pp.26–27.

Mackay, F. et al., 1997. Lymphotoxin but not tumor necrosis factor functions to maintain splenic architecture and humoral responsiveness in adult mice. *European journal of immunology*, 27(8), pp.2033–2042.

Mackay, L.K. et al., 2015. Cutting Edge: CD69 Interference with Sphingosine-1-Phosphate Receptor Function Regulates Peripheral T Cell Retention. *Journal of immunology (Baltimore, Md. : 1950)*, 194(5), pp.2059–2063.

MacKie, R.M., Reid, R. & Junor, B., 2003. Fatal melanoma transferred in a donated kidney 16 years after melanoma surgery. *The New England journal of medicine*, 348(6), pp.567–568.

Madorsky Rowdo, F.P. et al., 2015. Immunotherapy in Cancer: A Combat between Tumors and the Immune System; You Win Some, You Lose Some. *Frontiers in immunology*, 6, p.127.

Makkouk, A. & Weiner, G.J., 2015. Cancer immunotherapy and breaking immune tolerance: new approaches to an old challenge. *Cancer research*, 75(1), pp.5–10.

Malek, T.R., 2008. The biology of interleukin-2. *Annual Review of Immunology*, 26(1), pp.453–479.

Mamura, M. et al., 2004. CD28 disruption exacerbates inflammation in Tgf-beta1-/- mice: in vivo suppression by CD4+CD25+ regulatory T cells independent of autocrine TGF-beta1. *Blood*, 103(12), pp.4594–4601.

Maniotis, A.J. et al., 1999. Vascular channel formation by human melanoma cells in vivo and in vitro: vasculogenic mimicry. *The American journal of pathology*, 155(3), pp.739–752.

Marie, J.C. et al., 2005. TGF-beta1 maintains suppressor function and Foxp3 expression in CD4+CD25+ regulatory T cells. *The Journal of experimental medicine*, 201(7), pp.1061–1067.

Marinkovic, T. et al., 2006. Interaction of mature CD3+CD4+ T cells with dendritic cells triggers the development of tertiary lymphoid structures in the thyroid. *The Journal of clinical investigation*, 116(10), pp.2622–2632.

Martin, P. et al., 2010. The leukocyte activation antigen CD69 limits allergic asthma and skin contact hypersensitivity. *The Journal of allergy and clinical immunology*, 126(2), pp.355–65– 365.e1–3.

Martin-Liberal, J. et al., 2015. Anti-programmed cell death-1 therapy and insulin-dependent diabetes: a case report. *Cancer immunology, immunotherapy : CII*, 64(6), pp.765–767.

Martinet, L. & Girard, J.-P., 2013. Regulation of tumor-associated high-endothelial venules by dendritic cells: A new opportunity to promote lymphocyte infiltration into breast cancer? *Oncoimmunology*, 2(11), p.e26470.

Martinet, L. et al., 2013. High endothelial venule blood vessels for tumor-infiltrating lymphocytes are associated with lymphotoxin β-producing dendritic cells in human breast cancer. *Journal of immunology (Baltimore, Md. : 1950)*, 191(4), pp.2001–2008.

Martinet, L. et al., 2012. High endothelial venules (HEVs) in human melanoma lesions: Major gateways for tumor-infiltrating lymphocytes. *Oncoimmunology*, 1(6), pp.829–839.

Martinet, L. et al., 2011. Human solid tumors contain high endothelial venules: association with T- and B-lymphocyte infiltration and favorable prognosis in breast cancer. *Cancer research*, 71(17), pp.5678–5687.

Martín-Gayo, E. et al., 2010. Plasmacytoid dendritic cells resident in human thymus drive natural Treg cell development. *Blood*, 115(26), pp.5366–5375.

Matloubian, M. et al., 2004. Lymphocyte egress from thymus and peripheral lymphoid organs is dependent on S1P receptor 1. *Nature*, 427(6972), pp.355–360.

Matrougui, K. et al., 2011. Natural regulatory T cells control coronary arteriolar

endothelial dysfunction in hypertensive mice. *The American journal of pathology*, 178(1), pp.434–441.

Matsushita, H. et al., 2012. Cancer exome analysis reveals a T-cell-dependent mechanism of cancer immunoediting. *Nature*, 482(7385), pp.400–404.

Maude, S.L. et al., 2014. Chimeric antigen receptor T cells for sustained remissions in leukemia. *The New England journal of medicine*, 371(16), pp.1507–1517.

McGeachy, M.J., Stephens, L.A. & Anderton, S.M., 2005. Natural recovery and protection from autoimmune encephalomyelitis: contribution of CD4+CD25+ regulatory cells within the central nervous system. *Journal of immunology (Baltimore, Md. : 1950)*, 175(5), pp.3025–3032.

McMullen, T.P.W. et al., 2010. Survival in rectal cancer is predicted by T cell infiltration of tumour-associated lymphoid nodules. *Clinical and experimental immunology*, 161(1), pp.81–88.

McPherson, R.C. et al., 2015. T-bet Expression by Foxp3(+) T Regulatory Cells is Not Essential for Their Suppressive Function in CNS Autoimmune Disease or Colitis. *Frontiers in immunology*, 6, p.69.

Mebius, R.E., 2003. Organogenesis of lymphoid tissues. *Nature Reviews Immunology*, 3(4), pp.292–303.

Mebius, R.E. et al., 1996. A developmental switch in lymphocyte homing receptor and endothelial vascular addressin expression regulates lymphocyte homing and permits CD4+ CD3- cells to colonize lymph nodes. *Proceedings of the National Academy of Sciences of the United States of America*, 93(20), pp.11019–11024.

Mebius, R.E. et al., 1993. Expression of GlyCAM-1, an endothelial ligand for L-selectin, is affected by afferent lymphatic flow. *Journal of immunology (Baltimore, Md. : 1950)*, 151(12), pp.6769–6776.

Mebius, R.E. et al., 2001. The fetal liver counterpart of adult common lymphoid progenitors gives rise to all lymphoid lineages, CD45+CD4+CD3- cells, as well as macrophages. *Journal of immunology (Baltimore, Md. : 1950)*, 166(11), pp.6593–6601.

Mebius, R.E. et al., 1991. The influence of afferent lymphatic vessel interruption on vascular addressin expression. *The Journal of cell biology*, 115(1), pp.85–95.

Mebius, R.E., Rennert, P. & Weissman, I.L., 1997. Developing lymph nodes collect CD4+CD3- LTbeta+ cells that can differentiate to APC, NK cells, and follicular cells but not T or B cells. *Immunity*, 7(4), pp.493–504.

Mebius, R.E., Schadee-Eestermans, I.L. & Weissman, I.L., 1998. MAdCAM-1 dependent colonization of developing lymph nodes involves a unique subset of CD4+CD3- hematolymphoid cells. *Cell adhesion and communication*, 6(2-3), pp.97–103.

Medawar, P.B., 1944. The behaviour and fate of skin autografts and skin homografts in rabbits: A report to the War Wounds Committee of the Medical Research Council. *Journal of anatomy*, 78(Pt 5), pp.176–199.

Meier, D. et al., 2007. Ectopic lymphoid-organ development occurs through interleukin 7-mediated enhanced survival of lymphoid-tissue-inducer cells. *Immunity*, 26(5), pp.643–654.

Mellanby, R.J. et al., 2007. Diabetes in non-obese diabetic mice is not associated with quantitative changes in CD4+ CD25+ Foxp3+ regulatory T cells. *Immunology*, 121(1), pp.15–28.

Messina, J.L. et al., 2012. 12-Chemokine gene signature identifies lymph node-like structures in melanoma: potential for patient selection for immunotherapy? *Scientific reports*, 2, p.765.

Miller, F.R., 1983. Tumor subpopulation interactions in metastasis. *Invasion & metastasis*, 3(4), pp.234–242.

Miller, F.R., Miller, B.E. & Heppner, G.H., 1983. Characterization of metastatic heterogeneity among subpopulations of a single mouse mammary tumor: heterogeneity in phenotypic stability. *Invasion & metastasis*, 3(1), pp.22–31.

Misra, N. et al., 2004. Cutting edge: human CD4+CD25+ T cells restrain the maturation and antigen-presenting function of dendritic cells. *Journal of immunology (Baltimore, Md. : 1950)*, 172(8), pp.4676–4680.

Mittal, D. et al., 2014. New insights into cancer immunoediting and its three component phases--elimination, equilibrium and escape. *Current opinion in immunology*, 27, pp.16–25.

Miyagawa, S. et al., 2004. Prognostic significance of mature dendritic cells and factors associated with their accumulation in metastatic liver tumors from colorectal cancer. *Human pathology*, 35(11), pp.1392–1396.

Miyao, T. et al., 2012. Plasticity of Foxp3(+) T cells reflects promiscuous Foxp3 expression in conventional T cells but not reprogramming of regulatory T cells. *Immunity*, 36(2), pp.262–275.

Miyara, M., Wing, K. & Sakaguchi, S., 2009. Therapeutic approaches to allergy and autoimmunity based on FoxP3+ regulatory T-cell activation and expansion. *The Journal of allergy and clinical immunology*, 123(4), pp.749–55– quiz 756–7.

Miyawaki, S. et al., 1994. A new mutation, aly, that induces a generalized lack of lymph nodes accompanied by immunodeficiency in mice. *European journal of immunology*, 24(2), pp.429–434.

Morgan, M.E. et al., 2003. CD25+ cell depletion hastens the onset of severe disease in collagen-induced arthritis. *Arthritis and rheumatism*, 48(5), pp.1452–1460.

Morgan, R.A. et al., 2006. Cancer regression in patients after transfer of genetically engineered lymphocytes. *Science (New York, N.Y.)*, 314(5796), pp.126–129.

Morrissey, P.J. et al., 1993. CD4+ T cells that express high levels of CD45RB induce wasting disease when transferred into congenic severe combined immunodeficient mice. Disease development is prevented by cotransfer of purified CD4+ T cells. *The Journal of experimental medicine*, 178(1), pp.237–244.

Motallebzadeh, R. et al., 2012. Blocking lymphotoxin signaling abrogates the development of ectopic lymphoid tissue within cardiac allografts and inhibits effector antibody responses. *FASEB journal : official publication of the Federation of American Societies for Experimental Biology*, 26(1), pp.51–62.

Motz, G.T. & Coukos, G., 2011. The parallel lives of angiogenesis and immunosuppression: cancer and other tales. *Nature Publishing Group*, 11(10), pp.702–711.

Motz, G.T. et al., 2014. Tumor endothelium FasL establishes a selective immune barrier promoting tolerance in tumors. *Nature medicine*, 20(6), pp.607–615.

Moussion, C. & Girard, J.-P., 2011. Dendritic cells control lymphocyte entry to lymph nodes through high endothelial venules. *Nature*, 479(7374), pp.542–546.

Moyron-Quiroz, J.E. et al., 2006. Persistence and responsiveness of immunologic memory in the absence of secondary lymphoid organs. *Immunity*, 25(4), pp.643–654.

Moyron-Quiroz, J.E. et al., 2004. Role of inducible bronchus associated lymphoid tissue (iBALT) in respiratory immunity. *Nature medicine*, 10(9), pp.927–934.

Murakami, M. et al., 2002. CD25+CD4+ T cells contribute to the control of memory CD8+ T cells. *Proceedings of the National Academy of Sciences of the United States of America*, 99(13), pp.8832–8837.

Naito, Y. et al., 1998. CD8+ T cells infiltrated within cancer cell nests as a prognostic factor in human colorectal cancer. *Cancer research*, 58(16), pp.3491–3494.

Nakamura, K., Kitani, A. & Strober, W., 2001. Cell contact-dependent immunosuppression by CD4(+)CD25(+) regulatory T cells is mediated by cell surface-bound transforming growth factor beta. *The Journal of experimental medicine*, 194(5), pp.629–644.

Neumann, B. et al., 1996. Defective Peyer's patch organogenesis in mice lacking the 55-kD receptor for tumor necrosis factor. *The Journal of experimental medicine*, 184(1), pp.259–264.

Neurath, M.F. et al., 2002. The transcription factor T-bet regulates mucosal T cell activation in experimental colitis and Crohn's disease. *The Journal of experimental medicine*, 195(9), pp.1129–1143.

Neyt, K. et al., 2012. Tertiary lymphoid organs in infection and autoimmunity. *Trends in immunology*, 33(6), pp.297–305.

Ng, W.F. et al., 2001. Human CD4(+)CD25(+) cells: a naturally occurring population of regulatory T cells. *Blood*, 98(9), pp.2736–2744.

Nicholaou, T. et al., 2011. Immunoediting and persistence of antigen-specific immunity in patients who have previously been vaccinated with NY-ESO-1 protein formulated in ISCOMATRIX™. *Cancer immunology, immunotherapy : CII*, 60(11), pp.1625–1637.

Nielsen, J.S. et al., 2012. CD20+ tumor-infiltrating lymphocytes have an atypical CD27- memory phenotype and together with CD8+ T cells promote favorable prognosis in ovarian cancer. *Clinical cancer research : an official journal of the American Association for Cancer Research*, 18(12), pp.3281–3292.

Nishikawa, H. & Sakaguchi, S., 2010. Regulatory T cells in tumor immunity. *International journal of cancer. Journal international du cancer*, 127(4), pp.759–767.

Nishizuka, Y. & Sakakura, T., 1969. Thymus and reproduction: sex-linked dysgenesis of the gonad after neonatal thymectomy in mice. *Science (New York, N.Y.)*, 166(3906), pp.753–755.

North, R.J. & Bursuker, I., 1984. Generation and decay of the immune response to a

progressive fibrosarcoma. I. Ly-1+2- suppressor T cells down-regulate the generation of Ly-1-2+ effector T cells. *The Journal of experimental medicine*, 159(5), pp.1295–1311.

Nzula, S., Going, J.J. & Stott, D.I., 2003. Antigen-driven clonal proliferation, somatic hypermutation, and selection of B lymphocytes infiltrating human ductal breast carcinomas. *Cancer research*, 63(12), pp.3275–3280.

O'Connor, R.A. et al., 2012. Foxp3+ Treg cells in the inflamed CNS are insensitive to IL-6-driven IL-17 production. *European journal of immunology*, 42(5), pp.1174–1179.

Oberle, N. et al., 2007. Rapid suppression of cytokine transcription in human CD4+CD25 T cells by CD4+Foxp3+ regulatory T cells: independence of IL-2 consumption, TGF-beta, and various inhibitors of TCR signaling. *Journal of immunology (Baltimore, Md. : 1950)*, 179(6), pp.3578–3587.

Ohl, L. et al., 2003. Cooperating mechanisms of CXCR5 and CCR7 in development and organization of secondary lymphoid organs. *The Journal of experimental medicine*, 197(9), pp.1199–1204.

Old, L.J. & Boyse, E.A., 1964. IMMUNOLOGY OF EXPERIMENTAL TUMORS. *Annual review of medicine*, 15(1), pp.167–186.

Onder, L. et al., 2013. Endothelial cell-specific lymphotoxin-β receptor signaling is critical for lymph node and high endothelial venule formation. *The Journal of experimental medicine*, 210(3), pp.465–473.

Ondondo, B. et al., 2013. Home sweet home: the tumor microenvironment as a haven for regulatory T cells. *Frontiers in immunology*, 4, p.197.

Ondondo, B., et al., 2014[a]. A Distinct Chemokine Axis Does not Account for Enrichment of Foxp3(+) CD4(+) T cells in Carcinogen-Induced Fibrosarcomas. *Immunology*, pp.n/a–n/a.

Ondondo, B., et al., 2014[b]. Progression of carcinogen-induced fibrosarcomas is associated with the accumulation of naïve CD4+ T cells via blood vessels and lymphatics. *International journal of cancer. Journal international du cancer*, 134(9), pp.2156–2167.

Onizuka, S. et al., 1999. Tumor rejection by in vivo administration of anti-CD25 (interleukin-2 receptor alpha) monoclonal antibody. *Cancer research*, 59(13), pp.3128–3133.

Ono, M. et al., 2007. Foxp3 controls regulatory T-cell function by interacting with AML1/Runx1. *Nature*, 446(7136), pp.685–689.

Onodera, T. et al., 2009. Constitutive expression of IDO by dendritic cells of mesenteric lymph nodes: functional involvement of the CTLA-4/B7 and CCL22/CCR4 interactions. *Journal of immunology (Baltimore, Md. : 1950)*, 183(9), pp.5608–5614.

Outzen, H.C. et al., 1975. Spontaneous and induced tumor incidence in germfree "nude" mice. *Journal of the Reticuloendothelial Society*, 17(1), pp.1–9.

Pagès, F. et al., 2005. Effector memory T cells, early metastasis, and survival in colorectal cancer. *The New England journal of medicine*, 353(25), pp.2654–2666.

Pandiyan, P. & Lenardo, M.J., 2008. The control of CD4+CD25+Foxp3+ regulatory T cell survival. *Biology direct*, 3(1), p.6.

Pandiyan, P. et al., 2007. CD4+CD25+Foxp3+ regulatory T cells induce cytokine deprivation-mediated apoptosis of effector CD4+ T cells. *Nature Immunology*, 8(12), pp.1353–1362.

Parry, R.V. et al., 2005. CTLA-4 and PD-1 receptors inhibit T-cell activation by distinct mechanisms. *Molecular and cellular biology*, 25(21), pp.9543–9553.

Pasparakis, M. et al., 1996. Immune and inflammatory responses in TNF alpha-deficient mice: a critical requirement for TNF alpha in the formation of primary B cell follicles, follicular dendritic cell networks and germinal centers, and in the maturation of the humoral immune response. *The Journal of experimental medicine*, 184(4), pp.1397–1411.

Pasparakis, M. et al., 1997. Peyer's patch organogenesis is intact yet formation of B lymphocyte follicles is defective in peripheral lymphoid organs of mice deficient for tumor necrosis factor and its 55-kDa receptor. *Proceedings of the National Academy of Sciences of the United States of America*, 94(12), pp.6319–6323.

Peggs, K.S. et al., 2009. Blockade of CTLA-4 on both effector and regulatory T cell compartments contributes to the antitumor activity of anti-CTLA-4 antibodies. *The Journal of experimental medicine*, 206(8), pp.1717–1725.

Penhale, W.J. et al., 1973. Spontaneous thyroiditis in thymectomized and irradiated Wistar rats. *Clinical and experimental immunology*, 15(2), pp.225–236.

Penhale, W.J. et al., 1976. Thyroiditis in T cell-depleted rats: suppression of the autoallergic response by reconstitution with normal lymphoid cells. *Clinical and experimental immunology*, 25(1), pp.6–16.

Penn, I., 1999. Posttransplant malignancies. *Transplantation proceedings*, 31(1-2), pp.1260–1262.

Perrone, G. et al., 2008. Intratumoural FOXP3-positive regulatory T cells are associated with adverse prognosis in radically resected gastric cancer. *European journal of cancer (Oxford, England : 1990)*, 44(13), pp.1875–1882.

Peske, J.D. et al., 2015. Effector lymphocyte-induced lymph node-like vasculature enables naive T-cell entry into tumours and enhanced anti-tumour immunity. *Nature communications*, 6, p.7114.

Peters, A. et al., 2011. Th17 cells induce ectopic lymphoid follicles in central nervous system tissue inflammation. *Immunity*, 35(6), pp.986–996.

Peters, J.H. et al., 2013. Human secondary lymphoid organs typically contain polyclonally-activated proliferating regulatory T cells. *Blood*, 122(13), pp.2213–2223.

Pfeffer, K. et al., 1993. Mice deficient for the 55 kd tumor necrosis factor receptor are resistant to endotoxic shock, yet succumb to L. monocytogenes infection. *Cell*, 73(3), pp.457–467.

Piccirillo, C.A. et al., 2002. CD4(+)CD25(+) regulatory T cells can mediate suppressor function in the absence of transforming growth factor beta1 production and responsiveness. *The Journal of experimental medicine*, 196(2), pp.237–246.

Pierson, W. et al., 2013. Antiapoptotic Mcl-1 is critical for the survival and niche-filling capacity of Foxp3+ regulatory T cells. *Nature Immunology*, 14(9), pp.959–965.

Pitzalis, C. et al., 2014. Ectopic lymphoid-like structures in infection, cancer and autoimmunity. *Nature Publishing Group*, 14(7), pp.447–462.

Powrie, F. et al., 1993. Phenotypically distinct subsets of CD4+ T cells induce or protect from chronic intestinal inflammation in C. B-17 scid mice. *International immunology*, 5(11), pp.1461–1471.

Qiao, L. et al., 2015. Advanced research on vasculogenic mimicry in cancer. *Journal of cellular and molecular medicine*, 19(2), pp.315–326.

Qin, S. et al., 1987. CD4 monoclonal antibody pairs for immunosuppression and tolerance induction. *European journal of immunology*, 17(8), pp.1159–1165.

Qin, S.X. et al., 1989. Induction of classical transplantation tolerance in the adult. *The Journal of experimental medicine*, 169(3), pp.779–794.

Quezada, S.A. & Peggs, K.S., 2013. Exploiting CTLA-4, PD-1 and PD-L1 to reactivate the host immune response against cancer. *British journal of cancer*, 108(8), pp.1560–1565.

Quezada, S.A. et al., 2006. CTLA4 blockade and GM-CSF combination immunotherapy alters the intratumor balance of effector and regulatory T cells. *The Journal of clinical investigation*, 116(7), pp.1935–1945.

Quezada, S.A. et al., 2008. Limited tumor infiltration by activated T effector cells restricts the therapeutic activity of regulatory T cell depletion against established melanoma. *The Journal of experimental medicine*, 205(9), pp.2125–2138.

Quezada, S.A. et al., 2011. Shifting the equilibrium in cancer immunoediting: from tumor tolerance to eradication. *Immunological reviews*, 241(1), pp.104–118.

Qureshi, O.S. et al., 2011. Trans-endocytosis of CD80 and CD86: a molecular basis for the cell-extrinsic function of CTLA-4. *Science (New York, N.Y.)*, 332(6029), pp.600–603.

Radstake, T.R.D.J. et al., 2009. Increased frequency and compromised function of T regulatory cells in systemic sclerosis (SSc) is related to a diminished CD69 and TGFbeta expression. D. Unutmaz, ed. *PloS one*, 4(6), p.e5981.

Randall, T.D., Carragher, D.M. & Rangel-Moreno, J., 2008. Development of Secondary Lymphoid Organs. *Annual Review of Immunology*, 26(1), pp.627–650.

Rangel-Moreno, J. et al., 2007. Pulmonary expression of CXC chemokine ligand 13, CC chemokine ligand 19, and CC chemokine ligand 21 is essential for local immunity to influenza. *Proceedings of the National Academy of Sciences of the United States of America*, 104(25), pp.10577–10582.

Rangel-Moreno, J. et al., 2011. The development of inducible bronchus-associated lymphoid tissue depends on IL-17. *Nature Immunology*, 12(7), pp.639–646.

Read, S. et al., 2006. Blockade of CTLA-4 on CD4+CD25+ regulatory T cells abrogates their function in vivo. *Journal of immunology (Baltimore, Md. : 1950)*, 177(7), pp.4376–4383.

Read, S. et al., 1998. CD38+ CD45RB(low) CD4+ T cells: a population of T cells with

immune regulatory activities in vitro. *European journal of immunology*, 28(11), pp.3435–3447.

Read, S., Malmström, V. & Powrie, F., 2000. Cytotoxic T lymphocyte-associated antigen 4 plays an essential role in the function of CD25(+)CD4(+) regulatory cells that control intestinal inflammation. *The Journal of experimental medicine*, 192(2), pp.295–302.

Redjimi, N. et al., 2012. CXCR3+ T regulatory cells selectively accumulate in human ovarian carcinomas to limit type I immunity. *Cancer research*, 72(17), pp.4351–4360.

Remark, R. et al., 2013. Characteristics and clinical impacts of the immune environments in colorectal and renal cell carcinoma lung metastases: influence of tumor origin. *Clinical cancer research : an official journal of the American Association for Cancer Research*, 19(15), pp.4079–4091.

Rennert, P.D. et al., 1998. Lymph node genesis is induced by signaling through the lymphotoxin beta receptor. *Immunity*, 9(1), pp.71–79.

Rennert, P.D. et al., 1996. Surface lymphotoxin alpha/beta complex is required for the development of peripheral lymphoid organs. *The Journal of experimental medicine*, 184(5), pp.1999–2006.

Rennert, P.D., Browning, J.L. & Hochman, P.S., 1997. Selective disruption of lymphotoxin ligands reveals a novel set of mucosal lymph nodes and unique effects on lymph node cellular organization. *International immunology*, 9(11), pp.1627–1639.

Repasky, E.A., Evans, S.S. & Dewhirst, M.W., 2013. Temperature matters! And why it should matter to tumor immunologists. *Cancer immunology research*, 1(4), pp.210–216.

Robbins, P.F. et al., 2013. Mining exomic sequencing data to identify mutated antigens recognized by adoptively transferred tumor-reactive T cells. *Nature medicine*, 19(6), pp.747–752.

Robert, C. et al., 2014. Anti-programmed-death-receptor-1 treatment with pembrolizumab in ipilimumab-refractory advanced melanoma: a randomised dose-comparison cohort of a phase 1 trial. *Lancet (London, England)*, 384(9948), pp.1109–1117.

Robert, C. et al., 2011. Ipilimumab plus dacarbazine for previously untreated metastatic melanoma. *The New England journal of medicine*, 364(26), pp.2517–2526.

Robert, C. et al., 2015. Nivolumab in previously untreated melanoma without BRAF mutation. *The New England journal of medicine*, 372(4), pp.320–330.

Rojas, G. et al., 2014. Fine epitope specificity of antibodies against interleukin-2 explains their paradoxical immunomodulatory effects. *mAbs*, 6(1), pp.273–285.

Roncador, G. et al., 2005. Analysis of FOXP3 protein expression in human CD4+CD25+ regulatory T cells at the single-cell level. *European journal of immunology*, 35(6), pp.1681–1691.

Rooney, I., Butrovich, K. & Ware, C.F., 2000. Expression of lymphotoxins and their receptor-Fc fusion proteins by baculovirus. *Methods in enzymology*, 322, pp.345–363.

Roozendaal, R. & Mebius, R.E., 2011. Stromal cell-immune cell interactions. *Annual Review of Immunology*, 29(1), pp.23–43.

Rosen, S.D., 2004. Ligands for L-selectin: homing, inflammation, and beyond. *Annual Review of Immunology*, 22(1), pp.129–156.

Rosenberg, S.A. & Restifo, N.P., 2015. Adoptive cell transfer as personalized immunotherapy for human cancer. *Science (New York, N.Y.)*, 348(6230), pp.62–68.

Rosenberg, S.A. et al., 2005. Tumor progression can occur despite the induction of very high levels of self/tumor antigen-specific CD8+ T cells in patients with melanoma. *Journal of immunology (Baltimore, Md. : 1950)*, 175(9), pp.6169–6176.

Rothe, J. et al., 1993. Mice lacking the tumour necrosis factor receptor 1 are resistant to TNF-mediated toxicity but highly susceptible to infection by Listeria monocytogenes. *Nature*, 364(6440), pp.798–802.

Ruddle, N.H., 2014. Lymphatic vessels and tertiary lymphoid organs. *The Journal of clinical investigation*, 124(3), pp.953–959.

Ruddle, N.H. & Akirav, E.M., 2009. Secondary lymphoid organs: responding to genetic and environmental cues in ontogeny and the immune response. *Journal of immunology (Baltimore, Md. : 1950)*, 183(4), pp.2205–2212.

Ruffell, B. et al., 2010. Lymphocytes in cancer development: polarization towards pro-tumor immunity. *Cytokine & growth factor reviews*, 21(1), pp.3–10.

Rygaard, J. & Povlsen, C.O., 1974a. Is immunological surveillance not a cell-mediated immune function? *Transplantation*, 17(1), pp.135–136.

Rygaard, J. & Povlsen, C.O., 1974b. The mouse mutant nude does not develop spontaneous tumours. An argument against immunological surveillance. *Acta pathologica et microbiologica Scandinavica. Section B: Microbiology and immunology*, 82(1), pp.99–106.

Ryschich, E. et al., 2002. Transformation of the microvascular system during multistage tumorigenesis. *International journal of cancer. Journal international du cancer*, 97(6), pp.719–725.

Sacca, R. et al., 1998. Differential activities of secreted lymphotoxin-alpha3 and membrane lymphotoxin-alpha1beta2 in lymphotoxin-induced inflammation: critical role of TNF receptor 1 signaling. *Journal of immunology (Baltimore, Md. : 1950)*, 160(1), pp.485–491.

Sacca, R. et al., 1997. Transgenic expression of lymphotoxin restores lymph nodes to lymphotoxin-alpha-deficient mice. *Journal of immunology (Baltimore, Md. : 1950)*, 159(9), pp.4252–4260.

Sakaguchi, S., 2004. Naturally arising CD4+ regulatory t cells for immunologic self-tolerance and negative control of immune responses. *Annual Review of Immunology*, 22(1), pp.531–562.

Sakaguchi, S., 2005. Naturally arising Foxp3-expressing CD25+CD4+ regulatory T cells in immunological tolerance to self and non-self. *Nature Immunology*, 6(4), pp.345–352.

Sakaguchi, S. et al., 1995. Immunologic self-tolerance maintained by activated T cells

expressing IL-2 receptor alpha-chains (CD25). Breakdown of a single mechanism of self-tolerance causes various autoimmune diseases. *Journal of immunology (Baltimore, Md. : 1950)*, 155(3), pp.1151–1164.

Sakaguchi, S. et al., 2008. Regulatory T cells and immune tolerance. *Cell*, 133(5), pp.775–787.

Sakaguchi, S., Takahashi, T. & Nishizuka, Y., 1982. Study on cellular events in post-thymectomy autoimmune oophoritis in mice. II. Requirement of Lyt-1 cells in normal female mice for the prevention of oophoritis. *The Journal of experimental medicine*, 156(6), pp.1577–1586.

Sakaguchi, S.saka, 1985. Sakaguchi 1985. pp.1–16.

Sakai, Y. et al., 2014. High endothelial venule-like vessels and lymphocyte recruitment in testicular seminoma. *Andrology*, 2(2), pp.282–289.

Salomon, B. & Bluestone, J.A., 2001. Complexities of CD28/B7: CTLA-4 costimulatory pathways in autoimmunity and transplantation. *Annual Review of Immunology*, 19(1), pp.225–252.

Sancho, D. et al., 2003. CD69 downregulates autoimmune reactivity through active transforming growth factor-beta production in collagen-induced arthritis. *The Journal of clinical investigation*, 112(6), pp.872–882.

Sancho, D. et al., 2006. CD69 targeting differentially affects the course of collagen-induced arthritis. *Journal of leukocyte biology*, 80(6), pp.1233–1241.

Sato, E. et al., 2005. Intraepithelial CD8+ tumor-infiltrating lymphocytes and a high CD8+/regulatory T cell ratio are associated with favorable prognosis in ovarian cancer. *Proceedings of the National Academy of Sciences of the United States of America*, 102(51), pp.18538–18543.

Sawa, S. et al., 2010. Lineage relationship analysis of RORgammat+ innate lymphoid cells. *Science (New York, N.Y.)*, 330(6004), pp.665–669.

Scallon, B. et al., 2002. Binding and functional comparisons of two types of tumor necrosis factor antagonists. *The Journal of pharmacology and experimental therapeutics*, 301(2), pp.418–426.

Scanlan, M.J., Simpson, A.J.G. & Old, L.J., 2004. The cancer/testis genes: review, standardization, and commentary. *Cancer immunity*, 4, p.1.

Schadendorf, D. et al., 2015. Pooled Analysis of Long-Term Survival Data From Phase II and Phase III Trials of Ipilimumab in Unresectable or Metastatic Melanoma. *Journal of clinical oncology : official journal of the American Society of Clinical Oncology*, 33(17), pp.1889–1894.

Scheu, S. et al., 2002. Targeted disruption of LIGHT causes defects in costimulatory T cell activation and reveals cooperation with lymphotoxin beta in mesenteric lymph node genesis. *The Journal of experimental medicine*, 195(12), pp.1613–1624.

Schmidt, A., Oberle, N. & Krammer, P.H., 2012. Molecular mechanisms of treg-mediated T cell suppression. *Frontiers in immunology*, 3, p.51.

Schmidt, E.M. et al., 2009. Ctla-4 controls regulatory T cell peripheral homeostasis and is required for suppression of pancreatic islet autoimmunity. *Journal of immunology (Baltimore, Md. : 1950)*, 182(1), pp.274–282.

Schmutz, S. et al., 2009. Cutting edge: IL-7 regulates the peripheral pool of adult ROR gamma+ lymphoid tissue inducer cells. *Journal of immunology (Baltimore, Md. : 1950)*, 183(4), pp.2217–2221.

Schneider, M.A. et al., 2007. CCR7 is required for the in vivo function of CD4+ CD25+ regulatory T cells. *The Journal of experimental medicine*, 204(4), pp.735–745.

Schrama, D. et al., 2008. Immunological tumor destruction in a murine melanoma model by targeted LTalpha independent of secondary lymphoid tissue. *Cancer immunology, immunotherapy : CII*, 57(1), pp.85–95.

Schrama, D. et al., 2001. Targeting of lymphotoxin-alpha to the tumor elicits an efficient immune response associated with induction of peripheral lymphoid-like tissue. *Immunity*, 14(2), pp.111–121.

Schreiber, R.D., Old, L.J. & Smyth, M.J., 2011. Cancer immunoediting: integrating immunity's roles in cancer suppression and promotion. *Science (New York, N.Y.)*, 331(6024), pp.1565–1570.

Schreiber, T.H. et al., 2012. Tumor antigen specific iTreg accumulate in the tumor microenvironment and suppress therapeutic vaccination. *Oncoimmunology*, 1(5), pp.642–648.

Schumacher, T.N. & Schreiber, R.D., 2015. Neoantigens in cancer immunotherapy. *Science (New York, N.Y.)*, 348(6230), pp.69–74.

Scurr, M., Gallimore, A. & Godkin, A., 2012. T cell subsets and colorectal cancer: discerning the good from the bad. *Cellular immunology*, 279(1), pp.21–24.

Seleznik, G.M. et al., 2012. Lymphotoxin β receptor signaling promotes development of autoimmune pancreatitis. *Gastroenterology*, 143(5), pp.1361–1374.

Serra, P. et al., 2003. CD40 ligation releases immature dendritic cells from the control of regulatory CD4+CD25+ T cells. *Immunity*, 19(6), pp.877–889.

Setoguchi, R. et al., 2005. Homeostatic maintenance of natural Foxp3(+) CD25(+) CD4(+) regulatory T cells by interleukin (IL)-2 and induction of autoimmune disease by IL-2 neutralization. *The Journal of experimental medicine*, 201(5), pp.723–735.

Shankaran, V. et al., 2001. IFNgamma and lymphocytes prevent primary tumour development and shape tumour immunogenicity. *Nature*, 410(6832), pp.1107–1111.

Sharma, P. & Allison, J.P., 2015. The future of immune checkpoint therapy. *Science (New York, N.Y.)*, 348(6230), pp.56–61.

Shevach, E.M., 2009. Mechanisms of foxp3+ T regulatory cell-mediated suppression. *Immunity*, 30(5), pp.636–645.

Shevach, E.M. et al., 2006. The lifestyle of naturally occurring CD4+ CD25+ Foxp3+ regulatory T cells. *Immunological reviews*, 212(1), pp.60–73.

Shields, J.D. et al., 2010. Induction of lymphoidlike stroma and immune escape by tumors that express the chemokine CCL21. *Science (New York, N.Y.)*, 328(5979), pp.749–752.

Shimizu, J., Yamazaki, S. & Sakaguchi, S., 1999. Induction of tumor immunity by

removing CD25+CD4+ T cells: a common basis between tumor immunity and autoimmunity. *Journal of immunology (Baltimore, Md. : 1950)*, 163(10), pp.5211–5218.

Shinkura, R. et al., 1999. Alymphoplasia is caused by a point mutation in the mouse gene encoding Nf-kappa b-inducing kinase. *Nature genetics*, 22(1), pp.74–77.

Shiow, L.R. et al., 2006. CD69 acts downstream of interferon-alpha/beta to inhibit S1P1 and lymphocyte egress from lymphoid organs. *Nature*, 440(7083), pp.540–544.

Shrikant, P., Khoruts, A. & Mescher, M.F., 1999. CTLA-4 blockade reverses CD8+ T cell tolerance to tumor by a CD4+ T cell- and IL-2-dependent mechanism. *Immunity*, 11(4), pp.483–493.

Shrimali, R.K. et al., 2010. Antiangiogenic agents can increase lymphocyte infiltration into tumor and enhance the effectiveness of adoptive immunotherapy of cancer. *Cancer research*, 70(15), pp.6171–6180.

Simpson, T.R. et al., 2013. Fc-dependent depletion of tumor-infiltrating regulatory T cells co-defines the efficacy of anti-CTLA-4 therapy against melanoma. *The Journal of experimental medicine*, 210(9), pp.1695–1710.

Sinicrope, F.A. et al., 2009. Intraepithelial effector (CD3+)/regulatory (FoxP3+) T-cell ratio predicts a clinical outcome of human colon carcinoma. *Gastroenterology*, 137(4), pp.1270–1279.

Sistigu, A. et al., 2011. Immunomodulatory effects of cyclophosphamide and implementations for vaccine design. *Seminars in immunopathology*, 33(4), pp.369–383.

Skon, C.N. et al., 2013. Transcriptional downregulation of S1pr1 is required for the establishment of resident memory CD8+ T cells. *Nature Immunology*, 14(12), pp.1285–1293.

Small, E.J. et al., 2006. Placebo-controlled phase III trial of immunologic therapy with sipuleucel-T (APC8015) in patients with metastatic, asymptomatic hormone refractory prostate cancer. *Journal of clinical oncology : official journal of the American Society of Clinical Oncology*, 24(19), pp.3089–3094.

Soderberg, K.A. et al., 2004. MAdCAM-1 expressing sacral lymph node in the lymphotoxin beta-deficient mouse provides a site for immune generation following vaginal herpes simplex virus-2 infection. *Journal of immunology (Baltimore, Md. : 1950)*, 173(3), pp.1908–1913.

Sojka, D.K. & Fowell, D.J., 2011. Regulatory T cells inhibit acute IFN-γ synthesis without blocking T-helper cell type 1 (Th1) differentiation via a compartmentalized requirement for IL-10. *Proceedings of the National Academy of Sciences of the United States of America*, 108(45), pp.18336–18341.

Stranford, S. & Ruddle, N.H., 2012. Follicular dendritic cells, conduits, lymphatic vessels, and high endothelial venules in tertiary lymphoid organs: Parallels with lymph node stroma. *Frontiers in immunology*, 3, p.350.

Stutman, O., 1974. Tumor development after 3-methylcholanthrene in immunologically deficient athymic-nude mice. *Science (New York, N.Y.)*, 183(4124), pp.534–536.

Sugihara, S. et al., 1988. Autoimmune thyroiditis induced in mice depleted of particular

T cell subsets. I. Requirement of Lyt-1 dull L3T4 bright normal T cells for the induction of thyroiditis. *Journal of immunology (Baltimore, Md. : 1950)*, 141(1), pp.105–113.

Sugiyama, D. et al., 2013. Anti-CCR4 mAb selectively depletes effector-type FoxP3+CD4+ regulatory T cells, evoking antitumor immune responses in humans. *Proceedings of the National Academy of Sciences of the United States of America*, 110(44), pp.17945–17950.

Sun, Z. et al., 2000. Requirement for RORgamma in thymocyte survival and lymphoid organ development. *Science (New York, N.Y.)*, 288(5475), pp.2369–2373.

Sutmuller, R.P. et al., 2001. Synergism of cytotoxic T lymphocyte-associated antigen 4 blockade and depletion of CD25(+) regulatory T cells in antitumor therapy reveals alternative pathways for suppression of autoreactive cytotoxic T lymphocyte responses. *The Journal of experimental medicine*, 194(6), pp.823–832.

Suzuki, A. et al., 2002. Mature dendritic cells make clusters with T cells in the invasive margin of colorectal carcinoma. *The Journal of pathology*, 196(1), pp.37–43.

Swarte, V.V. et al., 1998. Regulation of fucosyltransferase-VII expression in peripheral lymph node high endothelial venules. *European journal of immunology*, 28(10), pp.3040–3047.

Szabo, S.J. et al., 2000. A novel transcription factor, T-bet, directs Th1 lineage commitment. *Cell*, 100(6), pp.655–669.

Szabo, S.J. et al., 2003. Molecular mechanisms regulating Th1 immune responses. *Annual Review of Immunology*, 21(1), pp.713–758.

Szymczak-Workman, A.L. et al., 2011. Cutting edge: regulatory T cells do not mediate suppression via programmed cell death pathways. *Journal of immunology (Baltimore, Md. : 1950)*, 187(9), pp.4416–4420.

Taams, L.S. et al., 2001. Human anergic/suppressive CD4(+)CD25(+) T cells: a highly differentiated and apoptosis-prone population. *European journal of immunology*, 31(4), pp.1122–1131.

Takahashi, T. et al., 2000. Immunologic self-tolerance maintained by CD25(+)CD4(+) regulatory T cells constitutively expressing cytotoxic T lymphocyte-associated antigen 4. *The Journal of experimental medicine*, 192(2), pp.303–310.

Takahashi, T. et al., 1998. Immunologic self-tolerance maintained by CD25+CD4+ naturally anergic and suppressive T cells: induction of autoimmune disease by breaking their anergic/suppressive state. *International immunology*, 10(12), pp.1969–1980.

Tanaka, H. et al., 2002. Depletion of CD4+ CD25+ regulatory cells augments the generation of specific immune T cells in tumor-draining lymph nodes. *Journal of immunotherapy (Hagerstown, Md. : 1997)*, 25(3), pp.207–217.

Tanchot, C. et al., 2013. Tumor-infiltrating regulatory T cells: phenotype, role, mechanism of expansion in situ and clinical significance. *Cancer microenvironment : official journal of the International Cancer Microenvironment Society*, 6(2), pp.147–157.

Tang, Q. et al., 2004. Distinct roles of CTLA-4 and TGF-beta in CD4+CD25+ regulatory T cell function. *European journal of immunology*, 34(11), pp.2996–3005.

Tawara, I. et al., 2002. Sequential involvement of two distinct CD4+ regulatory T cells during the course of transplantable tumor growth and protection from 3-methylcholanthrene-induced tumorigenesis by CD25-depletion. *Japanese journal of cancer research : Gann*, 93(8), pp.911–916.

Taylor, P.C., 2010. Pharmacology of TNF blockade in rheumatoid arthritis and other chronic inflammatory diseases. *Current opinion in pharmacology*, 10(3), pp.308–315.

Teng, M.W.L. et al., 2010. Conditional regulatory T-cell depletion releases adaptive immunity preventing carcinogenesis and suppressing established tumor growth. *Cancer research*, 70(20), pp.7800–7809.

Teng, M.W.L. et al., 2012. Opposing roles for IL-23 and IL-12 in maintaining occult cancer in an equilibrium state. *Cancer research*, 72(16), pp.3987–3996.

Terme, M. et al., 2013. VEGFA-VEGFR pathway blockade inhibits tumor-induced regulatory T-cell proliferation in colorectal cancer. *Cancer research*, 73(2), pp.539–549.

Thornton, A.M. & Shevach, E.M., 1998. CD4+CD25+ immunoregulatory T cells suppress polyclonal T cell activation in vitro by inhibiting interleukin 2 production. *The Journal of experimental medicine*, 188(2), pp.287–296.

Thornton, A.M. & Shevach, E.M., 2000. Suppressor effector function of CD4+CD25+ immunoregulatory T cells is antigen nonspecific. *Journal of immunology (Baltimore, Md. : 1950)*, 164(1), pp.183–190.

Thornton, A.M. et al., 2004. Cutting edge: IL-2 is critically required for the in vitro activation of CD4+CD25+ T cell suppressor function. *Journal of immunology (Baltimore, Md. : 1950)*, 172(11), pp.6519–6523.

Thornton, A.M. et al., 2010. Expression of Helios, an Ikaros transcription factor family member, differentiates thymic-derived from peripherally induced Foxp3+ T regulatory cells. *Journal of immunology (Baltimore, Md. : 1950)*, 184(7), pp.3433–3441.

Tong, R.T. et al., 2004. Vascular normalization by vascular endothelial growth factor receptor 2 blockade induces a pressure gradient across the vasculature and improves drug penetration in tumors. *Cancer research*, 64(11), pp.3731–3736.

Topalian, S.L. et al., 2012. Safety, activity, and immune correlates of anti-PD-1 antibody in cancer. *The New England journal of medicine*, 366(26), pp.2443–2454.

Topalian, S.L. et al., 2014. Survival, durable tumor remission, and long-term safety in patients with advanced melanoma receiving nivolumab. *Journal of clinical oncology : official journal of the American Society of Clinical Oncology*, 32(10), pp.1020–1030.

Tracey, D. et al., 2008. Tumor necrosis factor antagonist mechanisms of action: a comprehensive review. *Pharmacology & therapeutics*, 117(2), pp.244–279.

Tran, D.Q. et al., 2009. Selective expression of latency-associated peptide (LAP) and IL-1 receptor type I/II (CD121a/CD121b) on activated human FOXP3+ regulatory T cells allows for their purification from expansion cultures. *Blood*, 113(21), pp.5125–5133.

Tripathi, S.K. & Lahesmaa, R., 2014. Transcriptional and epigenetic regulation of T-

helper lineage specification. *Immunological reviews*, 261(1), pp.62–83.

Turk, M.J. et al., 2004. Concomitant tumor immunity to a poorly immunogenic melanoma is prevented by regulatory T cells. *The Journal of experimental medicine*, 200(6), pp.771–782.

Uchimura, K. et al., 2005. A major class of L-selectin ligands is eliminated in mice deficient in two sulfotransferases expressed in high endothelial venules. *Nature Immunology*, 6(11), pp.1105–1113.

Uchimura, K. et al., 2004. N-acetylglucosamine 6-O-sulfotransferase-1 regulates expression of L-selectin ligands and lymphocyte homing. *The Journal of biological chemistry*, 279(33), pp.35001–35008.

Valzasina, B. et al., 2006. Tumor-induced expansion of regulatory T cells by conversion of CD4+CD25- lymphocytes is thymus and proliferation independent. *Cancer research*, 66(8), pp.4488–4495.

van de Pavert, S.A. & Mebius, R.E., 2014. Development of secondary lymphoid organs in relation to lymphatic vasculature. *Advances in anatomy, embryology, and cell biology*, 214(Chapter 7), pp.81–91.

van de Pavert, S.A. & Mebius, R.E., 2010. New insights into the development of lymphoid tissues. *Nature Publishing Group*, 10(9), pp.664–674.

van de Pavert, S.A. et al., 2009. Chemokine CXCL13 is essential for lymph node initiation and is induced by retinoic acid and neuronal stimulation. *Nature Immunology*, 10(11), pp.1193–1199.

van der Bruggen, P. et al., 1991. A gene encoding an antigen recognized by cytolytic T lymphocytes on a human melanoma. *Science (New York, N.Y.)*, 254(5038), pp.1643–1647.

van der Vliet, H.J. et al., 2007. Effects of the administration of high-dose interleukin-2 on immunoregulatory cell subsets in patients with advanced melanoma and renal cell cancer. *Clinical cancer research : an official journal of the American Association for Cancer Research*, 13(7), pp.2100–2108.

van Rooij, N. et al., 2013. Tumor exome analysis reveals neoantigen-specific T-cell reactivity in an ipilimumab-responsive melanoma. *Journal of clinical oncology : official journal of the American Society of Clinical Oncology*, 31(32), pp.e439–42.

Végran, F. et al., 2014. The transcription factor IRF1 dictates the IL-21-dependent anticancer functions of TH9 cells. *Nature Immunology*, 15(8), pp.758–766.

Vignali, D.A.A., 2012. Mechanisms of T(reg) Suppression: Still a Long Way to Go. *Frontiers in immunology*, 3, p.191.

Vigneron, N. et al., 2013. Database of T cell-defined human tumor antigens: the 2013 update. *Cancer immunity*, 13, p.15.

Vogelstein, B. et al., 2013. Cancer genome landscapes. *Science (New York, N.Y.)*, 339(6127), pp.1546–1558.

Vondenhoff, M.F. et al., 2009. LTbetaR signaling induces cytokine expression and up-regulates lymphangiogenic factors in lymph node anlagen. *Journal of immunology (Baltimore, Md. : 1950)*, 182(9), pp.5439–5445.

Vukmanovic-Stejic, M. et al., 2006. Human CD4+ CD25hi Foxp3+ regulatory T cells are derived by rapid turnover of memory populations in vivo. *The Journal of clinical investigation*, 116(9), pp.2423–2433.

Vukmanovic-Stejic, M. et al., 2008. The kinetics of CD4+Foxp3+ T cell accumulation during a human cutaneous antigen-specific memory response in vivo. *The Journal of clinical investigation*, 118(11), pp.3639–3650.

Wainwright, D.A. et al., 2011. Thymus-derived rather than tumor-induced regulatory T cells predominate in brain tumors. *Neuro-oncology*, 13(12), pp.1308–1323.

Waitz, R., Fassò, M. & Allison, J.P., 2012. CTLA-4 blockade synergizes with cryoablation to mediate tumor rejection. *Oncoimmunology*, 1(4), pp.544–546.

Wald, O. et al., 2006. CD4+CXCR4highCD69+ T cells accumulate in lung adenocarcinoma. *Journal of immunology (Baltimore, Md. : 1950)*, 177(10), pp.6983–6990.

Walker, L.S.K. et al., 2003. Antigen-dependent proliferation of CD4+ CD25+ regulatory T cells in vivo. *The Journal of experimental medicine*, 198(2), pp.249–258.

Walter, S. et al., 2012. Multipeptide immune response to cancer vaccine IMA901 after single-dose cyclophosphamide associates with longer patient survival. *Nature medicine*, 18(8), pp.1254–1261.

Walunas, T.L. et al., 1994. CTLA-4 can function as a negative regulator of T cell activation. *Immunity*, 1(5), pp.405–413.

Wang, P. & Zheng, S.G., 2013. Regulatory T cells and B cells: implication on autoimmune diseases. *International journal of clinical and experimental pathology*, 6(12), pp.2668–2674.

Ware, C.F., 2005. Network communications: lymphotoxins, LIGHT, and TNF. *Annual Review of Immunology*, 23(1), pp.787–819.

Webster, B. et al., 2006. Regulation of lymph node vascular growth by dendritic cells. *The Journal of experimental medicine*, 203(8), pp.1903–1913.

Weiss, J.M. et al., 2012. Neuropilin 1 is expressed on thymus-derived natural regulatory T cells, but not mucosa-generated induced Foxp3+ T reg cells. *The Journal of experimental medicine*, 209(10), pp.1723–42– S1.

Wendland, M. et al., 2011. Lymph node T cell homeostasis relies on steady state homing of dendritic cells. *Immunity*, 35(6), pp.945–957.

Wengner, A.M. et al., 2007. CXCR5- and CCR7-dependent lymphoid neogenesis in a murine model of chronic antigen-induced arthritis. *Arthritis and rheumatism*, 56(10), pp.3271–3283.

Whiteside, T.L., 2012. What are regulatory T cells (Treg) regulating in cancer and why? *Seminars in cancer biology*, 22(4), pp.327–334.

Wildin, R.S. et al., 2001. X-linked neonatal diabetes mellitus, enteropathy and endocrinopathy syndrome is the human equivalent of mouse scurfy. *Nature genetics*, 27(1), pp.18–20.

Wilke, C.M. et al., 2010. Prognostic significance of regulatory T cells in tumor. *International journal of cancer. Journal international du cancer*, 127(4), pp.748–

758.

Willett, C.G. et al., 2004. Direct evidence that the VEGF-specific antibody bevacizumab has antivascular effects in human rectal cancer. *Nature medicine*, 10(2), pp.145–147.

Williams, E.L. et al., 2013. Immunotherapy targeting inhibitory Fcγ receptor IIB (CD32b) in the mouse is limited by monoclonal antibody consumption and receptor internalization. *Journal of immunology (Baltimore, Md. : 1950)*, 191(8), pp.4130–4140.

Williams, L.M. & Rudensky, A.Y., 2007. Maintenance of the Foxp3-dependent developmental program in mature regulatory T cells requires continued expression of Foxp3. *Nature Immunology*, 8(3), pp.277–284.

Williams, T.W. & Granger, G.A., 1968. Lymphocyte in vitro cytotoxicity: lymphotoxins of several mammalian species. *Nature*, 219(5158), pp.1076–1077.

Wing, K. et al., 2008. CTLA-4 control over Foxp3+ regulatory T cell function. *Science (New York, N.Y.)*, 322(5899), pp.271–275.

Winter, S. et al., 2010. The chemokine receptor CXCR5 is pivotal for ectopic mucosa-associated lymphoid tissue neogenesis in chronic Helicobacter pylori-induced inflammation. *Journal of molecular medicine (Berlin, Germany)*, 88(11), pp.1169–1180.

Wolchok, J.D. et al., 2013. Nivolumab plus ipilimumab in advanced melanoma. *The New England journal of medicine*, 369(2), pp.122–133.

World Health Organisation, http://www.who.int/mediacentre/factsheets/fs297/en/, Accessed September 2015

Wu, X. et al., 2013. Immune microenvironment profiles of tumor immune equilibrium and immune escape states of mouse sarcoma. *Cancer letters*, 340(1), pp.124–133.

Wu, Y. et al., 2006. FOXP3 controls regulatory T cell function through cooperation with NFAT. *Cell*, 126(2), pp.375–387.

Xu, B. et al., 2003. Lymphocyte homing to bronchus-associated lymphoid tissue (BALT) is mediated by L-selectin/PNAd, alpha4beta1 integrin/VCAM-1, and LFA-1 adhesion pathways. *The Journal of experimental medicine*, 197(10), pp.1255–1267.

Yagi, H. et al., 2004. Crucial role of FOXP3 in the development and function of human CD25+CD4+ regulatory T cells. *International immunology*, 16(11), pp.1643–1656.

Yamamoto, M. et al., 2000. Alternate mucosal immune system: organized Peyer's patches are not required for IgA responses in the gastrointestinal tract. *Journal of immunology (Baltimore, Md. : 1950)*, 164(10), pp.5184–5191.

Yang, L. et al., 2004. Expansion of myeloid immune suppressor Gr+CD11b+ cells in tumor-bearing host directly promotes tumor angiogenesis. *Cancer cell*, 6(4), pp.409–421.

Yin, L. et al., 2001. Defective lymphotoxin-beta receptor-induced NF-kappaB transcriptional activity in NIK-deficient mice. *Science (New York, N.Y.)*, 291(5511), pp.2162–2165.

Yokota, Y. et al., 1999. Development of peripheral lymphoid organs and natural killer cells depends on the helix-loop-helix inhibitor Id2. *Nature*, 397(6721), pp.702–706.

Yoshida, H. et al., 2002. Different cytokines induce surface lymphotoxin-alphabeta on IL-7 receptor-alpha cells that differentially engender lymph nodes and Peyer's patches. *Immunity*, 17(6), pp.823–833.

Yoshida, H. et al., 2001. Expression of alpha(4)beta(7) integrin defines a distinct pathway of lymphoid progenitors committed to T cells, fetal intestinal lymphotoxin producer, NK, and dendritic cells. *Journal of immunology (Baltimore, Md. : 1950)*, 167(5), pp.2511–2521.

Yoshida, H. et al., 1999. IL-7 receptor alpha+ CD3(-) cells in the embryonic intestine induces the organizing center of Peyer's patches. *International immunology*, 11(5), pp.643–655.

Yu, P. et al., 2005. Intratumor depletion of CD4+ cells unmasks tumor immunogenicity leading to the rejection of late-stage tumors. *The Journal of experimental medicine*, 201(5), pp.779–791.

Yu, P. et al., 2004. Priming of naive T cells inside tumors leads to eradication of established tumors. *Nature Immunology*, 5(2), pp.141–149.

Zang, X. et al., 2010. Tumor associated endothelial expression of B7-H3 predicts survival in ovarian carcinomas. *Modern pathology : an official journal of the United States and Canadian Academy of Pathology, Inc*, 23(8), pp.1104–1112.

Zhang, L. et al., 2003. Intratumoral T cells, recurrence, and survival in epithelial ovarian cancer. *The New England journal of medicine*, 348(3), pp.203–213.

Zhang, S., Zhang, D. & Sun, B., 2007. Vasculogenic mimicry: current status and future prospects. *Cancer letters*, 254(2), pp.157–164.

Zhao, D.-M. et al., 2006. Activated CD4+CD25+ T cells selectively kill B lymphocytes. *Blood*, 107(10), pp.3925–3932.

Zheng, W. & Flavell, R.A., 1997. The transcription factor GATA-3 is necessary and sufficient for Th2 cytokine gene expression in CD4 T cells. *Cell*, 89(4), pp.587–596.

Zheng, Y. & Rudensky, A.Y., 2007. Foxp3 in control of the regulatory T cell lineage. *Nature Immunology*, 8(5), pp.457–462.

Zheng, Y. et al., 2009. Regulatory T-cell suppressor program co-opts transcription factor IRF4 to control T(H)2 responses. *Nature*, 458(7236), pp.351–356.

Zhou, G. & Levitsky, H.I., 2007. Natural regulatory T cells and de novo-induced regulatory T cells contribute independently to tumor-specific tolerance. *Journal of immunology (Baltimore, Md. : 1950)*, 178(4), pp.2155–2162.

Zhu, J. & Paul, W.E., 2010. Peripheral CD4+ T-cell differentiation regulated by networks of cytokines and transcription factors. *Immunological reviews*, 238(1), pp.247–262.

Zou, W., 2006. Regulatory T cells, tumour immunity and immunotherapy. *Nature Reviews Immunology*, 6(4), pp.295–307.